



**HAL**  
open science

# Colloidal stability, intracellular fate and toxicology of drug nanocarriers - Application to polymerized micelles and organometallic nanogels

Federica Costamagna

► **To cite this version:**

Federica Costamagna. Colloidal stability, intracellular fate and toxicology of drug nanocarriers - Application to polymerized micelles and organometallic nanogels. Galenic pharmacology. Université Paris-Saclay, 2020. English. NNT : 2020UPASS128 . tel-03656228

**HAL Id: tel-03656228**

**<https://theses.hal.science/tel-03656228>**

Submitted on 2 May 2022

**HAL** is a multi-disciplinary open access archive for the deposit and dissemination of scientific research documents, whether they are published or not. The documents may come from teaching and research institutions in France or abroad, or from public or private research centers.

L'archive ouverte pluridisciplinaire **HAL**, est destinée au dépôt et à la diffusion de documents scientifiques de niveau recherche, publiés ou non, émanant des établissements d'enseignement et de recherche français ou étrangers, des laboratoires publics ou privés.

Stabilité colloïdale, devenir intracellulaire  
et toxicologie des nanovecteurs –  
Application aux micelles polymérisées  
et aux nanogels organométalliques

**Thèse de doctorat de l'université Paris-Saclay**

École doctorale n° 569, Innovation thérapeutique: du fondamental à l'appliqué  
(ITFA)

Spécialité de doctorat: Pharmacotechnie et Biopharmacie

Unité de recherche : Université Paris-Saclay, CNRS, Institut Galien Paris-Saclay, 92296,  
Châtenay-Malabry, France

Référent : Faculté de pharmacie

**Thèse présentée et soutenue en visioconférence totale,  
le 29 juin 2020, par**

**Federica COSTAMAGNA**

**Composition du Jury**

**Elias FATTAL**

Professeur, Université Paris-Saclay

Président

**Christophe SCHATZ**

MCF, HDR, Université de Bordeaux

Rapporteur & Examineur

**Ijeoma UCHEGBU**

Professeure, UCL School of Pharmacy

Rapporteur & Examinatrice

**Francoise CHUBURU**

Professeure, Université de Reims

Examinatrice

**Eric DORIS**

Directeur de recherche, Université Paris Saclay, CEA

Examineur

**Fabrice NESSLANY**

Directeur de recherche, Institut Pasteur de Lille

Examineur

**Hervé HILLAIREAU**

MCF, Université Paris-Saclay

Directeur de thèse



Colloidal stability, intracellular fate  
and toxicology of drug nanocarriers –  
Application to polymerized micelles  
and organometallic nanogels



To my family,



# Acknowledgements

This PhD thesis was performed at the Institut Galien Paris-Sud (Cnrs – Université Paris-Saclay) in the group of Prof. Elias Fattal. The work on chitosan-based nanogels was funded by an ANR fellowship (Kitostic) and supervised by Dr Hervé Hillaireau. The work on polydiacetylene micelles was supervised by Dr Hervé Hillaireau and Prof. Elias Fattal, in collaboration with the group of Eric Doris (Service de Chimie Bioorganique et de Marquage, CEA – Université Paris-Saclay) in the context of a LabEx Lermite project.

*Cette thèse de doctorat a été réalisée à l'Institut Galien Paris-Sud (Cnrs – Université Paris-Saclay) dans le groupe du Pr Elias Fattal. Les travaux sur les nanogels à base de chitosane ont été financés par une bourse ANR (Kitostic) et encadrés par le Dr Hervé Hillaireau. Les travaux sur les micelles de polydiacétylène ont été encadrés par le Dr Hervé Hillaireau et le Pr Elias Fattal, en collaboration avec le groupe d'Eric Doris (Service de Chimie Bioorganique et de Marquage, CEA – Université Paris-Saclay) dans le cadre d'un projet Labex Lermite.*

I would like to begin thanking Prof. Ijeoma UCHEGBU and Prof. Christophe SCHATZ, who did me the honor to accept to review this manuscript. Many thanks also to all the other members of the jury, Prof. Elias FATTAL, Prof. Françoise CHUBURU, Dr. Fabrice NESSLANY and Dr. Eric DORIS for accepting to read and evaluate my work.

I would like to express my sincere gratefulness to my advisor Dr. Hervé HILLAIREAU, for his support during my PhD, for his patience and big knowledge. More than anything, I appreciated the freedom and the trust you gave me on the management of the project. Your guidance taught me to do this job in a rigorous and in the same time creative way. Thanks for showing me this way of doing research.

I warmly wish to thank professor Elias FATTAL for welcoming me in his team long time ago and for his persistent help during this adventure. This thesis was made possible also by his masterly guidance and his very helpful advice. I want to thank you for our discussions about science, career and life in general, which made me grow up both scientifically and humanly.

A very special thanks to Dr. NICOLAS TSAPIS. We unfortunately didn't work together but you have been a great reference for me. Thank you for having always been there when I needed support at lab. My sincere thanks also goes to Dr. JULIETTE VERGNAUD who helped me a lot during this thesis. Thank you for having been always available, kind and interested to discuss about my results. I literally fell in love with cell biology during my experience at the Institut Galien and I learned a lot about that also thanks to you.

A big thanks to ERIC DORIS, EDMOND GRAVEL and the team of CEA for the synthesis of pDA-PEG micelles. A sincere thanks to STEPHANIE DENIS, who helped me to take care of my cells. The cell culture room has always been the place in which I loved to work, a kind of home for me at the Institut, and this is also thank to you. It has been a great pleasure to work with you. Thanks a lot to ASSIA HESSANI for her help and guidance in the experiments in radioactivity room (I hope I didn't leave any mess behind me). Thank you also for our cigarette breaks, it was good to have someone with whom complaining about experiments, life... A special thanks to MAGALI NOIRAY for her help with ITC experiments. It has been hard and I would probably not do it again (kidding) but I am happy and proud about the work we have done. My sincere thanks to VALERIE NICOLAS for her always optimistic help in performing the confocal microscopy experiments and to CLAIRE BOULOGNE for TEM experiments. A very special to MARION QUAILLET who taught me more or less everything I know about chitosan. You have been a great colleague and friend. Many thanks to Dr. SIMONA MURA, for being always available and kind when I asked her some advice.

I would like to thank the whole administration team of the Institut Galien (Dominique MARTIN, Fatiha HAMZA, Patricia LIVET) and especially Sylvie ZEMMOUR. You have been the only person

at the Institut who yelled at me but I think I was finally able to made myself lovable. Thanks a lot for fighting against FEDEX for me and for buying me my favorite vials all the time.

Next, a big thanks to all the students and the post-docs that I met during this amazing journey. I'm too scared to forget someone so I won't write all the names, sorry (you are so many!).

Just some special thanks. Sophie, for helping me a lot when I was just a new Italian not speaking French. Tanguy and Maria, for giving me wise advice. Isabella and Stefania, for creating the very first Italian team of my Parisian experience. Islam, for being a very good mate in congress and DPDD. Thanks a lot to Justine, Maud and Clelia for their smile, spontaneity, good mood. It has been a great pleasure to welcome you in the lab girls, I'm happy we found each other in Paris.

Thanks to Eleonore for having been my radioactivity partner, Badminton team mate and beer sponsor in Finland. Thanks to Renato for his sincere friendship, we miss you.

I want to warmly thank Raul, Balthazar, Arnaud and Quentin. We shared all these great (hard) years together and I'm so happy it has been with you. You are all good guys, excellent scientists and great friends. I would have not survive to the PhD without our "Trois Marches" moments. Thank you a lot. Thanks to Alessandro. I got really into nanomedicine by working with you in Italy and it has been a big gift for me having the opportunity to work together again in France. Everything would have been much more difficult without you.

Finally, thanks to my family in Paris.

Flavio, thanks for being the person I can call at any time. Thank you for our discussions about science, love, life, our fights (often), for the rum, the language exchanges, food experiences, travels we did and still have to do together. And for your basement, of course. The time I dived from a rock in Sicily just because you told me to do demonstrated all the trust I have in our friendship.

Serra. We fell in love immediately when we met. Having a person like you who always understand me and takes care of me is something I couldn't get without anymore. For sharing clothes, for supported each other against the difficulties of our Parisian life as foreigners. Thank you.

Celine. I couldn't imagine my adventure at the Institut without you. You have been on my side all the time, my rock. For having built a friendship that always growth up, your hugs, beers, IT help, for being the best room mate ever, for evenings at lab, for your car. Thank you.

Gianpiero. One of my best friends in Paris since the very beginning. We shared so much during these years, a lot of amazing moments and also many hard ones. We are growing up together and I hope we will always be able to preserve our great friendship despite difficulties of life.

Carlo. Thanks for being my favorite cook when I'm to lazy, for listening to my problems so patiently, for loving me as a very good friend. I'm lucky to have you in Paris.

It has been such a great journey guys, and we made it, together. I'm proud of us. I love you.

Finally, thanks to my family, that is far, but is always close to me.

# Summary

<b>Summary</b> .....	5
<b>Abbreviations</b> .....	7
<b>General introduction</b> .....	9
<b>Introduction générale</b> .....	13
<b>Literature Review</b> .....	17
1. Introduction.....	18
2. Colloidal stability of nanoparticles.....	22
2.1. Generalities.....	22
2.2. Colloidal stability of nanoparticles in physiological conditions.....	24
2.3. Colloidal stabilization of nanoparticles.....	28
2.4. The case of chitosan-based nanogels.....	30
2.4.1. Introduction to chitosan-based nanogels.....	30
2.4.2. Colloidal stability of chitosan-based nanogels.....	33
2.5. The case of polymeric micelles.....	35
2.5.1. Introduction to polymeric micelles.....	35
2.5.2. Colloidal stability of polymeric micelles.....	38
3. Biological fate and in vivo toxicity of nanoparticles.....	41
3.1. Generalities.....	41
3.2. In vivo fate and toxicity of chitosan-based nanogels.....	44
3.3 In vivo fate and toxicity of polymeric micelles.....	47
4. Intracellular fate and in vitro toxicity of nanoparticles.....	51
4.1 Generalities.....	51
4.2 Intracellular fate and in vitro toxicity of chitosan-based nanogels.....	56
4.3 Intracellular fate and in vitro toxicity of polymeric micelles.....	57
References.....	61
<b>Experimental work</b> .....	89
<b>Chapter 1: Influence of metals on the colloidal properties of chitosan-ATP nanogels</b> .....	91
Abstract.....	93
1. Introduction.....	94
2. Results.....	96
3. Discussion.....	105

4. Conclusions.....	108
5. Experimental.....	109
6. References.....	113
7. Supplementary.....	116
<b>Chapter 2: Influence of the nucleotide structure on the colloidal properties of chitosan-iron based nanogels.....</b>	<b>119</b>
Abstract.....	121
1. Introduction.....	122
2. Results.....	124
3. Discussion.....	133
4. Conclusions.....	134
5. Experimental.....	135
6. References.....	141
<b>Chapter 3: Intracellular fate and biological impact of Chitosan-Iron-based nanogels</b>	<b>145</b>
Abstract.....	147
1. Introduction.....	148
2. Results.....	150
3. Discussion.....	158
4. Conclusions.....	162
5. Experimental.....	163
6. References.....	169
7. Supplementary.....	173
<b>Chapter 4: Nanotoxicology at the particle/micelle frontier: influence of core-polymerization on the intracellular distribution, cytotoxicity and genotoxicity of polydiacetylene micelles</b>	<b>177</b>
Abstract.....	179
1. Introduction.....	181
2. Results.....	184
3. Discussion.....	194
4. Conclusions.....	198
5. Experimental.....	199
6. References.....	207
7. Supplementary.....	213
<b>General discussion.....</b>	<b>227</b>

# Abbreviations

BSA	Bovine Serum Albumine
PEG	Polyethylene Glycol
PVP	Poly(vinylpyrrolidone)
CS	Chitosan
TPP	Triphosphate
PEC	Polyelectrolytes Complexes
DD	Deacetylation Degree
PBS	Phosphate-Buffered Saline
ATP	Adenosine Triphosphate
CMC	Critical Micelle Concentration
PEO	Poly(ethylene oxide)
MePEG	Methoxy poly(ethylene glycol)
PDLLA	Poly(D,L-lactide)
PLGA	Poly(glycolic-co-lactic acid)
PCL	Poly( $\epsilon$ -caprolactone)
PEO–P(Asp)	Polyethylene Oxide-Poly(aspartic acid)
PEO–PCL	Polyethylene Oxide-Poly( $\epsilon$ -caprolactone)
pDA	Polydiacetylene
CARPA	Complement Activation-Related Pseudo-Allergy
RES	Reticuloendothelial System
ROS	Reactive Oxygen Species
GC	Chitosan Glycol
FRET	Fluorescence Resonance Energy Transfer
PLA	Poly(lactic Acid)
HA	Hyaluronic Acid
PMMA	Poly-hydroxymethyl methacrylate
HPMA	Hydroxypropyl Methacrylate
PPE	Polyphosphoester
NADPH	Nicotinamide Adenine Dinucleotide Phosphate
PAN	1.2-pyridylazo-2-naphthol
FBS	Fetal Bovine Serum

CS-Fe	Chitosan-iron
ICP-OES	Inductively Coupled Plasma-Optical Emission Spectrometry
FT-IR	Fourier-transform Infrared Spectroscopy
CS-Zn	Chitosan-Zinc
CS-M	Chitosan-Metal
DLS	Dynamic Light Scattering
ITC	Isothermal Titration Calometry
pDI	Polydispersity Index
AZT-TP	Azidothymidine Triphosphate
C-TP	Cytidine Triphosphate
dFdC-TP	2',2'-Difluorodeoxycytidine-Triphosphate
EMEM	Eagle's Minimum Essential Medium
DMEM	Dulbecco's Modified Eagle's Medium
Gem-TP	Gemcitabine Triphosphate
ELS	Electrophoretic Light Scattering
X-TP	Nucleotide Analogue
ADP	Adenosine Diphosphate
AMP	Adenosine Monophosphate
H <sub>2</sub> DCFDA	2',7'-Dichlorodihydrofluorescein Diacetate
LPS	Lipopolysaccharide
TMRE	Tetramethylrhodamine-ethyl Ester
CCCP	Carbonyl Cyanide 3-chlorophenylhydrazone
TEM	Transmission Electron Microscopy
SSC	Side Scattering
FSC-H	Height Forward Scattering
LDH	Lactate dehydrogenase
PI	Propidium Iodide
OTM	Olive Tail Moment
CBA	Cytometric Beads Array
EPR	Enhanced Permeability and Retention

# General Introduction

Nanotechnology has led to significant improvements in cancer therapy, diagnostic imaging of diseases, tissue engineering and most importantly in the development of drug delivery systems. However, the design of engineered nanoparticles is particularly challenging because the physicochemical properties of nanoparticles can be modified once the formulation is administered into the organism. In particular, the complex physiological fluid environment that nanoparticles encounter is populated with a wide range of components, notably proteins and salts, that can affect their colloidal stability and thus their fate at the tissue and cell level. Controlling and designing the drug/particle association is important, but anticipating the *in vivo* particles disassembly or aggregation is as much fundamental in order to predict the efficacy and toxicity of the nanoformulation. The first challenge for nanoformulations intended for intravenous injection is related to the colloidal stability of nanoparticles in the blood. After this, the fate of the drug nanocarrier at the cellular level is a key issue for the pharmacological activity and the eventual toxic effects.

To gain a better understanding of how the control of the colloidal stability of drug nanocarriers can influence their cellular effects in terms of efficacy and toxicity, the objectives of this thesis were (1) the improvement of the colloidal stability of drug nanocarriers in physiological conditions and (2) the *in vitro* investigation of the fate and toxicology of the stabilized nanocarriers in their interaction with cells. To do so, two types of drug nanocarriers particularly concerned by colloidal stability issues have been addressed in this study: chitosan-based nanogels and polydiacetylene micelles.

This manuscript is composed of two main parts. The first part is a literature review of:

- The colloidal stability of nanoparticles and different strategies adopted in order to control it in physiological conditions;
- The biodistribution of nanoparticles after injection and their cellular fate, with a special focus on the in vivo and in vitro toxicity.

For both themes, the specificities of chitosan-based nanogels and polymeric micelles have been developed.

The second part is an experimental section describing the work performed during this thesis and is composed by four chapters as follows:

- The first chapter reports the incorporation of different metal ions in the structure of chitosan-based nanogels with the aim of improving their colloidal stability, and the investigation of the mechanisms underlying their disassembly and aggregation in physiological conditions;
- The second chapter describes the application of chitosan-iron nanogels to the delivery of different nucleotide analogues, with additional studies on the formation of nanogels and their colloidal stability;
- The third chapter reports the evaluation of the intracellular fate of chitosan-iron nanogels and their potential toxic effects arising from the presence of iron;
- The fourth chapter is devoted to polydiacetylene micelles and investigates their in vitro intracellular distribution and the cytotoxicity either in their polymerized and non-polymerized form, with the aim of evaluating the influence of their stabilization by core-polymerization on their toxicological profile.

The manuscript is concluded by a general discussion of the obtained results and the future perspectives of this work.

This PhD thesis was performed at the Institut Galien Paris-Sud (Cnrs – Université Paris-Saclay) in the group of Prof. Elias Fattal, under the supervision of Dr Hervé Hillaireau. The work on chitosan-based nanogels was funded by an ANR fellowship (Kitostic). The work on polydiacetylene micelles was done in collaboration with the group of Eric Doris (Service de Chimie Bioorganique et de Marquage, CEA – Université Paris-Saclay) in the context of a LabEx Lermite project.



## Introduction générale

*Les nanotechnologies ont permis d'améliorer considérablement la thérapie du cancer, l'imagerie diagnostique des maladies, l'ingénierie tissulaire et, surtout, la vectorisation des médicaments. Cependant, la conception de nanoparticules artificielles est particulièrement difficile car leurs propriétés physicochimiques peuvent être modifiées une fois que la formulation est administrée dans l'organisme. En particulier, l'environnement complexe des fluides physiologiques rencontré par les nanoparticules est peuplé d'une grande variété de composants, notamment des protéines et des sels, qui peuvent affecter leur stabilité colloïdale et, par conséquent, leur devenir au niveau des tissus et des cellules. Le contrôle et la conception de l'association médicament/particule sont importants, mais il est tout aussi fondamental d'anticiper l'agrégation ou la désagrégation des particules in vivo afin de prévoir l'efficacité et la toxicité de la formulation. Le premier défi pour les nanoformulations destinées à l'injection intraveineuse est lié à la stabilité colloïdale des nanoparticules dans le sang. Par la suite, le devenir du nanovecteur au niveau cellulaire conditionne l'activité pharmacologique et les éventuels effets toxiques.*

*Pour mieux comprendre comment le contrôle de la stabilité colloïdale des nanovecteurs peut influencer leurs effets cellulaires en termes d'efficacité et de toxicité, les objectifs de cette thèse étaient (1) l'amélioration de la stabilité colloïdale de nanovecteurs en conditions physiologiques et (2) l'étude in vitro du devenir et de la toxicologie des nanovecteurs ainsi stabilisés dans leur interaction avec les cellules. Pour ce faire, deux types de nanovecteurs particulièrement concernés par des problématiques de stabilité colloïdale ont été utilisés dans cette étude : les nanogels à base de chitosane et les micelles de polydiacétylène.*

*Ce manuscrit se compose de deux parties principales. La première partie bibliographique porte sur:*

- La stabilité colloïdale des nanoparticules et les différentes stratégies adoptées pour la contrôler dans des conditions physiologiques;*
- La biodistribution des nanoparticules après l'injection et leur devenir cellulaire, avec un accent particulier sur la toxicité in vivo et in vitro.*

*Pour les deux thèmes, les spécificités des nanogels à base de chitosane et des micelles polymérisées ont été approfondies.*

*La deuxième partie concerne les travaux expérimentaux réalisées au cours de cette thèse et se compose de quatre chapitres:*

- Le premier chapitre décrit l'incorporation de différents ions métalliques dans la structure des nanogels à base de chitosane dans le but d'améliorer leur stabilité colloïdale, et l'étude des mécanismes sous-jacents à leur agrégation et désagrégation dans des conditions physiologiques;*
- Le deuxième chapitre décrit l'application de nanogels de chitosane-fer à l'administration de différents analogues nucléotidiques, avec des études supplémentaires sur la formation de nanogels et leur stabilité colloïdale;*
- Le troisième chapitre porte sur l'évaluation du devenir intracellulaire des nanogels de chitosane-fer et de leurs potentiels effets toxiques découlant de la présence de fer;*
- Le quatrième chapitre est consacré aux micelles de polydiacétylène et étudie la distribution intracellulaire et la toxicité in vitro des micelles sous leur forme polymérisée ou non polymérisée, dans le but d'évaluer l'influence de la stabilisation par polymérisation sur leur profil toxicologique.*

*Le manuscrit est conclu par une discussion générale des résultats obtenus et des perspectives futures de ce travail.*

*Cette thèse de doctorat a été réalisée à l'Institut Galien Paris-Sud (Cnrs – Université Paris-Saclay) dans le groupe du Prof. Elias Fattal, sous la direction du Dr Hervé Hillaireau. Les travaux sur les nanogels à base de chitosane ont été financés par une bourse ANR (Kitostic). Les travaux sur les micelles de polydiacétylène ont été réalisés en collaboration avec le groupe d'Eric Doris (Service de Chimie Bioorganique et de Marquage, CEA – Université Paris-Saclay) dans le cadre d'un projet Labex Lermite.*



# Literature review

## **1. Introduction**

The application of nanotechnology to biomedical sciences and healthcare is called ‘nanomedicine’ and requires the intersection of many disciplines including biology, chemistry, physics, chemical and mechanical engineering, material science and clinical medicine. Engineered nanoparticles offer the possibility to administer poorly soluble drugs, protect fragile therapeutic molecules, and modify their blood circulation and tissue distribution. The nanoparticle entrapment of drugs can therefore enhance their delivery to, or uptake by, target organs and cells and conversely reduce the toxicity of the free drug to non-target ones, resulting in an increased therapeutic index.

The composition and the structure of engineered nanoparticles for drug delivery may vary, depending on the source material and the formulation process. At present nanomedicines on the market consist of nanocrystals, liposomes and lipid nanoparticles, polymeric nanoparticles, protein-based nanoparticles and metal-based nanoparticles<sup>1</sup>, for the delivery of small molecules and macromolecules. **Table 1** summarize different types of nanocarriers and their main advantages in the biomedical field. These nanotechnologies have been applied in oncology, infectiology, pain medicine, cardiology, ophthalmology, endocrinology, orthopedics, neurology, dentistry.

Type	Description	Advantages	Applications
Nanocrystals	Crystalline particles produced by different methods such as pearl milling, high pressure homogenization (HPH), precipitation process	<ul style="list-style-type: none"> <li>Improving the dissolution rate of drugs</li> <li>Improving the saturation solubility</li> <li>Safe composition</li> <li>Suitable for intravenous injection</li> <li>High drug bioavailability</li> </ul>	<ul style="list-style-type: none"> <li>Cancer treatment</li> <li>Controlling the level of triglyceride and cholesterol</li> <li>Hyperthermic chemotherapy</li> </ul>
Polymeric NPs	Can be prepared as nanospheres or nanocapsules by different methods such as nanoprecipitation, double emulsification, polymer coating and emulsification diffusion	<ul style="list-style-type: none"> <li>Can be administered by infusion, different types of injection or oral ingestion</li> <li>Tunable characteristics</li> <li>Able to carry multifunctional agents</li> <li>Improved thermodynamic stability of cargo</li> <li>Deep penetration to cells and tissues</li> </ul>	<ul style="list-style-type: none"> <li>Drug delivery</li> <li>Gene delivery</li> <li>Tissue engineering</li> </ul>
Liposomes	Synthetic vesicles formed from lipid bilayers, which are divided into two groups: unilamellar and multilamellar able to dissolve both water-soluble (interior) and lipid soluble drugs (bilayer) at the same time	<ul style="list-style-type: none"> <li>Passive targeting of drugs</li> <li>Highly efficient cargo delivery</li> <li>Reducing the cargo toxicity</li> </ul>	Delivery of various biomolecules such as enzymes, hormones, anti-sense oligonucleotides, ribozyme, proteins/peptides, DNA and anticancer drug
Nanogels	Hydrogel materials composed of polymers in the nanoscale size range formed by crosslinked swellable polymer networks with a high capacity to hold water, without actually dissolving into the aqueous medium	<ul style="list-style-type: none"> <li>Highly biocompatible</li> <li>High loading</li> <li>Ability to incorporate entities with very different physical properties within the same carrier</li> <li>Stimuli-responsive behavior</li> </ul>	<ul style="list-style-type: none"> <li>Delivery of therapeutic oligonucleotides, proteins and small molecules</li> <li>Diagnostic and imaging</li> </ul>
Magnetic NPs	These types of nanosystems can respond to external magnetic fields in a nanoscale size	<ul style="list-style-type: none"> <li>Accumulation at desired sites via delivery guidance using a magnetic field</li> <li>A promising choice for MRI application</li> </ul>	<ul style="list-style-type: none"> <li>Surface functionalization</li> <li>Use as a contrast agent</li> <li>Gene delivery</li> </ul>
Micelles	Spherical amphiphilic copolymer NPs formed by supramolecular assembly, having a core-shell structure with hydrophobic interior separated from the aqueous exterior	<ul style="list-style-type: none"> <li>High loading capacity</li> <li>Good stability in blood</li> <li>Prolonged circulation time</li> <li>Low number of side effects</li> <li>Protects internal drugs from degradation</li> </ul>	Carrying various water insoluble drugs including: paclitaxel, doxorubicin, C6-ceramide
Dendrimers	Synthetic tree-shaped macromolecules having a 3D monodisperse structure with branches extended from a central molecule; predictable size according to generation number	<ul style="list-style-type: none"> <li>Defined MW</li> <li>Uniform in shape</li> <li>Host-guest entrapment properties</li> <li>Extremely low polydispersity</li> </ul>	Carrying various drugs including: piroxicam, paclitaxel, ketoprofen, methotrexate
Mesoporous silica NPs	Mesoporous form of silica particles in nanoscale sizes with a large surface area and a solid structure	<ul style="list-style-type: none"> <li>High loading capacity</li> <li>Good protection ability by keeping cargo molecules inside pores</li> <li>Controlled drug-release ability</li> </ul>	<ul style="list-style-type: none"> <li>Drug and gene delivery</li> <li>Bio-sensing</li> <li>Target specific deliver</li> <li>Diagnostic agent</li> <li>Antidote agent</li> </ul>
Carbon nanotubes	Needle-like carriers, which can easily diffuse into cell membranes by perforation. CNTs are categorized as SWCNTs which have a high near infrared optical absorbance and MWCNTs having unique physical properties such as young modulus and electrical conductivity	<ul style="list-style-type: none"> <li>Very high elastic modulus and mechanical strength</li> <li>High electrical and thermal conductivity</li> <li>Prolonged circulating time</li> <li>Cell membrane permeability</li> <li>High aspect ratio allowing high drug loading</li> </ul>	<ul style="list-style-type: none"> <li>Use in scaffolds for supporting bone cell growth</li> <li>Chemo-photothermal therapy</li> <li>Vaccine delivery</li> <li>Cancer treatment</li> <li>Brain glioma therapy</li> <li>Spinal cord injury repair</li> </ul>
Au NPs	First synthesized over 150 years ago; wide use in drug delivery applications	<ul style="list-style-type: none"> <li>Low cytotoxicity</li> <li>Controlled size and surface</li> <li>Easy synthesis</li> <li>High cell permeability</li> <li>Ability to bind many molecules on their surface</li> <li>High drug loading capacity</li> </ul>	<ul style="list-style-type: none"> <li>Drug delivery</li> <li>Diagnosis</li> <li>Treatment of various diseases including: cancer, Alzheimer, diabetes, arthritis, heart failure</li> </ul>
QD	Semiconductor crystals with a nearly spherical structure; metalloid crystalline semiconductor that controls fluorescence emission	<ul style="list-style-type: none"> <li>Small size</li> <li>Good intracellular uptake and drug release</li> <li>Easy surface modification</li> </ul>	<ul style="list-style-type: none"> <li>Biological optical detection</li> <li>Cellular and intracellular targeting</li> </ul>

**Table 1.** Different types of nanocarriers and their main advantages and applications in biomedical field (based on ref.<sup>2</sup>).

The most common routes of administration of nanoparticles in drug delivery include intravenous injection, oral administration, inhalation, transdermal administration and implantation. The intravenous injection is one of the most efficient and common routes of administration of drugs and it provides the most rapid effects. The major potential clinical benefits of using drug delivery nanosystems include a reduction in toxicity by replacing solubilizing agents, the possibility of altering the pharmacokinetics of the drug leading to higher dosing and less frequent administration, and possibly passive or even active targeting for drug delivery. For these reasons, nowadays many organic and inorganic engineered nanoparticles are used in the clinic for intravenous administration, for both therapeutic and imaging purposes.<sup>3,4,5</sup> Approved nanomedicines designed for parenteral administration are varied with respect to their chemical composition, size, geometry, surface properties, and intended clinical uses. These formulations share certain physicochemical properties, such as the shape (they are mostly spherical) and the size (they have particle diameter below one micron).<sup>6</sup> However, knowledge about their behavior or safety after injection is still lacking. Svenson et al. put in evidence the fact that the formation of nanocarriers is usually confirmed *in vitro* but available informations *in vivo* are not sufficient.<sup>7</sup> Moreover, many formulations that have been translated into the clinic or entered the market (Taxol, Genexol-PM, and Abraxane) and are benefitting patients, don't actually maintain their structure in systemic circulation.<sup>8</sup> Functionalized micellar systems for cancer targeted drug delivery. *Pharm Res* 2007, 24:1029–1046. The authors suggest therefore that the formulation composition, before and after injection, can be more important than nanoparticle presence for clinical success. However, it must be kept in mind that most nanoparticles form and dissociate in response to the local environment, and given the small amount of studies available on this subject, it is still difficult to claim that improvements we see from some nanomedicines are structure-related or consequences of

improved formulations. Many efforts are done in order to control the drug/particle association but anticipating the *in vivo* solubilization/release is just as important in order to predict efficacy and toxicity of the nanoformulation. In order to do that, the *in vivo* colloidal stability of nanoparticles must be studied. In fact, a fundamental understanding of colloidal stability is important to rationally design nanoparticles whereby it can be understood how they may behave at molecular, cellular, and systemic levels within biological systems.

There is evidence that, depending on their colloidal properties, nanoparticles can interact with cells and be taken up. However, the subsequent release and/or intracellular degradation of the materials, transfer to other cells, and/or translocation across tissue barriers are still poorly understood. Furthermore, biodistribution and longterm fate of nanomaterials, although crucial for drug efficacy as well as safety, have only rarely been investigated. Bourquin et al. recently reviewed studies on the long-term biological fate of clinically interesting nanomaterials and put in evidence the need to develop and optimize (novel) analytical methods to detect and quantify the distribution of nanomaterials in cells, tissues, and/ or organs.<sup>9</sup> Nanoparticles in the biological environment behave differently owing to the complex environment; however, the *in vitro* tests currently used are not adept in reproducing this complexity.

The aim of this introduction chapter is to address the biological fate of clinically interesting nanocarriers for drug delivery administered by intravenous injection, and particularly how the colloidal stability of the nano-systems can affect their interaction with biological systems at extracellular and intracellular level. Two different nanocarrier types, which exhibit typical colloidal stability challenges, will be discussed more in depth: chitosan-based nanoparticles and polymeric micelles.

## **2. Colloidal stability of nanoparticles**

### **2.1 Generalities**

Nanoparticle dispersions are usually considered not thermodynamically stable. In fact, such particles tend to be unstable because of the solid-solution interfacial tension.<sup>10</sup> In order to reduce the surface area and minimize the dispersion free enthalpy, an increase in the average particle size tends to occur. This phenomenon, called surface energy minimization, is mainly due to the tendency of smaller particles in a suspension to dissolve and re-grow on bigger particles (Ostwald ripening). The Ostwald ripening mostly originates from the re-crystallization of smallest particles on the larger ones leading to a decreased total surface area of the system and consequent reduced free enthalpy of formation of the system. This phenomenon can be minimized if the particle distribution is narrow. It is also possible to obtain dispersions consisting of very fine particles due to a very slow ripening, i.e. by growth limitation due to surface-active compounds (surfactants).

The dispersion state of nanoparticles results from an energetic barrier, which is opposed to the approach of particles due to Brownian motion. Such stability is called kinetic stability and is due to the energy barrier resulting from the balance of attractive (van der Waals) and repulsive forces (electrostatic) between the particles' surfaces. **(Fig.1)**

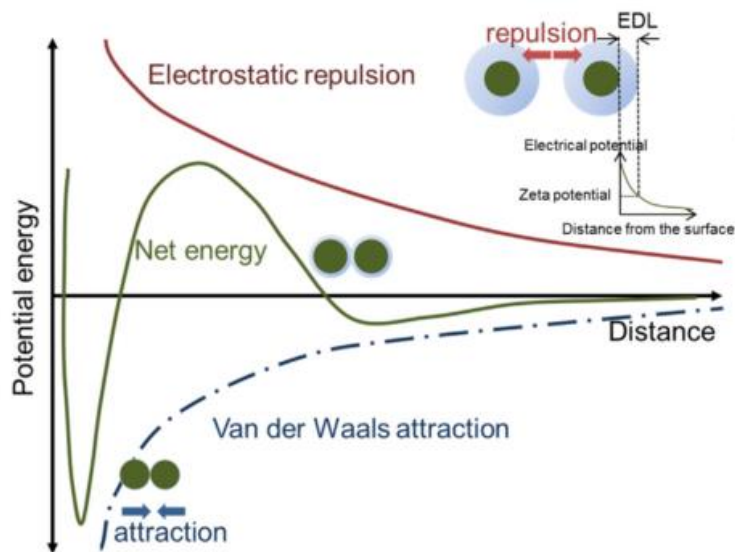


**Fig.1** Schematic showing potential energy governed by electrostatic repulsion and van der Waals attraction between nanoparticles, which can lead to particle aggregation.<sup>11</sup>

The zeta potential of the nanoparticles is the common indicator of their kinetic stability based on the electrostatic repulsion between similarly charged particles. This means that a higher magnitude potential translates into increased electrostatic repulsion and therefore, increased stability. However, it has to be taken into account that the degree of charge on the nanoparticles surface is related to the pH of the solution, as pH influences protonation and deprotonation of the nanoparticles. The zeta potential, besides being an important indicator of the colloidal stability of the formulation, can also have an impact on the interactions of nanoparticles with the biological systems. Many studies have been performed *in vitro* in order to predict the influence of the zeta potential on the biological behavior of nanocarriers. Upon incubation with BSA (Bovine Serum Albumine), particles with positively charged were found to adsorb more BSA compared to negatively ones.<sup>12</sup> It is also well known that the zeta potential can have a strong impact on the cellular uptake of nanoparticles.<sup>13</sup>

Usually, the stability of nanoparticles intended to intravenous administration is measured *in vitro*. However, surprisingly, a generally accepted protocol is still missing. Despite that, it is commonly admitted that nanoparticles should have particle size distributions below 20% (polydispersity indices of  $< 0.2$ ) as determined in a physiological buffer system and their aqueous stability should not be affected when measured at 37 °C. For formulations intended for intravenous administration, the colloidal stability of nanoparticles should always be determined at pH 7.4.

## **2.2 Colloidal stability of nanoparticles in physiological conditions**

The colloidal destabilization of nanoparticles occurs when van der Waals attraction dominates over the electrostatic repulsion, which results in particle aggregation and precipitation. The nanoparticles destabilization largely depends on the magnitude of surface charge and the thickness of electrical double layer, both of which depend from properties of the solution, such as pH, ionic strength and electrolytes.<sup>11</sup> Therefore, many factors can impact the colloidal stability of nanoparticles in physiological conditions. In fact, after intravenous administration, nanoparticles inevitably encounter a complex physiological fluid environment populated with a wide range of biomacromolecules, e.g., proteins, vitamins, lipids, and salts/ions.<sup>14</sup> Upon contact with physiological fluids, the formation of a surface-bound protein layer, particle dissolution, or aggregation might occur, which are expected to have a crucial impact on cellular, tissue, and organ interaction.<sup>15</sup> For example, negatively charged citrate-coated gold nanoparticles are stable in  $<10$  nM NaCl but aggregate with increasing salt concentration due to charge screening.<sup>16</sup> The aggregated nanoparticles exhibit severe cytotoxicity, e.g., their intravenous aggregation blocks blood capillary and disturbs blood flow.<sup>17,18</sup> On the other hand, when nanoparticles are injected into the bloodstream they are subjected to an instantaneous important dilution, in so-called sink

conditions. Under such a situation, some types of particles may dissolve completely, immediately upon injection, and release the drug in the blood.<sup>19</sup>

Another fundamental parameter affecting the colloidal stability of nanoparticles in physiological conditions is represented by the formation of a protein corona. Indeed, once in the body, the surface of nanoparticles is rapidly covered by proteins. The affinity of the proteins for the surface of nanoparticles is governed by a variety of complementary physical forces: van der Waals interactions, hydrogen bonding, as well as electrostatic and hydrophobic interactions.<sup>20</sup> When nanoparticles come into contact with biological material, the physicochemical properties of nanoparticles may change.<sup>21</sup> Here also, a key physicochemical property is surface electric charge. The amount of surface charge (i.e., as evaluated by the absolute zeta potential) is reduced in the case of protein adsorption to the nanoparticle surface, which in turn influences the interaction with cells. An increase in size due to the presence of the protein corona is another common effect. By altering the structure, dynamics and functions of nanoparticles, the protein corona can lead to changes in the intracellular recognition of nanoparticles. In this manner, the protein corona can influence intracellular uptake, inflammation, accumulation, degradation and clearance of nanoparticles from biological stream<sup>22, 14, 23</sup>. Moreover, the protein corona can seriously affect the drug release in the blood. In fact, the formation of the protein corona impacts the colloidal stability of nanoparticles. In many cases, the presence of proteins can increase the resistance of nanoparticles against agglomeration even in the presence of physiological electrolyte concentrations by steric or electrosteric effects.<sup>24, 25</sup> In other cases, the nanoparticles/biomolecules interaction can lead to agglomeration (i.e. weakly bonded particles) and aggregation (i.e. strongly bonded or fused particles).<sup>26, 27</sup>

The ideal drug nanocarrier should be able to stay in the blood circulation long enough, bypass biological membranes, carry and release the drug to the target site and disintegrate into bioinert and non-toxic components that can be easily eliminated. In this regard, understanding the dynamic behavior of all drug delivery nanosystems is crucial to ensure the drug release and the desired biological effect. If the disassembly of nanoparticles is uncontrolled and immediate, it can lead to a drug burst release before reaching the target site, affecting the pharmacological action and eventually the adverse effects.

The drug release can occur by nanoparticles degradation, swelling of the carrier matrix, drug diffusion through the matrix, loss of drug–polymer linkage<sup>28</sup> (**Fig.2**). The drug liberation can take place at the extracellular or intracellular level. In particular, the intracellular fate of the nanocarrier is a key issue for the drug to be efficient. In fact, the release of the drug into the enzymatic environment of the lysosomes or directly in the cell cytoplasm have important impact on the pharmacological activity. In order to control the nanoparticles disassembling and the drug biodistribution, many nanoscale stimuli-responsive systems have been designed. These systems are able to control the drug release in response to specific stimuli, either exogenous or endogenous.<sup>29</sup> The central operating principle of these systems lies in the fact that a specific cellular/extracellular stimulus of chemical, biochemical, or physical origin can modify the structural composition/conformation of the nanocarriers, thereby promoting release of the active species to specific biological environment. Changes are mainly decomposition, isomerization, polymerization, activation of supramolecular aggregation among many others.<sup>30</sup> In the case in which the active molecule is physically encapsulated, the release can be triggered by structural change within the nanoparticle scaffold (i.e., carrier degradation, cleavage of shell, charging of functional groups), while in case of chemical encapsulation the mechanism of release involves the

splitting of the linker between the carrier and the bioactive agent. Exogenous stimuli-responsive drug delivery systems take advantage of externally applied stimuli such as temperature changes, magnetic fields, ultrasounds, light and electric fields.<sup>31,32,33</sup> The behavior of endogenous stimuli-responsive drug delivery systems depends on variations in pH, redox potential, or the concentrations of enzymes or specific analytes.<sup>34,35,36,37,38,39,40</sup>

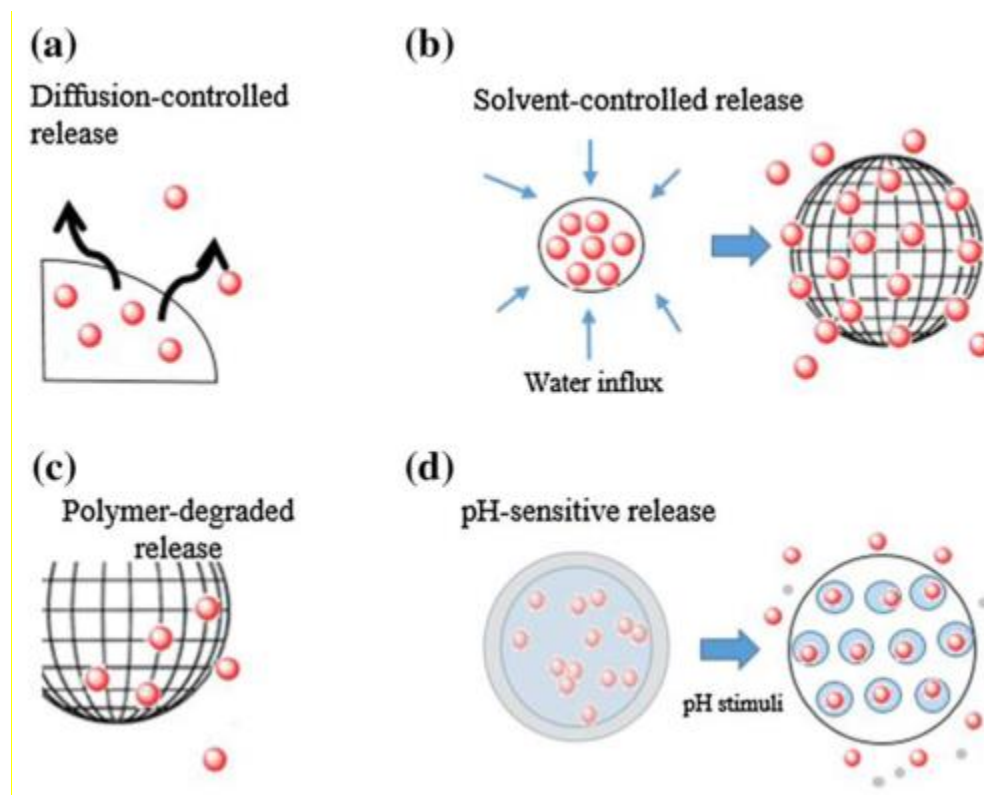


**Fig.2** Various mechanisms of drug release from nanocarriers: a) diffusion-controlled release; b) solvent-controlled release; c) polymer-degraded release; d) pH-sensitive release.<sup>28</sup>

### 2.3 Colloidal stabilization of nanoparticles

The colloidal stability of the nanoparticles after injection depends on a number of properties such as: drug particle dissolution rate, morphology of particles, type and density of coating, size of the particles. In order to improve the stability of nanoparticles in biological fluids with the aim of avoiding the early carrier destabilization and the burst drug release, many strategies have been adopted. Nanoparticles are stabilized by modifying either their surface or their core properties.

The surface modifications include steric stabilization and electrostatic stabilization.<sup>41</sup> (**Fig.3**)

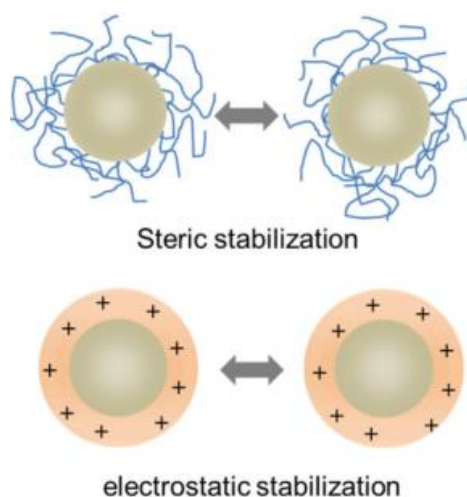


**Fig.3** Schematic showing the steric and electrostatic contribution to the colloidal stability aggregation.<sup>11</sup>

The stabilization through electrostatic repulsion relies on the adsorption of polyelectrolytes to oppositely charged nanoparticles surface and the formation of an adsorbed polyelectrolyte layer.<sup>42</sup> At low ionic strengths, the diffuse double layer extends far from the particle surface, facilitating particle–particle repulsions. However, at high ionic strengths, typical of biological media, this double layer can be compressed and neutralized triggering the destabilization of nanoparticles

through aggregation driven by van der Waals forces. For instance, Mahl et al. reported gold NPs electrostatically stabilized with a tris(sodium-m-sulfonatophenyl)phosphine (TPPTS) coating.<sup>43</sup> The hydrodynamic diameter of TPPTS-stabilized gold NPs in H<sub>2</sub>O was 25 nm, but dispersion in RPMI-1640 cell culture medium without serum caused their aggregation into particles of 750 nm. Similar results have been reported for other nanomaterials,<sup>44,45,46</sup> demonstrating that electrostatic stabilization is not sufficient to avoid aggregation in biological media.

The steric stabilization consists in the generation of a physical barrier at the particle surface. Coating materials are mostly adsorbed on the surface of the nanoparticles. The stability of coated particles also depends on the strength of the bond between particle and coating. Hydrophilic polymers attached to the particle surface are often used to increase nanoparticles physical stability and dispersibility. The hydrophilic nature of these polymers also induces an extra stabilization through the short-range repulsive hydration forces. Thus, steric stabilization results more adequate for biological systems. Several polymers can be used to prevent agglomeration and keep the particles in colloidal suspension, including various synthetic polymers such as polyethylene glycol (PEG) and poly(vinylpyrrolidone) (PVP), or natural polymers such as dextran, chitosan, pullulan etc, and surfactants such as sodium oleate and dodecylamine.<sup>47</sup> It should be stressed that the zeta potential is greatly affected by the nature of coating.

Poly(ethylene glycol) (PEG) is a biocompatible polymer, usually covalently attached to the nanoparticle surface providing an hydrophilic steric barrier around particles. This protective layer prevents agglomeration during the production and/or storage, and subsequently, improves the physical stability and dispersibility of the particles. Coating with PEG increases also the stability and plasma half-life even by decreasing the adhesion of opsonins and thus the phagocytic uptake and clearance from bloodstream.<sup>1</sup> Another strategy proposed to inhibit the adsorption of plasma

proteins is based on the preformation of a protein corona on the nanoparticles surface. Peng et al. successfully reduced the opsonization by performing an albumin corona on nanoparticles.<sup>48</sup>

Regarding the improvement of the colloidal stability by modifying the core of nanoparticles, the common strategy consists on the introduction of cross-links that reinforce the internal structure and usually prevent the dissolution and disassembling of nanoparticles. The cross-linkage can be performed by the introduction of covalent bonds (such as disulfide bonds)<sup>49,50,51,52</sup> or by the addition of metals.<sup>53</sup> For instance, lipoprotein-based nanoparticles formed by a discoidal phospholipid lipid bilayer and confined by an apolipoprotein belt were stabilized through the incorporation and subsequent UV-mediated intermolecular crosslinking of photoactive DiynePC (1,2-bis(10,12-tricosadiynoyl)-sn-glycero-3-phosphocholine) phospholipids in the lipid bilayer.<sup>54</sup> Such cross-linked lipoprotein nanoparticles displayed enhanced stability in serum and in the blood after injection. Many examples of structural stabilization are related to nanogels and micellar systems for drug delivery and will be discussed in sections 2.4.2 and 2.5.2.

## **2.4 The case of chitosan-based nanogels**

### **2.4.1 Introduction to chitosan-based nanogels**

Chitosan (CS) is a natural, biocompatible and biodegradable polycation used in many areas such as food, cosmetics, textiles and biomedicine (tissue engineering and drug delivery). It is obtained by partial (>50%) deacetylation of chitin, a polysaccharide of natural origin, mainly extracted from shellfish shells (shrimps, crabs) and consisting of monomer units of N-acetyl-D-glucosamine bound together by  $\beta$ -(1-4) glycosidic bonds. As shown in **Fig.4** chitosan is a positively charged (pKa around 6.5) linear copolymer constituted by N-acetyl-D-glucosamine and D-glucosamine

units randomly distributed. Chitosan is insoluble in alkaline solutions and organic solvents but soluble in an acidic aqueous medium when its deacetylation degree (DA) is less than 50%.<sup>55</sup> It is commonly solubilized in aqueous solutions of acetic acid (0,1 M or 1% w/v) or strong acids such as hydrochloric acid.<sup>56,57</sup>

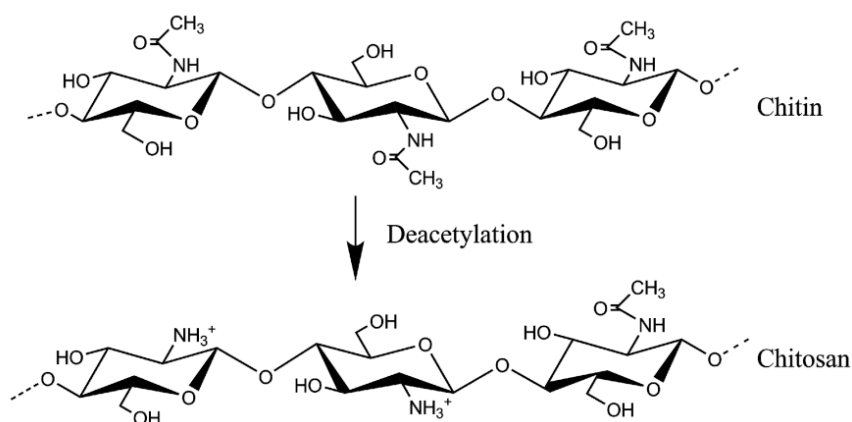


**Fig.4** Structure of chitin and chitosan.<sup>58</sup>

Chitosan has been widely used for the formulation of nanogels encapsulating active molecules for various administration routes over the past twenty years. Chitosan-based nanogels can be obtained in different ways:

1. by chemical cross-linking,
  2. by ionic cross-linking,
  3. by self-assembly,
  4. by polymerization.
1. The first chitosan-based nanogels were obtained by chemical cross-linking. The most commonly used cross-linking agent is glutaraldehyde, which binds covalently by its aldehyde groups the primary amine groups of chitosan and in some cases the primary amino groups of

the active substance (Schiff reaction), allowing the formation of nanogels under certain concentration and ratio conditions.<sup>59,60,61</sup> Because of the cytotoxicity of glutaraldehyde, recent studies proposed the use of other cross-linking agents such as genipine, a naturally occurring agent.<sup>62,63,64</sup> Thanks to its resistance to the enzymatic degradation and lower cytotoxicity, genipine is actually a relevant alternative.

2. Because of its polycationic nature, chitosan can interact with negative charges carried by an ionic cross-linking agent, an active substance or a polymer. Two approaches have been developed: the ionotropic gelation and the complexation with polyelectrolytes. Alonso et al. first formulated chitosan-based nanogels by ionotropic gelation.<sup>18</sup> This technique is based on the addition on a chitosan solution, drop by drop, of a solution containing the polyanion sodium triphosphate (TPP) that is used as ionic cross-linking agent.<sup>65,66,67</sup> Nanogels spontaneously form thanks to electrostatic interactions between negatively charged phosphate groups of the TPP and amino groups of chitosan positively charged. Alternatively, chitosan can also interact with polyanions to form polyelectrolytes complexes (PEC).<sup>68</sup> In the literature, different PECs were proposed based on chitosan and several polyanions such as alginates,<sup>69</sup> carrageenan,<sup>70</sup> glucomannan,<sup>71,72</sup> pectin,<sup>73</sup> hyaluronic acid,<sup>74,75</sup> chondroitin sulfate,<sup>69,76</sup> poly-glutamic acid,<sup>69</sup> heparin,<sup>77</sup> dextran sulfate.<sup>69,78,79</sup>
3. While native chitosan does not have the ability to self-assemble into nanogels in aqueous medium, grafting hydrophobic fragments such as fatty acids by acylation or certain polymers to chitosan allows the resulting conjugates to self-assemble into nano-objects in an aqueous medium thanks to hydrophobic interactions.<sup>69,80,81,82,83,84</sup>

4. Chitosan-based nanogels were also obtained by grafting a polymerizable group on chitosan leading to a polymer chain formation (“grafting-from”). The polymerization results in the formation of inter- and intra-molecular bonds between the carboxylic groups of the new polymer and amino groups of chitosan forming nanogels.<sup>85,86</sup>

#### **2.4.2 Colloidal stability of chitosan-based nanogels**

Chitosan-based nanogels present some issues in their colloidal stability in physiological media. Their colloidal instability can result either in the dissociation of their or in their aggregation (**Fig.5**).

Nanogels obtained by chemical cross-linking present a good physiological stability thanks to the intermolecular covalent bonds involved. However, the preparation of these nanogels requires aggressive experimental conditions that may impair the integrity of the drug encapsulated. In addition, problems of solvent and reagent removal can be encountered. Therefore, chitosan nanogels obtained by softer manufacturing methods such as the ionotropic gelation has gained more interest. The colloidal properties (size, surface charge, compactness) of nanogels prepared by ionotropic gelation are influenced by many parameters, such as CS and TPP concentrations, CS/TPP ratio, molar mass and deacetylation degree of chitosan (DD), pH of the chitosan solution, addition of another polymer like polyethylene glycol (PEG).<sup>65,66,67,87,88,89,90</sup> The colloidal properties of CS/TPP can be also impacted by the ionic strength. Increasing the ionic strength in the medium of formation of nanogels by the addition of salt (NaCl 150 mM) leads to the formation of more compact and stable nanogels.<sup>89,91,92</sup> Indeed, the addition of salt allows to screen the positive charges of chitosan and decreasing the electrostatic repulsions between positive groups promoting the formation of nanogels. Even after nanogels formation, the ionic strength plays a key role in their

colloidal stability. It has been shown that in NaCl (150 mM, pH = 4), a lower DD leads to the decrease of the aggregation but also to the increase of the dissociation of nanogels, reflecting weaker electrostatic interactions in case of more deacetylated chitosan. On the contrary, in PBS (pH= 7,4), nanogels based on highly deacetylated chitosan do not dissociate but precipitate. The dissociation or the aggregation of chitosan nanogels depends therefore on the strength of the interactions between chitosan and TPP, which is influenced by the ionic force and the pH.<sup>93,94,95</sup>

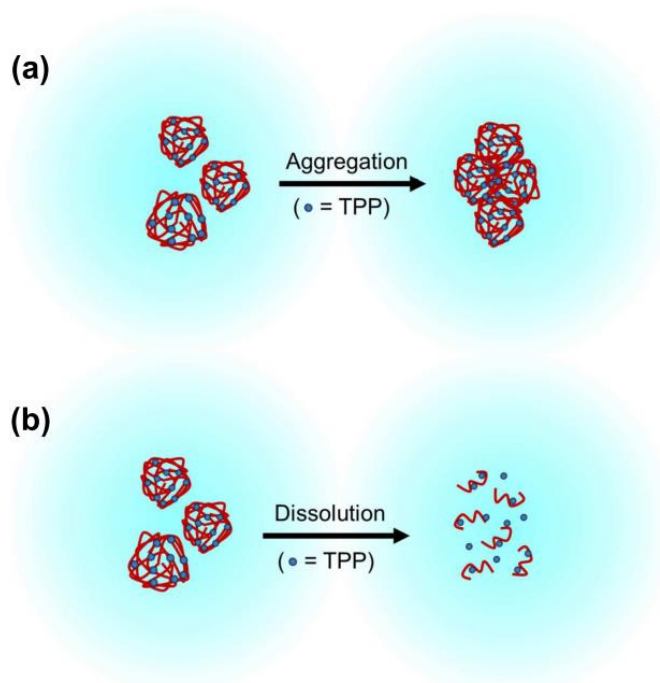


**Fig.5** Chitosan/TPP nanogels can be unstable due to their: (a) aggregation and subsequent precipitation, and (b) dissolution (reproduced from ref.<sup>94</sup>).

Because of this instability, the use of chitosan nanogels obtained by ionic cross-linkage has been limited to mucosal delivery purposes.<sup>96</sup> Several strategies have been proposed to improve the colloidal stability of these systems, which mainly consist in decorating the nanoparticle surface with additional components, like alginates<sup>97</sup> or hyaluronic acid<sup>98,99</sup>, or in using chemical crosslinking, often glutaraldehyde or genipin.<sup>100,62</sup> Giacalone et al. reported the possibility to

improve the stability of chitosan nanogels prepared with the ionic cross-linker TPP or the ATP drug by modifying chitosan before nanoparticle preparation, namely complexing it with ferric ions.<sup>4</sup> The rationale behind this approach is based on the ability of chitosan to bind to metal ions including iron, leading to strong coordination complexes<sup>101,102</sup> and on the capacity of iron to bind to phosphate groups,<sup>103,104</sup> creating an additional and strong 'bridge' in the nanoparticle formation. Similarly, it has been reported that the colloidal stability of PEC can be improved by the use of zinc.<sup>53</sup>

## **2.5 The case of polymeric micelles**

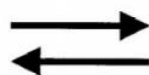
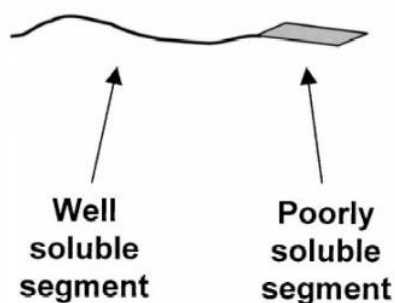
### **2.5.1 Introduction to polymeric micelles**

Micelles are amphiphilic colloids that form spontaneously under certain conditions (concentration, temperature). These systems are characterized by two distinct regions (core and shell) with opposite affinities towards a given solvent. The concentration of amphiphile above which micelles are formed is called critical micelle concentration (CMC). Micellar systems based on low-molecular-weight surfactants have the ability to increase the solubility of poorly water soluble substances that can be solubilized in the lipophilic core,<sup>105</sup> and for this reason have been widely used in pharmaceutical technology.<sup>106,107</sup> Contrary to high-molecular weight surfactants, low-molecular-weight oligo-ethyleneglycol based surfactants (for instance, Polysorbate 80) have been broadly used for drug solubilization<sup>107</sup> mainly because of their lower toxicity.<sup>108,109,110</sup> However, the definite drawback of such systems is that micelles composed of low molecular weight surfactants are not stable in aqueous media at concentrations lower than their CMC and are therefore subject to dissociation upon dilution. Hence, there is a need to find a new class of

surfactants molecules able to form more stable micelles with lower CMC values. Amphiphilic polymers can form polymeric micelles in an aqueous solution and are therefore good candidates.

(Fig.6)

### SINGLE POLYMER CHAIN



### MICELLE

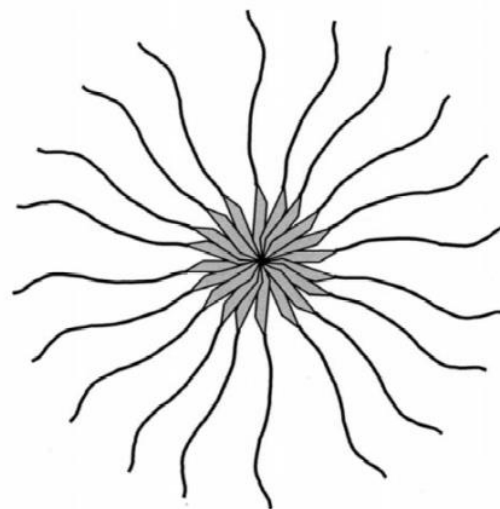


**Fig.6** The general scheme of micelle formation from amphiphilic molecules.<sup>109</sup>

Polymeric micelles represent a separate class of micelles and are formed from copolymers consisting of both hydrophilic and hydrophobic monomer units or different copolymers.<sup>109</sup> The copolymers can be made of two (di-block) or three (tri-block) alternate segments (hydrophobic and hydrophilic).<sup>111</sup> The hydrophilic segment that is most commonly used is PEG (1–15 kDa) since it is highly soluble in water and exhibits poor toxicity. The hydrophobic portion of the micelle can be selected from various types of polymers that are usually biodegradable, such as polyethers, polypeptides or polyesters. Nanoparticles based on amphiphilic block copolymers composed of hydrophilic blocks of poly(ethylene oxide) (PEO) or methoxy poly(ethylene glycol) (MePEG) and a variety of polyester hydrophobic blocks, including poly(D,L-lactide) (PDLLA), poly(glycolic-

co-lactic acid) (PLGA) and poly( $\epsilon$ -caprolactone) (PCL) have been extensively explored. Drug-loaded polymeric micelles, constituted by a hydrophobic core as a drug reservoir (for hydrophobic drugs, proteins or DNA) and an hydrophilic shell have demonstrated outstanding features as tumor-targeted nanocarriers with high translational potential, and several formulations are currently under clinical evaluation.<sup>112,113,114,115,116</sup> Genexol®-PM (Samyang Biopharmaceuticals, South Korea) is a formulation of paclitaxel based on polymeric micelles that was launched in Korean market for breast cancer and non-small cell lung cancer in February 2007 and is currently undergoing clinical trials in the US. Genexol®-PM micelles were formed through the self-assembly of low molecular weight diblock copolymer, polyethylene glycol PEG-block-poly(D,L-lactide) and PEG-block- PDLLA.<sup>117</sup>

The miscibility between polymers and drugs plays an important role in drug loading efficiency of polymeric micelles.<sup>113</sup> The fabrication methods to prepare polymeric micelle can be classified into four categories:<sup>118</sup>

1. direct dissolution
2. dialysis
3. film casting
4. oil- in-water emulsions

1. The direct dissolution method simply involves the addition of block or graft copolymers to water or other aqueous medium such as phosphate buffer saline, without using any organic solvents and surfactants.<sup>119,120,121,122</sup>

2. The film casting method involves the dissolution of copolymer (or copolymer and drug mixtures) in a volatile organic solvent. The solvent is first evaporated to create a thin film and then a buffer solution or water is added under agitation to dissolve the polymer film.<sup>123,124,125,126</sup>
  
3. The dialysis method can be used if the copolymer has a low solubility in water. The copolymer is first dissolved in a water miscible organic solvent, such as ethanol, acetone, dimethylsulfoxide, dimethylformamide, N,N-dimethylacetamide, tetrahydrofuran, acetonitrile. Dialysis is subsequently carried out against the aqueous media to remove the solvent.<sup>127,128,129,130</sup>
  
4. The oil-in-water (O/W) emulsion method involves the dissolution of drug and copolymer in a volatile, non-water-miscible organic solvent, such as dichloromethane, ethyl acetate or chloroform. The O/W emulsion is subsequently formed in an aqueous medium by vortexing and sonicating, which is followed by the evaporation of the organ solvent.<sup>131,132,133</sup>

### **2.5.2 Colloidal stability of polymeric micelles**

Micellar systems for drug delivery should be stable enough to give maximum retention time to drug in the target zone without having any side effect until its removal from the body.

Thermodynamic and kinetic parameters can be used to understand the stability of a micellar system. The thermodynamic stability is directly linked with the CMC. Micelles composed of low molecular weight surfactants have generally a low thermodynamic stability and are subjected to rapid dissociation upon strong dilution. This instability is due to the relatively high CMC of the amphiphiles. This means that upon dilution in the blood volume after intravenous administration, micelles may dissociate into unimers, releasing the drug in the blood.

Polymeric micelles based on copolymers generally have a lower CMC and therefore a better thermodynamic stability. The thermodynamic stability depends on the length of the hydrophobic block and, to a lesser degree, the hydrophilic block, the molecular weight of the unimers, the hydrophobic/hydrophilic ratio and the properties of the core like its viscosity.<sup>114</sup> By increasing the hydrophobic part of the polymer, the CMC decreases while the stability is enhanced. For example, the attachment of various fatty acids to the core of PEO–P(Asp) micelles was shown to decrease their CMC.<sup>113</sup> Those polymers which have low CMC can retain their stability even in very diluted conditions within the blood circulatory system.

In contrast to the thermodynamic stability, the kinetic stability is related to the dissociation of polymeric micelles into single chain at concentration below their CMC values. Fundamentally, kinetic stability depends upon the physical state of the core, the amount of solvent inside the core, the size of hydrophobic block and the hydrophobic/hydrophilic ratio.<sup>134</sup> The micellar kinetic stability can be increased by increasing the intra-micellar interactions or by forming covalent cross linking at the core level. For instance, the introduction of benzyl groups to PEO–PCL polymers has been reported to increase the rigidity of the micelle core due to intra- micellar interactions. Similarly the micelle stability can be enhanced by electrostatic ionic interactions through the formation of polyionic complexes<sup>135</sup> or by covalent cross linking that can be attained by different

methods.<sup>136</sup> There are several potential locations for cross-linking within polymer micelles, including at the core chain end, within the core domain, at the core–shell interface, throughout the shell layer, and on the surface. The incorporation of crosslinks has been shown to provide for enhanced structural stability, while retaining tunability of size and shape.<sup>137</sup> Chemistries employed for core cross-linking of micelles are the incorporation of polymerizable or photo/UV cross-linkable groups and the introduction of cross-linking reagents. The cross-linking can be established with disulfides and other redox-sensitive bonds, temperature, and pH-sensitive functional groups. For instance, Barkey et al. reported a cross-linking procedure that relies on the pH sensitivity of metal–oxygen coordination bonds.<sup>138</sup> Some groups recently proposed photo cross-linked polydiacetylene micelles (PDA-micelles) as robust carriers.<sup>139,140,141</sup> Cross-linked polydiacetylene micelles (PDA-micelles) have been shown to be well suitable for drug delivery and imaging applications.

Moreover, external stimuli such as pH-, thermo-, ultrasound-, enzyme- and light-sensitive block-copolymers can be used to control micelles dissociation and trigger drug release in response to the pathological environment-specific stimuli and/or externally applied signals.<sup>142,143</sup>

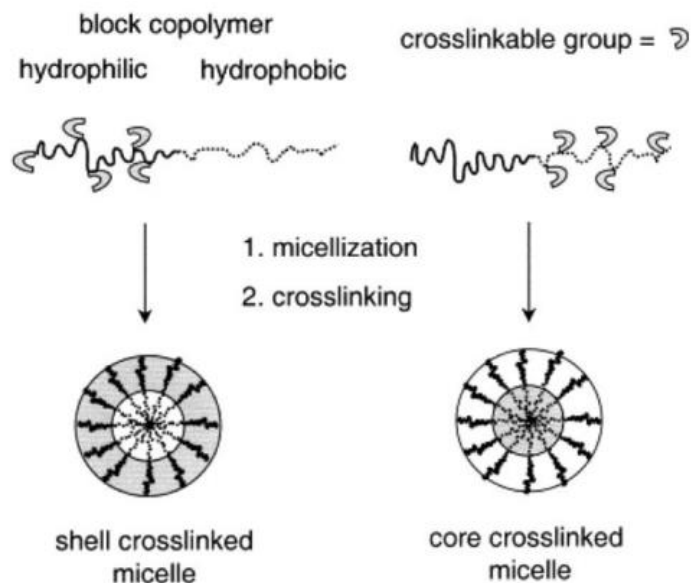


**Fig.7** Schematic representation of the different types of functional amphiphilic block copolymers used in the formation of shell cross-linked or core cross-linked nanoparticles (reproduced from ref.<sup>136</sup>).

### 3. Biological fate and *in vivo* toxicity of nanoparticles

#### 3.1 Generalities

Nanoparticles are potentially able to induce adverse effects and toxicity *in vitro* and *in vivo*. Nanoparticles' toxicity can be influenced by their core chemistry, shape, crystallinity, surface properties, but also by their dissolution and aggregation state, which depend on the environment they encounter.<sup>144,145,146</sup> Therefore the complexity of nanotoxicology studies comes with the complexity and variety of the particles' properties, their ability to bind and interact with biological systems and change their characteristics, depending on the environment they are in. Generally, the nanoparticles toxicity is related to their ability to affect the normal physiology and structure of

organs and tissues. Toxic effects strongly depend on the administration route and the resulting biodistribution of nanoparticles.

The *in vivo* toxicity following intravenous administration of nanoparticles is associated to the augmented circulation time, off-target interactions, accumulation, retarded clearance, hemolysis, activation of the complement, which can lead in the worst cases to the so-called complement activation-related pseudo-allergy (CARPA), organ damage, and chronic adverse effects.<sup>147,148</sup> The exact underlying mechanisms are still poorly understood and need to be fully investigated.

Size is another important parameter regarding circulation and distribution within the organism. In the bloodstream, particles with an excessive size may cause embolism with a potentially fatal outcome. Moreover, large particles tend to accumulate after intravenous administration within the lungs. *In vivo* studies in the rat using polystyrene particles demonstrated a passive accumulation in the lung for particles with a size exceeding a threshold of 10  $\mu\text{m}$ .<sup>149</sup> Thus, some findings of lung targeting of nanoparticles may be indicative of “accidental” trapping of agglomerates.<sup>150</sup> Indeed, lack of colloidal stability of nanoparticles in the blood after injection can lead to particles aggregation. Agglomerates can block the systemic circulation and are also more prone to be engulfed by RES. Agglomeration-flocculates can sediment and in extreme cases could clot capillaries causing mechanical distress and serious pain. Furthermore, the aggregation may trigger immune responses such as increased phagocytosis, generation of reactive oxygen species (ROS), and inflammatory reactions.<sup>151</sup>

Nanoparticles are distributed throughout the body via the bloodstream and extravasate this transport system depending on their size. Extravasation is restricted to specific tissues since the presence of tight junctions prevents nanoparticles larger than 2  $\mu\text{m}$  to leave the circulation.<sup>152</sup> Nanoparticles are often trapped in the liver and spleen as these organs host the largest

concentration of tissue resident macrophages. Liver overload of nanoparticulate material may induce insurgence of severe liver injury and irreversible impairment of its functionality.

The elimination from the blood can occur by two main mechanisms: (i) renal elimination and (ii) hepatobiliary elimination.<sup>153,154</sup> Glomerular filtration eliminates nanoparticles with a maximal hydrodynamic diameter of 5 nm to 10 nm.<sup>155</sup> Many strategies for tuning nanoparticles renal elimination have been developed from this fundamental understanding using nanoparticle size, core density, surface charge, and surface chemistry.<sup>156</sup> Conversely, the principles governing nanoparticle hepatobiliary elimination are relatively unexplored.

The degradation of nanoparticles can involve multiple processes such as erosion, deagglomeration, disintegration, dissolution, or chemical degradation of particles. Anticipating the biological fate and the *in vivo* degradation of nanoparticles is of primary importance to design biocompatible and safe nanocarriers for drug delivery. However, nowadays model studies to the *in vivo* behavior of nanoparticles have largely been conducted with non-degradable particles. Indeed, most data reported concern the biological behavior and toxicity of inhaled nanoparticles as part of the unintended release of ultrafine or nanoparticles by combustion derived processes such as diesel exhaust particles.<sup>157</sup>

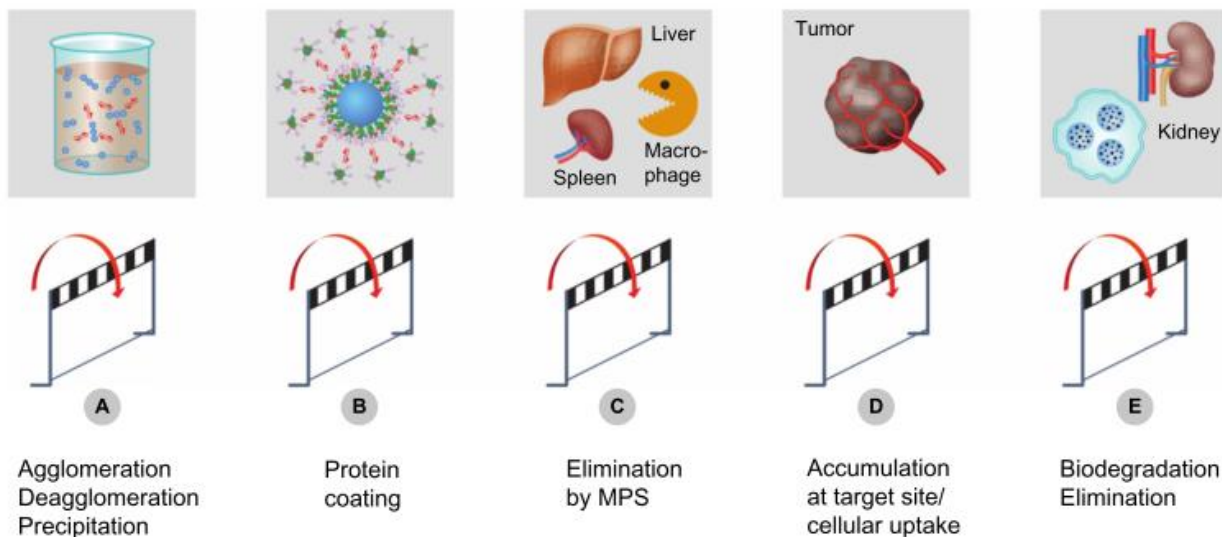


**Fig.8** Experimental challenges and hurdles. Particle agglomeration (A) reduces dosing accuracy or may lead to embolism after IV injection. Plasma-protein binding and opsonization of nanoparticles (B) may trigger a humoral immune response. Interaction of nanoparticles with cells of the MPS leads to accelerated plasma clearance (C). Accumulation of particles at a defined target site (D) might be impeded by their premature degradation and elimination (E). Abbreviations: ENMs, engineered nanomaterials; IV, intravenous; MPS, mononuclear phagocytic system (reproduced from ref.<sup>158</sup>).

### 3.2 In vivo fate and toxicity of chitosan-based nanogels

Chitosan is considered to be biocompatible and biodegradable. Indeed chitosan polymer can be degraded by hydrolysis of the glycosidic  $\beta$  1-4 bonds, by enzymes such as lysozymes and chitinases.<sup>159</sup> Chitosan hydrolysis leads to the production of glucosamine oligosaccharides and hetero-oligosaccharides of glucosamine and N-acetyl-D-glucosamine.<sup>160</sup> These saccharides can participate to the glycoprotein synthesis pathways or can be excreted. An increase in lysozyme activity has been reported in rabbit serum, after intravenous injections of chitosan. This increase

would be due to the activation of macrophages releasing lysozymes as body's defense mechanism. Varum et al. also observed in vitro that chitosan is mainly degraded by lysozymes in human serum.<sup>161</sup> The deacetylation degree (DD) plays an important role in chitosan degradation. Zhang et al. demonstrated that chitosan with lower molar mass and lower DD showed a faster rate of degradation.<sup>160,162</sup> The rate of degradation is also affected by the availability of amino groups. In fact, the chemical modifications of chitosan may limit the accessibility of amino groups for the hydrolysis of glycosidic bonds  $\beta$  1-4.<sup>163</sup> On the other hand, the deacetylation diminish the degradation rate of chitosan.<sup>164</sup> The presence of a cross-linking agent significantly affects chitosan degradation by preventing the access of the enzymes to  $\beta$ -4 glycosidic bonds.<sup>165</sup> This effect is strongly dependent on the nature of the cross-linking agent. For instance, glutaraldehyde forms covalent and rigid bonds while TPP forms ionic and flexible bonds between chitosan chains leading to a lower resistance.<sup>166</sup>

The biodistribution of chitosan after injection has been established after intravenous administration in rats. Chitosan showed to have a fast plasmatic clearance and a liver accumulation dependent on its molar mass. Chitosan with low molar mass (<5 kDa) exhibited slower clearance and the polymer was also detected in kidneys and urine suggesting urinary elimination.<sup>167</sup> After injection, chitosan can potentially activate the complement and the coagulation system because of the interaction of its cationic groups with plasma proteins or blood cells.<sup>168,169,170</sup> After intravenous injection of chitosan solutions at a dose of 4.5 mg/kg, Hirano et al. did not observe any physiological symptoms in rabbits. However, a dose of 50 mg/kg caused the death of animals probably due to blood coagulation. Another study reported that after repeated intraperitoneal injections of 5 mg chitosan as a solution, mice showed weight loss and inactivity, while by subcutaneous route no clinical abnormalities were observed.<sup>171</sup>

In the form of nanogels, the impact of the molar mass of chitosan glycol (GC) conjugated was studied in mice with subcutaneous tumors.<sup>172</sup> Conjugates were detected in liver, lung, kidneys, spleen and heart. Nanogels showed a tumor accumulation dependent on the molar mass of chitosan: nanogels based on 20 kDa and 100 kDa chitosan displayed lower tumor accumulation compared to 250 kDa chitosan-based nanogels. This difference suggests a longer blood circulation time for bigger nanogels. According to Park et al., this could be related to the difference in stability of nanogels in the bloodstream. Many other studies investigated the biodistribution of chitosan glycol nanogels for the delivery of different anticancer showing accumulation in the tumors.<sup>81,173</sup> He et al. were interested in the impact of the surface properties of chitosan nanogels on their biodistribution.<sup>174</sup> Two types of chitosan (carboxymethyl-chitosan and chitosan hydrochloride) conjugated with rhodamine, forming nanogels with different physico-chemical properties were studied. Results showed that the surface charge plays a key role in the biodistribution of chitosan. Negatively charged nanogels accumulated more in the tumor than those positively charged, which are more rapidly removed from the blood and accumulate in liver and spleen. The size of the nanogels has also an impact: larger nanogels are more captured by the liver. In the lungs, the accumulation of nanogels depends on the surface charge, probably because of the formation of aggregates in the case of positively charged nanogels.

Regarding the nanogels' form, CS-TPP nanogels with different sizes (200 nm and 360 nm) were tested on zebrafish, a model commonly used in genotoxicity studies. A decrease of hatching and a concentration-dependent mortality have been shown. Malformations were observed only in zebrafish embryos treated with high concentrations of small nanogels, showing an impact of the size on the toxicity.<sup>175</sup> N-octyl-O-sulfate chitosan micelles have been reported to not induce anaphylactic and histopathological reactions or hemolytic effects after intravenous injection at 6

mg/kg/day in mice.<sup>176</sup> Song et al. evaluated the toxicity of N-succinyl-chitosan, after peritoneal injection. The polymer did not demonstrated any significant toxicity with an LD50 of 2000 mg/kg.<sup>177</sup>

### **3.3 In vivo fate and toxicity of polymeric micelles**

Toxicologically relevant organs for polymeric micelles include the major organs involved in the reticuloendothelial system, and clearance organs such as the liver, spleen, kidneys, bone marrow, lungs, and heart. Unlike vesicular colloids such as liposomes, micelles gradually dissociate in the blood, so it is often difficult to delineate their fate after injection.<sup>178</sup> After intravenous injection, polymeric micelles become much diluted by blood and they are confronted with numerous blood components, such as proteins and cells. **Fig.9** describes the complexity of their in vivo behavior. Savic et al. showed in vitro that a conventional polymer micelle of PEG-b-PCL is unstable in serum-containing culture media with or without cells, but stable in phosphate-buffered saline.<sup>179</sup> Recently, Chen et al. demonstrated that polymer micelle made of PEG-b-PDLLA are not stable in blood.<sup>180</sup> The authors used the FRET technique to monitor the stability of polymer micelles in real time after intravenous administration, using micelles loaded with a pair of FRET dyes. The FRET ratio detected in the blood vessels of the mice ears was reduced to half of the initial value at 15 min post intravenous injection, indicating that the dyes were released from the core of the micelles. It was further revealed that the main components responsible for the release of lipophilic dyes from micelles into the blood are a- and b-globulins rather than g-globulin or serum albumin. Genexol®-PM micelles are well known to increase the water-solubility of paclitaxel allowing higher dose administration than paclitaxel alone.<sup>181</sup> It has been suggested that saturated paclitaxel in the polymeric micelles is quickly released (95%) followed by being bound to plasma proteins within

about 2.5 h. This immediate offloading of the paclitaxel dose is consistent with another work on PEG-block-PLA micelles that reported micelles disruption/instability within 15 min after IV injection.<sup>180</sup> However, another in vitro release study reported that Genexol-PM demonstrated first-order release kinetics with ~65% drug release within 24 h and 95% drug release at 48 h.L<sup>182</sup>ong circulating PEG-block-PDLLA micelles have previously been developed by another group who reported that the integrity of the micelles could be preserved up to 24 h.<sup>183</sup> Liu et Al. administered MePEG5000-b-PCL5000 micelles to mice at different copolymer doses to examine the distribution kinetics of (1) copolymer assembled as thermodynamically stable micelles, (2) copolymer assembled as thermodynamically unstable micelles and (3) copolymer unimers, respectively. Overall, they found that when the copolymer is assembled as thermodynamically stable micelles the material is effectively restricted to the plasma compartment. Interestingly, the copolymer was found to have a relatively long circulation half-life, even when administered at a dose that would likely fall to concentrations below the CMC following distribution. Analysis of plasma samples from this group revealed that even 24 h after administration, a significant portion of the copolymer remained assembled as intact micelles.<sup>184</sup> Another study showed that after intravenous injection, PEG-PCL and PEG-PDLLA micelles were quickly sequestered into the liver as unimers and the micelle degree in the blood quickly decreased to about 20%. Intact micelles were difficult to be cleared. These micelles were able to arrive tumors and were very stable with cell membrane, but dissociate gradually inside cells.<sup>185</sup> Micellar systems with a reinforced structure showed longer circulation half-life. It has been shown that hyaluronic acid micelles core-crosslinked by disulfide bonds have enhanced in vivo tumor-targetability and therapeutic efficacy compared to the non-crosslinked ones, which can be attributed to the improved blood stability.<sup>186</sup> Also core polymerized

polydiacetylene micelles display an overall slower clearance from blood when compared to non-polymerized ones.<sup>140</sup>

Thanks to their small size, polymeric micelles can theoretically evade the renal excretion, during the drug delivery to their target, and also eventually disassemble into single polymer chains that can be excreted from the bloodstream in the kidneys.<sup>187</sup> This dual status of polymeric micelles can provide high targeting efficiency with being free from toxicities. The polymeric micelles' disassembling rate is therefore an important factor for a good balance between the targeting efficiency and the low toxicity. Designing degradable nanomaterials is currently receiving great impetus due to their ability to degrade after delivering their therapeutic cargoes.<sup>188</sup> In addition, the degradation rate might be tuned via incorporating various functionalities to control the degradation and/or to respond to a particular enzyme or pH, and hence allowing for controlled or stimuli-responsive drug delivery applications.<sup>189</sup> A representative example are the pH-sensitive polymeric micelle, which destabilize and liberate drugs depending on the environmental pH. Cancer or inflammation makes the extracellular pH at the disease site acidic by means of hypoxia or over-producing metabolic wastes. Therefore by using pH-sensitive polymers it is possible to specifically unload drugs at a diseased tissues.<sup>37, 113</sup>

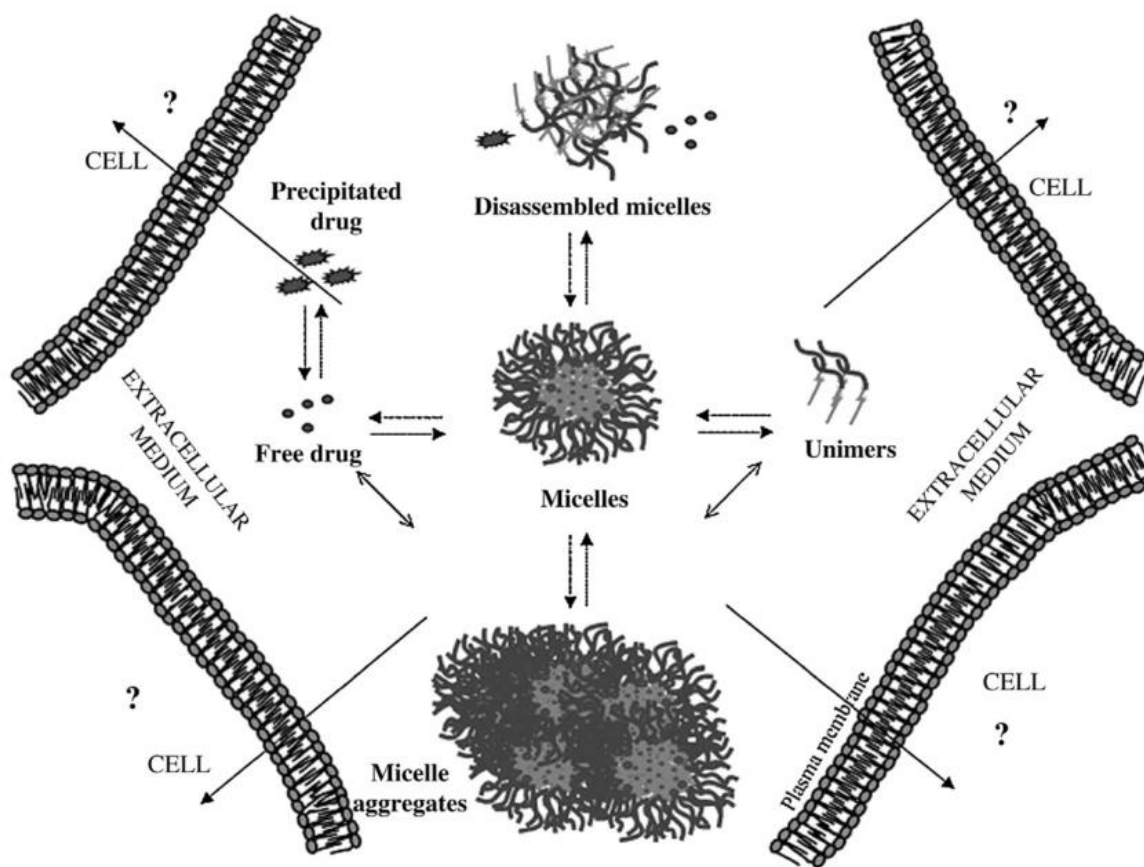


**Fig.9** The in vivo behavior of polymeric micelles is complex and hard to anticipate. Micelles can accumulate in the target tissue and intracellularly deliver the drug or release the drug in the extracellular medium through different mechanisms (reproduced from ref.<sup>190</sup>).

The physico-chemical properties of micelles (surface charge, hydrophobicity, size, shape, and aggregation tendencies) are found to trigger different biological responses.<sup>191,192</sup> Generally, biodegradable polymers with an electric neutrality, such as polyesters (PLGA), pegylated polyesters and so on, show low toxicity.<sup>193,194</sup> On the contrary, polycations present higher toxicity, inducing hemolysis and complement activation. Polyanions are poorly toxic but still induce

anticoagulant activity and cytokine release.<sup>195</sup> Currently, the main concerns on toxicity of polymers focus on their metabolism, immunotoxicity and complement activation.<sup>191</sup>

For poly(ethylene glycol)-b-poly(amino acid) block copolymer-based polymeric micelle anti-cancer drugs, carrier-derived toxic side effects were not observed both in animal experiments or in clinical evaluations, while typical toxicities of anti-cancer drugs loaded in the polymeric micelles were observed.<sup>196</sup> Kawaguchi et al. examined toxicities of a polymeric micelle carrier which did not load any drug, and found no pathological abnormality at a considerably high dose.<sup>197</sup> They, however, observed significant activation of the mononuclear phagocytic system (MPS) in several organs such as the spleen and liver, even though this activation was transient.

#### **4. Intracellular fate and in vitro toxicity of nanoparticles**

##### **4.1. Generalities**

The cellular uptake as well as the intracellular fate of the drug nanocarrier is a key issue for the pharmacological activity, especially when it is expected to occur on an intracellular target. The intracellular liberation of the active molecule takes generally place through the loss of the particle status from the nanocarrier and is crucial for the drug to be active and efficient. The intracellular release of the drug occurs into the enzymatic environment of the lysosomes or directly in the cell cytoplasm.

The ability of nanoparticles to enter cells may be predicted based on their physicochemical properties. Besides their size,<sup>198, 199</sup> shape,<sup>200</sup> and surface properties,<sup>194</sup> their aggregation status also plays an important role. It is important also to keep in mind that the protein corona leads to changes in nanoparticles surface charge, composition and dispersion/aggregation degree, and for this reason strongly influences the cellular entrance.

According to the physicochemical characteristics of the nanocarrier and the nature of the target cells, two main internalization pathways may occur: either the phagocytosis or the endocytic pathways (i.e., clathrin- and caveolae-mediated endocytosis).<sup>201</sup> In general, larger particles experience more efficient uptake by phagocytosis.<sup>202</sup> During the endocytosis, nanoparticles are enclosed by early or late endosomes, and their environment pH is shifted from 7.4 in the extracellular medium to nearly 6.0 in the early endosomes, and further to 4.5 in the lysosomes.<sup>158</sup>

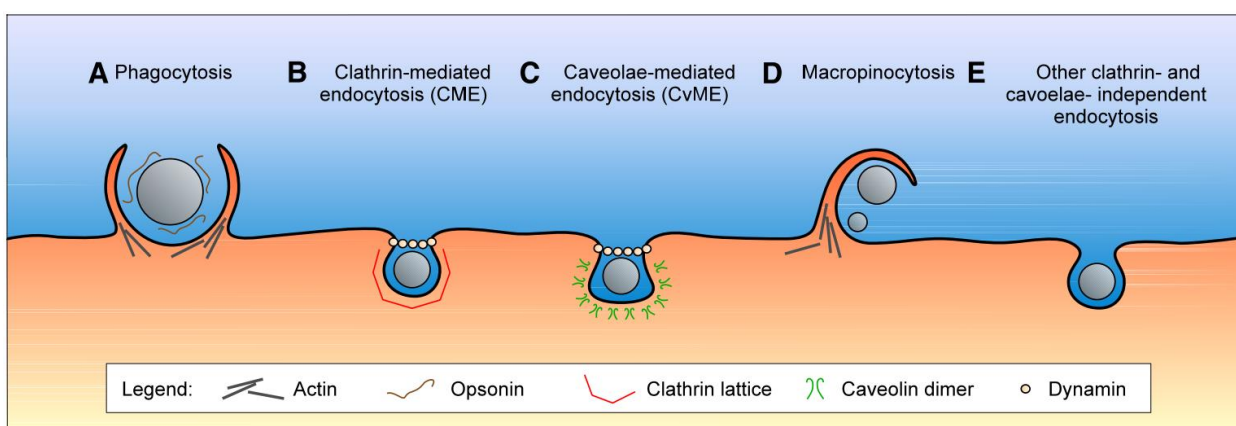


**Fig.10** Principal nanocarrier internalization pathways in mammalian cells. (A) Phagocytosis is an actin-based mechanism occurring primarily in professional phagocytes, such as macrophages, and closely associated with opsonization. (B) Clathrin-mediated endocytosis is a widely shared pathway of nanoparticle internalization, associated with the formation of a clathrin lattice and depending on the GTPase dynamin. (C) Caveolae-mediated endocytosis occurs in typical flask-shaped invaginations of the membrane coated with caveolin dimers, also depending on dynamin. (D) Macropinocytosis is an actin-based pathway, engulfing nanoparticles and the extracellular milieu with a poor selectivity. (E) Other endocytosis pathways can be involved in the nanoparticle internalization, independent of both clathrin and caveolae (reproduced from ref.<sup>201</sup>).

Physicochemical properties of colloids can undergo significant changes upon cellular uptake.<sup>203</sup> Inorganic particles cores, organic particle components and surface coatings, as well as the protein corona may be subjected to dissolution, exchange or degradation processes.<sup>204</sup>

After degradation of the surface molecules of nanoparticles, the acidic environment may lead to acid etching of the particles and to the gradual decrease in the nanoparticles core diameter or morphology. In addition to the acidic pH, nanoparticles may also be exposed to various degradable enzymes such as cathepsin L, which has recently been reported to be able to degrade almost all of the bio-conjugated nanoparticles.<sup>205</sup> The nanoparticles intracellular degradation is mainly dependent on their original properties and surface coating. The use of inert nanoparticles, stabilizing coatings or specific ligand coatings and pH-responsive polymers, which allow nanoparticles to escape rapidly from lysosomes, are of great importance.<sup>206,207</sup>

It is well known that the cellular uptake and the intracellular persistence of nanoparticles can provide preliminary information on the *in vivo* toxicity.<sup>208</sup> This is why studying the intracellular fate of nanoparticles is crucial to better understand the mechanisms of toxicity of engineered nanoparticles. Siegrist et al. proposed the Hazard Evaluation Strategy (HES) based on cellular uptake and intracellular persistence to predict the suitability of injectable nanoparticles.<sup>146</sup> In particular, after intravenous injection, the uptake of nanoparticles by macrophages and endothelial cells should be closely monitored, as it can lead to severe cytotoxic effects that in turn damage the vascular system and potentially the tissue residing behind it, causing complications and pain to the patient. The intracellular persistence is not equivalent to chemical or colloidal stability. Even though the two parameters can certainly be linked, the ability of an organism to degrade or

eliminate nanoparticles underlies different and often more complex mechanisms than particle agglomeration or disintegration in aqueous solution.

The intracellular degradation of nanoparticles can trigger different mechanisms of toxicity that have been widely investigated by *in vitro* studies. During their degradation inside of lysosomes, nanoparticles may release their components like ions or molecules and the degradation products can affect cell homeostasis and functions. In particular, it is now well known that ions derived from nanoparticles degradation can induce high levels of reactive oxygen species (ROS), which can directly provoke DNA damage (e.g. DNA point mutations or single/ double strand break) and mRNA degradation, activate signaling pathways, affect gene expression and induce apoptosis. Moreover, ROS are one of the main factors involved in inflammation processes. Cell membrane stability can be affected by nanoparticles either directly (e.g. physical damage) or indirectly (e.g. oxidation) which can lead to cell death. All cell organelles (primarily lysosomes and mitochondria) can be damaged by nanoparticles through physical or chemical mechanisms. **Fig.11** show the main nanoparticles intracellular targets and the related nanotoxicological mechanisms.

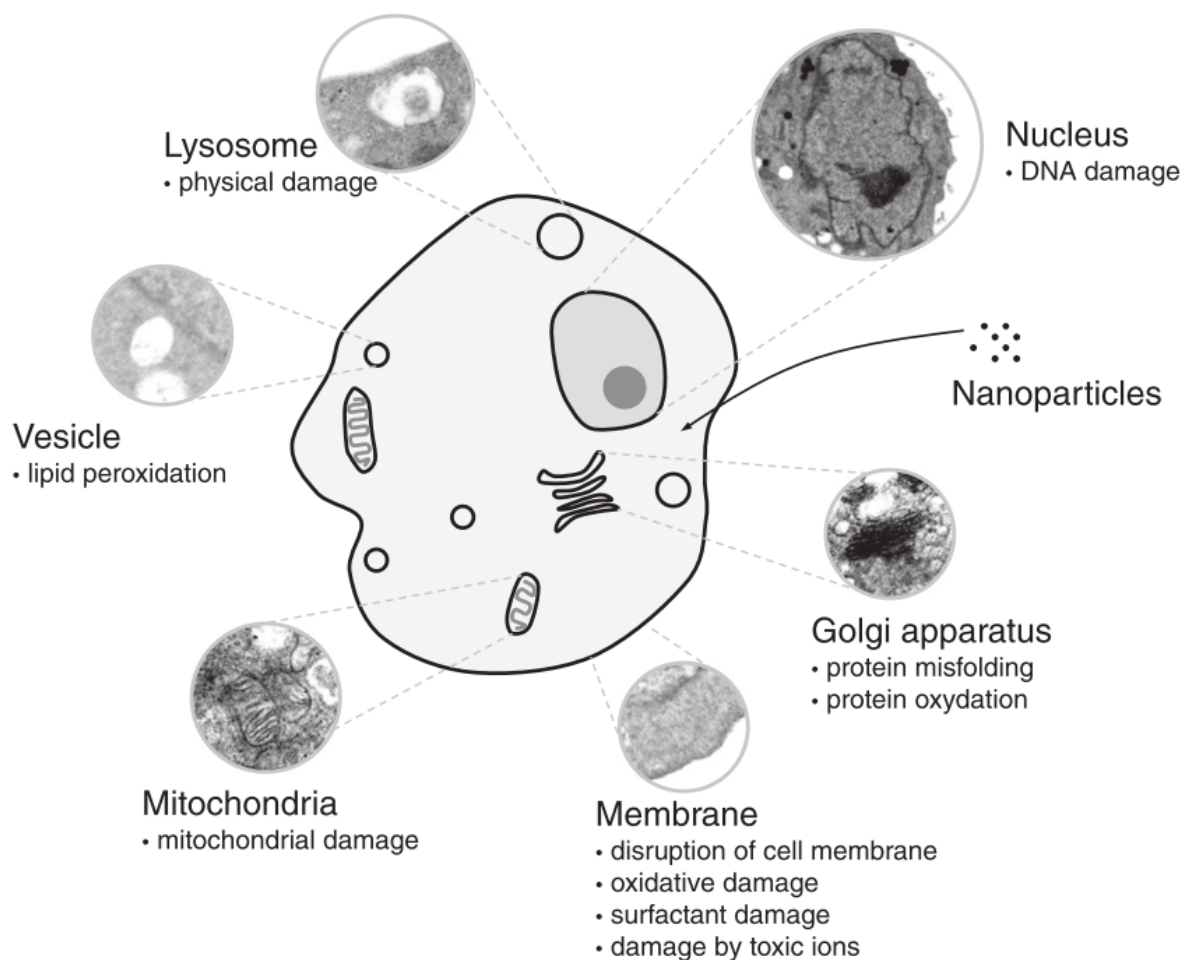


**Fig.11** Nanoparticle interaction with cells: intracellular targets and nanotoxicological mechanisms (reproduced from ref.<sup>144</sup>).

Until today, most of *in vitro* studies have been conducted on inorganic nanoparticles.<sup>6</sup> Under the acidic environment of the lysosomes, many inorganic nanoparticles (e.g. metallic, metal oxide, and semiconductor nanoparticles) have been reported to dissolve and release metallic ions such as  $\text{Ag}^+$ ,  $\text{Gd}^{2+}$ ,  $\text{Fe}^{2+/3+}$ ,  $\text{Zn}^{2+}$ , and  $\text{Au}^{+/3+}$ . The induction of oxidative stress has been reported to be the main common toxic effect upon exposure to inorganic nanoparticles.<sup>209</sup> Most inorganic nanoparticles are formulated with a hydrophilic surface coating, since their metallic core is hydrophobic, and the core itself is toxic since it is composed of heavy metals. In these cases,

biocompatible polymers (such as PEG) used as coating materials to enhance the colloidal stability are also of primary importance in order to prevent the dissolution and the release of toxic ions.<sup>210,211,212</sup>

Biodegradable polymeric nanoparticles (based on polyesters, polysaccharides and poly(amino acids)) are expected to demonstrate fewer toxic events than the non-biodegradable ones. For example, a naturally occurring component such as a phospholipid is not expected to interact with cells similarly to non-natural ones such as metals. Nevertheless, the degradation products of the polymeric biodegradable nanoparticles may still induce cytotoxicity to some extent.<sup>205</sup> Therefore the intracellular fate of the products of enzymatic and hydrolytic degradation of polymer or lipid-based nanoparticles should be investigated.

#### **4.2 Intracellular fate and in vitro toxicity of chitosan-based nanogels**

Many studies have investigated the impact of the physico-chemical properties of chitosan on cell viability.<sup>213,214,215,216</sup> Some modifications of chitosan structure have been shown to modify its cytotoxicity. For instance, PEG grafting reduces the surface charge of chitosan resulting in a decrease in the interactions with cells and hence in the cytotoxicity.<sup>213</sup> Opanasopit et al. showed that chitosan cytotoxicity varied according to the type of chitosan salts.<sup>214,215</sup> Another factor affecting chitosan toxicity is its molar mass: chitosan toxicity increases with molar mass. Chitosan with low molar mass (<10 kDa) do not exhibit significant cytotoxicity.<sup>217</sup> It is difficult to conclude on the toxicity of chitosan because all cytotoxicity studies are not comparable, since they use different cell lines and different incubation conditions. Nonetheless in comparison with reference

cationic polymers such as PEI or poly-L-lysine, chitosan and its derivatives display very low toxicity with an IC<sub>50</sub> values ranging from 0.2 to 2 mg/mL in most cellular models.<sup>96</sup>

It is well known that size, surface charge and composition of nanogels have key roles in the cellular uptake of nanogels.<sup>96</sup> It has been observed that chitosan-TPP nanogels cytotoxicity diminish with the decrease in polymer DD.<sup>218</sup> Qui et al. studied the impact of the surface charge and the size of the CS/TPP nanogels by comparing small chitosan-TPP nanogels (40 nm, +51 mV) with nanogels charged with Cu(II) (257 nm, +96 mV).<sup>219</sup> The increase in the surface charge increased electrostatic interactions with the components of the cell membrane leading to higher cytotoxicity. The cytotoxicity was also impacted by the size: larger nanogels size displayed higher cytotoxicity. Both types of nanogels showed higher toxicity than chitosan in solution. Another study reported the evaluation of the impact of a hyaluronic acid (HA) coating on the cytotoxicity.<sup>98</sup> CS-TPP-HA nanogels exhibited lower cytotoxicity compared to CS/TPP ones. All studies present in the literature show that the cytotoxicity of chitosan nanogels is directly related to the surface charge density, the nanogels size but also at to the tridimensional conformation of the polymer.<sup>213,216,160</sup> In particular, the interactions with the anionic components of cellular membranes seems to play a key role on chitosan-based nanogels cellular toxicity.

#### **4.3 Intracellular fate and in vitro toxicity of polymeric micelles**

It could be assumed that polymeric micelles enter cells mainly by endocytosis. However, micelle–cell interaction as well as the cellular uptake of polymeric micelles could be mediated by means of complicated molecular and cellular events, which should be clarified by continuous research. In fact, micelles and unimers might have different behaviors in regard to cellular uptake,

membrane accumulation, and intracellular distribution. Beside this, cellular uptake, intracellular fate and cytotoxicity are dependent on the properties of the specific polymers and on the physico-chemical properties of micelles, such as size, structure and surface charge. Generally, biodegradable polymers with electric neutrality such as polyesters show low toxicity.<sup>193,194</sup> Polycations display generally higher cytotoxicity and polyanions are less cytotoxic but still induce cytokine release.<sup>195</sup> All biological properties are molecular weight dependent and can change once the respective conjugates are prepared. Therefore, careful characterization of the potential toxicity of both the polymer — this will be a primary metabolite — and the final construct is required.

Crosslinking of micelles has increasingly been proposed as a strategy to create stable nanoparticles. Crosslinking of the polymeric nanomaterials forms robust structures that have lower tendency of dissociation and aggregation than the parent micellar structures and also allows to control the release rates of cargos. Kim et al. showed that the shell-crosslinking has an impact on exocytosis by accelerating it.<sup>220</sup> In the same way, it has been reported that the stability of micelles plays a crucial role in the penetration in multicellular tumor spheroids: fast disassembly of non-crosslinked P(HPMA-co-MAA)-b-PMMA micelles and quick release of the loaded drug can provoke the apoptosis of peripheral cells and cease the transport from outer part to inner part of the spheroids.<sup>221</sup>

In addition, the presence of stabilizing crosslinks has been recently shown to reduce the toxicity and immunotoxicity of micelles, eventually by limiting the release of free polymeric units and reducing the interactions with the surrounding cells and biomacromolecules.<sup>222</sup> Elsbahy et al. reported that by increasing the degree of crosslinking it is possible to reduce the accessibility of biomolecules to the core of PEG-poly(acrylamidoethylamine)-block-poly(DL-lactide)(PAEA<sub>90</sub>-b-PDLLA<sub>40</sub>) micelles and to decrease their cytotoxicity and immunotoxicity.<sup>223</sup> A study on

polyphosphoester (PPE)-based degradable micelles showed that crosslinking plays an important role in controlling stability, cytotoxicity and immunotoxicity of micelles. Shell crosslinking of zwitterionic micelles significantly reduced the immunotoxicity.<sup>188</sup>

In recent years, smart bio-responsive micellar nanoparticles have received particular attention. These systems exhibit extremely fast response to the intracellular environment and are intended to disassemble and release drugs inside of cells while being stable under extracellular conditions and during workup. Smart micelles for intracellular drug delivery can be sensitive to pH, redox potential and enzymes.<sup>142</sup> pH-responsive polymeric micelles take advantage of the acidic environments in the endo/ lysosomal compartments and are based on titratable anionic groups such as poly(acrylic acid), poly(methacrylic acid), poly(glutamic acid) and polymer having sulphonamide group, titratable cationic groups (dimethylamino)ethyl methacrylate, poly(vinylpyridine), poly(histidine), poly(amino ester) and acid-labile polymers (containing any of hydrazone, acetal, benzoic imine, poly(ortho-ester) bonds).<sup>224</sup> Enzyme-responsive systems present esters or short peptide sequences that can be cleaved by esterases or proteases. The most used linker is the tetrapeptide Gly–Phe–Leu–Gly, which can be cleaved by the lysosomal enzyme cathepsin B that is usually overexpressed in tumor cells. Reduction-sensitive micellar nanoparticles are sensitive to the difference of redox potential between the extracellular and the intracellular space.<sup>225,226</sup> The extracellular space is oxidative while the intracellular is reductive. The high reducing potential in the cytosol and cell nucleus is mainly due to presence of 2-10 mM glutathione tripeptide (g-glutamyl-cysteinyl-glycine, GSH) which is the most abundant low molecular weight biological reducing agent and is kept reduced by NADPH and glutathione reductase.

## Conclusions

Based on all the available literature, the interactions between drug nanocarriers and biological systems appear very dependent on the type and the dynamic attitude of the nanoparticles. Such knowledge is key to predict the efficacy but also the potential toxicity of the drug nanocarriers. This is especially true for the two types of drug nanocarriers studied in this thesis, chitosan-based nanogels and polymeric micelles. Starting from this principle, in the experimental part of this thesis, the intracellular fate of chitosan based nanogels and polydiacetylene micelles have been systematically investigated.

The experimental work explained below aim to improve the colloidal stability of nanocarriers and to study the specific interactions of the nanocarriers with cells relating them with the colloidal stability of nanoparticles in physiological conditions.

## REFERENCES

1. Üner, M. Importance of solid lipid nanoparticles ( SLN ) in various administration routes and future perspectives. **2**, 289–300 (2007).
2. Farjadian, F. *et al.* Nanopharmaceuticals and nanomedicines currently on the market: Challenges and opportunities. *Nanomedicine* **14**, (2019).
3. Farokhzad, O. C. & Langer, R. Nanomedicine : Developing smarter therapeutic and. **58**, 1456–1459 (2006).
4. Giacalone, G. *et al.* Stabilization and cellular delivery of chitosan – polyphosphate nanoparticles by incorporation of iron. *J. Control. Release* **194**, 211–219 (2014).
5. Anselmo, A. C. & Mitragotri, S. Nanoparticles in the clinic. 10–29 (2016).
6. Buzea, C., Pacheco, I. I. & Robbie, K. Nanomaterials and nanoparticles : Sources and toxicity Nanomaterials and nanoparticles : Sources and toxicity. **17**, (2017).
7. Svenson, S. What nanomedicine in the clinic right now really forms nanoparticles ? **6**, 125–135 (2014).
8. Sparreboom, A. *et al.* Cancer Therapy : Clinical Comparative Preclinical and Clinical Pharmacokinetics of a ( ABI-007 ) and Paclitaxel Formulated in Cremophor ( Taxol ). **11**, 4136–4144 (2005).
9. Bourquin, J. *et al.* Biodistribution , Clearance , and Long-Term Fate of Clinically Relevant Nanomaterials. **1704307**, 1–31 (2018).
10. Vayssieres, L. On the thermodynamic stability of metal oxide nanoparticles in aqueous

- solutions. **2**, (2005).
11. Seo, S. J. *et al.* Extra- and intra-cellular fate of nanocarriers under dynamic interactions with biology. *Nano Today* **14**, 84–99 (2017).
  12. Pareek, V., Bhargava, A., Bhanot, V. & Gupta, R. Formation and Characterization of Protein Corona Around Nanoparticles : A Review. **18**, 6653–6670 (2018).
  13. Gustafson, H. H., Holt-Casper, D., Grainger, D. W. & Ghandehari, H. Nanoparticle uptake: The phagocyte problem. *Nano Today* **10**, 487–510 (2015).
  14. Nel, A. E. *et al.* Understanding biophysicochemical interactions at the nano–bio interface. *Nat. Publ. Gr.* **8**, 543–557 (2009).
  15. Moore, T. L. *et al.* Chem Soc Rev media and impact on cellular interactions †. 6287–6305 (2015).
  16. Enustun, B. Y. B. V. *TOURNAL.* **730**, (1963).
  17. Biswas, P. Characterization of size , surface charge , and agglomeration state of nanoparticle dispersions for toxicological studies. 77–89 (2009).
  18. Wu, L., Zhang, J. & Watanabe, W. Physical and chemical stability of drug nanoparticles ☆. *Adv. Drug Deliv. Rev.* **63**, 456–469 (2011).
  19. Wong, J. *et al.* Suspensions for intravenous ( IV ) injection : A review of development , preclinical and clinical aspects ☆. **60**, 939–954 (2008).
  20. Mahmoudi, M., Bertrand, N., Zope, H. & Farokhzad, O. C. Emerging understanding of the protein corona at the nano-bio interfaces. *Nano Today* **11**, 817–832 (2016).

21. Johnston, B. D. *et al.* Colloidal Stability and Surface Chemistry Are Key Factors for the Composition of the Protein Corona of Inorganic Gold Nanoparticles. *Adv. Funct. Mater.* **27**, 1–9 (2017).
22. Hellstrand, E. *et al.* Complete high-density lipoproteins in nanoparticle corona. **276**, 3372–3381 (2009).
23. Milani, S., Bombelli, F. B., Pitek, A. S. & Dawson, K. A. Reversible versus Irreversible Binding of Transferrin to Polystyrene Nanoparticles : Soft and Hard Corona. 2532–2541 (2012).
24. Gebauer, J. S. *et al.* Impact of the nanoparticle-protein corona on colloidal stability and protein structure. *Langmuir* **28**, 9673–9679 (2012).
25. Safi, M., Courtois, J., Seigneuret, M., Conjeaud, H. & Berret, J. F. The effects of aggregation and protein corona on the cellular internalization of iron oxide nanoparticles. *Biomaterials* **32**, 9353–9363 (2011).
26. Argentiere, S., Cella, C., Cesaria, M., Milani, P. & Lenardi, C. Silver nanoparticles in complex biological media: assessment of colloidal stability and protein corona formation. *J. Nanoparticle Res.* **18**, (2016).
27. Oliveira, C. L. *et al.* Characterization of polymeric nanoparticles for intravenous delivery: Focus on stability. *Colloids Surfaces B Biointerfaces* **150**, 326–333 (2017).
28. Ho, G., Beom, S., Lee, J. & Weon, C. Mechanisms of drug release from advanced drug formulations such as polymeric-based drug-delivery systems and lipid nanoparticles. *J. Pharm. Investig.* **0**, 0 (2017).

29. Mura, S., Nicolas, J. & Couvreur, P. Stimuli-responsive nanocarriers for drug delivery. *Nat. Publ. Gr.* **12**, 991–1003 (2013).
30. Fleige, E., Quadir, M. A. & Haag, R. Stimuli-responsive polymeric nanocarriers for the controlled transport of active compounds: Concepts and applications. *Adv. Drug Deliv. Rev.* **64**, 866–884 (2012).
31. Paola, S., Vicente, J. De, Nardecchia, S., Marchal, J. A. & Boulaiz, H. Thermo-Sensitive Nanomaterials: Recent Advance in Synthesis and Biomedical Applications. 1–32 doi:10.3390/nano8110935
32. Gill, S. L. M., Cuylear, C. L., Adolphi, N. L., Osi, M. & Smyth, H. D. C. Magnetically Responsive Nanoparticles for Drug Delivery Applications Using Low Magnetic Field Strengths. **8**, 33–42 (2009).
33. Boissenot, T., Bordat, A., Fattal, E. & Tsapis, N. Ultrasound-triggered drug delivery for cancer treatment using drug delivery systems: From theoretical considerations to practical applications. *J. Control. Release* (2016). doi:10.1016/j.jconrel.2016.09.026
34. Wanakule, P. & Roy, K. Disease-Responsive Drug Delivery: The Next Generation of Smart Delivery Devices. *Curr. Drug Metab.* **13**, 42–49 (2011).
35. Malcolm, D. W., Varghese, J. J., Sorrells, J. E., Ovitt, C. E. & Benoit, D. S. W. The Effects of Biological Fluids on Colloidal Stability and siRNA Delivery of a pH-Responsive Micellar Nanoparticle Delivery System. *ACS Nano* **12**, 187–197 (2018).
36. Guan, X. *et al.* Ultrasensitive pH Triggered Charge/Size Dual-Rebound Gene Delivery System. *Nano Lett.* **16**, 6823–6831 (2016).

37. Chen, J., Ouyang, J., Kong, J., Zhong, W. & Xing, M. M. Photo-cross-linked and pH-sensitive biodegradable micelles for doxorubicin delivery. *ACS Appl. Mater. Interfaces* **5**, 3108–3117 (2013).
38. Fan, Y., Li, F. & Chen, D. Biomaterials Scavenger receptor-recognized and enzyme-responsive nanoprobe for fluorescent labeling of lysosomes in live cells. *Biomaterials* **35**, 7870–7880 (2014).
39. Song, S. J., Lee, S., Lee, Y. & Choi, J. S. Enzyme-responsive destabilization of stabilized plasmid-lipid nanoparticles as an efficient gene delivery. *Eur. J. Pharm. Sci.* **91**, 20–30 (2016).
40. Biswas, D., An, S. Y., Li, Y., Wang, X. & Oh, J. K. Intracellular Delivery of Colloidally Stable Core-Cross-Linked Triblock Copolymer Micelles with Glutathione-Responsive Enhanced Drug Release for Cancer Therapy. *Mol. Pharm.* **14**, 2518–2528 (2017).
41. Guerrini, L., Alvarez-puebla, R. A. & Pazos-perez, N. Surface Modifications of Nanoparticles for Stability in Biological Fluids. 1–28 (2018). doi:10.3390/ma11071154
42. Sadeghpour, A., Szilagyi, I., Vaccaro, A. & Borkovec, M. Electrostatic Stabilization of Charged Colloidal Particles with Adsorbed Polyelectrolytes of Opposite Charge. **26**, 15109–15111 (2010).
43. Mahl, D., Greulich, C., Meyer-zaika, W., Manfred, K. & Epple, M. Gold nanoparticles : dispersibility in biological media and cell-biological effect. 6176–6181 (2010). doi:10.1039/c0jm01071e
44. Chen, Z. P. *et al.* Preparation and characterization of water-soluble monodisperse magnetic

- iron oxide nanoparticles via surface double-exchange with DMSA. **316**, 210–216 (2008).
45. Engineering, E., Sciences, E. H. & Angeles, L. Dispersion and Stability Optimization of TiO<sub>2</sub> Nanoparticles in Cell Culture Media. **44**, 7309–7314 (2010).
  46. Cohen, J. M., Teegarden, J. G. & Demokritou, P. An integrated approach for the in vitro dosimetry of engineered nanomaterials. 1–12 (2014).
  47. Kumar, A. & Gupta, M. Synthesis and surface engineering of iron oxide nanoparticles for biomedical applications. **26**, 3995–4021 (2005).
  48. Peng, Q. *et al.* Enhanced biostability of nanoparticle-based drug delivery systems by albumin corona. *Nanomedicine* **10**, 205–214 (2015).
  49. Du, X. *et al.* Disulfide-Bridged Organosilica Frameworks: Designed, Synthesis, Redox-Triggered Biodegradation, and Nanobiomedical Applications. *Adv. Funct. Mater.* **28**, (2018).
  50. Zheng, N. *et al.* Redox-responsive, reversibly-crosslinked thiolated cationic helical polypeptides for efficient siRNA encapsulation and delivery. *J. Control. Release* **205**, 231–239 (2015).
  51. Li, Y. *et al.* Probing of the assembly structure and dynamics within nanoparticles during interaction with blood proteins. *ACS Nano* **6**, 9485–9495 (2012).
  52. Novo, L., Van Gaal, E. V. B., Mastrobattista, E., Van Nostrum, C. F. & Hennink, W. E. Decationized crosslinked polyplexes for redox-triggered gene delivery. *J. Control. Release* **169**, 246–256 (2013).

53. Wu, D. & Delair, T. Stabilization of chitosan/hyaluronan colloidal polyelectrolyte complexes in physiological conditions. *Carbohydr. Polym.* **119**, 149–158 (2015).
54. Gilmore, S. F. *et al.* Lipid Cross-Linking of Nanolipoprotein Particles Substantially Enhances Serum Stability and Cellular Uptake. *ACS Appl. Mater. Interfaces* **8**, 20549–20557 (2016).
55. Kubota, N. & Eguchi, Y. Facile preparation of water-soluble N-acetylated chitosan and molecular weight dependence of its water-solubility. *Polymer Journal* **29**, 123–127 (1997).
56. Rinaudo, M., Pavlov, G. & Desbrières, J. Influence of acetic acid concentration on the solubilization of chitosan. *Polymer (Guildf)*. **40**, 7029–7032 (1999).
57. Rinaudo, M. & Pavlov, G. of Polymer Analysis and Characterization Solubilization of Chitosan in Strong Acid Medium. *Science (80-. )*. 37–41
58. Nilsen-nygaard, J., Strand, S. P., Vårum, K. M., Draget, K. I. & Nordgård, C. T. Chitosan: Gels and Interfacial Properties. 552–579 (2015). doi:10.3390/polym7030552
59. Agnihotri, S. A., Mallikarjuna, N. N. & Aminabhavi, T. M. Recent advances on chitosan-based micro- and nanoparticles in drug delivery. *Journal of Controlled Release* **100**, 5–28 (2004).
60. Wang, J. J. *et al.* Recent advances of chitosan nanoparticles as drug carriers. *International journal of nanomedicine* **6**, 765–774 (2011).
61. Xu, J. *et al.* Design and characterization of antitumor drug paclitaxel-loaded chitosan nanoparticles by W/O emulsions. *Int. J. Biol. Macromol.* **50**, 438–443 (2012).

62. Sung, H., Liang, I., Chen, C., Huang, R. & Liang, H. Stability of a biological tissue fixed with a naturally occurring crosslinking agent ( genipin ). (2000).
63. Sung, H. W., Huang, R. N., Huang, L. H. & Tsai, C. C. In vitro evaluation of cytotoxicity of a naturally occurring cross-linking reagent for biological tissue fixation. *J. Biomater. Sci. Polym. Ed.* **10**, 63–78 (1999).
64. Mi, F. L., Sung, H. W. & Shyu, S. S. Synthesis and characterization of a novel chitosan-based network prepared using naturally occurring crosslinker. *J. Polym. Sci. Part A Polym. Chem.* **38**, 2804–2814 (2000).
65. Alonso, M. J., Calvo, P. & Remun, C. Novel Hydrophilic Chitosan – Polyethylene Oxide Nanoparticles as Protein Carriers. 125–132
66. Liu, H. & Gao, C. Preparation and properties of ionically cross-linked chitosan nanoparticles. *Polym. Adv. Technol.* **20**, 613–619 (2009).
67. Gan, Q., Wang, T., Cochrane, C. & McCarron, P. Modulation of surface charge, particle size and morphological properties of chitosan-TPP nanoparticles intended for gene delivery. *Colloids Surfaces B Biointerfaces* **44**, 65–73 (2005).
68. Schatz, C. *et al.* Formation and properties of positively charged colloids based on polyelectrolyte complexes of biopolymers. *Langmuir* **20**, 7766–7778 (2004).
69. Sankalia, M. G., Mashru, R. C., Sankalia, J. M. & Sutariya, V. B. Reversed chitosan-alginate polyelectrolyte complex for stability improvement of alpha-amylase: Optimization and physicochemical characterization. *Eur. J. Pharm. Biopharm.* **65**, 215–232 (2007).
70. Grenha, A. *et al.* Development of new chitosan/carrageenan nanoparticles for drug delivery

- applications. *J. Biomed. Mater. Res. - Part A* **92**, 1265–1272 (2010).
71. Alonso-Sande, M. *et al.* Formation of new glucomannan - chitosan nanoparticles and study of their ability to associate and deliver proteins. *Macromolecules* **39**, 4152–4158 (2006).
  72. Du, J., Dai, J., Liu, J. L. & Dankovich, T. Novel pH-sensitive polyelectrolyte carboxymethyl Konjac glucomannan-chitosan beads as drug carriers. *React. Funct. Polym.* **66**, 1055–1061 (2006).
  73. Birch, N. P. & Schiffman, J. D. Characterization of self-Assembled polyelectrolyte complex nanoparticles formed from chitosan and pectin. *Langmuir* **30**, 3441–3447 (2014).
  74. Denuziere, A., Ferrier, D., Damour, O. & Domard, A. Chitosan - chondroitin sulfate and chitosan - hyaluronate polyelectrolyte complexes: Biological properties. *Biomaterials* **19**, 1275–1285 (1998).
  75. Lalevée, G. *et al.* Polyelectrolyte complexes via desalting mixtures of hyaluronic acid and chitosan—Physicochemical study and structural analysis. *Carbohydr. Polym.* **154**, 86–95 (2016).
  76. Hu, C. S., Chiang, C. H., Hong, P. Da & Yeh, M. K. Influence of charge on FITC-BSA-loaded chondroitin sulfate-chitosan nanoparticles upon cell uptake in human Caco-2 cell monolayers. *Int. J. Nanomedicine* **7**, 4861–4872 (2012).
  77. Martins, A. F., Piai, J. F., Schuquel, I. T. A., Rubira, A. F. & Muniz, E. C. Polyelectrolyte complexes of chitosan/heparin and N,N,N-trimethyl chitosan/heparin obtained at different pH: I. Preparation, characterization, and controlled release of heparin. *Colloid Polym. Sci.* **289**, 1133–1144 (2011).

78. Chaiyasan, W., Praputbut, S., Kompella, U. B., Srinivas, S. P. & Tiyaboonchai, W. Penetration of mucoadhesive chitosan-dextran sulfate nanoparticles into the porcine cornea. *Colloids Surfaces B Biointerfaces* **149**, 288–296 (2017).
79. Sarmiento, B., Ribeiro, A., Veiga, F. & Ferreira, D. Development and characterization of new insulin containing polysaccharide nanoparticles. *Colloids Surfaces B Biointerfaces* **53**, 193–202 (2006).
80. Qu, G., Yao, Z., Zhang, C., Wu, X. & Ping, Q. PEG conjugated N-octyl-O-sulfate chitosan micelles for delivery of paclitaxel: In vitro characterization and in vivo evaluation. *Eur. J. Pharm. Sci.* **37**, 98–105 (2009).
81. Jae, H. P. *et al.* Self-assembled nanoparticles based on glycol chitosan bearing hydrophobic moieties as carriers for doxorubicin: In vivo biodistribution and anti-tumor activity. *Biomaterials* **27**, 119–126 (2006).
82. Xiangyang, X. *et al.* Preparation and characterization of N-succinyl-N-octyl chitosan micelles as doxorubicin carriers for effective anti-tumor activity. *Colloids Surfaces B Biointerfaces* **55**, 222–228 (2007).
83. Son, Y. J. *et al.* Biodistribution and anti-tumor efficacy of doxorubicin loaded glycol-chitosan nanoaggregates by EPR effect. in *Journal of Controlled Release* **91**, 135–145 (2003).
84. Opanasopit, P. *et al.* Incorporation of camptothecin into N-phthaloyl chitosan-g-mPEG self-assembly micellar system. *Eur. J. Pharm. Biopharm.* **64**, 269–276 (2006).
85. Qian, F., Cui, F., Ding, J., Tang, C. & Yin, C. Chitosan graft copolymer nanoparticles for

- oral protein drug delivery: Preparation and characterization. *Biomacromolecules* **7**, 2722–2727 (2006).
86. Heidari, A., Younesi, H., Mehraban, Z. & Heikkinen, H. Selective adsorption of Pb(II), Cd(II), and Ni(II) ions from aqueous solution using chitosan-MAA nanoparticles. *Int. J. Biol. Macromol.* **61**, 251–263 (2013).
87. Csaba, N. *et al.* Ionically crosslinked chitosan nanoparticles as gene delivery systems: Effect of PEGylation degree on in vitro and in vivo gene transfer. *J. Biomed. Nanotechnol.* **5**, 162–171 (2009).
88. Wu, Y., Yang, W., Wang, C., Hu, J. & Fu, S. Chitosan nanoparticles as a novel delivery system for ammonium glycyrrhizinate. *Int. J. Pharm.* **295**, 235–245 (2005).
89. Sreekumar, S., Goycoolea, F. M., Moerschbacher, B. M. & Rivera-Rodriguez, G. R. Parameters influencing the size of chitosan-TPP nano- and microparticles. *Sci. Rep.* **8**, (2018).
90. Zhang, H., Oh, M., Allen, C. & Kumacheva, E. Monodisperse chitosan nanoparticles for mucosal drug delivery. *Biomacromolecules* **5**, 2461–2468 (2004).
91. Jonassen, H., Kjøniksen, A. L. & Hiorth, M. Stability of chitosan nanoparticles cross-linked with tripolyphosphate. *Biomacromolecules* **13**, 3747–3756 (2012).
92. Huang, Y. & Lapitsky, Y. Monovalent salt enhances colloidal stability during the formation of chitosan/tripolyphosphate microgels. *Langmuir* **27**, 10392–10399 (2011).
93. López-León, T., Carvalho, E. L. S., Seijo, B., Ortega-Vinuesa, J. L. & Bastos-González, D. Physicochemical characterization of chitosan nanoparticles: Electrokinetic and stability

- behavior. *J. Colloid Interface Sci.* **283**, 344–351 (2005).
94. Huang, Y., Cai, Y. & Lapitsky, Y. Factors affecting the stability of chitosan/tripolyphosphate micro- and nanogels: Resolving the opposing findings. *J. Mater. Chem. B* **3**, 5957–5970 (2015).
95. Dautzenberg, H. & Kriz, J. Response of polyelectrolyte complexes to subsequent addition of salts with different cations. *Langmuir* **19**, 5204–5211 (2003).
96. Garcia-Fuentes, M. & Alonso, M. J. Chitosan-based drug nanocarriers: Where do we stand? *Journal of Controlled Release* **161**, 496–504 (2012).
97. Borges, O., Borchard, G., Verhoef, J. C., Sousa, A. De & Junginger, H. E. Preparation of coated nanoparticles for a new mucosal vaccine delivery system. **299**, 155–166 (2005).
98. Nasti, A. *et al.* Chitosan/TPP and chitosan/TPP-hyaluronic acid nanoparticles: Systematic optimisation of the preparative process and preliminary biological evaluation. *Pharm. Res.* **26**, 1918–1930 (2009).
99. Schmitt, F. *et al.* Chitosan-based nanogels for selective delivery of photosensitizers to macrophages and improved retention in and therapy of articular joints. *J. Control. Release* **144**, 242–250 (2010).
100. Mi, F., Sung, H., Shyu, S., Su, C. & Peng, C. Synthesis and characterization of biodegradable TPP / genipin co- crosslinked chitosan gel beads. **44**, 6521–6530 (2003).
101. Bhatia, S. C. & Ravi, N. A Magnetic Study of an Fe - Chitosan Complex and Its Relevance to Other Biomolecules. 413–417 (2000).

102. Reynaud, F., Tsapis, N., Deyme, M., Vasconcelos, G. & Gueutin, C. Spray-dried chitosan-metal microparticles for ciprofloxacin adsorption: 7304–7312 (2011). doi:10.1039/c1sm05509g
103. Lijklema, L. Interaction of Orthophosphate with Iron( 111) and Aluminum Hydroxides. 537–541 (1980).
104. Follmann, B. K. S. H. *et al.* Characterization and Extracorporeal Application of a New Phosphate-Binding Agent. **32**, 733–739 (1994).
105. Attwood, D., & Florence, A. T. *Surfactant systems: their chemistry, pharmacy, and biology.* (1983).
106. micelles\_diazepam.pdf.
107. Kabanov, A. V *et al.* The neuroleptic activity of haloperidol increases after its solubilization in surfactant micelles Micelles as microcontainers for drug targeting of Mol ~ adar. **258**, 343–345 (1989).
108. © 19 9 2 Nature Publishing Group.
109. Torchilin, V. P. Structure and design of polymeric surfactant -based drug delivery systems. *J. Control. Release* **73**, 137–172 (2001).
110. Schmolka, I. R. A review of block polymer surfactants. *J. Am. Oil Chem. Soc.* **54**, 110–116 (1977).
111. Ogier, J., Arnauld, T. & Doris, E. Recent advances in the field of nanometric drug carriers. *Future Med. Chem.* **1**, 693–711 (2009).

112. Cabral, H. & Kataoka, K. Progress of drug-loaded polymeric micelles into clinical studies. *J. Control. Release* **190**, 465–476 (2014).
113. Ahmad, Z., Shah, A., Siddiq, M. & Kraatz, H.-B. Polymeric micelles as drug delivery vehicles. *RSC Adv.* **4**, 17028–17038 (2014).
114. Jones, M. & Leroux, J. Polymeric micelle sea new generation of colloidal drug carriers. *Eur J Pharm Biopharm* **48**, 101–111 (1999).
115. Lu, Y. & Park, K. Polymeric micelles and alternative nanonized delivery vehicles for poorly soluble drugs. *Int. J. Pharm.* **453**, 198–214 (2013).
116. Eetezadi, S., Ekdawi, S. N. & Allen, C. The challenges facing block copolymer micelles for cancer therapy: In vivo barriers and clinical translation. *Adv. Drug Deliv. Rev.* **91**, 7–22 (2015).
117. Tan, Y. F., Lao, L. L., Xiong, G. M. & Venkatraman, S. Controlled-release nanotherapeutics: State of translation. *J. Control. Release* **284**, 39–48 (2018).
118. Tang, Z. *et al.* Polymeric nanostructured materials for biomedical applications. *Prog. Polym. Sci.* **60**, 86–128 (2016).
119. Kabanov, A. V. *et al.* Micelle Formation and Solubilization of Fluorescent Probes in Poly(oxyethylene-6-oxypropylene-6-oxyethylene) Solutions. *Macromolecules* **28**, 2303–2314 (1995).
120. Li, M. *et al.* Nanoscaled poly(l-glutamic acid)/doxorubicin-amphiphile complex as pH-responsive drug delivery system for effective treatment of nonsmall cell lung cancer. *ACS Appl. Mater. Interfaces* **5**, 1781–1792 (2013).

121. Lv, S. *et al.* Doxorubicin-loaded amphiphilic polypeptide-based nanoparticles as an efficient drug delivery system for cancer therapy. *Acta Biomater.* **9**, 9330–9342 (2013).
122. Cabral, H., Nishiyama, N., Okazaki, S., Koyama, H. & Kataoka, K. Preparation and biological properties of dichloro(1,2-diaminocyclohexane) platinum(II) (DACHPt)-loaded polymeric micelles. *J. Control. Release* **101**, 223–232 (2005).
123. Lee, H., Zeng, F., Dunne, M. & Allen, C. Methoxy poly(ethylene glycol)-block-poly( $\delta$ -valerolactone) copolymer micelles for formulation of hydrophobic drugs. *Biomacromolecules* **6**, 3119–3128 (2005).
124. Letchford, K. & Burt, H. A review of the formation and classification of amphiphilic block copolymer nanoparticulate structures: micelles, nanospheres, nanocapsules and polymersomes. *Eur. J. Pharm. Biopharm.* **65**, 259–269 (2007).
125. Tyrrell, Z. L., Shen, Y. & Radosz, M. Fabrication of micellar nanoparticles for drug delivery through the self-assembly of block copolymers. *Prog. Polym. Sci.* **35**, 1128–1143 (2010).
126. Ke, X. Y. *et al.* Co-delivery of thioridazine and doxorubicin using polymeric micelles for targeting both cancer cells and cancer stem cells. *Biomaterials* **35**, 1096–1108 (2014).
127. Sant, V. P., Smith, D. & Leroux, J. C. Novel pH-sensitive supramolecular assemblies for oral delivery of poorly water soluble drugs: Preparation and characterization. *J. Control. Release* **97**, 301–312 (2004).
128. Huh, K. M. *et al.* Hydrotropic polymer micelle system for delivery of paclitaxel. *J. Control. Release* **101**, 59–68 (2005).
129. Zhou, Z. *et al.* Linear-dendritic drug conjugates forming long-circulating nanorods for

- cancer-drug delivery. *Biomaterials* **34**, 5722–5735 (2013).
130. Wang, H. X., Xiong, M. H., Wang, Y. C., Zhu, J. & Wang, J. N-acetylgalactosamine functionalized mixed micellar nanoparticles for targeted delivery of siRNA to liver. *J. Control. Release* **166**, 106–114 (2013).
131. Sant, V. P., Smith, D. & Leroux, J. C. Enhancement of oral bioavailability of poorly water-soluble drugs by poly(ethylene glycol)-block-poly(alkyl acrylate-co-methacrylic acid) self-assemblies. *J. Control. Release* **104**, 289–300 (2005).
132. Waldrop, M. M. After the Fall Published by : American Association for the Advancement of Science . **239**, 17–18 (2016).
133. Elhasi, S., Astaneh, R. & Lavasanifar, A. Solubilization of an amphiphilic drug by poly(ethylene oxide)-block-poly(ester) micelles. *Eur. J. Pharm. Biopharm.* **65**, 406–413 (2007).
134. Creutz, S., Van Stam, J., De Schryver, F. C. & Jérôme, R. Dynamics of poly((dimethylamino)alkyl methacrylate-block-sodium methacrylate) micelles. Influence of hydrophobicity and molecular architecture on the exchange rate of copolymer molecules. *Macromolecules* **31**, 681–689 (1998).
135. Segments, P. Formation of Polyion Complex Micelles in an Aqueous Milieu from a Pair of Oppositely-Charged Block Copolymers with. 5294–5299 (1996).
136. O'Reilly, R. K., Hawker, C. J. & Wooley, K. L. Cross-linked block copolymer micelles: functional nanostructures of great potential and versatility. *Chem. Soc. Rev.* **35**, 1068 (2006).

137. Zhang, F. *et al.* Shell crosslinked knedel-like nanoparticles for delivery of cisplatin: Effects of crosslinking. *Nanoscale* **5**, 3220–3225 (2013).
138. Barkey, N. M. *et al.* Development and in vivo quantitative magnetic resonance imaging of polymer micelles targeted to the melanocortin 1 receptor. *J. Med. Chem.* **56**, 6330–6338 (2013).
139. Gravel, E. *et al.* Drug delivery and imaging with polydiacetylene micelles. *Chem. - A Eur. J.* **18**, 400–408 (2012).
140. Theodorou, I. *et al.* Stable and compact zwitterionic polydiacetylene micelles with tumor-targeting properties. *Chem. Commun.* **51**, 14937–14940 (2015).
141. Neuberg, P. *et al.* Photopolymerized micelles of diacetylene amphiphile : physical characterization and cell delivery properties †. 15–17 (2015).
142. Movassaghian, S., Merkel, O. M. & Torchilin, V. P. Applications of polymer micelles for imaging and drug delivery. *Wiley Interdiscip. Rev. Nanomedicine Nanobiotechnology* **7**, 691–707 (2015).
143. Liu, M. *et al.* Crosslinked self-assembled nanoparticles for chemo-sonodynamic combination therapy favoring antitumor, antimetastasis management and immune responses. *J. Control. Release* **290**, 150–164 (2018).
144. Elsaesser, A. & Howard, C. V. Toxicology of nanoparticles. *Adv. Drug Deliv. Rev.* **64**, 129–137 (2012).
145. Turci, F. *et al.* An Integrated Approach to the Study of the Interaction between Proteins and Nanoparticles. **26**, 8336–8346 (2010).

146. Siegrist, S. *et al.* Preclinical hazard evaluation strategy for nanomedicines. *Nanotoxicology* **0**, 1–27 (2018).
147. Bazile, D. V. Nanotechnologies in drug delivery – An industrial perspective. *J. Drug Deliv. Sci. Technol.* **24**, 12–21 (2014).
148. Yildirimer, L., Thanh, N. T. K., Loizidou, M. & Seifalian, A. M. Toxicological considerations of clinically applicable nanoparticles. (2011).
149. Kutscher, H. L. *et al.* Threshold size for optimal passive pulmonary targeting and retention of rigid microparticles in rats. *J. Control. Release* **143**, 31–37 (2010).
150. Aneja, M. K. *et al.* Targeted gene delivery to the lung Targeted gene delivery to the lung. **5247**, (2015).
151. Fu, P. P., Xia, Q., Hwang, H. & Ray, P. C. ScienceDirect Mechanisms of nanotoxicity : Generation of reactive oxygen species 5. *J. Food Drug Anal.* **22**, 64–75 (2014).
152. Garnett, M. C. & Kallinteri, P. Nanomedicines and nanotoxicology : some physiological principles. 307–311 (2006).
153. Poon, W. *et al.* Elimination Pathways of Nanoparticles. *ACS Nano* **13**, 5785–5798 (2019).
154. Zhang, Y., Poon, W., Tavares, A. J., Mcgilvray, I. D. & Chan, W. C. W. AC SC. *J. Control. Release* (2016).
155. Choi, H. S. *et al.* Renal clearance of quantum dots. **25**, 1165–1170 (2007).
156. Du, B., Yu, M. & Zheng, J. Transport and interactions of nanoparticles in the kidneys. *Nat. Rev. Mater.* (2018).

157. Oberdörster, G. *et al.* Brogan & Partners Nanotoxicology: An Emerging Discipline Evolving from Studies of Ultrafine Particles. **113**, 823–839 (2014).
158. Kettiger, H., Schipanski, A., Wick, P. & Huwyler, J. Engineered nanomaterial uptake and tissue distribution: From cell to organism. *Int. J. Nanomedicine* **8**, 3255–3269 (2013).
159. Rinaudo, M. Chitin and chitosan: Properties and applications. *Prog. Polym. Sci.* **31**, 603–632 (2006).
160. Omar Zaki, S. S., Ibrahim, M. N. & Katas, H. Particle size affects concentration-dependent cytotoxicity of chitosan nanoparticles towards mouse hematopoietic stem cells. *J. Nanotechnol.* (2015).
161. Vårum, K. M., Myhr, M. M., Hjerde, R. J. N. & Smidsrød, O. In vitro degradation rates of partially N-acetylated chitosans in human serum. *Carbohydr. Res.* **299**, 99–101 (1997).
162. Zhang, H. & Neau, S. H. In vitro degradation of chitosan by bacterial enzymes from rat cecal and colonic contents. *Biomaterials* **23**, 2761–2766 (2002).
163. Thiomers, V. *et al.* Evaluation of In Vitro Enzymatic Degradation of Evaluation of In Vitro Enzymatic Degradation of Various Thiomers and. **9045**, (2015).
164. Lim, S. M., Song, D. K., Oh, S. H. & Sin, D. Journal of Biomaterials Science , In vitro and in vivo degradation behavior of acetylated chitosan porous beads. 37–41 (2012).
165. Jameela, S. R. & Jayakrishnan, A. Glutaraldehyde cross-linked chitosan microspheres as a long acting biodegradable drug delivery vehicle: studies on the in vitro release of mitoxantrone and in vivo degradation of microspheres in rat muscle. *Biomaterials* **16**, 769–775 (1995).

166. McConnell, E. L., Murdan, S. & Basit, A. W. An Investigation into the Digestion of Chitosan ( Noncrosslinked and Crosslinked ) by Human Colonic Bacteria. **97**, 3820–3829 (2008).
167. Richardson, S. C. W., Kolbe, H. V. J. & Duncan, R. Potential of low molecular mass chitosan as a DNA delivery system: Biocompatibility, body distribution and ability to complex and protect DNA. *Int. J. Pharm.* **178**, 231–243 (1999).
168. Suzuki, Y., Miyatake, K., Okamoto, Y., Muraki, E. & Minami, S. Influence of the chain length of chitosan on complement activation. *Carbohydr. Polym.* **54**, 465–469 (2003).
169. Minamia, S., Suzuki, H., Okamoto, Y., Fujinagab, T. & Shigemasa, Y. Carbohydrate Polymers Chitin and chitosan activate complement via the alternative pathway. **8617**, (1998).
170. Baraghis, E. *et al.* C3 , C5 , and factor B bind to chitosan without complement activation. (2009).
171. Tanaka, Y., Tanaka, M., Minamis, S., Miyashitas, M. & Nanno, M. Effects of chitin and chitosan particles on BALB/c mice by oral and parenteral administration. **18**, 591–595 (1997).
172. Park, K. *et al.* Effect of polymer molecular weight on the tumor targeting characteristics of self-assembled glycol chitosan nanoparticles. *J. Control. Release* **122**, 305–314 (2007).
173. Kim, J. H. *et al.* Antitumor efficacy of cisplatin-loaded glycol chitosan nanoparticles in tumor-bearing mice. *J. Control. Release* **127**, 41–49 (2008).
174. He, C., Hu, Y., Yin, L., Tang, C. & Yin, C. Effects of particle size and surface charge on cellular uptake and biodistribution of polymeric nanoparticles. *Biomaterials* **31**, 3657–3666

- (2010).
175. Hu, Y. Toxicity evaluation of biodegradable chitosan nanoparticles using a zebrafish embryo model. 3351–3359 (2011).
  176. Zhang, C. *et al.* Pharmacokinetics , biodistribution , efficacy and safety of N -octyl- O -sulfate chitosan micelles loaded with paclitaxel. **29**, (2008).
  177. University, H. Conjugate of mitomycin C with N-succinyl-chitosan : In vitro drug release properties , toxicity and antitumor activity. **98**, 121–130 (1993).
  178. Sakai-Kato, K. *et al.* General considerations regarding the in vitro and in vivo properties of block copolymer micelle products and their evaluation. *J. Control. Release* **210**, 76–83 (2015).
  179. Azzam, T., Eisenberg, A. & Maysinger, D. Assessment of the Integrity of Poly ( caprolactone ) - b -poly ( ethylene oxide ) Micelles under Biological Conditions : A Fluorogenic-Based Approach. 3570–3578 (2006).
  180. Chen, H. *et al.* Fast Release of Lipophilic Agents from Circulating PEG-PDLLA Micelles Revealed by in Vi W o Fo " rster Resonance Energy Transfer Imaging. 5213–5217 (2008).
  181. Manuscript, A. NIH Public Access. **4**, 1–35 (2013).
  182. Werner, M. E. *et al.* Preclinical Evaluation of Genexol-PM , a Nanoparticle Formulation of Paclitaxel , as a Novel Radiosensitizer for the Treatment of Non-Small Cell Lung Cancer. *Radiat. Oncol. Biol.* **86**, 463–468 (2013).
  183. Yamamoto, Y., Nagasaki, Y., Kato, Y. & Sugiyama, Y. Long-circulating poly ( ethylene

- glycol )– poly ( D , L -lactide ) block copolymer micelles with modulated surface charge. *77*, 27–38 (2001).
184. Liu, J., Zeng, F. & Allen, C. In vivo fate of unimers and micelles of a poly(ethylene glycol)-block-poly(caprolactone) copolymer in mice following intravenous administration. *Eur. J. Pharm. Biopharm.* **65**, 309–319 (2007).
185. Sun, X. *et al.* The Blood Clearance Kinetics and Pathway of Polymeric Micelles in Cancer Drug Delivery. *ACS Nano* **12**, 6179–6192 (2018).
186. Han, H. S. *et al.* Bioreducible core-crosslinked hyaluronic acid micelle for targeted cancer therapy. *J. Control. Release* **200**, 158–166 (2015).
187. Yokoyama, M. Polymeric micelles as drug carriers: Their lights and shadows. *J. Drug Target.* **22**, 576–583 (2014).
188. Elsabahy, M. *et al.* Surface charges and shell crosslinks each play significant roles in mediating degradation, biofouling, cytotoxicity and immunotoxicity for polyphosphoester-based nanoparticles. *Sci. Rep.* **3**, (2013).
189. Samarajeewa, S., Shrestha, R., Li, Y. & Wooley, K. L. Degradability of poly(lactic acid)-containing nanoparticles: Enzymatic access through a cross-linked shell barrier. *J. Am. Chem. Soc.* **134**, 1235–1242 (2012).
190. Kedar, U., Phutane, P., Shidhaye, S. & Kadam, V. Advances in polymeric micelles for drug delivery and tumor targeting. *Nanomedicine Nanotechnology, Biol. Med.* **6**, 714–729 (2010).
191. Fischer, H. C. & Chan, W. C. Nanotoxicity: the growing need for in vivo study. *Curr. Opin.*

- Biotechnol.* **18**, 565–571 (2007).
192. Dobrovolskaia, M. A. & McNeil, S. E. Immunological properties of engineered nanomaterials. *Nanosci. Technol. A Collect. Rev. from Nat. Journals* 278–287 (2009). doi:10.1142/9789814287005\_0029
193. Naahidi, S. *et al.* Biocompatibility of engineered nanoparticles for drug delivery. *J. Control. Release* **166**, 182–194 (2013).
194. Verma, A. & Stellacci, F. Effect of surface properties on nanoparticle-cell interactions. *Small* **6**, 12–21 (2010).
195. Duncan, R. The dawning era of polymer therapeutics. *Nat. Rev. Drug Discov.* **2**, 347–360 (2003).
196. Matsumura, Y. *et al.* Phase I clinical trial and pharmacokinetic evaluation of NK911, a micelle-encapsulated doxorubicin. *Br. J. Cancer* **91**, 1775–1781 (2004).
197. Kawaguchi, T., Honda, T., Nishihara, M., Yamamoto, T. & Yokoyama, M. Histological study on side effects and tumor targeting of a block copolymer micelle on rats. *J. Control. Release* **136**, 240–246 (2009).
198. Meng, H., Chen, Z., Xing, G. & Yuan, H. Ultrahigh reactivity provokes nanotoxicity: Explanation of oral toxicity of nano-copper particles. **175**, 102–110 (2007).
199. Ma, X. *et al.* Gold Nanoparticles Induce Autophagosome Accumulation through Size-Dependent Nanoparticle Uptake and Lysosome Impairment. 8629–8639 (2011).
200. Qiu, Y. *et al.* Biomaterials Surface chemistry and aspect ratio mediated cellular uptake of

- Au nanorods. *Biomaterials* **31**, 7606–7619 (2010).
201. Hillaireau, H. & Couvreur, P. Nanocarriers' entry into the cell: Relevance to drug delivery. *Cell. Mol. Life Sci.* **66**, 2873–2896 (2009).
202. Beddoes, C. M., Case, C. P. & Briscoe, W. H. Understanding nanoparticle cellular entry: A physicochemical perspective. *Adv. Colloid Interface Sci.* **218**, 48–68 (2015).
203. Feliu, N. *et al.* Quantitative uptake of colloidal particles by cell cultures. *Sci. Total Environ.* **568**, 819–828 (2016).
204. Feliu, N. *et al.* Quantitative uptake of colloidal particles by cell cultures. *Sci. Total Environ.* **568**, 819–828 (2016).
205. Deng, J. & Gao, C. Recent advances in interactions of designed nanoparticles and cells with respect to cellular uptake , intracellular fate , degradation and cytotoxicity. *Nanotechnology* **27**, 1–10
206. Zhu, Y. *et al.* Negative Surface Shielded Polymeric Micelles with Colloidal Stability for Intracellular Endosomal/Lysosomal Escape. *Mol. Pharm.* **15**, 5374–5386 (2018).
207. Nelson, C. E. *et al.* Balancing cationic and hydrophobic content of PEGylated siRNA polyplexes enhances endosome escape, stability, blood circulation time, and bioactivity in vivo. *ACS Nano* **7**, 8870–8880 (2013).
208. Press, D. Endocytosis and exocytosis of nanoparticles in mammalian cells. 51–63 (2014).
209. Soenen, S. J. *et al.* Cellular toxicity of inorganic nanoparticles: Common aspects and guidelines for improved nanotoxicity evaluation. *Nano Today* **6**, 446–465 (2011).

210. Soenen, S. J., Parak, W. J., Rejman, J. & Manshian, B. (Intra)cellular stability of inorganic nanoparticles: Effects on cytotoxicity, particle functionality, and biomedical applications. *Chem. Rev.* **115**, 2109–2135 (2015).
211. Levy, M., Angeles, L., Maraloiu, V. & Wilhelm, C. Degradability of superparamagnetic nanoparticles in a model of intracellular environment : Follow-up of magnetic , structural and chemical properties Degradability of superparamagnetic nanoparticles in a model of intracellular environment : follow-up of m. (2010).
212. Soenen, S. J. H. *et al.* Intracellular nanoparticle coating stability determines nanoparticle diagnostics efficacy and cell functionality. *Small* **6**, 2136–2145 (2010).
213. Mao, S. *et al.* Synthesis , characterization and cytotoxicity of poly ( ethylene glycol ) - graft-trimethyl chitosan block copolymers. **26**, 6343–6356 (2005).
214. Opanasopit, P. *et al.* Effect of salt forms and molecular weight of chitosans on in vitro permeability enhancement in intestinal epithelial cells (Caco-2). *Pharm. Dev. Technol.* **12**, 447–455 (2007).
215. Carrefio-gmez, B. & Duncan, R. *intemational journal of pharmaceutics* Evaluation of the biological properties of soluble chitosan and chitosan microspheres. **148**, (1997).
216. Kean, T., Roth, S. & Thanou, M. Trimethylated chitosans as non-viral gene delivery vectors: Cytotoxicity and transfection efficiency. *J. Control. Release* **103**, 643–653 (2005).
217. Kean, T. & Thanou, M. Biodegradation, biodistribution and toxicity of chitosan. *Advanced Drug Delivery Reviews* **62**, 3–11 (2010).
218. Huang, M., Khor, E. & Lim, L. Y. Uptake and cytotoxicity of chitosan molecules and

- nanoparticles: Effects of molecular weight and degree of deacetylation. *Pharm. Res.* **21**, 344–353 (2004).
219. Qi, L., Xu, Z., Jiang, X., Li, Y. & Wang, M. Cytotoxic activities of chitosan nanoparticles and copper-loaded nanoparticles. *Bioorganic Med. Chem. Lett.* **15**, 1397–1399 (2005).
220. Kim, Y., Pourgholami, M. H., Morris, D. L., Lu, H. & Stenzel, M. H. Effect of shell-crosslinking of micelles on endocytosis and exocytosis: Acceleration of exocytosis by crosslinking. *Biomater. Sci.* **1**, 265–275 (2013).
221. Lu, H. *et al.* Enhanced transcellular penetration and drug delivery by crosslinked polymeric micelles into pancreatic multicellular tumor spheroids. *Biomater. Sci.* **3**, 1085–1095 (2015).
222. Klyachko, N. L. *et al.* Cross-linked antioxidant nanozymes for improved delivery to CNS. *Nanomedicine Nanotechnology, Biol. Med.* **8**, 119–129 (2012).
223. Mathias, J. R. *et al.* NIH Public Access. **33**, 1212–1217 (2010).
224. Quader, S. *et al.* Selective intracellular delivery of proteasome inhibitors through pH-sensitive polymeric micelles directed to efficient antitumor therapy. *J. Control. Release* **188**, 67–77 (2014).
225. Sun, H., Meng, F., Cheng, R., Deng, C. & Zhong, Z. Reduction-sensitive degradable micellar nanoparticles as smart and intuitive delivery systems for cancer chemotherapy. *Expert Opin. Drug Deliv.* **10**, 1109–1122 (2013).
226. Zou, Y. *et al.* Self-crosslinkable and intracellularly decrosslinkable biodegradable micellar nanoparticles: A robust, simple and multifunctional nanoplatform for high-efficiency targeted cancer chemotherapy. *J. Control. Release* **244**, 326–335 (2016).





# Experimental work



# Experimental work

---

## Chapter 1

*Influence of metals on the colloidal properties  
of chitosan-ATP nanogels*

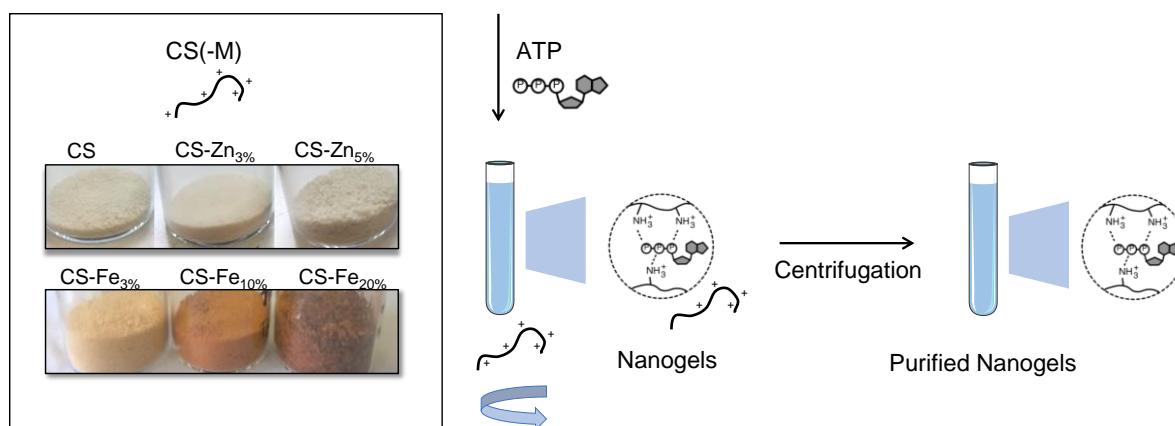


## **Influence of metals on the colloidal properties of chitosan-ATP nanogels**

**ABSTRACT:** Chitosan (CS) nanogels are typically obtained by complexation with tripolyphosphate (TPP) ions, or more recently using triphosphate group-containing drugs such as adenosine triphosphate (ATP). Despite high interest in CS nanogels for drug delivery, due to the biodegradability of CS and to the simple method of preparation, these systems tend to readily disintegrate when diluted in physiological media. Recently, our group proposed the stabilization of the nanogels structure by complexing CS with iron prior to nanogels formation. In this study, we selected iron (III) and zinc (II) to investigate the influence of metal modification on the nanogels' colloidal properties. Moreover, we studied the mechanisms underlying the destabilization of nanogels in physiological conditions and the impact of two physiological factors, notably the ionic strength and the presence of proteins.

Chitosan has been modified with two different metal ions ( $\text{Fe}^{3+}$  and  $\text{Zn}^{2+}$ ) and modified polymers were then used to prepare ATP-loaded nanogels. The formation of nanogels was assessed by Isothermal Titration Calorimetry (ITC) and Dynamic Light Scattering (DLS). The stability of nanogels was evaluated by DLS upon dilutions in NaCl 0,9% or in presence of Fetal Bovine Serum.

The presence of iron showed to strongly limit the phenomenon of nanogels disintegration due to the ionic strength, proving that iron effectively forms new "bridges" between the polymer and the nucleotide leading to the formation of resistant nanoparticles.



## INTRODUCTION

Chitosan-based nanogels are typically obtained by complexation with triphosphate (TPP) ions,<sup>1</sup> or more recently with triphosphate group-containing drugs such as adenosine triphosphate (ATP).<sup>2</sup> Besides the high interest in nanogels prepared by ionotropic gelation,<sup>3</sup> thanks to the biodegradability and biocompatibility of chitosan (CS) and to the easily scalable preparation process, the lack of stability of chitosan-based nanogels in physiological conditions still represents a major concern.<sup>4</sup> In fact, only a few nanogel-based formulations have reached clinical trials for subcutaneous delivery of vaccine antigens, while the clinical translation for all other diverse applications remains to be realized.<sup>5</sup> Literature describing nanogels colloidal stability in physiological conditions is still lacking and filled with opposite reports.

Upon contact with physiological fluids, nanoparticles are generally subjected to a variety of forces, coming from the presence of electrolytes, proteins, lipids, etc. All these factors affect the colloidal stability of nanoparticles in the biological media and consequently their behavior in this environment, in terms of pharmacokinetics, biodistribution, cellular uptake and eventually toxicity.<sup>6</sup> Understanding the factors driving the colloidal stability is therefore essential for the development of safe and effective nano-therapeutics for clinical use. In the case of chitosan-based nanogels, the chitosan molecular weight and concentration have been initially

reported to play an important role in the drug-release pattern.<sup>7</sup> It is also known that the physiological ionic strength can weaken the electrostatic interactions between chitosan chains and the phosphate-containing molecules, leading to nanogels disintegration and dissolution of their components; moreover, the physiological pH neutralizes the cationic amine groups of chitosan (pKa around 6.5), promoting aggregation between the more lyophobic chains.<sup>8</sup> Several approaches have been investigated in order to improve nanogels colloidal stability, in terms of resistance to both disintegration and aggregation. To counter aggregation, many strategies have been proposed based on the surface modification with alginates, hyaluronic acid and poly(lactic-co-glycolic acid) or on the formation of polymer/layered silicate composites.<sup>9</sup> Furthermore, the addition of a monovalent salt in the solvent employed during the preparation process have been shown to improve the colloidal stability of chitosan/TPP nanogels and microgels,<sup>10,11</sup> as well as having an impact on their size and compactness.<sup>12</sup> In a previous work, we proposed the complexation of CS with iron (III) ions prior to nanogels formation with ATP as a strategy to improve their resistance to physiological ionic strength.<sup>13</sup> This can be achieved thanks to the ability of iron (III) to strongly bind to both chitosan and phosphate groups.<sup>14,15</sup> Indeed, CS is known to form coordination complexes with various metal cations, through the oxygen of the C-6 hydroxyl group and the nitrogen of the aminosaccharide group.<sup>16</sup>

In the present study, we attempt to shed lights on the influence of metal modification on the nanogels' colloidal properties in a biological environment. To do so, we selected iron (III) and zinc (II), based on their ability to complex with chitosan,<sup>17,18,19,20,21,22,23,24</sup> and we investigated their ability to efficiently complex chitosan and to form nanogels as a function of the type of metal ions and the metal quantity. More importantly, we tried to give insight into the mechanism of nanogels formation as well as destabilization in physiological conditions, not only by disintegration but also by aggregation, induced by ionic strength and proteins.

## RESULTS

### 1. Synthesis of chitosan-metal (CS-M) complexes

Chitosan–iron (CS–Fe) complexes containing increasing iron content were obtained by complexation of chitosan using iron (III) nitrate at different initial concentrations. This concentration was found to be the key factor to control the amount of bound iron, since it determines the pH of the solution and, consequently, the protonation degree of chitosan. As evaluated by a phenanthroline-based assay and confirmed by inductively coupled plasma-optical emission spectrometry (ICP-OES), CS-Fe complexes containing around 3%, 10% and 20% w/w of iron were obtained. Elemental analysis results (**Table S1**) are consistent with iron dosage and suggest the presence of nitrate impurities in the final complexes, difficult to eliminate. To assess the efficacy of iron complexation, CS-Fe complexes were also analyzed by infrared spectroscopy. The FT-IR spectra of CS and CS-Fe complexes are given in **Fig. 1**. All CS–Fe complexes present a similar spectrum, clearly different from CS. The two large absorption bands in the region  $> 3000\text{ cm}^{-1}$  of the CS spectrum, typically due to -OH and -NH stretching, clearly disappear along with the iron content. This is consistent with the limitation of movements of these bonds following interaction with iron. Moreover, the binding of the metal with the ammine group is confirmed by the decrease of intensity of the N-H bending peak at  $1630\text{ cm}^{-1}$  and by the decrease in intensity between  $1000$  and  $1350\text{ cm}^{-1}$  due to the C-N bending. These observations are consistent with proposed models of chitosan-iron complexes describing two amino groups and four hydroxyl groups for each Fe (III) ion.<sup>14</sup> Taking into account the average molar weight of a chitosan monomer and an iron atom, the maximum theoretical iron content of the complex is around 20% w/w. This means that in CS-Fe<sub>20%</sub> all chitosan monomers are bound to iron.

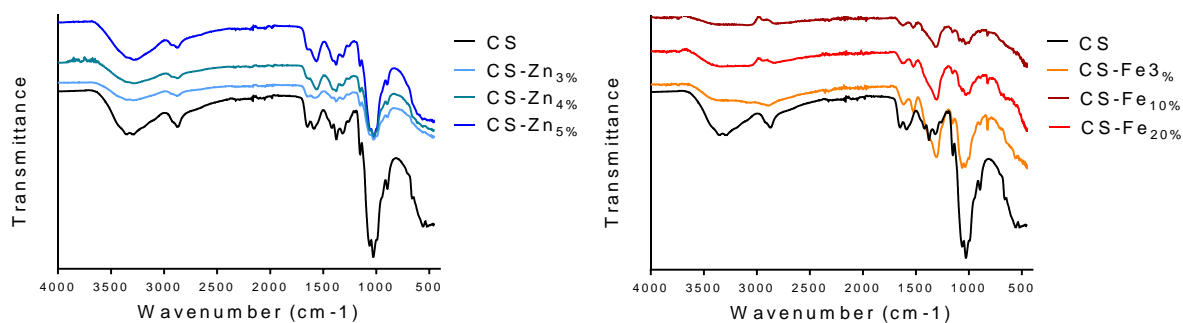


**Figure 1.** IR spectra of CS-Zn and CS-Fe complexes, compared to unmodified CS. For each curve, the highest point has to be considered as 100% of transmittance.

Chitosan–zinc (CS–Zn) complexes were obtained by complexation of chitosan using zinc (II) acetate at different concentrations and keeping the pH at around 4 during the reaction. The concentration of zinc (II) nitrate did not play a key role in controlling the amount of bound zinc. Indeed, complexes obtained presented closed values of zinc content (3-5%), as evaluated by UV–vis spectroscopy. Elemental analysis (**Table S1**) results are consistent with the zinc dosage. To assess the efficacy of zinc complexation, CS-Zn complexes were analyzed by infrared spectroscopy. The FT-IR spectra of CS and CS-Zn complexes are given in **Fig. 1**. The two absorption bands in the region  $> 3000 \text{ cm}^{-1}$  of the CS spectrum, due to -OH and -NH stretching, appear less visible. This is in agreement with the limitation of movements of -OH and -NH groups following interaction with zinc. This observation is consistent with proposed models of chitosan-zinc complexes according to which the zinc bond to one or two amino groups and hydroxyl groups of one or more CS chains.<sup>18</sup> However, the zinc content of the complex is far from the theoretical maximum value, which vary from 20% to 40% w/w depending on the chosen model.

## 2. Formation and characterization of nanogels from CS(-M) and ATP

### 2.1 Size, polydispersity and zeta potential of CS-M/ATP nanogels

Colloidal suspensions were successfully obtained from all chitosan-iron and chitosan-zinc complexes described above and ATP, similarly to what was known for chitosan<sup>2</sup> and chitosan complexes containing lower amounts of iron.<sup>13</sup> The resulting nanogels have been characterized as a function of ATP amounts added to CS(-M) solutions, expressed using classical N/P ratios (triphosphate derivative concentrations are expressed as phosphate groups “P” and CS concentration as nitrogen “N” from amine and amide groups). Increasing ATP/CS-M ratios correspond to decreasing N/P ratios. As shown in **Fig.2**, the addition of ATP to various CS-M complexes led to nanoparticles formation until a critical N/P ratio in a similar way to CS. At the so-called “critical N/P ratio” (that presented comparable values for all CS-M/ATP nanogels) (**Tab.1**), the smallest nanoparticles with the narrowest size distribution were obtained. For N/P ratios lower than the critical ones, visible aggregation and immediate sedimentation were observed for all CS(-M) formulations. However, the evolution of nanoparticle size, polydispersity and surface charge as a function of the N/P ratio is strongly influenced by the metal presence. CS-Fe based nanogels exhibit a smaller size (< 150 nm diameter) at any N/P ratio, independently from the iron content. CS-Zn based nanoparticles size show intermediate values between CS and CS-Fe nanogels at all N/P ratios higher than the critical one. This may be explained by a denser condensation of nanogels in presence of metal ions, which is even more pronounced in the case of nanogels containing iron. The particle size distribution of CS-Fe nanogels is less polydisperse at any N/P ratio with pDI values always below 0.23. Iron seems then to play a role also in reducing particles polydispersion, contrary to the zinc.

Concerning the zeta potential evolution, the same trend was observed, with a progressive decrease until reaching the minimum value around the N/P that is consistent with the formation

of ionic bonds between ammine groups of chitosan and phosphate groups of ATP. The presence of metals has been showed to decrease the zeta potential at N/P higher than the critical N/P ratio. This could be explained by the involvement of ammine groups in the coordination complex with metals.

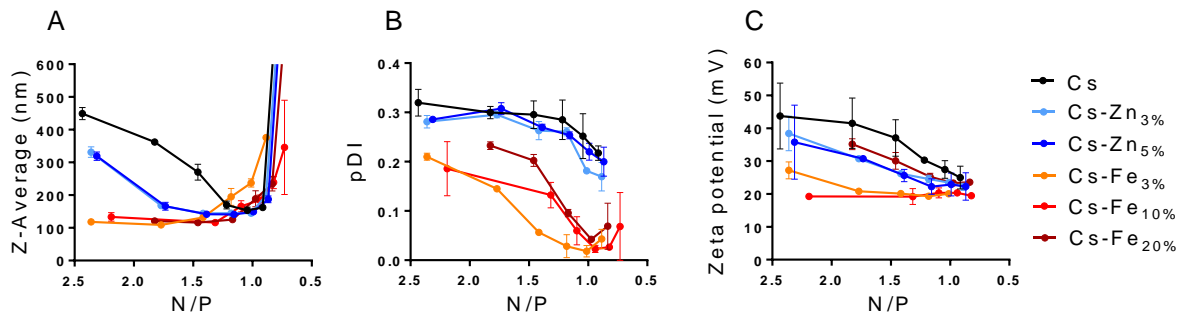


**Figure 2.** (A) Mean hydrodynamic size (Z-Average), (B) polydispersity index (pDI), and (C) zeta potential of CS-M/ATP nanogels obtained from CS-M solutions (M = Fe, Zn) and increasing amounts of ATP solution, expressed as a function of the N/P ratio, and compared to CS/ATP nanogels (increasing ATP/CS-M ratios correspond to decreasing N/P ratios).

**Table 1.** Average size, pDI and zeta potential of nanogel formulations prepared from ATP and CS-M (M = Fe, Zn) at the corresponding critical N/P ratio, compared to CS/ATP nanogels.

Nanogel formulation	Critical N/P ratio	Corresponding ATP/CS ratio	Size (nm)	pDI	Zeta potential (mV)
CS/ATP	1.04	0.32	154 ± 9	0.25 ± 0.04	27.4 ± 10
CS-Zn <sub>3%</sub> /ATP	1.01	0.33	145 ± 1	0.18 ± 0.01	23.5 ± 0.35
CS-Zn <sub>5%</sub> /ATP	0.99	0.34	149 ± 6	0.22 ± 0.02	22.8 ± 3.4
CS-Fe <sub>3%</sub> /ATP	1.42	0.23	132 ± 6	0.06 ± 0.01	20,1 ± 0.72
CS-Fe <sub>10%</sub> /ATP	1.31	0.25	116 ± 0.16	0.13 ± 0.02	19.2 ± 2.43
CS-Fe <sub>20%</sub> /ATP	1.17	0.28	125 ± 4.84	0.09 ± 0.01	25.3 ± 1.04

## 2.2 Isothermal titration calorimetry studies

The thermodynamics of nanogels formation was determined by isothermal titration calorimetry in the same mixing conditions. Results (**Fig. 3**) show similar thermodynamic profiles for all different CS(-M), with two different steps. The first part is endothermic and occurs for ATP/CS(M) ratios below around 0.2 (ie. N/P ratios above around 1.66) corresponding to the electrostatic interactions between the ammine groups of chitosan and the phosphate groups of ATP and to the formation of a colloidal suspension, similarly to what was observed above. The second part (higher ATP/CS(-M) ratios, or lower N/P ratios) is exothermic and corresponds mainly to the domain of macroscopic aggregation determined similarly. For the first part of the curves, all thermodynamic parameters were extracted from the two set of sites fitting model. Importantly, the molar ratios of the reactions were consistent with the critical N/P ratios observed by DLS analysis. As shown in **table 2**, in all cases, isotherms obtained after subtraction of the integrated heat of dilution revealed endothermic reactions, implying higher entropic contributions to account for the thermodynamically favorable ( $\Delta G < 0$ ) reaction. The entropic gain may be due to the release of counterions from ammonium groups of chitosan and phosphate groups of ATP and this phenomenon appeared to be much more pronounced in presence of metals. As for the enthalpy, the absolute values are clearly higher in presence of metals compared to non-modified chitosan. According to the binding constants  $K$ , the amino groups of chitosan-metal complexes (CS-M), probably sterically hindered because of the metal cross-linkage, seems less suitable for the electrostatic interaction compared to the less obstructed amino groups of native chitosan (CS).

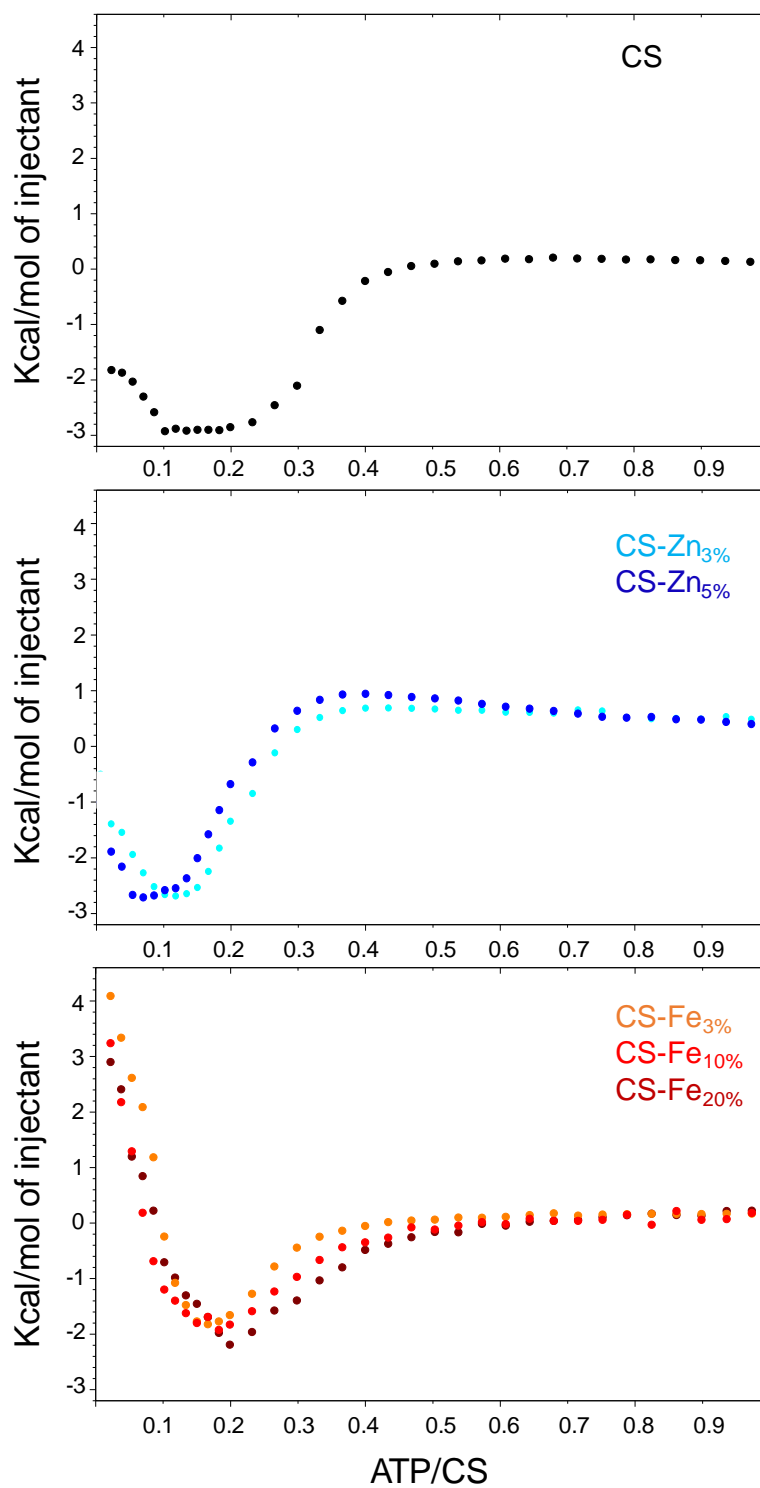


**Figure 3.** Isothermal titration calorimetry study of the interaction between ATP and CS(-M). Titration curves show the integrated heat plotted against the ATP/CS molar ratio.

**Table 2.** Binding affinity (K) and thermodynamic parameters ( $\Delta H$ ,  $-T\Delta S$ ,  $\Delta G$ ) calculated according to the one site binding model for the electrostatic interactions of chitosan and chitosan-metal complexes with ATP, on the first part of the titration

Nanogel formulation	Ka, 10 <sup>3</sup> M	$\Delta H$	$-T\Delta S$	$\Delta G$
CS/ATP	177000	1328	-8497	-7169
CS-Zn <sub>3%</sub> /ATP	36600	7141	-13357	-6216
CS-Zn <sub>5%</sub> /ATP	34100	11140	-17322	-6182
CS-Fe <sub>3%</sub> /ATP	135000	6778	-13774	-6996
CS-Fe <sub>10%</sub> /ATP	65000	7487	-14042	-6555
CS-Fe <sub>20%</sub> /ATP	29300	8691	-14788	-6097

### 3. Influence of Metals on nanogels colloidal stability in physiological media

#### 3.1 Impact of ionic strength on nanogels colloidal stability

The resistance of all nanogels formulations to the ionic strength was evaluated by following the relative intensity of the scattered light by DLS after incubating nanogels at 37°C in isotonic conditions (0.9% w/v NaCl). The results obtained (**Fig.4**) confirmed previous studies showing that CS-ATP nanoparticles readily dissociate in a physiological solution without aggregation or swelling but rather through chitosan dissolution. The stability profile of CS-Zn nanogels did not exhibit any significant differences compared to CS-ATP nanogels. In these cases, the ionic bond between CS and phosphate groups seems to be easily displaced by the electrolyte ions. On the contrary, nanoparticle stability was found to be clearly increased by the presence of iron, consistently with the metal content. By comparing nanogels containing the same amount of Fe or Zn (3%) it can be confirmed that iron-containing nanogels are more stable in the time. CS-Fe<sub>20%</sub> nanogels presented a good stability until 72h, which means that the interactions between iron and phosphate groups are not displaced by the electrolyte ions.

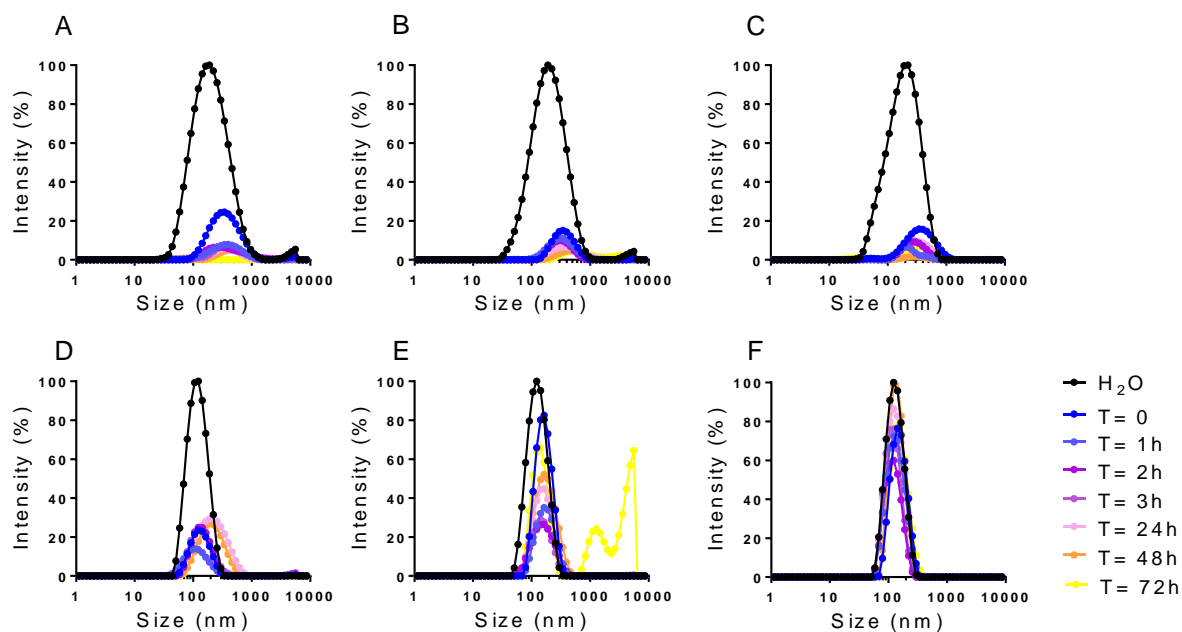


**Figure 4.** Representative size distribution as a function of relative intensity of dynamic light scattering (DLS) of CS/ATP (A), CS-Zn<sub>3</sub>%/ATP (B), CS-Zn<sub>5</sub>%/ATP (C), CS-Fe<sub>3</sub>%/ATP (D), CS-Fe<sub>10</sub>%/ATP (E) and CS-Fe<sub>20</sub>%/ATP nanogels (F) during incubation at 37°C in a physiological solution (0.9% NaCl).

The purification of nanogels consists in eliminating by centrifugation the chitosan and ATP fractions that are not involved in the nanogel formation. The impact of this step on the nanogels colloidal properties was also investigated. In all cases, this purification step was proved to have no influence on the stability of nanogels in presence of NaCl compared to non-purified ones.

### 3.2 Impact of proteins on nanogels colloidal stability

The stability of all nanogels formulations in presence of proteins was evaluated by DLS analysis after incubating nanogels at 37°C in presence of 10% of fetal bovine serum. All non-purified nanogel formulations investigated (CS/ATP, CS-Zn/ATP, CS-Fe/ATP) lead to immediate and macroscopic aggregation upon dilution in FBS-containing media. This nanogel destabilization,

could be due to the surface charge neutralization of nanogels by negatively-charged proteins or to a bridging flocculation phenomenon, but could also involve residual free chitosan chains present in the medium.

The same study was performed on purified nanogel formulations, ie. after removal of free chitosan fractions. The results showed that purified CS/ATP and CS-Zn/ATP nanogels readily aggregate in presence of proteins, as non-purified ones. In contrast, CS-Fe/ATP nanogels exhibit a significantly increased resistance to the aggregation, consistently with the metal content (**Fig.6**).

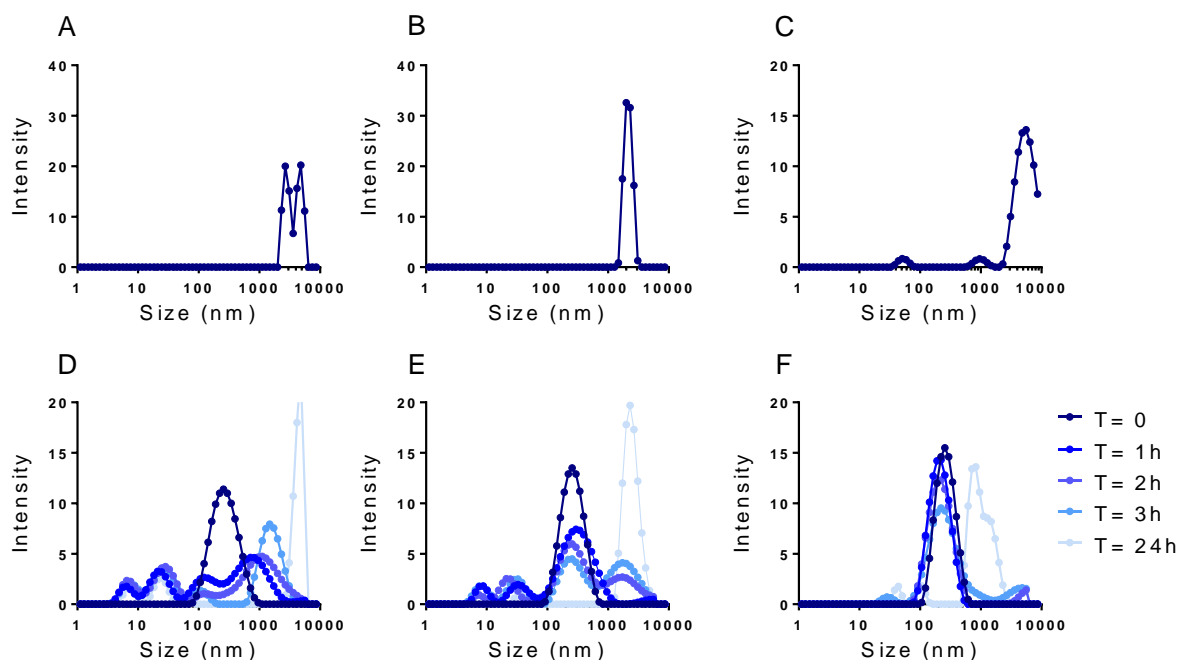


**Figure 6.** Representative size distribution of CS/ATP (A), CS-Zn<sub>3%</sub>/ATP (B), CS-Zn<sub>5%</sub>/ATP (C), CS-Fe<sub>3%</sub>/ATP (D), CS-Fe<sub>10%</sub>/ATP (E) and CS-Fe<sub>20%</sub>/ATP (F) nanogels after removal of free CS(-M) fraction by purification, during incubation at 37°C in presence of 10% of fetal bovine serum (FBS), evaluated by dynamic light scattering (DLS).

These results show that both the presence of iron in the nanogel together with the removal of free CS-Fe chains in the formulation confer a unique resistance to aggregation induced by

proteins. The existence of an interaction between free, soluble CS and CS-M and serum proteins has been confirmed by the observation of macroscopic aggregates upon incubation of CS(-M) solutions in FBS-containing medium in the same conditions (**Fig.S2**). **Table 2** summarizes the observations.

**Table 2.** Summary of the behavior of CS(-M)/ATP nanogels, in terms of disassembly in a salt-containing medium and in terms of aggregation in a protein-containing medium, highlighting the role of the metal used, the role of free CS(-M) chains and of their removal by purification (na, non applicable).

	Disassembly in isotonic NaCl medium	Aggregation in proteins-containing medium
Free CS or CS-M	na	+
CS/ATP nanogels		
-Non-Purified	+	+
-Purified	+	+
CS-Zn/ATP nanogels		
-Non-Purified	+	+
-Purified	+	+
CS-Fe/ATP nanogels		
-Non-Purified	-	+
-Purified	-	-

## DISCUSSION

Our group has previously shown that the incorporation of moderate amounts of iron (III) into CS/ATP nanogels improves their resistance to dissociation in salt-containing media.<sup>13</sup> In this study, to further understand the role of the nature and the proportion of metal ions in the behavior of these organometallic colloids in several physiological media, chitosan was first modified by complexation with different amounts of Zn (II) and Fe (III). FT-IR, UV-vis spectroscopy and elemental analysis were used to characterize all the complexes obtained and provide concordant results. The synthesis of chitosan-iron complexes from Fe(NO<sub>3</sub>)<sub>3</sub> showed

to be strongly influenced by the pH and can be tuned to achieve up to 20% w/w of iron content in the complex. In contrast, the maximum amount of metal for the chitosan-zinc complexation stood at 5% w/w.

Nanogels were successfully obtained by ionic cross-linking of positively charged chitosan or chitosan-metal complexes with negatively charged ATP. The mechanism of formation of nanoparticles has been analyzed by dynamic light scattering and by isothermal titration calorimetry. According to both techniques, all ATP-loaded nanogels formed in a similar way, from the point of view of N/P ratios range and zeta potential decrease until the critical N/P ratio, after which all nanoparticles aggregate and precipitate. Nanogels formation is usually a multiple process, mainly driven by the electrostatic interactions between amine groups and phosphate groups in the case of CS/ATP nanogels, and extremely influenced by conformational rearrangements, desolvation and reduced flexibility in the case of metal-modified chitosan. The presence of metals exhibited a reducing effect on the size and the polydispersity of nanoparticles. At the critical N/P ratio smaller and more homogenous nanoparticles can be obtained in presence of chitosan-iron complexes, suggesting a higher degree of compactness of nanogels.

The stability of nanogels has been studied in isotonic NaCl solutions and in presence of proteins (1/10 serum). According to previous studies, the ionic strength tends to weaken electrostatic interactions inside of nanogels leading to their disassembly by dissolution, which has been mitigated by the use of chemical cross-linking,<sup>25</sup> nanogel formation in presence of high salt concentration,<sup>10</sup> or incorporation of moderate amounts of iron (III).<sup>13</sup> We show here that the stabilization effect of iron is maximal at a 20% w/w content in the CS-Fe complex, for as long as 72 h. However, this effect cannot be obtained from CS-Zn complexes, which could be due to the lower Zn content of the CS-Zn complex and to a lower affinity of Zn ions towards phosphate groups of ATP.

The instability of chitosan-based nanogels in presence of serum proteins causing aggregation has long been reported, and may have restricted their application mostly to mucosal routes.<sup>26</sup> This aggregation behavior is classically believed to result from the interaction between negatively-charged proteins and positively-charged nanogel surface. In contrast, we show here that CS-Fe<sub>20%</sub>/ATP nanogels, despite exhibiting a positive surface charge, resist aggregation in presence of serum proteins, provided that the fraction of free CS-Fe chains are removed from the formulation. This pivotal role of both iron and free CS(-M) chains appears in our systematic comparison (**Table 2**) and provides the basis of a hypothetical mechanism of CS(-M)-based nanogel aggregation in presence of proteins (**Fig. 8**). This mechanism can be described in three cases: (i) whenever free CS(-M) chains are present, they will induce aggregation in presence of proteins; (ii) when purified nanogels are not resistant to ionic strength (ie., CS/ATP, CS-Zn/ATP), they may be disassembled in presence of serum, releasing CS or CS-Zn chains, inducing in turn aggregation; (iii) only nanogels resistant to ionic strength and devoid of free CS-M chains (ie., purified CS-Fe<sub>20%</sub>/ATP) may resist aggregation induced by serum proteins.

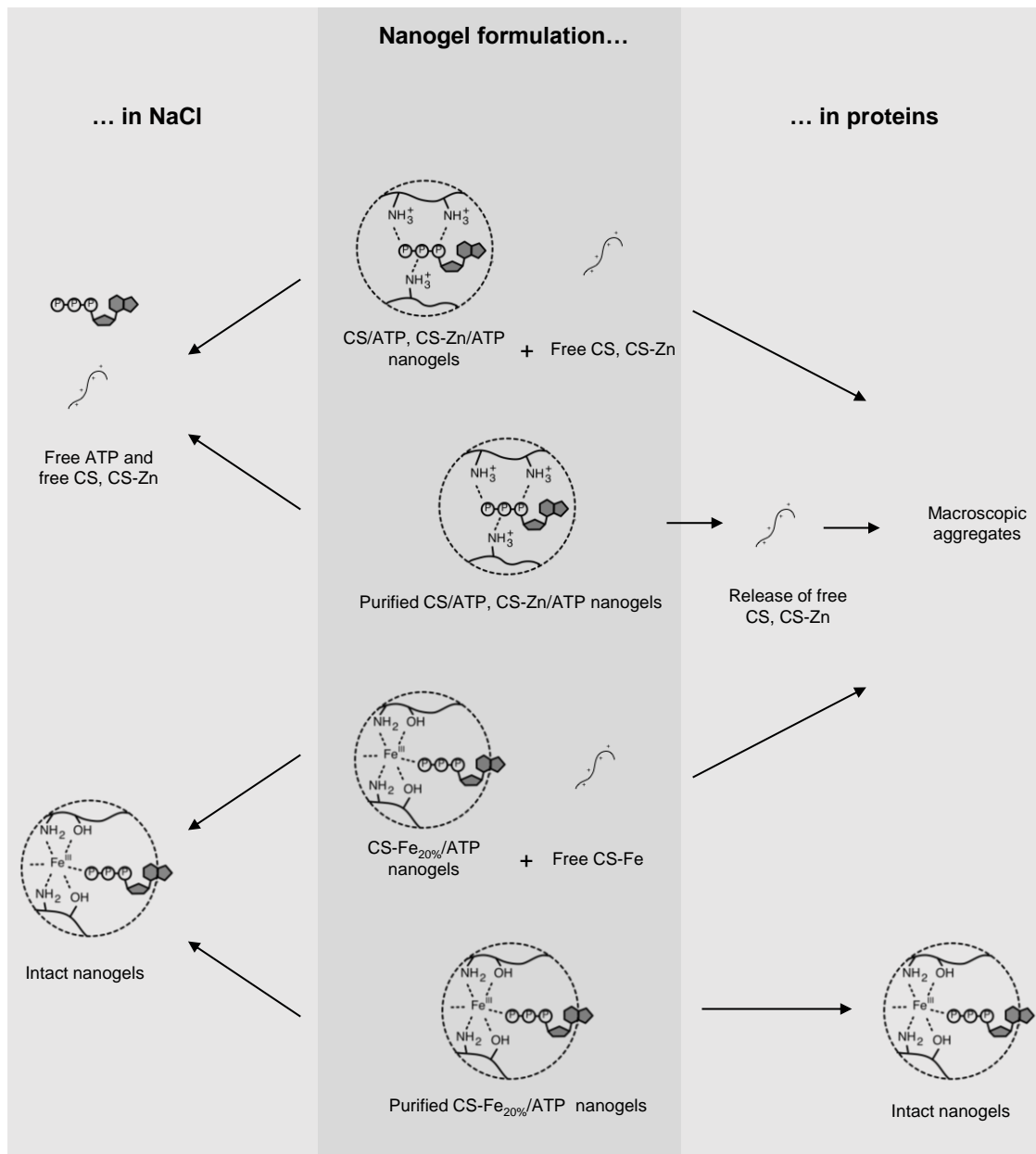


**Figure 8.** Proposed mechanism of nanogel instability in physiological conditions.

## CONCLUSIONS

In this work, CS-Fe complexes and CS-Zn complexes were synthesized and investigated for their ability to form colloids by ionotropic gelation in presence of ATP. Only iron significantly impacts nanogel size and homogeneity, contrary to zinc, suggesting a condensation and reinforcement of nanogels structure by organometallic bounds. The impact of two physiological

factors, notably the ionic strength and the presence of proteins, on ATP nanogels stability also highlighted the specific role of iron. Our outcomes suggest that two different mechanisms of nanogels destabilization in physiological conditions (disassembly caused by the presence of electrolytes and aggregation in presence of proteins) can be addressed by the use of CS-Fe<sub>20%</sub> for nanogel preparation combined with the removal of free CS-Fe. This also suggests a more complex mechanism of chitosan-based nanogel aggregation than mere electrostatic interaction with serum proteins.

## EXPERIMENTAL

### *Materials*

Nanogels were prepared using low viscosity chitosan and ATP purchased from Sigma-Aldrich (France). The degree of N-deacetylation of commercial chitosan was determined to be 84% by <sup>1</sup>H NMR spectroscopy. In the following, water refers to MilliQ® purified water of resistivity ≥ 18.2 MΩ.cm (Millipore, France). Complexation of CS with iron was achieved with iron (III) nitrate nonahydrate, 1,10-phenanthroline monohydrate and hydroxylamine hydrochloride from Sigma. Complexation of CS with zinc (II) was achieved with zinc (II) acetate dihydrate and 1,2-pyridylazo-2-naphtol (PAN) from Fluka. Fetal bovine serum (FBS) was from Gibco. Other reagents used were purchased from Sigma; all solvents were of analytical grade.

### *Preparation and characterization of CS-Fe complexes*

Three different chitosan-iron (CS-Fe) complexes were prepared as described previously.<sup>13</sup> Briefly, 1 g of CS was added under mechanical stirring to 100 mL of 0.1 M Fe(NO<sub>3</sub>)<sub>3</sub> solution (pH = 2.3), 100 mL of 0.5 M Fe(NO<sub>3</sub>)<sub>3</sub> solution (pH = 1.9) or 100 mL of 1 M Fe(NO<sub>3</sub>)<sub>3</sub> solution (pH = 1.6) in the case of CS-Fe<sub>20%</sub>, Cs-Fe<sub>10%</sub> and Cs-Fe<sub>30%</sub> respectively, and stirred overnight at RT to yield CS-Fe complexation. The resulting complexes were then precipitated

through the addition of 500 mL acetone and repeatedly washed with acetone to remove unbound iron. The presence of free iron in the filtrate was assessed through the addition of ascorbic acid, which turns brown in presence of iron. The fractions of carbon, hydrogen and nitrogen present in the complexes were determined by elemental analysis. The association of iron to chitosan was quantified after hydrolysis of CS-Fe complexes in concentrated nitric acid and chloridric acid 1:1 at 200 °C. The iron was dosed by inductively coupled plasma-optical emission spectrometry (ICP-OES) using an iCAP 6300 series Duo ICP spectrometer (Thermo Scientific, Waltham, USA) and through a colorimetric UV-vis spectroscopy dosage using phenanthroline, as described previously.<sup>13</sup> These conditions yielded three different CS-Fe complexes with approximately 3%, 10% and 20% iron content (named respectively CS-Fe<sub>3%</sub>, CS-Fe<sub>10%</sub> and CS-Fe<sub>20%</sub> in the following). FT-IR spectra of CS-Fe complexes were acquired using a Spectrum Two FT-IR Spectrometer (Perkin Elmer) with a Diamond ATR accessory, between 4000 and 400 cm<sup>-1</sup>. The spectral resolution was 4 cm<sup>-1</sup> and 20 scans were averaged. Data were acquired using the software Spectrum Touch and processed with Time Base v.3.1.2.

### ***Preparation and characterization of Cs-Zn complexes***

Three different chitosan-zinc (CS-Zn) complexes were prepared according to a previously described method,<sup>24</sup> with some modifications. 1 g of CS was added under mechanical stirring to 100 mL of 0.1 M Zn(CH<sub>3</sub>COO)<sub>2</sub> solution (pH = 6.4), 0.5M Zn(CH<sub>3</sub>COO)<sub>2</sub> solution (pH = 5.9) or 1M Zn(CH<sub>3</sub>COO)<sub>2</sub> solution (pH = 5.6). The pH was adjusted at 4 with NaOH and the mixture was stirred overnight at RT to yield CS-Zn complexation. The resulting complexes were then precipitated through the addition of 500 mL acetone, washed with ethanol and dried. Powders were then suspended in EtOH:H<sub>2</sub>O 1:1, repeatedly washed and dried. The fractions of carbon, hydrogen and nitrogen present in the complexes were determined by elemental analysis. The association of zinc to chitosan was quantified after hydrolysis of CS-Zn complexes in

concentrated nitric acid and chloridric acid 1:1 at 200 °C. The quantity of Zn(II) associated to chitosan was determined by UV–vis spectroscopy using according to a procedure described in the literature.<sup>24</sup> These conditions yielded three different CS-Zn complexes with approximately 3%, 4% and 5% iron content (named respectively CS-Zn<sub>3%</sub>, CS-Zn<sub>4%</sub> and CS-Zn<sub>5%</sub> in the following). FT-IT spectra of CS–Zn complexes were acquired using a Spectrum Two FT-IR Spectrometer (Perkin Elmer) with a Diamond ATR accessory, between 4000 and 400 cm<sup>-1</sup>. The spectral resolution was 4 cm<sup>-1</sup> and 20 scans were averaged. Data were acquired using the software Spectrum Touch and processed with Time Base v.3.1.2.

### ***Preparation and characterization of ATP-loaded nanoparticles***

CS and CS-M solutions were obtained by dissolving low viscosity CS powder or CS-M powder at a final concentration of 1 mg/mL in a 1.75% v/v acetic acid aqueous solution, stirring overnight and filtrating through 0.22 µm filter. A freshly prepared solution of ATP at a concentration of 15 mg/mL was added dropwise to the CS and CS-M solutions under stirring at 1000 rpm to allow nanogels formation. To study the nanogels formation domains, increasing amounts of ATP solution, from 0.02 to 0.2 mL, were added dropwise to 0.5 mL of a 1 mg/mL CS solution or CS-M solution under magnetic stirring at 1000 rpm. For further studies, nanoparticles have been prepared at the so-called critical N/P ratio (triphosphate derivative concentrations are expressed as phosphate groups “P” and CS concentration as nitrogen “N” from amine and amide groups). To study the impact of the elimination of the free CS(-M) on the colloidal stability, nanogels have been purified as follows: 1 mL of nanogels suspension was centrifuged on a 20 µL glycerol layer at 2000 × g for 1 h. 0.92 mL of supernatant was then removed and pellet was redispersed in 1 mL (final volume) of water. The mean hydrodynamic diameter and the polydispersity index (PdI) of nanogels were determined in triplicate by dynamic light scattering (DLS) and the zeta potential by electrophoretic light scattering (ELS)

after 1/20 sample dilution in 1 mM NaCl solution, using a Zetasizer Nano ZS (Malvern Instrument, Malvern, UK) with a 173° scattering angle at a temperature of 25°C. The results were represented as the size distribution by intensity percentage.

### ***Isothermal titration calorimetry studies***

Isothermal titration calorimetry (ITC) measurements were performed on a Microcal VP-ITC with a cell volume of 1.441 mL at 25° C. For each experiment, a 5.4 mM ATP solution was injected into the cell containing a CS or CS-M dissolved in a 1.75% v/v acetic acid aqueous solution at the concentration of 0.3 mg/mL CS (which corresponds to 1.192 mM as CS monomer unit). Volumes of 5 µL or 10 µL of ATP solution were injected with spacing times ranging from 800 to 1000 s, while the solution/suspension was stirred at 394 rpm. The heat of dilution was measured by injecting the ATP solution into the buffer solution, and these values were then subtracted in order to obtain the actual heat of binding. The fit of the curves was calculated with Origin7 (Chi-square values between 900 and 7000) and values found were used to determine the free Gibbs energy.

### ***Impact of ionic strength on nanogels colloidal stability***

The impact of the ionic strength on nanogels colloidal stability was evaluated by dynamic light scattering (DLS) by comparing nanogels at the same concentration in water or in a physiological saline solution (0.9% w/v NaCl). The relative intensity (corresponding to the scattered light intensity corrected by the derived count rate) was measured using a Zetasizer Nano ZS (Malvern Instrument, Malvern, UK) with a 173° scattering angle at 25°C. For each condition, the laser power (attenuation index) and the measurement position from the “outer” square cuvette wall were fixed to have similar light intensity entering the sample cuvette. Data are expressed as the

relative intensity of the nanogel suspension diluted in the saline solution compared to the nanogel suspension diluted in water.

### ***Impact of proteins on nanogels colloidal stability***

The impact of proteins on nanogels colloidal stability was evaluated by dynamic light scattering by comparing nanogel at the same concentration in water or in an aqueous solution containing 10% fetal bovine serum (FBS), as described above. Data are expressed as the relative intensity of the nanogel suspension diluted in the protein solution compared to the nanogel suspension diluted in water.

## **ACKNOWLEDGMENTS**

Thanks to Najet Yagoubi for the IR Analysis, Françoise Chuburu for ICP measurements, Paul van Tassel for helpful discussions on ITC experiments, Magali Noiray for ITC experiments, Nelly Alaglo for contribution on the synthesis of CS-Zn complexes and Marion Quaillet for her help in the experiments.

## **REFERENCES**

1. Alonso, M. J., Calvo, P. & Remun, C. Novel Hydrophilic Chitosan – Polyethylene Oxide Nanoparticles as Protein Carriers. 125–132.
2. Giacalone, G., Fattal, E. & Hillaireau, H. Drug-Induced Nanocarrier Assembly as a Strategy for the Cellular Delivery of Nucleotides and Nucleotide Analogues. 0–5 (2013).
3. Wang, H., Qian, J. & Ding, F. Recent advances in engineered chitosan-based nanogels

- for biomedical applications. *J. Mater. Chem. B* **5**, 6986–7007 (2017).
4. Huang, Y., Cai, Y. & Lapitsky, Y. tripolyphosphate micro- and nanogels : 5957–5970 (2015).
  5. Soni, K. S., Desale, S. S. & Bronich, T. K. Nanogels: an overview of properties, biomedical applications and obstacles to clinical translation. 109–126 (2017).
  6. Moore, T. L. *et al.* Chem Soc Rev media and impact on cellular interactions †. 6287–6305 (2015).
  7. Ko, J. A., Park, H. J., Hwang, S. J., Park, J. B. & Lee, J. S. Preparation and characterization of chitosan microparticles intended for controlled drug delivery. **249**, 165–174 (2002).
  8. López-león, T., Carvalho, E. L. S., Seijo, B., Ortega-vinuesa, J. L. & Bastos-gonzález, D. Physicochemical characterization of chitosan nanoparticles : electrokinetic and stability behavior. **283**, 344–351 (2005).
  9. Press, D. Preparation , characterization , and potential application of chitosan , chitosan derivatives , and chitosan metal nanoparticles in pharmaceutical drug delivery. 483–507 (2016).
  10. Huang, Y. & Lapitsky, Y. Monovalent Salt Enhances Colloidal Stability during the Formation of Chitosan / Tripolyphosphate Microgels. 10392–10399 (2011).
  11. Jonassen, H., Kjøniksen, A. & Hiorth, M. Stability of Chitosan Nanoparticles Cross-Linked with Tripolyphosphate. (2012).
  12. Jonassen, H., Kjøniksen, A. & Hiorth, M. Effects of ionic strength on the size and compactness of chitosan nanoparticles. 919–929 (2012).

13. Giacalone, G. *et al.* Stabilization and cellular delivery of chitosan – polyphosphate nanoparticles by incorporation of iron. *J. Control. Release* **194**, 211–219 (2014).
14. Bhatia, S. C. & Ravi, N. A Magnetic Study of an Fe - Chitosan Complex and Its Relevance to Other Biomolecules. 413–417 (2000).
15. Follmann, B. K. S. H. *et al.* Characterization and Extracorporeal Application of a New Phosphate-Binding Agent. **32**, 733–739 (1994).
16. Varma, A. J., Deshpande, S. V & Kennedy, J. F. Metal complexation by chitosan and its derivatives : a review. **55**, 77–93 (2004).
17. Deshpande, P., Dapkekar, A., Oak, M. D., Paknikar, K. M. & Rajwade, J. M. Zinc complexed chitosan / TPP nanoparticles : a promising micronutrient nanocarrier suited for foliar application. *Carbohydr. Polym.* (2017).
18. Wang, X., Du, Y. & Liu, H. Preparation , characterization and antimicrobial activity of chitosan – Zn complex. **56**, 21–26 (2004).
19. Ou, C. *et al.* Journal of Analytical and Applied Pyrolysis Study on the thermal degradation kinetics and pyrolysis characteristics of chitosan-Zn complex. *J. Anal. Appl. Pyrolysis* **122**, 268–276 (2016).
20. Khan, A., Mehmood, S., Sha, M. & Yasin, T. Structural and antimicrobial properties of irradiated chitosan and its complexes with zinc. **91**, 138–142 (2013).
21. Wang, R. *et al.* Preparation of low-molecular-weight chitosan derivative zinc complexes and their effect on the growth of liver cancer cells in vitro \*. **81**, 2397–2405 (2009).
22. Vlasov, P. S., Kiselev, A. A., Domnina, N. S., Popova, E. V & Tyuterev, S. L. Synthesis and Biological Activity of Metal Chitosan Complexes. **82**, 1675–1681 (2009).

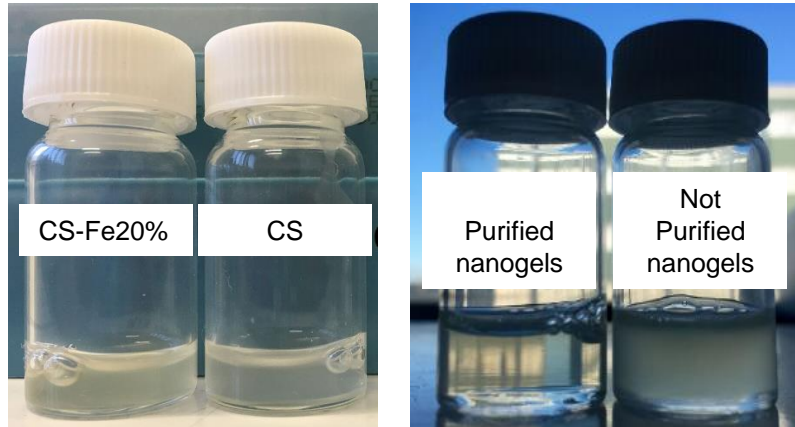
23. Taylor, P. Journal of Liquid Chromatography & Related PREPARATION , CHARACTERIZATION , AND CHROMATOGRAPHY PROPERTIES OF CHITIN MODIFIED WITH FeCl<sub>3</sub>. 37–41 doi:10.1081/JLC-100101697.
24. Reynaud, F., Tsapis, N., Deyme, M., Vasconcelos, G. & Gueutin, C. Kinetic and equilibrium studies. 7304–7312 (2011).
25. Mi, F., Sung, H., Shyu, S., Su, C. & Peng, C. Synthesis and characterization of biodegradable TPP / genipin co- crosslinked chitosan gel beads. **44**, 6521–6530 (2003).
26. Garcia-fuentes, M. & Alonso, M. J. Chitosan-based drug nanocarriers : Where do we stand ? *J. Control. Release* **161**, 496–504 (2012).

## SUPPLEMENTARY

**Table S1.** Elemental analysis results on chitosan and chitosan-metal complexes.

	C %	H %	N%
CS	41.31	7.24	7.325
CS-Zn <sub>3%</sub>	36.00	6.41	6.26
CS-Zn <sub>4%</sub>	36.34	6.47	6.00
CS-Zn <sub>5%</sub>	35.20	6.45	5.88
CS-Fe <sub>3%</sub>	21.87	4.52	8.18
CS-Fe <sub>10%</sub>	26.98	5.39	9.705
CS-Fe <sub>20%</sub>	29.03	5.66	10.43

**Fig.S2** (Left) Representative images of free CS-Fe<sub>20%</sub> solution and free Chitosan solutions at the concentration of 1 mg/mL diluted 1:10 in 10% of fetal bovine serum. (Right) Representative images of purified and not purified CS-Fe<sub>20%</sub>/ATP nanogels prepared at 1 mg/mL diluted 1:10 in 10% of fetal bovine serum.





# Experimental work

---

## Chapter 2

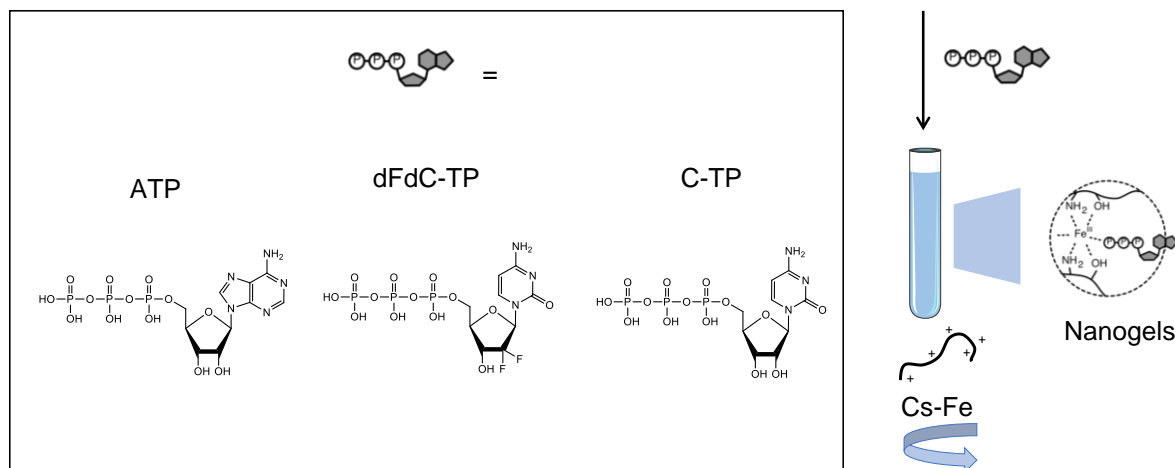
*Influence of the nucleotide  
on the colloidal properties  
of chitosan-iron based nanogels*



## **Influence of the nucleotide on the colloidal properties of chitosan-iron based nanogels**

**ABSTRACT:** Nucleotides and nucleotide analogues display important pharmacological activities. However, their clinical use is limited due to the presence of a triphosphate group, which is prone to hydrolysis and enzymatic degradation, and responsible for the high hydrophilicity of the molecules, thereby strongly limiting their uptake by target cells. This study describes the application of nanogels based on chitosan complexed with iron to the delivery of different nucleotides (ATP, C-TP) or a nucleotide analogue (gemcitabine-triphosphate), with the aim of proposing chitosan-iron nanogels as efficient and versatile platform for the delivery of these molecules. The formation of nanogels and their colloidal stability have been investigated by isothermal titration calorimetry and by dynamic light scattering and the drug release evaluated by HPLC measurements. The biological activity of gemcitabine triphosphate-loaded nanogels has been studied on gemcitabine-resistant cancer cell lines.

Results obtained showed that chitosan-iron is able to form stable nanogels with all tested nucleotides/nucleotide analogues, with a sustained drug release in physiological conditions. Moreover, nanogels can efficiently deliver the active triphosphate form of gemcitabine to breast cancer cells, colorectal cancer cells and lymphoblastic cells inducing an *in vitro* cytotoxic activity similar to that observed with the parental drug.



## INTRODUCTION

Adenosine Triphosphate (ATP) has been shown to induce ionotropic gelation of chitosan,<sup>1</sup> leading to the formation of nanoparticles with a high drug loading. In order to improve the stability of nanogels, that represented the major concern related to their application, a new formulation based on CS complexed with iron ions have been proposed.<sup>2</sup> According to results presented in chapter 1, chitosan-iron based nanogels demonstrated a good resistance towards dissolution and aggregation in physiological conditions, thanks to the “cross-linker” role of iron that reinforce nanogels structure.

In this chapter, we applied the promising nanogels formulation based on chitosan-iron to the delivery of other nucleotides, such as cytidine triphosphate (C-TP) and gemcitabine triphosphate (dFdC-TP, 2',2'-difluorodeoxycytidine-triphosphate). It is already known that the presence of the triphosphate group allows electrostatic interactions with chitosan that are the driving force of the particle formation. However, the influence of the pending moiety on nanogels properties and stability has not been investigated yet. Cytidine triphosphate (C-TP) is a natural nucleotide containing a pyrimidine (contrary to ATP which is a purine based nucleotide) involved in many metabolic reactions and in the synthesis of RNA. Gemcitabine triphosphate (dFdC-TP) is an analogue of deoxycytidine in which two fluorine atoms have been

inserted into the deoxyribose ring. dFdC-TP has a very short plasma half-life and is rapidly metabolized to its inactive form by cytidine deaminase. The non-triphosphate analogue gemcitabine is commonly used in anticancer therapy (Gemzar, Eli Lilly ®) taking advantage of the intracellular kinases that transform it in his active form gemcitabine triphosphate.<sup>3,4,5</sup> However, patients treated with a gemcitabine-based chemotherapy usually develop resistance, which can result from many molecular and cellular changes,<sup>6</sup> and severe side effects. With the aim of improving the therapeutic index of gemcitabine, many pro-drugs and nanocarriers have been proposed,<sup>7</sup> including chitosan nanogels,<sup>8,9,10</sup> liposomes, polymeric nanoparticles,<sup>11</sup> micelles, inorganic carriers, prodrugs.<sup>12</sup> Since an important cause of the eventual decline in clinical efficacy of gemcitabine is the selection of resistant cancer cells with deficiencies in the expression of nucleoside-activating kinases, some groups recently suggested a new strategy based on the nano-encapsulation of the active triphosphate form of gemcitabine.<sup>13,14,15,16,17</sup>

The present study aimed to achieve two main objectives. The first consisted in investigating how the structure of nucleotides/nucleotide analogue impacts nanogel formation based on chitosan-iron (CS-Fe<sub>20%</sub>), and the colloidal properties and stability of the resulting nanogels. The second objective consisted in investigating the intracellular delivery of gemcitabine-triphosphate by such nanogels. For this purpose, the biological activity of gemcitabine triphosphate-loaded nanogels has been evaluated on resistant cancer cell lines.

## RESULTS

### 1. Formation and characterization of CS-Fe-based nanogels

#### *1.1 Size, polydispersity and Zeta potential of CS-Fe-based nanogels*

Nanogels were successfully obtained by ionotropic gelation from CS-Fe<sub>20%</sub> and X-TP (ATP, C-TP or Gem-TP). The resulting nanogels have been characterized as a function of X-TP amounts added to the CS-Fe solution, expressed using classical N/P ratios (triphosphate derivative concentrations are expressed as phosphate groups “P” and CS concentration as nitrogen “N” from amine and amide groups). Increasing X-TP/CS-Fe ratios corresponds to decreasing N/P ratios. As shown in **Fig.1**, the addition of triphosphate derivatives to the CS-Fe<sub>20%</sub> solution led to nanogels formation until a critical N/P ratio, at which the smallest nanoparticles with the narrowest size distribution were obtained. For N/P ratios lower than the critical ones, visible aggregation and sedimentation were observed for all CS-Fe<sub>20%</sub> formulations. However, the nanogels formation, the evolution of nanoparticle size, the polydispersity and the surface charge as a function of the N/P ratio appeared to be strongly influenced by the nucleotide structure. ATP and Gem-TP showed a similar behavior in producing nanogels, even if ATP-loaded nanogels present a smaller polydispersity at any N/P ratio. Concerning the zeta potential evolution, the same trend was observed, with a progressive decrease until reaching the minimum value around the N/P ratio that is consistent with the formation of ionic bonds between ammine groups of chitosan and phosphate groups of ATP or Gem-TP. On the contrary, by visual observation, C-TP showed to form nanogels at lower N/P ratios. Indeed, for formulations with N/P ratios higher than 1 the DLS analysis was not possible. Moreover, the aggregation of C-TP loaded nanogels occurs smoothly after the critical N/P ratio

and the sedimentation is not immediate. **Tab.1** summarizes the colloidal properties of CS-Fe/X\_TP nanogels and their critical N/P ratio.

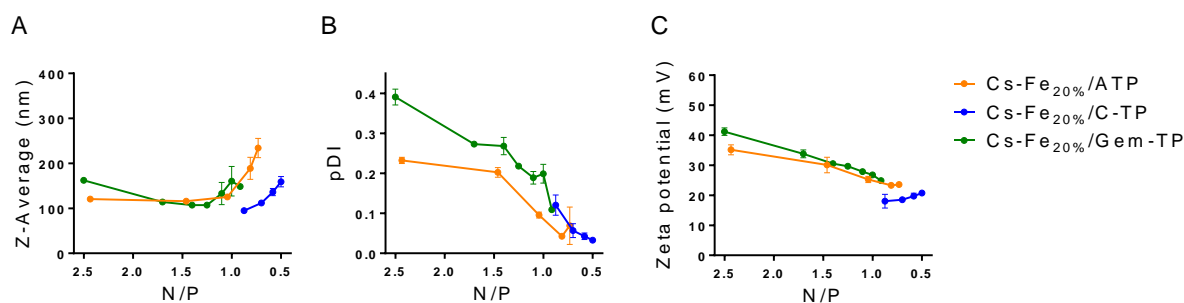


**Figure 1.** (A) Mean hydrodynamic size (Z-Average), (B) polydispersity index (pDI), and (C) zeta potential of CS-Fe<sub>20%</sub>/X-TP nanogels obtained from CS-Fe<sub>20%</sub> solutions and increasing amounts of XTP solution, expressed as a function of the N/P ratio.

**Table 1.** Average size, pDI and zeta potential of nanogel formulations prepared from CS-Fe<sub>20%</sub> and ATP, C-TP or Gem-TP at the corresponding critical N/P ratio.

Nanogel formulation	Critical N/P ratio	Corresponding X-TP/CS ratio	Size (nm)	pDI	Zeta potential (mV)
CS-Fe <sub>20%</sub> /ATP	1.17	0.28	125 ± 5	0.09 ± 0.01	25 ± 1
CS-Fe <sub>20%</sub> /C-TP	0.87	0.38	95 ± 3	0.12 ± 0.01	18 ± 3
CS-Fe <sub>20%</sub> /Gem-TP	1.1	0.30	133 ± 25	0.19 ± 0.02	27 ± 1

### 1.2 Isothermal titration calorimetry studies

The thermodynamics of nanogels formation were determined by isothermal titration calorimetry in the same mixing conditions. Results (**Fig. 2**) show similar thermodynamic profiles for all different formulations characterized by two different steps, with some noticeable differences. The first part is endothermic and correspond to the formation of the colloidal

suspension, similarly to what was observed above. The molar ratio ranges of nanogels formation were similar for CS-Fe<sub>20%</sub>/ATP and CS-Fe<sub>20%</sub>/Gem-TP, while the formation of CS-Fe<sub>20%</sub>/CTP clearly occurs at higher CTP/CS-Fe ratios (lower N/P ratios), in accordance with the DLS results. Indeed, the endothermic part of the reaction occurs for ATP/CS-Fe ratios below around 0.2 (ie. N/P ratios above around 1.66), for C-TP/CS-Fe ratios below 0.45 (ie. N/P ratios above around 0.74) and for Gem-TP/CS-Fe ratios below 0.3 (ie. N/P ratios above around 1.1). Importantly, the molar ratios of the reactions were consistent with the critical N/P ratios observed by DLS analysis. The second part (higher X-TP/CS-Fe ratios, or lower N/P ratios) is exothermic and corresponds mainly to the domain of macroscopic aggregation determined similarly.

For the first part of the curves, all thermodynamic parameters were extracted from the two set of sites fitting model. As shown in **table 2**, in all cases, isotherms obtained after subtraction of the integrated heat of dilution revealed endothermic reactions, implying higher entropic contributions to account for the thermodynamically favorable ( $\Delta G < 0$ ) reaction. The entropic gain may be due to the release of counterions from ammonium groups of chitosan and phosphate groups of X-TP and this phenomenon appeared to be much more pronounced for CS-Fe<sub>20%</sub>/ATP and CS-Fe<sub>20%</sub>/Gem-TP. The binding constants  $K_a$  are clearly higher for CS-Fe<sub>20%</sub>/ATP and CS-Fe<sub>20%</sub>/Gem-TP compared to CS-Fe<sub>20%</sub>/C-TP.

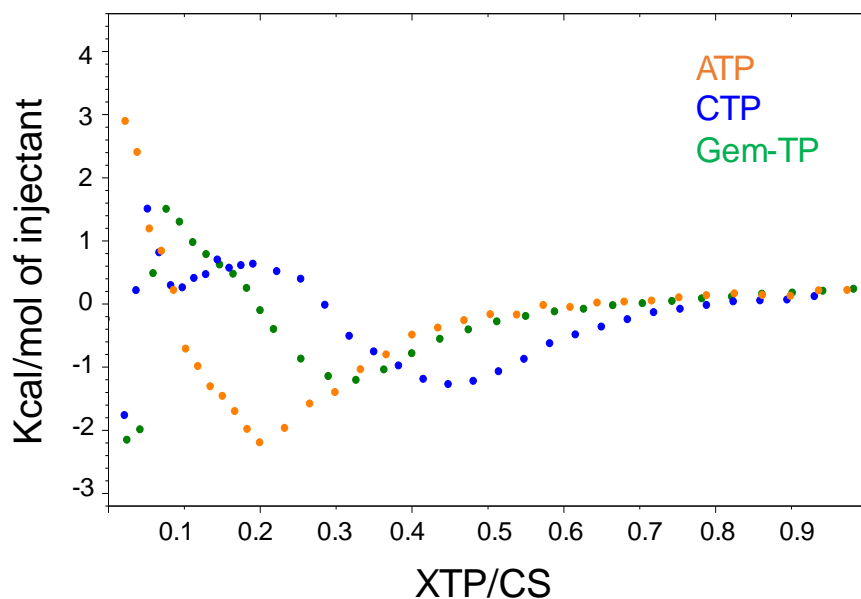


**Figure 2.** Isothermal titration calorimetry study of the interaction between ATP, CTP or Gem-TP and CS-Fe<sub>20%</sub>. Titration curves show the integrated heat plotted against the XTP/CS ratio.

**Table 2.** Binding affinity ( $K_a$ ) and thermodynamic parameters ( $\Delta H$ ,  $-T\Delta S$ ,  $\Delta G$ ) calculated according to the one site binding model for the electrostatic interactions of chitosan-iron with ATP, C-TP and Gem-TP, on the first part of the titration.

Nanogel formulation	$K_a$ , $10^3$ M	$\Delta H$	$-T\Delta S$	$\Delta G$
CS-Fe <sub>20%</sub> /ATP	29300	8691	-14788	-6097
CS-Fe <sub>20%</sub> /C-TP	5600	2547	-9361	-6814
CS-Fe <sub>20%</sub> /Gem-TP	11700	8065	-13625	-5560

### 1.3 Determination of nanogels composition

The fraction of CS-Fe<sub>20%</sub> and X-TP (ATP, C-TP or Gem-TP) constitutive of the nanogels present in the colloidal suspension was quantified after separation of the particles from the dispersing phase by centrifugation. As shown in **Fig.3**, the association of X-TP increase with

decreasing N/P ratios, according to the nanogels formation, reaching around 70% for ATP and around 50% for C-TP and Gem-TP at the corresponding critical N/P ratios (**Tab.3**). The fraction of CS-Fe<sub>20%</sub> involved in nanogels formation was around 90% at the critical N/P ratio for all the formulations. The drug loading of nanogels was then calculated according to the fractions of CS-Fe<sub>20%</sub> and X-TP constitutive of nanogels. **Fig.3** showed the trend of the drug loading and the effective N/P ratio with decreasing the N/P ratio of the formulation. For all triphosphate derivatives, the drug loading (DL% w/w) (around 40-45%) does not vary significantly. In the same way the effective N/P ratio does not vary much across the N/P range of nanogels formation.

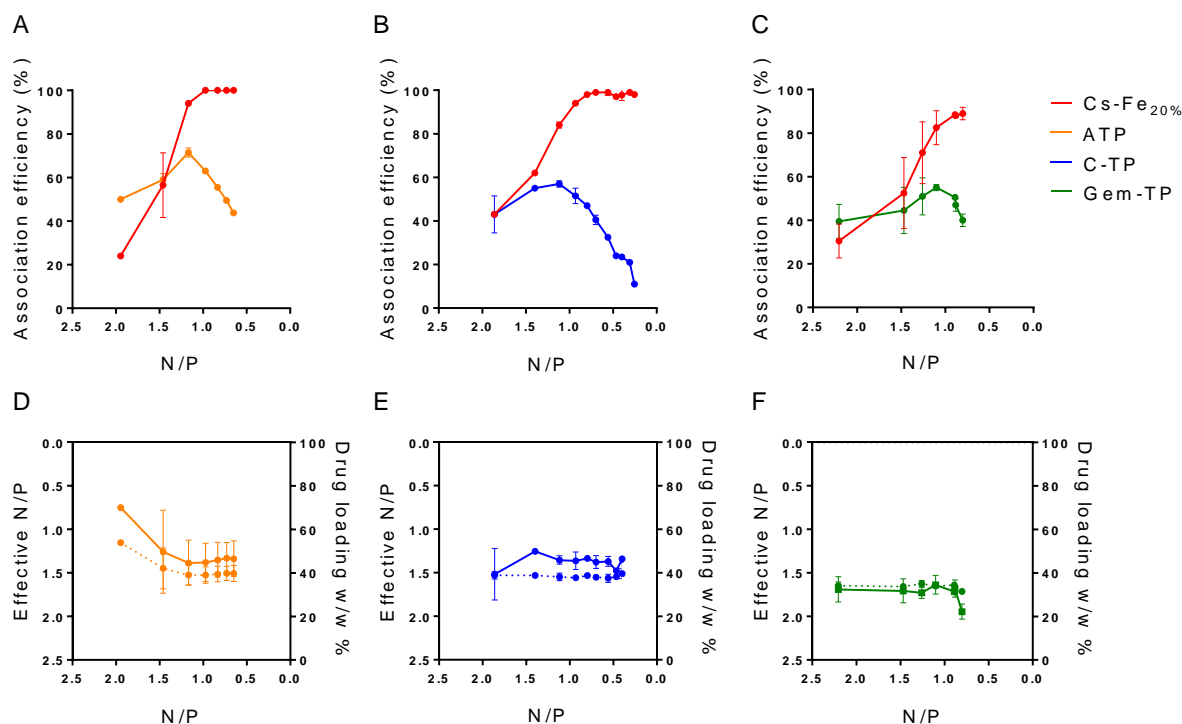


**Figure 3.** Association efficiency of CS-Fe<sub>20%</sub> and ATP (A), C-TP (B) or Gem-TP (C) to nanogels. Drug loading % (···) and effective N/P ratio (—) of CS-Fe<sub>20%</sub>/ATP nanogels (D), CS-Fe<sub>20%</sub>/CTP nanogels (E) and CS-Fe<sub>20%</sub>/Gem-TP nanogels (F). All results are expressed as a function of the N/P ratio used for the preparation of nanogels.

**Table 3.** Drug loading (DL%) and Encapsulation Efficiency (EE%) of CS-Fe20%/ATP, CS-Fe20%/C-TP and CS-Fe20%/Gem-TP nanogels at the critical N/P ratio.

Nanogel formulation	DL%	EE%
CS-Fe <sub>20%</sub> /ATP	39 ± 4	72 ± 2
CS-Fe <sub>20%</sub> /C-TP	38 ± 2	50 ± 5
CS-Fe <sub>20%</sub> /Gem-TP	34 ± 2	55 ± 2

## 2. In vitro release of ATP from CS-Fe20%/ATP nanogels

The in vitro release of ATP from CS-Fe20%/ATP nanogels has been evaluated after dilution in NaCl 0.9% at 37°C. Since ATP is prone to hydrolysis in aqueous solution, the products of degradation have been simultaneously quantified. Results obtained by HPLC measurements indicate that, after immediately after dilution in NaCl%, around 6% ATP is released, which can be seen as a limited burst release. Interestingly, this small amount of ATP then decreases, while the metabolites ADP and finally AMP appear, which is consistent with the progressive hydrolysis of the released ATP. Overall, the total drug release (ATP and metabolites) remains below 8% over one week, showing that CS-Fe based nanogels efficiently protect ATP from premature release and degradation.

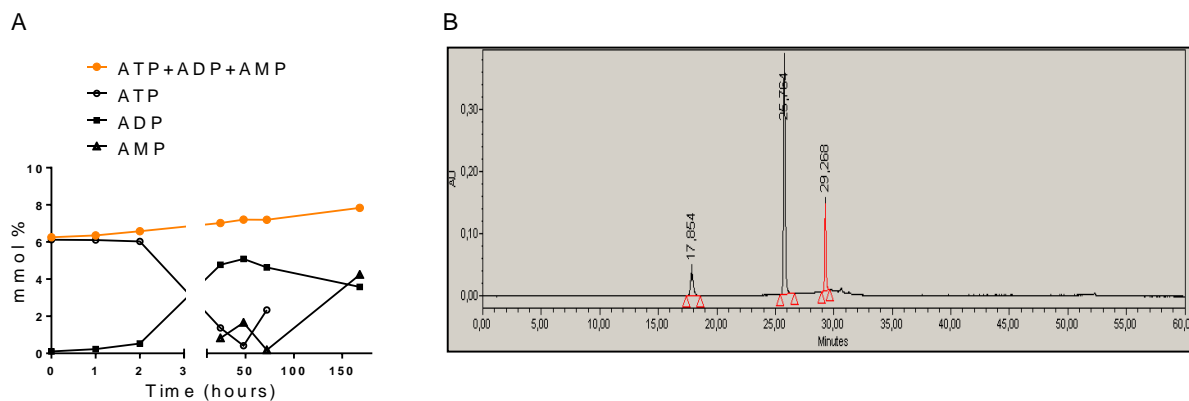


**Figure 4.** In vitro release (mol %) from CS-Fe<sub>20%</sub>/ATP nanogels in NaCl 0.9 % w/w (A), representative chromatogram of ATP, ADP and AMP aqueous mixture separated from nanogels after 24 h of incubation and analyzed using ion-pair reversed-phase HPLC coupled to a UV detector (set at 260 nm) (B).

### 3. Influence of nucleotide structure on nanogels colloidal stability in physiological media

#### 3.1 Impact of ionic strength on nanogels colloidal stability

The resistance of all nanogels formulations to the ionic strength was evaluated by following the relative intensity of the scattered light by DLS after incubating nanogels at 37°C in isotonic conditions (0.9% w/v NaCl) up to 72 h. The results obtained (**Fig.5**) showed that all nanogels exhibit a good resistance towards dissociation in a physiological solution, independently to the nucleotide structure. ATP-loaded nanogels seem to be slightly more stable at long incubation times, compared to the other two formulations.

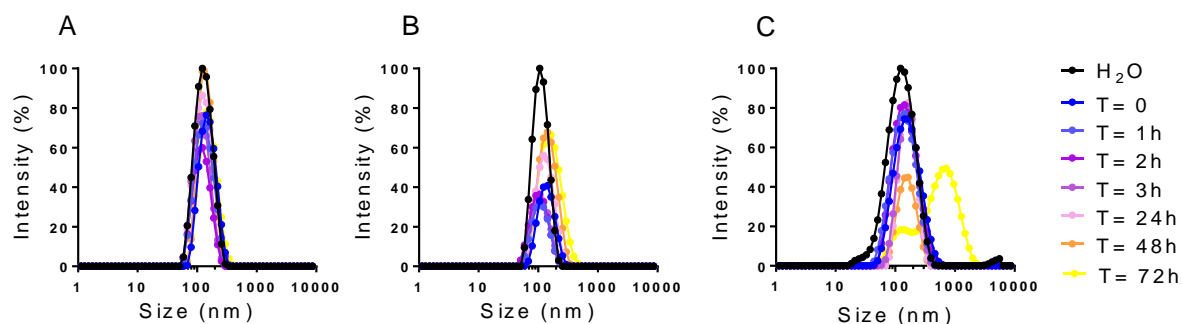


**Figure 5.** Representative size distribution as a function of relative intensity of dynamic light scattering (DLS) of CS-Fe<sub>20</sub>%/ATP nanogels (A), CS-Fe<sub>20</sub>%/C-TP nanogels (B), CS-Fe<sub>20</sub>%/Gem-TP nanogels (C) during incubation at 37°C in a physiological solution (0.9% NaCl).

### 3.2 Impact of proteins on nanogels colloidal stability

The stability of all nanogels formulations in presence of proteins was evaluated by DLS analysis after incubating purified nanogels at 37°C in presence of 10% of fetal bovine serum up to 72 h. The results (**Fig.6**) showed that CS-Fe<sub>20</sub>%/ATP nanogels, CS-Fe<sub>20</sub>%/C-TP nanogels and CS-Fe<sub>20</sub>%/Gem-TP nanogels exhibit a good resistance to the aggregation. No significant impact of the nucleotide structure is noticeable in DLS measurements.

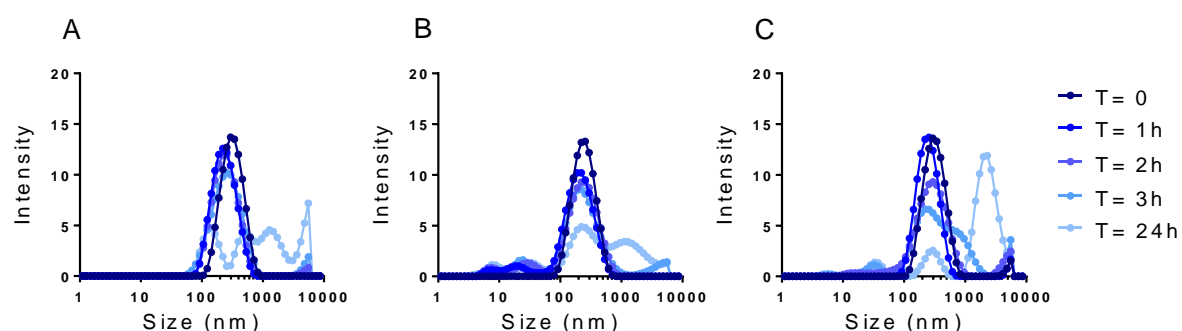


**Figure 6.** Representative size distribution of CS-Fe<sub>20</sub>%/ATP nanogels (A), CS-Fe<sub>20</sub>%/C-TP nanogels (B), CS-Fe<sub>20</sub>%/Gem-TP nanogels (C), during incubation at 37°C in presence of 10% of Fetal Bovine Serum (FBS) evaluated by Dynamic light scattering (DLS).

#### 4. Biological activity of Gem-TP-loaded nanogels

Four cancer cell lines (PANC-1, BxPC-3, MCF-7, CCRF-CEM and CCRF-CEM Ara 8C) have been exposed to CS-Fe<sub>20%</sub>/Gem-TP nanogels for 24 h and 72 h. The cytotoxic activity of the formulation has been compared to the cytotoxic activity of the free Gem-TP. CS-Fe<sub>20%</sub>/TPP nanogels have been used as a control for a potential cytotoxicity of the nanocarrier.

As shown in **Table 4**, similarly to the free molecule Gem-TP, CS-Fe<sub>20%</sub>/Gem-TP nanogels exert a cytotoxic activity on the pancreatic cancer cells PANC-1 and BxPC-3 and the breast cancer cells MCF-7 only after 72 h. In all cases, nanoformulations containing TPP exhibited no cytotoxicity, demonstrating the absence of intrinsic toxicity of CS-Fe<sub>20%</sub>-based nanogels. In the case of lymphoblastic cells CCRF-CEM (sensitive to gemcitabine) and CCRF-CEM-araC/C8 (resistant to gemcitabine), the drug resistance index was calculated as a ratio of IC<sub>50</sub> values obtained in drug-resistant cells to regular cells. This index was around 5500 to 500 for Gem-TP and CS-Fe<sub>20%</sub>/Gem-TP nanogels respectively.

**Table 4.** Cytotoxicity of Gem-TP, CS-Fe<sub>20%</sub>/TPP and CS-Fe<sub>20%</sub>/Gem-TP nanogels on PANC-1, BxPC-3, MCF-7, CCRF-CEM and CCRF-CEM Ara 8C cells expressed as IC<sub>50</sub> in  $\mu$ M, after 24 h and 72 h of treatment. Resistance Index (RI) of the compounds are calculated in the case of CCRF-CEM cells as a ratio of IC<sub>50</sub> values obtained in drug-resistant cells to regular cells. “/” indicates that IC<sub>50</sub> is not reached even at the highest tested concentration.

	PANC-1		MCF-7		BxPC-3		CCRF-CEM		CCRF-CEM Ara8C		RI	
	24 h	72 h	24 h	72 h	24 h	72 h	24 h	72 h	24 h	72 h	24 h	72 h
Gem-TP	/	1	/	0.02	/	0.01	0.1	0.02	/	110	/	5500
CS-Fe <sub>20%</sub> /TPP	/	/	/	/	/	/	/	/	/	/	/	/
CS-Fe <sub>20%</sub> /Gem-TP	/	0.09	/	0.03	/	0.03	0.5	0.2	/	100	/	500

## DISCUSSION

The obtention of colloidal suspensions from the complexation of chitosan to TPP (“ionotropic gelation”) has been well established and has led to many developments of such “chitosan nanogels”.<sup>18,19,20,21,22</sup> Recently this strategy has been applied to triphosphate group-containing molecules such as the nucleotide ATP and the nucleotide analogue AZT-TP.<sup>1</sup> In this study, we selected chitosan modified with iron for the delivery of other nucleotide analogues, according to previous studies showing the capacity of chitosan-iron to form stable nanogels in physiological conditions<sup>2</sup> (chapter 1). The ionotropic gelation has been successfully applied to the encapsulation of cytidine triphosphate (C-TP) and gemcitabine triphosphate (Gem-TP) and compared with ATP nanogels. By DLS analysis, it has been demonstrated that, independently from the nucleotide structure, modified chitosan can form nanoparticles with small size (diameter < 200 nm) and narrow polydispersity, confirming that the electrostatic interactions are the driving force of the nanogels formation. However, C-TP nanogels require a very different ratio between chitosan-iron and triphosphate derivative in the preparation, suggesting an influence of the nucleotide structure on mechanism of formation of nanogels. The thermodynamic parameters of the nanogels formation suggest that the nucleoside structure influence the affinity between the two components and the rearrangements that lead to the formation of colloidal suspensions. Here also, ATP and Gem-TP showed to have a similar behavior in their interactions with chitosan-iron, contrary to C-TP. The actual composition of nanogels have been analyzed at different N/P ratios used in the preparation, by quantifying free chitosan-iron and free nucleotide analogue in the suspension. Results indicate that, to allow the nanogels formation, the effective N/P ratio in the nanoparticle has to be around 1.5. For this reason, the maximum drug loading reaches values as high as 40% w/w for all formulations.

The colloidal stability assessment confirms that CS-Fe<sub>20%</sub> leads to stable nanogels, regardless the structure of the nucleotide analogues encapsulated, with only slight differences. The stability of the formulation in physiological conditions has been confirmed by evaluating the ATP release from CS-Fe<sub>20%</sub>/ATP nanogels in NaCl 0.9%. The drug showed to remain encapsulated in nanogels for up to several days, with a very slow drug release, which is consistent with the objective of an intracellular delivery for this type of nanocarriers.

Finally, to prove the effective interest as chitosan-iron based nanogels for the delivery of therapeutic molecules, CS-Fe<sub>20%</sub>/Gem-TP nanogels have been tested on gemcitabine-resistant cancer cell lines. Nanogels showed a similar cytotoxicity on PANC-1, BxPC-3 and MCF-7 cells compared to the free drug. In regular CCRF-CEM cell line, nanogels showed higher IC<sub>50</sub> values after 24 h and 72 h compared to the free molecule, but in gemcitabine-resistant CEM-araC/C8 cells the cytotoxicity was slightly improved by the nanoformulation. The calculated resistance index indicate that nanogels may be able to mitigate the drug-resistant phenotype of CEM/araC/C8 cancer cell line, which could be explained by a specific mechanism of cellular delivery in the case of nanogels.

The *in vitro* anticancer activity presented by our formulation is similar to other systems previously proposed<sup>14,13</sup>, with the difference that CS-Fe<sub>20%</sub> based nanocarrier did not exhibit any sign of intrinsic cytotoxicity.

## CONCLUSIONS

In this study, we applied chitosan-iron based nanogels to encapsulation of C-TP and Gem-TP. Results obtained evidenced for the first time that the structure of the triphosphate molecule has an impact on the mechanism of nanogels formation. Despite that, the composition of obtained nanogels is similar and all the formulations present a satisfactory colloidal stability in physiological conditions, combined with a protection of the encapsulated triphosphate

molecule. Moreover, we showed that such nanogels loaded with the active triphosphate form of gemcitabine exert similar in vitro cytotoxic activity compared to the parental drug on classical breast and colorectal cancer cells.

## **EXPERIMENTAL**

### ***Materials***

Nanogels were prepared using low viscosity chitosan purchased from Sigma-Aldrich (France) complexed with Iron and ATP (Sigma), CTP (Sigma) or Gem-TP (Syncom, Netherland). The degree of N-deacetylation of commercial chitosan was determined to be 84% by <sup>1</sup>H NMR spectroscopy. In the following, water refers to MilliQ® purified water (Millipore, France). Complexation of CS with iron was achieved with iron (III) nitrate nonahydrate, 1,10-Phenanthroline monohydrate and hydroxylamine hydrochloride from Sigma. Eagle's Minimum Essential Medium (EMEM) and fetal bovine serum (FBS) were purchased from Dulbecco (Invitrogen, France). Penicillin and streptomycin were obtained from Lonza (Verviers, Belgium). Other reagents used were purchased from Sigma; all solvents were of analytical grade.

### ***Cell culture***

The MCF-7 human breast cancer cell line was obtained from American Type Culture Collection (ATCC) (catalog number HTB-22) and cultured in Eagle's Minimum Essential Medium (EMEM) from Sigma, supplemented with 50 U/mL penicillin, 50 U/mL streptomycin, 10% heat-inactivated fetal bovine serum (FBS) (56 °C, 30 min) from Gibco, 1% non-essential amino acids (NEAA) and 5 mL glutamine. Cells were maintained at 37 °C in a 5% CO<sub>2</sub> humidified atmosphere. Twice a week, cells were divided at 1:5 ratio by using trypsin/EDTA.

The PANC-1 human pancreatic cancer cell line was obtained from ATCC (catalog number CRL-1469) and cultured in Dulbecco's Modified Eagle's Medium (DMEM), supplemented with 50 U/mL penicillin, 50 U/mL streptomycin and 10% heat-inactivated FBS (56 °C, 30 min) fetal bovine serum. Cells were maintained at 37 °C in a 5% CO<sub>2</sub> humidified atmosphere. Twice a week, cells were divided at 1:4 ratio by using trypsin/EDTA. The Bx-PC3 human pancreatic cancer cell line was obtained from ATCC (catalog number CRL-187) and cultured in Eagle's Minimum Essential Medium (RPMI), supplemented with 50 U/mL penicillin, 50 U/mL streptomycin and 10% heat-inactivated FBS (56 °C, 30 min) fetal bovine serum, Twice a week, cells were divided at 1:5 ratio by using trypsin/EDTA. The CCRF-CEM human acute lymphoblastic leukemia cell line and the CCRF-CEM-ARA 8C aracytidin-resistant variant of CCRF CEM were obtained from ATCC (catalog numbers CCC-119 and CCC-119 Modified) and cultured in Eagle's Minimum Essential Medium (RPMI), supplemented with 50 U/mL penicillin, 50 U/mL streptomycin and 10% heat-inactivated FBS (56 °C, 30 min) fetal bovine serum. Twice a week, cells were diluted 1:5.

### ***Preparation and characterization of CS-Fe-based nanogels***

A chitosan-iron complex (CS-Fe<sub>20%</sub>) containing 20% m/m of iron was prepared as described previously (chapter 1). CS-Fe solution was obtained by dissolving CS-Fe<sub>20</sub> powder at a final concentration of 1 mg/mL in a 1.75% v/v acetic acid aqueous solution, stirring overnight and filtrating through 0.22 µm filter. Freshly prepared solutions of ATP and CTP at a concentration of 15 mg/mL and dFdC-TP at a concentration of 10 mg/mL were added dropwise to the CS-Fe solution under magnetic stirring at 1000 rpm to allow nanogels formation. For the study of the nanoparticle formation domains, increasing amounts of ATP, CTP and dFdC-TP solutions, from 0.01 to 0.08 mL, were added dropwise to 0.5 mL of a 1 mg/mL Cs-Fe<sub>20</sub> solution. For further studies, ATP, CTP and Gem-TP nanogels have been prepared respectively at N/P ratios

of 1.1, 1, 0.8. Nanogels were purified from free ATP, CTP or dFdC-TP and CS-Fe through centrifugation of 1 mL suspension on a 20  $\mu$ L glycerol layer at  $2000 \times g$  for 1 h, removal of 0.92 mL supernatant, and redispersion in 1 mL (final volume) of water. The mean hydrodynamic diameter and the polydispersity index (PdI) of nanogels were determined in triplicate by dynamic light scattering (DLS) and the zeta potential by electrophoretic light scattering (ELS) after 1/20 sample dilution in 1 mM NaCl solution, using a Zetasizer Nano ZS (Malvern Instrument, Malvern, UK) with a  $173^\circ$  scattering angle at a temperature of  $25^\circ\text{C}$ . The results were represented as the size distribution by intensity percentage.

### ***Isothermal titration calorimetry studies***

Isothermal titration calorimetry (ITC) measurements were performed on a Microcal VP-ITC with a cell volume of 1.441 mL at  $25^\circ\text{C}$ . In each experiment, the triphosphate derivative solution (ATP 5.4 mM, C-TP 5.16 mM, dFdC-TP 5.9 mM) was titrated into the cell containing CS-Fe<sub>20%</sub> dissolved in a 1.75% v/v acetic acid aqueous solution at the concentration of 0.3 mg/mL CS (which corresponds to 1.192 mM as CS monomer unit). Volumes of 5  $\mu$ L or 10  $\mu$ L of ATP, C-TP or dFdC-TP solution were injected with spacing times ranging from 800 to 100 s, while the solution/suspension was stirred at 394 rpm. The heat of dilution was measured by titrating the triphosphate derivative solution into the buffer solution, and these values were then subtracted in order to obtain the actual heat of binding. The fit of the curves was calculated with Origin7 (Chi-square values between 900 and 7000) and values found were used to determine the free Gibbs energy.

### ***Determination of nanogels composition***

To study ATP, C-TP and dFdC-TP association efficiency, nanogels with N/P ranging from 2 to 0.5 were prepared as described above using CS-Fe<sub>20%</sub> and aqueous solutions of ATP, C-TP

and dFdC-TP. The purification step was replaced by a step of separation of free triphosphate derivative and free CS-Fe<sub>20%</sub> from nanogels by centrifugation at 12000 g for 1 h. The concentration of free triphosphate derivatives and free CS-Fe<sub>20%</sub> in the supernatant was measured by UV-spectroscopy at  $\lambda = 320$  nm for CS-Fe<sub>20%</sub>, at  $\lambda = 260$  nm for ATP, and at  $\lambda = 270$  nm for C-TP and dFdC-TP. The amount of ATP, C-TP or dFdC-TP, and CS-Fe<sub>20%</sub> associated to nanogels was calculated by subtraction of free triphosphate derivatives and free CS-Fe<sub>20%</sub> to the total amounts used for the preparation. The association efficiency of the drug and the CS-Fe<sub>20%</sub> to nanogels was calculated as the ratio between the quantities used for the preparation and the quantities involved in the formation of nanogels. After determination of the association efficiency, the drug loading was calculated as the ratio between the nanoparticle-associated drug weight and the nanoparticle (drug + CS-Fe<sub>20%</sub>) weight.

#### ***In vitro release of ATP from CS-Fe<sub>20%</sub>/ATP nanogels***

The ATP release from CS-Fe<sub>20%</sub>/ATP nanogels was studied by preparing the formulation at 1 mg/mL and subsequently purifying it by free CS-Fe<sub>20%</sub> and ATP. After dilution 1:10 in NaCl 0,9%, nanogels were incubated at 37 °C for 1 h, 2 h, 24 h, 48 h, 72 h, one week. After incubation, nanogels were centrifuged for 1 h at 12 000g, in order to separate them from free ATP. The ATP present in the supernatant was quantified by HPLC. HPLC analysis was performed using a Ion-pair reversed phase high-performance liquid chromatography ultraviolet (UV)-coupled method reported in the literature,<sup>23</sup> allowing to rapidly and simultaneously quantify ATP and its products of hydrolysis ADP and AMP. A Synergi Hydro-RP 80 Å 250 X 4.6 mm column fitted with a guard column (Phenomenex, Macclesfield, UK) was used for chromatographic separation. The column was kept at 40 °C, and the detection absorption wavelength set at 254 nm. The mobile phase consisted of a gradient mix of phosphate buffer (39 mM K<sub>2</sub>HPO<sub>4</sub>, 26 mM KH<sub>2</sub>PO<sub>4</sub>, and 10 mM TBAHS (Tetrabutylammonium hydrogen sulfate) adjusted to pH

6.0 with orthophosphoric acid (solution A) and ACN (solution B) at concentrations that varied from 2 % to 30 % over the duration of the HPLC run as follows: 0 min (98 % solution A, 2 % solution B), 10 min (92 % solution A, 8 % solution B), 20 min (70 % solution A, 30 % solution B), 20.5 min (98 % solution A, 2 % solution B), 35 min (98 % solution A, 2 % solution B). The flow rate was set at 1 mL.min<sup>-1</sup>, and an injection volume of 100 µL was used for all analyzed samples. Retention times were: 17.9, 25.8 and 29.3 min for AMP, ADP and ATP, respectively.

### ***Impact of ionic strength and proteins on nanogels colloidal stability***

The impact of the ionic strength and proteins on nanogels colloidal stability was evaluated by comparing nanogel suspensions in aqueous solution and in physiological solution (0.9% NaCl) or in aqueous solution containing 10% of Fetal Bovine Serum (FBS) at the same concentration by dynamic light scattering (DLS). The relative intensity (corresponding to the scattered light intensity corrected by the derived count rate) was measured using a Zetasizer Nano ZS (Malvern Instrument, Malvern, UK) with a 173° scattering angle at 25°C. For each condition, the laser power (attenuation index) and the measurement position from the “outer” square cuvette wall were fixed to have similar light intensity entering the sample cuvette. Data are represented as relative intensity of nanogel suspension diluted in 0.9% NaCl compared to the nanogel suspension diluted in milliQ water. In the the case of the dilution in FBS, the results were represented as the size distribution by intensity percentage.

### ***Cytotoxicity of Gem-TP -loaded nanogels***

The mitochondrial activity was evaluated using the 3-[4,5-dimethylthiazol-2-yl]-3,5-diphenyl tetrazolium bromide (MTT) test. This colorimetric test measures the mitochondrial dehydrogenase cell activity, an indicator of cell viability. The assay is based on the reduction, by living cells, of the tetrazolium salt, MTT, which forms a blue formazan product. PANC-1 cells were seeded onto 96-well plates (TTP, Zurich, Switzerland) with 100  $\mu$ L of growth medium per well at a density of 6,000 cells/well, MCF7 cells at a density of 7,000 cells/well, Bx-PC-3 cells at a density of 7,000 cells/well. CCRF-CEM cells were seeded at a density of 60,000 cells/well for 24h treatment and 30,000 cells/well for 72h treatment, while CCRF-CEM-Ara8C at a density of 50,000 cells/well for 24h treatment and 30,000 cells/well for 72h treatment. After 24 h (pre-incubation), 100  $\mu$ L of CS-Fe/GemTP nanogels dispersed in growth medium were added onto cells at various final concentrations. After 24 h, 48 h or 72 h of incubation with nanogels, 20  $\mu$ L of a 5 mg/mL MTT solution was added to each well and incubated for 4 h in the case of PANC-1, MCF7 and Bx-PC-3 cells after 24 h and 48 h of treatment, 1 h in the case of PANC-1, MCF7 and Bx-PC-3 cells after 72 h of treatment, 2 h in the case of CCRF-CEM cells and CCRF-CEM-Ara8C cells, 1 h in the case of CCRF-CEM cells and CCRF-CEM-Ara8C cells. The medium was then discarded and 200  $\mu$ L of dimethyl sulfoxide (DMSO) were added to dissolve formazan crystals. The absorbance was measured at 570 nm with a microplate reader (Metertech  $\Sigma$  960, Fisher Bioblock, France). The fraction of viable cells was calculated as the absorbance ratio between nanogels-treated and untreated cells. Wells without the addition of MTT were used as blank. The impact on cell viability of nanogels was compared to the effect of same concentrations of free Gem-TP. CS-Fe/TPP nanogels were used as control for the toxicity of the carrier. The IC<sub>50</sub> was calculated as the sample concentration, which inhibits the growth of 50% of cells relative to untreated cells, using the

sigmoidal fitting from GraphPad Prism Software. All measurements were performed in triplicate.

## ACKNOWLEDGMENTS

Thanks to Balthazar Toussaint for help with HPLC experiments and Stéphanie Denis for help with cell culture experiments.

## REFERENCES

1. Giacalone, G., Fattal, E. & Hillaireau, H. Drug-Induced Nanocarrier Assembly as a Strategy for the Cellular Delivery of Nucleotides and Nucleotide Analogues. 0–5 (2013).
2. Giacalone, G. *et al.* Stabilization and cellular delivery of chitosan – polyphosphate nanoparticles by incorporation of iron. *J. Control. Release* **194**, 211–219 (2014).
3. Rizzuto, I. Pharmacogenomics. (2017).
4. Ueno, H., Kiyosawa, K. & Kaniwa, N. Pharmacogenomics of gemcitabine : can genetic studies lead to tailor-made therapy ? 145–151 (2007).
5. Rompay, A. R. Van, Johansson, M. & Karlsson, A. Substrate specificity and phosphorylation of antiviral and anticancer nucleoside analogues by human deoxyribonucleoside kinases and ribonucleoside kinases. **100**, 119–139 (2003).
6. Samulitis, B. K. *et al.* Gemcitabine resistant pancreatic cancer cell lines acquire an invasive phenotype with collateral hypersensitivity to histone deacetylase inhibitors. 43–51 (2015).
7. Birhanu, G., Akbari, H., Seyedjafari, E. & Zandi-karimi, A. ScienceDirect Nanotechnology for delivery of gemcitabine to treat pancreatic cancer. *Biomed. Pharmacother.* **88**, 635–643 (2017).
8. Arias, L., Reddy, L. H. & Couvreur, P. Superior Preclinical Efficacy of Gemcitabine

- Developed As Chitosan Nanoparticulate System. 97–104 (2011).
9. Derakhshandeh, K. & Fathi, S. Role of chitosan nanoparticles in the oral absorption of Gemcitabine. *Int. J. Pharm.* **437**, 172–177 (2012).
  10. Arya, G., Vandana, M., Acharya, S. & Sahoo, S. K. Enhanced antiproliferative activity of Herceptin ( HER2 ) -conjugated gemcitabine-loaded chitosan nanoparticle in pancreatic cancer therapy. *Nanomedicine Nanotechnology, Biol. Med.* **7**, 859–870 (2011).
  11. Bildstein, L. *et al.* Transmembrane diffusion of gemcitabine by a nanoparticulate squalenoyl prodrug : An original drug delivery pathway. *J. Control. Release* **147**, 163–170 (2010).
  12. Fang, Y., Du, F., Xu, Y., Meng, H. & Huang, J. Colloids and Surfaces B : Biointerfaces Enhanced cellular uptake and intracellular drug controlled release of VESylated gemcitabine prodrug nanocapsules. *Colloids Surfaces B Biointerfaces* **128**, 357–362 (2015).
  13. Galmarini, C. M. *et al.* Polymeric nanogels containing the triphosphate form of cytotoxic nucleoside analogues show antitumor activity against breast and colorectal cancer cell lines. **7**, 3373–3381 (2008).
  14. Galmarini, C. M., Warren, G., Senanayake, M. T. & Vinogradov, S. V. Efficient overcoming of drug resistance to anticancer nucleoside analogs by nanodelivery of active phosphorylated drugs. **395**, 281–289 (2010).
  15. Zhang, Y., Kim, W. Y. & Huang, L. Biomaterials Systemic delivery of gemcitabine triphosphate via LCP nanoparticles for NSCLC and pancreatic cancer therapy. *Biomaterials* **34**, 3447–3458 (2013).
  16. Manuscript, A. & Therapy, P. C. NIH Public Access. **34**, 3447–3458 (2014).
  17. Rodriguez-ruiz, V. *et al.* Positively charged cyclodextrins as effective molecular

- transporters of active phosphorylated forms of gemcitabine into cancer cells. 1–10 (2017).
18. Garcia-fuentes, M. & Alonso, M. J. Chitosan-based drug nanocarriers : Where do we stand ? *J. Control. Release* **161**, 496–504 (2012).
  19. Soliman, G. M., Zhang, Y. L., Merle, G., Cerruti, M. & Barralet, J. Hydrocaffeic acid-chitosan nanoparticles with enhanced stability, mucoadhesion and permeation properties. *Eur. J. Pharm. Biopharm.* **88**, 1026–1037 (2014).
  20. Schmitt, F. *et al.* Chitosan-based nanogels for selective delivery of photosensitizers to macrophages and improved retention in and therapy of articular joints. *J. Control. Release* **144**, 242–250 (2010).
  21. Huang, Y., Cai, Y. & Lapitsky, Y. tripolyphosphate micro- and nanogels : 5957–5970 (2015).
  22. Csaba, N. *et al.* Ionically crosslinked chitosan nanoparticles as gene delivery systems: Effect of PEGylation degree on in vitro and in vivo gene transfer. *J. Biomed. Nanotechnol.* **5**, 162–171 (2009).
  23. Contreras-sanz, A. *et al.* Simultaneous quantification of 12 different nucleotides and nucleosides released from renal epithelium and in human urine samples using ion-pair reversed-phase HPLC. 741–751 (2012).



# Experimental work

---

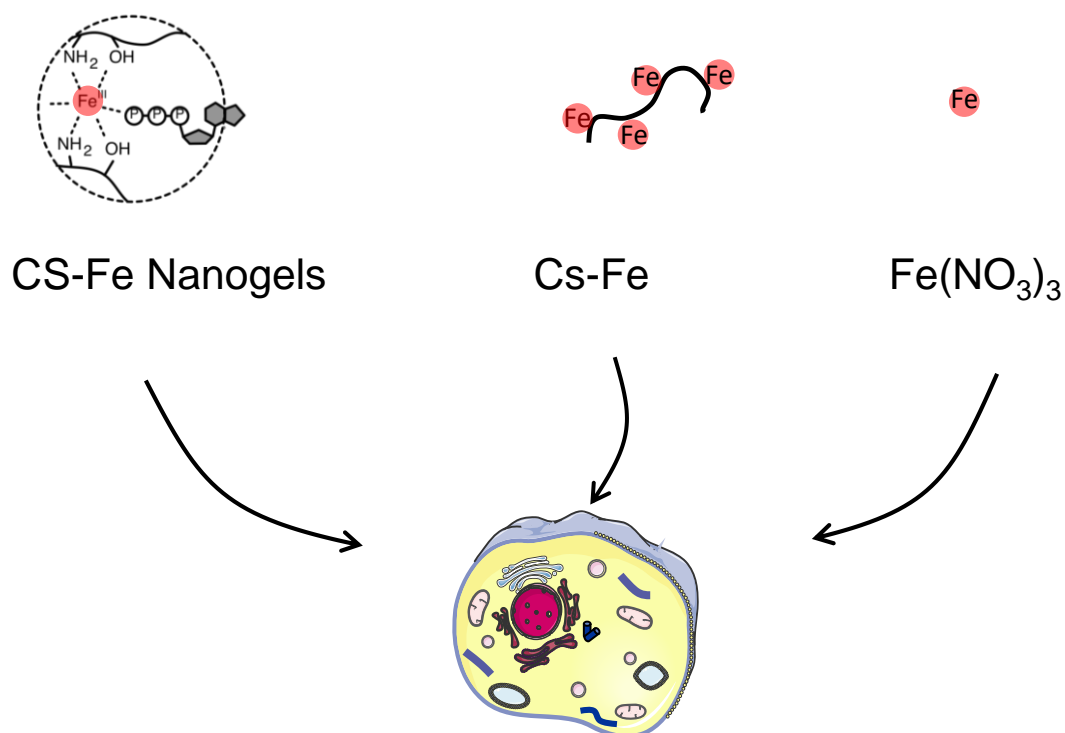
## Chapter 3

*Intracellular fate and biological impact  
of Chitosan-iron based nanogels*



## **Intracellular fate and biological impact of Chitosan-iron based nanogels**

**ABSTRACT:** The potential applications of chitosan-iron nanogels as nucleotides delivery platform are extremely interesting. However, iron-based nanoparticles have been frequently associated with toxic effects towards immune cells. In the present study, the role played by the iron present in the nanogels structure on the eventual toxicity has been investigated. In order to do that, CS-Fe<sub>20%</sub>/ATP nanogels have been compared to CS-Fe<sub>20%</sub> soluble polymer and to free Fe<sup>3+</sup> in their toxicological profile on immortalized RAW 264.7 murine macrophages. The intracellular fate of nanogels has been investigated by confocal microscopy and by Transmission Electron Microscopy. The toxicity of the formulation has been evaluated in terms impact on cell viability, oxidative stress, mitochondrial damage, organelles deformation. Nanogels did not show any toxicity in terms of necrosis induction and oxidative stress for concentrations up to 20 µg/mL iron, contrary to the treatment with Fe(NO<sub>3</sub>)<sub>3</sub> (free Fe<sup>3+</sup>). Results obtained in this study put in evidence the in vitro safety profile of CS-Fe<sub>20%</sub> based nanogels.



## INTRODUCTION

Chitosan is a polysaccharide obtained by deacetylation of chitin, a naturally occurring biopolymer. Because of its low toxicity and biodegradability, chitosan has been widely used in the medical field.<sup>1</sup> To date, many studies have been conducted on drug delivery applications of chitosan,<sup>2</sup> even if it is not yet approved by FDA for this purpose. Our group recently proposed chitosan-iron (CS–Fe) complexes as original scaffold for the production of nanogels intended to the delivery of nucleotide analogues. CS–Fe-based nanogels have been previously applied to the delivery of ATP for its relevant pharmacological activity, eg. to circumvent hypoxia in ATP-depleted macrophages,<sup>3</sup> but also serves as a model molecule for nucleotide analogues such as gemcitabine-triphosphate. The presence of iron in the nanogels structure is crucial to obtain ATP-loaded nanogels with a good stability and a controlled release in physiological conditions.<sup>4</sup> While chitosan is widely considered as safe, a detailed understanding of the eventual

interactions of chitosan-iron-based nanoparticles with cellular processes, especially at high doses, is needed. Indeed, iron itself has been shown to be involved in a new type of cell death mechanism called “ferroptosis”. The morphological, biochemical, and genetic features of ferroptosis are quite different from the other types of regulated cell death, such as apoptosis, necrosis, necroptosis, and autophagy,<sup>5</sup> and are still subject of study. Ferroptosis results from iron-dependent lipid peroxide and ROS accumulation and is characterized mainly by cell volume shrinkage and increased mitochondrial membrane density without typical apoptotic and necrotic manifestations.<sup>6</sup> It is known that the process derives from iron metabolism but the mechanism is not clear yet. Recently, many groups proposed iron-based nanomaterials such as iron oxide nanoparticles and metal-organic frameworks as cytotoxic compounds for cancer therapy because of their ability to accumulate in tumor cells and release  $\text{Fe}^{2+}$  or  $\text{Fe}^{3+}$  ions in lysosomes, which participate in the Fenton reaction and induce ferroptosis.<sup>7,8</sup> In parallel, several iron-based nanoparticles used for drug delivery and imaging purposes have been reported to have toxic effects on immune cells.<sup>9,10,11,12</sup> In particular, many studies describe increased production of reactive oxygen species (ROS) and cytokines, mitochondrial dysfunctions and autophagy in immune cells following exposition to iron-based nanoparticles. It is well known that many parameters can influence the effects on immune cells, such as size (smaller nanoparticles are generally more toxic), shape (the spherical shape seems to be the less toxic), hydrophobicity and surface functionalities and charge.<sup>13,14,15</sup> However, a clear understanding of the mechanism of immunotoxicity of iron-based nanoparticles is missing and systematic studies are needed to inform the design of safe iron-based nanomaterials. In contrast to widely used iron oxide nanoparticles, the choice of chitosan-iron nanogels offers the potential to investigate the role of iron in various states, ie. in a colloidal state (chitosan-iron-based nanogel), in a soluble, organometallic state (chitosan-iron polymer), compared to free iron ions.

In this study, immortalized RAW 264.7 murine macrophages were chosen as a model to investigate chitosan-iron nanogels toxicity and to compare it with those of the polymer (chitosan-iron) and with those of free iron (iron nitrate). Cellular uptake and cells morphology studies were conducted together with toxicity assessments (cell viability, oxidative stress, mitochondrial damage, organelles deformation) with the aim of clarify the mechanisms of cellular toxicity of iron-based nanoparticles.

## **RESULTS**

### **1. Intracellular fate of chitosan-iron/ATP nanogels**

#### ***1.1 Intracellular delivery of fluorescent ATP by nanogels***

The intracellular fate of fluorescent ATP delivered by nanogels was evaluated by confocal laser microscopy after 24 h incubation on RAW 264.7 cells and compared to that of free fluorescent ATP in solution. The nanoparticle concentration used was 0.1 mg/mL, as a safe concentration determined through Propidium Iodide Assay. In both cases, the fluorescence is found intracellularly, mostly in the cytoplasm. As observed in Fig. 1, this fluorescence is clearly higher for nanogels-treated cells compared to cells treated with the free molecule, confirming the ability of nanogels to deliver intracellularly ATP by crossing cell membranes and releasing therefore the molecule in the cytoplasm. Images did not show any effect of nanogels and ATP on cells morphology at the concentration tested.

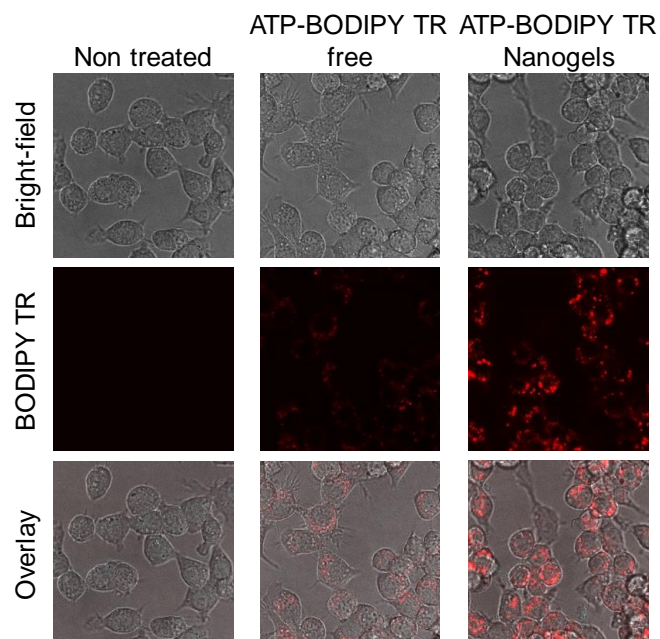


**Figure 1.** Intracellular distribution of fluorescent ATP delivered as free molecule or as CS-Fe<sub>20%</sub>/ATP nanogels in RAW 264.7 cells, after 24 h incubation at 37 °C, observed by confocal laser microscopy on a 0.8 μm thick midpoint optical slice.

### ***1.2 Cellular uptake of Cs-Fe/ATP nanogels by confocal microscopy in reflection mode***

The kinetics of internalization of CS-Fe/ATP nanogels on RAW 264.7 cells was followed up to 24 h, by confocal laser microscopy in reflection mode, in order to monitor ion-containing material present in the cells. The nanoparticle concentration used was 0.1 mg/mL, to avoid any effect on cell viability. The signal is found intracellularly, mostly in the cytoplasm. As observed in Fig. 2, non-treated cells produce a signal that has to be taken into account. The signal on treated cells becomes higher for nanogels-treated cells after 2 h of incubation, suggesting the presence of iron inside of cells. Furthermore, few aggregates of CS-Fe/ATP can be observed in the medium from 1 h exposure. The highest internalization of CS-Fe/ATP nanogels was observed after 6 h of exposure. The reduction in nanogels loading after 24 h could be due to

mechanisms of exocytosis or to nanogels degradation. Images also show the absence of any effect of nanogels on cell morphology for all incubation times.

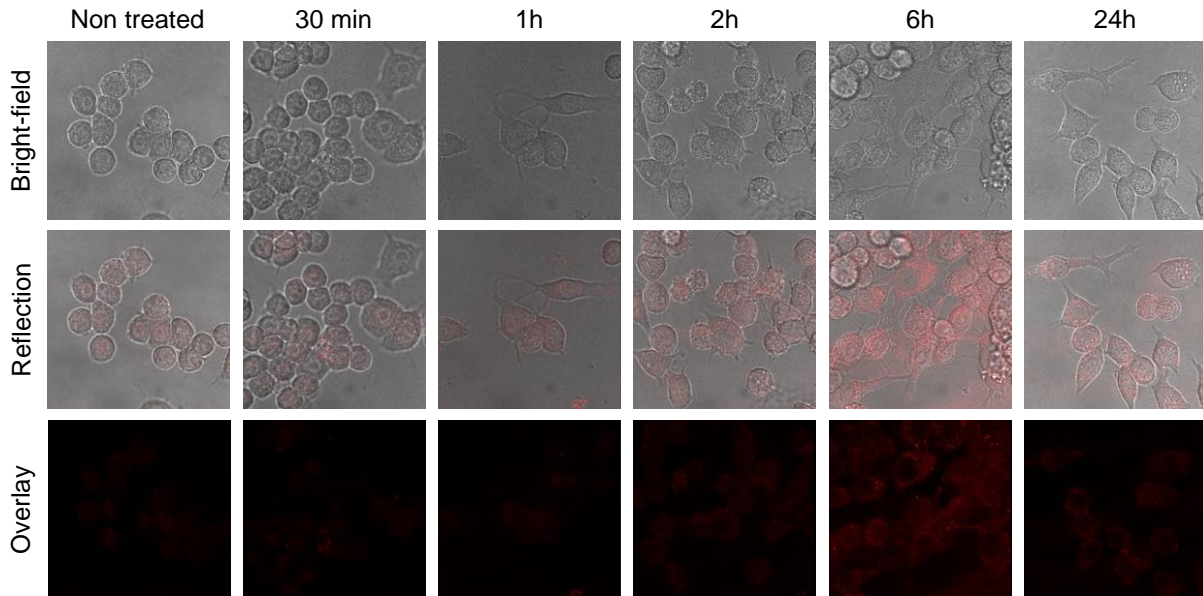


**Figure 2.** Intracellular distribution of CS-Fe<sub>20%</sub>/ATP nanogels in RAW 264.7 cells, after 30 min, 1 h, 2 h, 6 h and 24 h incubation at 37 °C, as observed by confocal laser microscopy by reflection on a 0.8 μm thick midpoint optical slice.

### *1.3 Transmission electron microscopy of cells treated with Cs-Fe/ATP nanogels*

RAW 264.7 cells treated with CS-Fe<sub>20%</sub>/ATP nanogels at high concentration (100 μg/mL of iron) were successfully observed by TEM (images shown in Figure 3). As a control measure, untreated cells were imaged in the same conditions (Fig. A, B, C, D). Cell sections show a variety of noticeable features, including the plasma membrane, the nucleus, the mitochondria and the lysosomes (electron dense zones). The increase in the number of intracellular vacuoles containing dark, electron-dense entities in treated cells is evident. These cytoplasmic structures resembled phagosomes or autophagosomes, which typically have size > 500 nm. Cells treated with nanogels exhibit also an increased quantity of ingested material in the cytoplasm

corresponding to electron-dense zones with a size around 500 nm (Fig. I, J, K, L). Furthermore, after treatment with nanogels, electron-dense zones with a size > 500 nm were observed in correspondence with mitochondria (Fig.3 E, F, G).

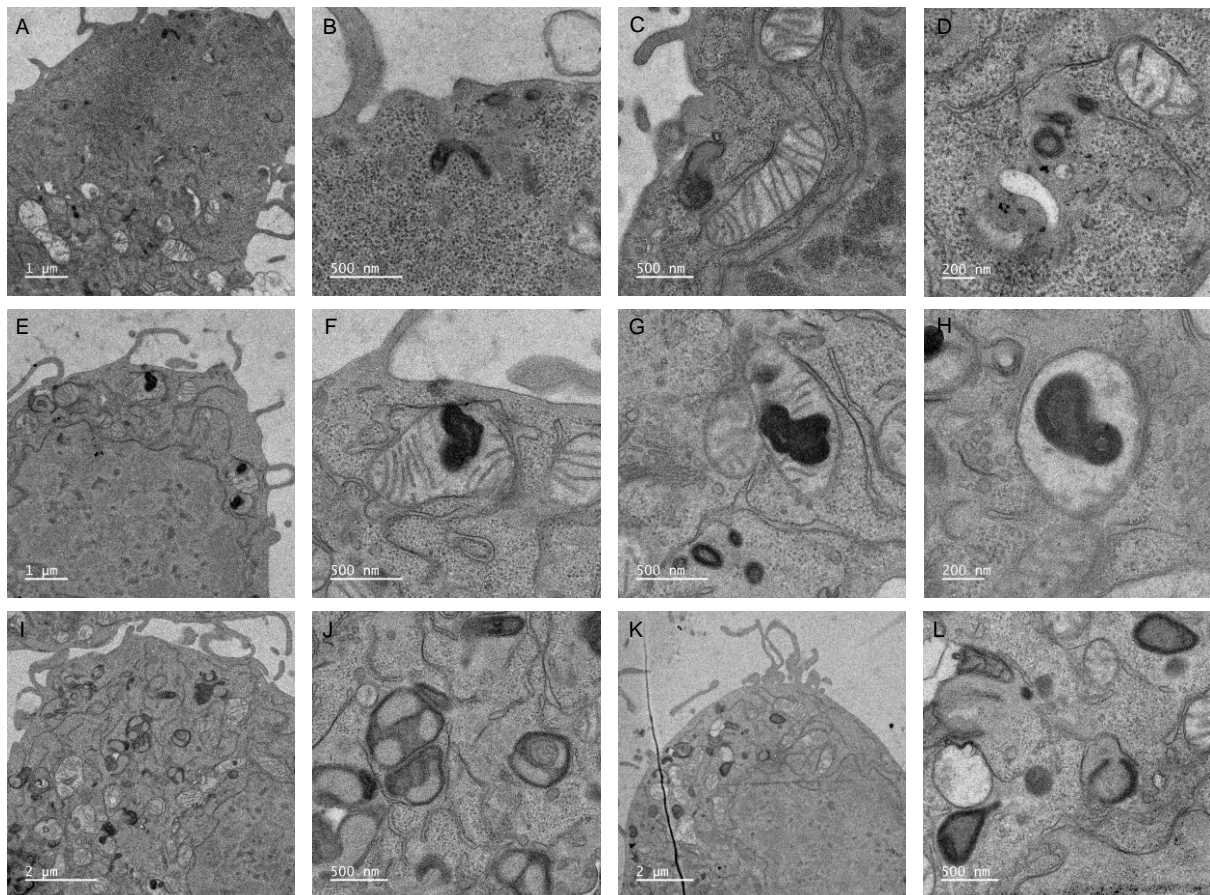


**Figure 3.** Overview of the uptake of CS-Fe<sub>20%</sub>/ATP nanogels in RAW 264.7 cells after 12 h incubation at the concentration of 0.1 mg/mL of iron. (A, B, C, D) Non-treated cells. (E, F, G, H, I, J, K, L) Cells incubated with nanogels.

## 2. Comparative toxicity of iron-containing nanogels, iron-containing polymer and free iron

### 2.1 Cell morphology analysis

The impact of nanogels on cell morphology was investigated through flow cytometry analysis and compared with the effects of the CS-Fe<sub>20%</sub> polymer and Fe(NO<sub>3</sub>)<sub>3</sub>. In particular, two parameters were taken into account: the side scattering (SSC) pattern and the height forward scattering (FSC-H). Results showed in Figure 4 evidenced that neither CS-Fe<sub>20%</sub>/ATP nanogels nor CS-Fe<sub>20%</sub> polymer affected the SSC pattern and at any tested concentrations and incubation time. On the contrary, Fe(NO<sub>3</sub>)<sub>3</sub> treatment did increase the SSC after 24 h exposure at high concentrations ( $\geq 20 \mu\text{g/mL}$ ). Regarding the FSC-H patterns, slight increases were observed after 24 h exposure to each compound at the highest concentration (20  $\mu\text{g/mL}$  iron).

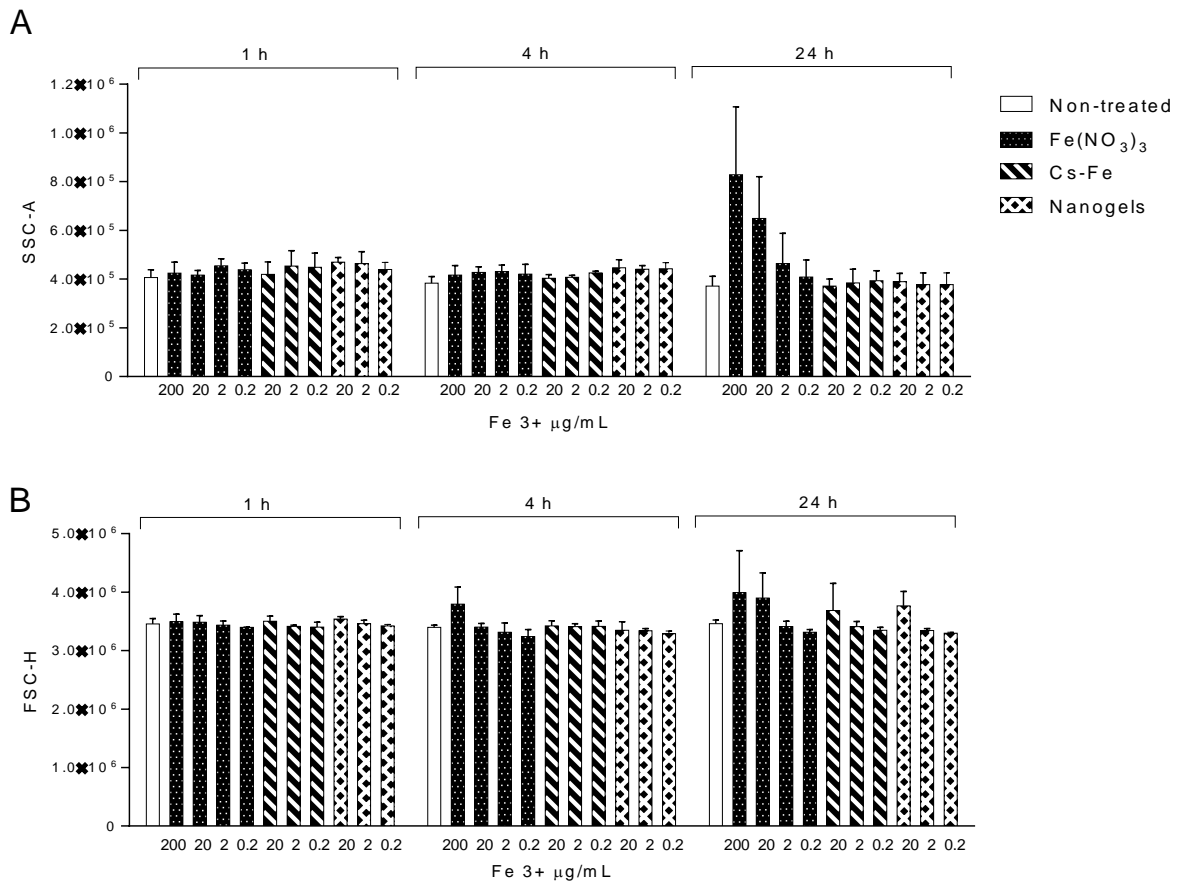


**Figure 4.** Side scatter (SSC) values of RAW cells treated different concentration of  $\text{Fe}(\text{NO}_3)_3$ , CS- $\text{Fe}_{20\%}$  polymer and CS- $\text{Fe}_{20\%}$ ,/ATP nanogels (A). Forward scatter (FSC-H) values of RAW cells treated different concentration of  $\text{Fe}(\text{NO}_3)_3$ , CS- $\text{Fe}_{20\%}$  polymer and CS- $\text{Fe}_{20\%}$ ,/ATP nanogels (B). Concentrations are expressed as  $\mu\text{g}/\text{mL}$  of  $\text{Fe}^{3+}$ . Data are presented as mean  $\pm$  S.D, n = 3.

### 2.2 Cellular viability by Propidium Iodide Assay

The cellular viability was evaluated by flow cytometry after incubation with propidium iodide (PI) that can stain permeabilized cells. Unlabeled cells are considered as viable, PI-positive cells as necrotic or late apoptotic. Results (Fig.5) show that compared to non-treated cells, there was no increase of necrosis in cells exposed for 24 h to CS- $\text{Fe}_{20\%}$ ,/ATP nanogels or to CS- $\text{Fe}_{20\%}$  polymer, at any concentration. On the contrary, cells treated with  $\text{Fe}(\text{NO}_3)_3$  from 2  $\mu\text{g}/\text{mL}$  exhibited significantly higher fractions of necrotic cells.

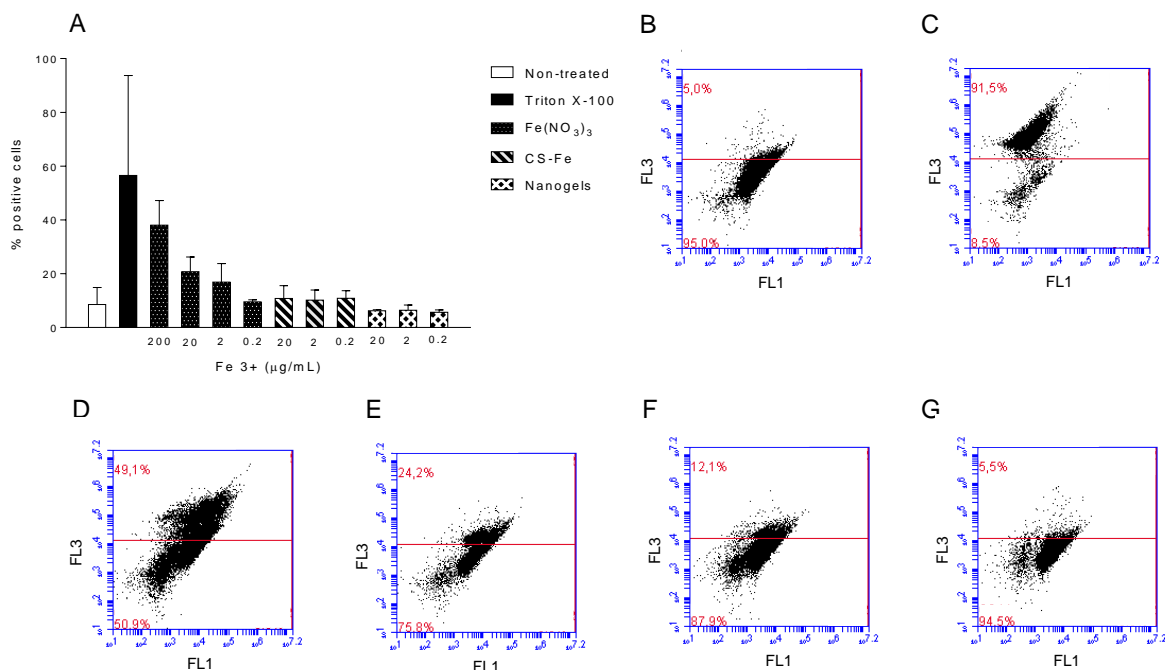


**Figure 5.** Percentages of necrotic RAW cells detected by PI assay after 24 h of exposure to Triton X-100 (necrosis control) and different concentration of  $\text{Fe}(\text{NO}_3)_3$  salt, CS- $\text{Fe}_{20\%}$  polymer, CS- $\text{Fe}_{20\%}$ ,/ATP nanogels (A). Concentrations are expressed as mg/mL of  $\text{Fe}^{3+}$ . Data presented as mean  $\pm$  S.D., n = 3. Representative flow cytometry analysis of non-treated cells (B), cells treated with Triton X-100 (0.1 mg/mL) (C), cells treated with  $\text{Fe}(\text{NO}_3)_3$  (0.2 mg/mL of  $\text{Fe}^{3+}$ ) (D), cells treated with  $\text{Fe}(\text{NO}_3)_3$  (0.02 mg/mL of  $\text{Fe}^{3+}$ ) (E), cells treated with CS- $\text{Fe}_{20\%}$  polymer, (0.02 mg/mL of  $\text{Fe}^{3+}$ ) (F), CS- $\text{Fe}_{20\%}$ ,/ATP nanogels (0.02 mg/mL of  $\text{Fe}^{3+}$ ) (G).

### ***2.3 Detection of intracellular Reactive Oxygen Species (ROS)***

The intracellular production of reactive oxygen species (ROS) was investigated using the  $\text{H}_2\text{DCFDA}$  probe, which becomes fluorescent after cellular internalization and oxidation. LPS was used as positive control in such conditions (1  $\mu\text{g/mL}$ ) that cells retain a good viability according to preliminary MTT tests. As shown in Fig.6, LPS induces oxidative stress only after 24 h treatment. On the contrary, the exposure to  $\text{Fe}(\text{NO}_3)_3$  at the iron concentration of 20  $\mu\text{g/mL}$  and 2  $\mu\text{g/mL}$  causes a strong production of ROS as soon as after 1 h of treatment and diminishes with the time. In contrast, neither CS- $\text{Fe}_{20\%}$  polymer nor CS- $\text{Fe}_{20\%}$ ,/ATP nanogels induced significant ROS production at any concentration and incubation time tested.

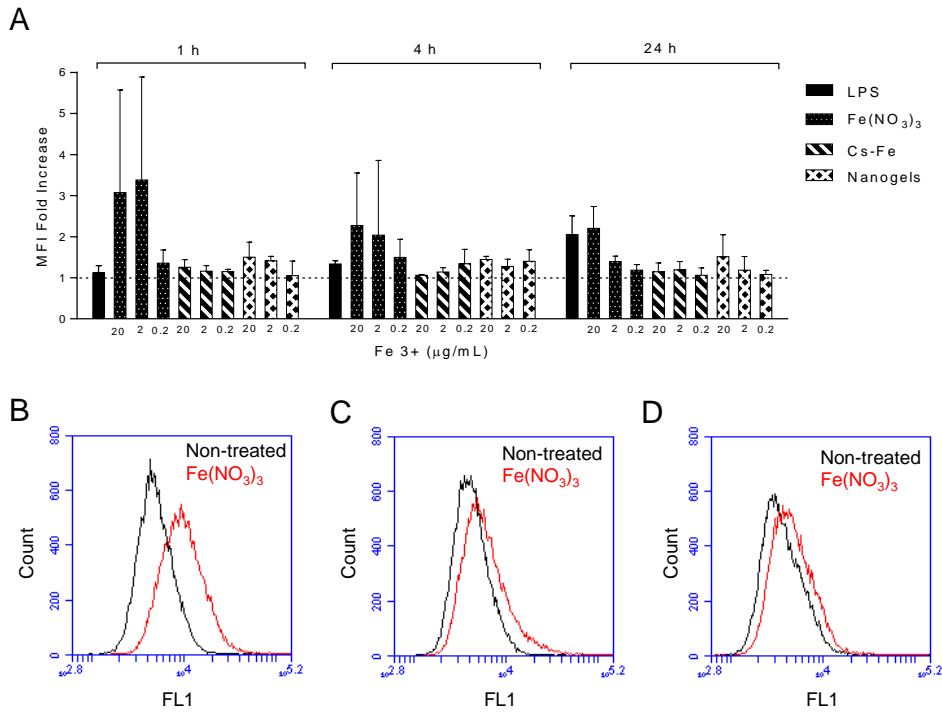


**Figure 6.** H2DCFDA fluorescence increase of RAW cells treated with LPS (1 μg/mL) and different concentrations of Fe(NO<sub>3</sub>)<sub>3</sub> salt, CS-Fe<sub>20%</sub> polymer, CS-Fe<sub>20%</sub>/ATP nanogels compared to non-treated cells (A). Concentrations are expressed as mg/mL of Fe<sup>3+</sup>. Data presented as mean ± S.D., n = 3. Representative FL-1 intensities of cells exposed to Fe(NO<sub>3</sub>)<sub>3</sub> (0.02 mg/mL of Fe<sup>3+</sup>) for 1 h (B), 4 h (C), 24 h (D), compared to untreated cells.

#### 2.4 Impact on mitochondrial membrane potential

The mitochondrial damage consequent to iron treatment was evaluated through the assessment of the mitochondrial membrane potential by TMRE staining. All treatments were found to induce a slight decrease of this potential, indicating a mitochondrial impairment. Fe(NO<sub>3</sub>)<sub>3</sub> has a higher impact on mitochondria compared to CS-Fe<sub>20%</sub>/ATP nanogels, and the CS-Fe<sub>20%</sub> polymer has an intermediate effect.

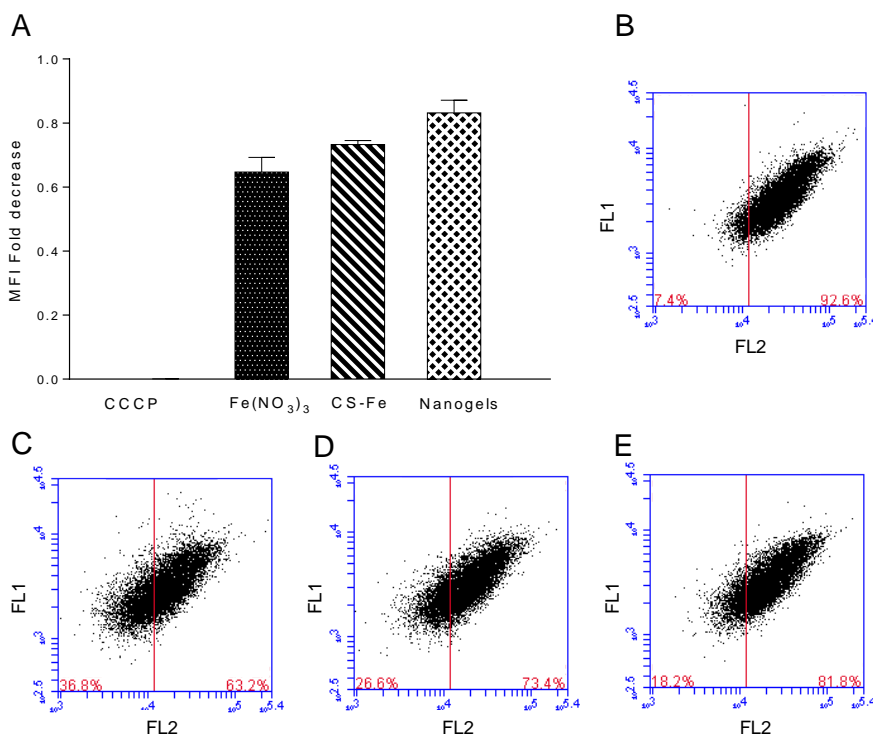


**Figure 7.** MFI Fold decrease of RAW cells treated with CCCP (1  $\mu\text{g}/\text{mL}$ ) and different concentrations of  $\text{Fe}(\text{NO}_3)_3$  salt, CS- $\text{Fe}_{20\%}$  polymer, CS- $\text{Fe}_{20\%}$ /ATP nanogels compared to non-treated cells, after exposure to tetramethylrhodamine-ethyl ester (TMRE) (A).. Data presented as mean  $\pm$  S.D.,  $n = 3$ . Representative flow cytometry analysis of non-treated cells (B), cells treated with  $\text{Fe}(\text{NO}_3)_3$  (C), cells treated with CS- $\text{Fe}_{20\%}$  (D), cells treated with CS- $\text{Fe}_{20\%}$ /ATP at the concentration (E) at the concentration of 0.02  $\text{mg}/\text{mL}$  of  $\text{Fe}^{3+}$ .

## DISCUSSION

The biological effects of CS- $\text{Fe}/\text{ATP}$  nanogels were evaluated on RAW 264.7 murine macrophages and compared to those of the CS- $\text{Fe}/\text{ATP}$  free polymer and to  $\text{Fe}(\text{NO}_3)_3$  (free  $\text{Fe}^{3+}$ ), by treating cells with the same amounts of iron (III). The objective of this approach was to clarify the intracellular behavior of iron, when added on cells in its free form, complexed to chitosan or inside of the nanogels structure.

In the first part of the work, the intracellular fate of nanogels was investigated using complementary techniques. Fluorescent ATP, one of the nanogel component, was first monitored by confocal laser microscopy. Although free fluorescent ATP exhibited a certain degree of uptake, suggesting that the molecule can be uptaken by RAW macrophages probably thanks to nucleoside transporters on the cell membrane, the uptake was found to be clearly higher when the molecule was delivered by nanogels compared to the free molecule, confirming previous results performed on other cells.<sup>4</sup> Furthermore, the perinuclear fluorescence observed in median optical slices showed that the molecule was delivered in the cell cytoplasm rather than merely bound to the cell membrane.

The kinetics of the cellular internalization of nanogels has been investigated by confocal microscopy through reflection mode. RAW 264.7 cells were shown to internalize nanogels with a time-dependent trend that reaches a maximum after 6 h and then decreases. These results are consistent with previous studies on the intracellular uptake of chitosan nanogels by macrophages.<sup>16</sup> Indeed, it was proven that, after reaching the highest degree of internalization around 6-8 h of incubation, a large proportion of chitosan nanogels are exocytosed by macrophages within 24 h. Moreover, it was shown by a resonance energy transfer (FRET) method that most of chitosan nanogels that are not exocytosed are degraded in lysosomes after internalization within 0–8 h. This report could explain the absence of clearly visible nanogels in TEM images reported in this work: after treating RAW cells for 12 h with CS-Fe/ATP nanogels, some electron-dense entities were observed but not resembling chitosan nanogels. Regarding other types of iron-based nanoparticles, a lysosome-degradating pathway has been also reported as common metabolic pathway.<sup>17,18,10</sup> In fact, both the low pH environment of endosomes/lysosomes and some intracellular Fe-chelating substances (i.e., phosphate, nucleotides and dicarboxylic acids, etc.) can solubilize iron oxide particles and free iron can be released into the intracellular iron metabolic pool.<sup>19,20</sup>

The impact of nanogels treatment on cell morphology was then investigated by flow cytometry. A slight increase in the cell volume was observed after 24 h of incubation, consistent with the uptake of nanogels by the macrophages. The treatment with CS-Fe free polymer and  $\text{Fe}(\text{NO}_3)_3$  provoked as well a FSC-H increase, which could be explained by the phagocytosis of aggregates formed following the interactions between the plasmatic proteins and both CS-Fe and free  $\text{Fe}^{3+}$ , as observed macroscopically. On the contrary, only the exposure to  $\text{Fe}(\text{NO}_3)_3$  induced an increase of cells granularity upon 24 h at high concentrations ( $\geq 20 \mu\text{g/mL Fe}^{3+}$ ). These data can be related to the presence of aggregates on the cell membrane or to changes in the organelles within cells related to cells suffering. Images obtained by confocal microscopy confirmed the absence of any effect on cells morphology after treatment with nanogels at the tested concentrations.

Before investigating specific endpoints of iron toxicity, we evaluated the toxicity of all compounds on macrophages in terms of induction of necrosis by Propidium Iodide Assay. All the compounds exhibited no cytotoxicity, for iron concentrations up to  $20 \mu\text{g/mL}$  of iron. When added to cells at low concentrations, none of the compounds induced a decrease of cell viability. At high concentrations ( $> 20 \mu\text{g/mL}$ ), significant differences appeared between free iron (III) and CS-Fe/ATP free polymer or CS-Fe/ATP nanogels. In a previous study, it was reported that chitosan oligosaccharide coating on iron oxide nanoparticles results in a decreased cytotoxic impact of bare iron oxide nanoparticles.<sup>21</sup> The authors attribute the reduced toxicity to the controlled release of iron from nanoparticles into the acidic environment of lysosomes. Indeed, the intracellular degradation has been shown to be also a key factor in the toxicity determination of iron-based nanoparticles.<sup>20,22</sup> It is well known that free iron has the potential to become cytotoxic when electron exchange with oxygen is unrestricted and catalyzes the production of reactive oxygen species.<sup>23</sup> Recently, a new form of iron-dependent cell death, named ferroptosis, was discovered. Ferroptosis result from iron-dependent lipid peroxide and ROS

accumulation. It is characterized by mitochondrial damage without typical apoptotic and necrotic manifestations. In fact, the expansion of the catalytically active iron pool in the mitochondria may play a central role in iron toxicity, leading to lipid peroxidation of mitochondrial membranes, perturbation in mitochondrial  $\text{Ca}^{2+}$  transport and decreased production of ATP.<sup>24</sup> An alternative proposed mechanism for the toxic effects of iron on cells involves the proposition that an accumulation of iron within the cellular lysosomal compartment sensitizes the lysosomes to damage and rupture, with release of damaging lysosomal digestive enzymes into the cytoplasm of the cell. Minimal release of lysosomal enzymes may induce transient reparative autophagocytosis.<sup>25</sup> To evaluate the possible induction of ferroptosis by nanogels, the oxidative stress and the mitochondrial damage were evaluated. The exposure to  $\text{Fe}(\text{NO}_3)_3$  induced an immediate strong production of ROS that diminishes with the time, whereas all compounds showed to have a toxic effect on mitochondria, with the higher effects still observed in the case of  $\text{Fe}(\text{NO}_3)_3$  and lower in the case of nanogels.

In order to investigate the potential effects on macrophages of high concentrations of CS-Fe/ATP nanogels, cells were observed by TEM after exposure to high concentrations of nanogels (100  $\mu\text{g}/\text{mL}$  of iron). Images obtained evidenced an increased number of vacuoles resembled phagosomes or autophagosomes. Autophagy is an innate defense mechanism in which the cells degrade dysfunctional cellular organelles and misfolded proteins. This mechanism can be induced in nanoparticles uptake leading to inflammatory responses such as specified polarization of immune cells and release of pro-inflammatory cytokines.<sup>26,27</sup> Our hypothesis is that after internalization, Cs-Fe20% nanogels are gradually dissolved inside of cells, releasing intracellularly iron that can become toxic in high amounts. Unexpectedly, TEM images evidenced also the presence of large electron-dense regions in mitochondria in cells treated with nanogels. These observations could be related to iron accumulation in mitochondria<sup>28,29</sup>, as reported in cases of iron metabolism dysregulation. These observations,

together with the data provided on the mitochondrial membrane potential depletion, indicate that the accumulation of CS-Fe<sub>20%</sub>/ATP nanogels inside of macrophages may have a potential toxic effect on mitochondria.

## **CONCLUSIONS**

The potential applications of chitosan-iron nanogels as nucleotides delivery systems are extremely interesting based on the cell-nano interaction. However, the mechanisms underlying cell uptake, intracellular trail and possible mechanisms of toxicity have to be clearly elucidated. In fact, iron-based nanoparticles have been frequently associated with toxic effects towards immune cells. In the present study, various cellular toxicity endpoints have been used in order to understand the role played by the iron present in the nanogels structure on the eventual toxicity. The comparison of CS-Fe<sub>20%</sub>/ATP nanogels to the CS-Fe<sub>20%</sub> soluble polymer and to free Fe<sup>3+</sup> showed that the toxicological profile of nanogels can be very different from the sum of their components studied separately. In fact, nanogels did not show any toxicity in terms of necrosis induction and oxidative stress for concentrations up to 20 µg/mL iron, contrary to the treatment with Fe(NO<sub>3</sub>)<sub>3</sub> (free Fe<sup>3+</sup>).

Data obtained in this study put in evidence the *in vitro* safety profile of CS-Fe<sub>20%</sub> based nanogels. Moreover, results obtained by the comparison with free iron can provide an additional understanding of the cellular effects of iron-based nanoparticles and may contribute to their safe use in medicine.

## EXPERIMENTAL

### *Materials*

Nanogels were prepared using low viscosity chitosan purchased from Sigma-Aldrich (France) complexed with Iron and ATP (Sigma). The degree of N-deacetylation of commercial chitosan was determined to be 84% by  $^1\text{H}$  NMR spectroscopy. In the following, water refers to MilliQ® purified water (Millipore, France) of resistivity  $\geq 18.2 \text{ M}\Omega\cdot\text{cm}$ . Complexation of CS with iron was achieved with iron (III) nitrate nonahydrate, 1,10-Phenanthroline monohydrate and hydroxylamine hydrochloride from Sigma. Fetal bovine serum (FBS) was from Gibco, 2',7'-dichlorodihydrofluorescein diacetate ( $\text{H}_2\text{DCFDA}$ ) and lipopolysaccharide from Escherichia coli (LPS) were from Sigma. BODIPY®-TR ATP was from Invitrogen, propidium iodide was from BD Biosciences and the Mitochondrial Potential assay kit was from Cell Signaling Technology. Glutaraldehyde and Osmium were purchased from EMS and resine Epon Low Viscosity Premix Kit Medium from Agar Scientific. Other reagents used were purchased from Sigma; all solvents were of analytical grade.

### *Cell culture*

The macrophage-like murine cell line RAW 264.7 was obtained from ATCC (catalog number TIB-71) and cultured in high glucose Dulbecco's Modified Eagle's Medium (Sigma), supplemented with 50 U/mL penicillin, 50 U/mL streptomycin, and 10% fetal bovine serum (Gibco). Cells were maintained at 37 °C in a 5%  $\text{CO}_2$  humidified atmosphere. Twice a week, cells were divided at 1:10 ratio by scraping.

### ***Preparation and characterization of Cs-Fe/ATP nanogels***

A CS-Fe solution was obtained by dissolving CS-Fe<sub>20%</sub> powder in water at a final concentration of 1 mg/mL without addition of acetic acid, stirring overnight and filtrating through 0.22 µm filter. A freshly prepared solution of ATP at a concentration of 15 mg/mL was added dropwise to the Cs-Fe solution under magnetic stirring at 1000 rpm to allow nanogels formation. For fluorescence studies, nanogels were formed from a 15 mg/mL ATP solution prepared using BODIPY®-TR ATP as a tracer (0.5%). Nanogels were purified from free ATP and free CS-Fe<sub>20%</sub>, through centrifugation of 1 mL suspension on a 20 µL glycerol layer at 2000 × g for 1 h, removal of 0.92 mL supernatant, and redispersion in water at a final volume of 1 mL or lower in order to concentrate nanogels.

### ***Cellular uptake of fluorescent ATP-loaded nanogels***

RAW 264.7 cells were seeded on coverslips previously placed in 6-well plates, having respectively 300,000 cells and 2 mL medium per well, and pre-incubated for 24 h. Preparation of nanogels was realized using fluorescent BODIPY®-TR ATP as a tracer, and a free fluorescent ATP solution was prepared as a control using the same concentration. CS-Fe/ATP nanogels at the concentration of 1 mg/mL and the control solution were diluted 1:10 in cell culture medium and incubated with cells for 24h. After incubation, the supernatant was removed and cells were washed with fresh medium. The coverslips with the cells were removed from the well and mounted on a microscope slide previously prepared with a drop of Vectashield® mounting medium. Cells were then imaged by confocal microscopy.

### ***Cellular uptake of non-labeled Cs-Fe/ATP nanogels***

RAW 264.7 cells were seeded on coverslips previously placed in 6-well plates, having respectively 300,000 cells and 2 mL medium per well, and pre-incubated for 24 hours. CS-Fe/ATP nanogels at the concentration of 1 mg/mL were diluted 1:10 in cell culture medium and incubated with the cells for 24h. Untreated cells were used as control. After 30 min, 1 h, 2 h, 6 h or 24 h incubation, the supernatant was removed and cells were washed with fresh medium. The coverslips with the cells were removed from the well and mounted on a microscope slide previously prepared with a drop of Vectashield® mounting medium. Cells were then imaged by confocal microscopy by reflection mode.

### ***Confocal microscopy***

The samples were imaged with an inverted confocal laser scanning microscope TCS SP8 – gSTED Leica (Leica, Germany) using a HC PL APO CS2 63x/1.40 oil immersion objective lens. The instrument was equipped with a WLL Laser (592 nm excitation wavelength for Bodipy and 488 nm for the reflexion mode). Red fluorescence emission was collected with a 608-745 nm wide emission slits and a 478-507 nm wide emission slits for the reflexion signal under a sequential mode. Transmission images were acquired with a PMT-trans detector. The pinhole was set at 1.0 Airy unit. 12 bit numerical images were done with the Leica Application Suite X software (Version 3.5.5; Leica, Germany).

### ***Transmission Electron Microscopy on cells treated with Cs-Fe/ATP nanogels***

RAW 264.7 cells were seeded on coverslips previously placed in 12-well plates, having respectively 200,000 cells and 1 mL medium per well, and pre-incubated for 24 hours. CS-Fe/ATP nanogels at the iron concentration of 100 µg/mL were diluted 1:10 in cell culture

medium and incubated with the cells for 12 h. Untreated cells were used as control. After incubation, cells were rinsed twice with phosphate buffer 0.2 M at pH 7.4 at 37°C and then fixed at RT with Glutaraldehyde 2.5% in phosphate buffer 0.1M at pH 7.4 for 2 h. After fixation, cells were rinsed with phosphate buffer four times for 5 min and then post-fixed in 1% osmium and 1.5% potassium ferrocyanide in the same buffer. Cells were then rinsed five times in water, dehydrated in ethanol 50%, 70%, 90%, 2x100% (10 min for each bath) and finally embedded 2 h in 1:1 epoxy resin:ethanol and 2 h in pure resin. Polymerisation was performed 24 h at 60°C. The glass coverslip was removed from the resin by a heat shock and cells were sectioned with ultramicrotome (UC6) and a diamond knife (ultra 35°, Diatome). 70 nm-sections were collected on formvar-coated copper grids, stained with 2% uranyl acetate and lead citrate before observation in TEM operating at 80 kV (JEOL1400 equipped with a RIO9 camera (Gatan)).

### ***Cell morphology analysis***

Cell morphology was studied by analyzing height forward scatter (FSC-H) and side scatter (SSC) using flow cytometry (Accuri C6, BD Biosciences). RAW 264.7 cells were seeded onto 6-wells plate with 2 mL of growth medium at a density of 300,000 cells/well for 1 h and 4 h incubation and 150,000 cells for 24 h incubation. After 24 h of pre-incubation, cells were treated for 1 h, 4 h and for 24 h with CS-Fe/ATP nanogels, free CS-Fe<sub>20%</sub> or Fe(NO<sub>3</sub>)<sub>3</sub> diluted in culture media at different final concentrations of iron (0.2, 2 and 20 µg/mL). For Fe(NO<sub>3</sub>)<sub>3</sub>, an additional very high concentration corresponding to a Fe<sup>3+</sup> concentration of 200 µg/mL was tested. Afterward, cells were rinsed with ice-cold PBS, detached by scraping and suspended in PBS for flow cytometry analysis. All measurements were performed in triplicate.

***Cellular viability by Propidium Iodide Assay***

Necrosis detection following exposure to CS-Fe/ATP nanogels were performed using propidium iodide (PI, BD Biosciences) (red fluorescence). RAW 264.7 cells were seeded with 2 mL of growth medium in 6-wells plates (200,000 cells/well) and pre-incubated for 24h. Culture medium was then replaced with dilutions of CS-Fe/ATP nanogels, CS-Fe<sub>20%</sub> or Fe(NO<sub>3</sub>)<sub>3</sub> in culture medium at different final concentrations of iron (0.2, 2 and 20 µg/mL). For Fe(NO<sub>3</sub>)<sub>3</sub>, an additional high concentration corresponding to a Fe<sup>3+</sup> concentration of 200 µg/mL was tested. After 24 h of incubation, plates were centrifuged (200×g, 5 min), the culture medium was discarded, and cells were rinsed twice with ice-cold PBS. Cells were incubated with PI at RT in the dark for 15 min, then rinsed with ice-cold PBS and scraped. Cells were suspended in ice-cold PBS and immediately analyzed by flow cytometry (Accuri C6, BD Biosciences) using the fluorescent channel FL-3. Triton X-100 (0.1 mg/mL) was used as positive control for necrosis induction.

***Detection of intracellular reactive oxygen species (ROS)***

RAW 264.7 cells were seeded in 6-well plates with 2 mL of growth medium (450,000 cells/well for 1 h and 4 h treatments and 250,000 cells/well for 24 h treatment) and pre-incubated for 24 h. Culture medium was then replaced with dilutions of CS-Fe/ATP nanogels, CS-Fe<sub>20%</sub> or Fe(NO<sub>3</sub>)<sub>3</sub> at different final concentrations of iron (0.2, 2 and 20 µg/mL). After 1 h, 4 h or 24 h of incubation, cells were rinsed twice with PBS at 37°C and then exposed for 45 min to 5 µM H<sub>2</sub>DCFDA in PBS at 37°C. Cells were then washed twice with PBS and incubated with fresh growth medium for 30 min at 37°C. Afterwards, cells were rinsed with cold PBS, recovered and immediately analyzed by flow cytometry (Accuri C6, BD Biosciences), on FL-1 channel. LPS (1 µg/mL) was used as positive control for necrosis induction.

### ***Impact on mitochondrial membrane potential***

RAW 264.7 cells were seeded with 1 mL of growth medium in 12-wells plates (90,000 cells/well). After 24 h of pre-incubation, culture medium was replaced with dilutions of CS-Fe/ATP nanogels, free CS-Fe<sub>20%</sub> or Fe(NO<sub>3</sub>)<sub>3</sub> in culture medium at the concentrations of iron 0.2 µg/mL. After 24 h of incubation, tetramethylrhodamine-ethyl ester (TMRE) was added to wells at the concentration of 200 nM and incubated for 20 min at 37°C. Cells were rinsed with cold PBS, recovered and immediately analyzed by flow cytometry (Accuri C6, BD Biosciences) using the fluorescent channel FL-2. The mitochondrial membrane potential disruptor carbonyl cyanide 3-chlorophenylhydrazone (CCCP) (100 µM) was used as positive control for depolarization induction.

### **ACKNOWLEDGMENTS**

Thanks to Valérie Nicolas for confocal microscopy observations, Juliette Vergnaud for help with mitochondrial potential experiments, Claire Boulogne and Cynthia Dupas for cell inclusions and TEM observations. The present work has benefited from Imagerie-Gif core facility supported by l'Agence Nationale de la Recherche (ANR-11-EQPX-0029/Morphoscope, ANR-10-INBS-04/FranceBioImaging ; ANR-11-IDEX-0003-02/ Saclay Plant Sciences).

## REFERENCES

1. Kean, T. & Thanou, M. Biodegradation, biodistribution and toxicity of chitosan. *Advanced Drug Delivery Reviews* **62**, 3–11 (2010).
2. Amidi, M. & Hennink, W. E. Chitosan-based formulations of drugs , imaging agents and biotherapeutics ☆. *Adv. Drug Deliv. Rev.* **62**, 1–2 (2010).
3. Giacalone, G., Fattal, E. & Hillaireau, H. Drug-Induced Nanocarrier Assembly as a Strategy for the Cellular Delivery of Nucleotides and Nucleotide Analogues. 0–5 (2013). doi:10.1021/bm301832v
4. Giacalone, G. *et al.* Stabilization and cellular delivery of chitosan – polyphosphate nanoparticles by incorporation of iron. *J. Control. Release* **194**, 211–219 (2014).
5. Dixon, S. J. *et al.* NIH Public Access. **149**, 1060–1072 (2013).
6. Yu, H., Guo, P., Xie, X., Wang, Y. & Chen, G. Ferroptosis , a new form of cell death , and its relationships with tumourous diseases Definition and discovery of ferroptosis Differences between ferroptosis and apoptosis / necrosis. **21**, 648–657 (2017).
7. Shen, Z. *et al.* Emerging Strategies of Cancer Therapy Based on Ferroptosis. **1704007**, 1–15 (2018).
8. Wang, S. *et al.* Iron and magnetic : new research direction of the ferroptosis-based cancer therapy. **8**, 1933–1946 (2018).
9. Shah, A. & Dobrovolskaia, M. A. Immunological effects of iron oxide nanoparticles and iron-based complex drug formulations : Therapeutic benefits , toxicity , mechanistic insights , and translational considerations. *Nanomedicine Nanotechnology, Biol. Med.* **14**, 977–990 (2018).

10. Beck-speier, I. *et al.* Soluble iron modulates iron oxide particle-induced inflammatory responses via prostaglandin E 2 synthesis : In vitro and in vivo studies. **12**, (2009).
11. Press, D. Concentration-dependent toxicity of iron oxide nanoparticles mediated by increased oxidative stress. 983–989 (2010). doi:10.2147/IJN.S13244
12. Tamames-tabar, C., Cunha, D., Imbuluzqueta, E., Ragon, F. & Serre, C. frameworks †. 262–271 (2014). doi:10.1039/c3tb20832j
13. Feng, Q. *et al.* Uptake , distribution , clearance , and toxicity of iron oxide nanoparticles with different sizes and coatings. *Sci. Rep.* 1–13 (2018). doi:10.1038/s41598-018-19628-z
14. Sun, H. *et al.* Induction of oxidative stress and sensitization of cancer cells to paclitaxel by gold nanoparticles. 1633–1639 (2018). doi:10.1039/c7tb03153j
15. Jackson, T. C., Patani, B. O. & Israel, M. B. Nanomaterials and Cell Interactions : A Review. 220–228 (2017). doi:10.4236/jbnb.2017.84015
16. Wang, T. Y. & Webster, T. J. Intracellular disposition of chitosan nanoparticles in macrophages : intracellular uptake , exocytosis , and intercellular transport. 6383–6398 (2017).
17. Ning, G. U., Haiyan, X. U. & Jimin, C. A. O. The internalization pathway , metabolic fate and biological effect of superparamagnetic iron oxide nanoparticles in the macrophage-like RAW264 . 7 cell. **54**, 793–805 (2011).
18. Sci, J. M. HHS Public Access. **51**, 513–553 (2017).
19. Kornberg, T. G. *et al.* Potential Toxicity and Underlying Mechanisms Associated with Pulmonary Exposure to Iron Oxide Nanoparticles : Conflicting Literature and Unclear Risk. 1–26 doi:10.3390/nano7100307

20. Levy, M., Angeles, L., Maraloiu, V. & Wilhelm, C. Degradability of superparamagnetic nanoparticles in a model of intracellular environment : Follow-up of magnetic , structural and chemical properties Degradability of superparamagnetic nanoparticles in a model of intracellular environment : follow-up of m. (2010). doi:10.1088/0957-4484/21/39/395103
21. Shukla, S., Jadaun, A., Arora, V. & Kumar, R. In vitro toxicity assessment of chitosan oligosaccharide coated iron oxide nanoparticles. **2**, 27–39 (2015).
22. Yarjanli, Z., Ghaedi, K., Esmaeili, A., Rahgozar, S. & Zarrabi, A. Iron oxide nanoparticles may damage to the neural tissue through iron accumulation , oxidative stress , and protein aggregation. *BMC Neurosci.* 1–12 (2017). doi:10.1186/s12868-017-0369-9
23. Soares, M. P. & Hamza, I. Review Macrophages and Iron Metabolism. *Immunity* **44**, 492–504 (2016).
24. Hershko, C. Mechanism of iron toxicity. **28**, 500–509 (2007).
25. Bases, M., Cellular, O. F. & Toxicity, I. Serial Review : Iron and Cellular Redox Status. **32**, 833–840 (2002).
26. Jung, E., Ha, P., Umh, N. & Wook, S. ERK pathway is activated in bare - FeNPs - induced autophagy. 323–336 (2014). doi:10.1007/s00204-013-1134-1
27. Stern, S. T., Adiseshaiyah, P. P. & Crist, R. M. Autophagy and lysosomal dysfunction as emerging mechanisms of nanomaterial toxicity Autophagy and lysosomal dysfunction as emerging mechanisms of nanomaterial toxicity. **20**, (2012).
28. Rouault, T. A. & Tong, W. Iron – sulphur cluster biogenesis and mitochondrial iron homeostasis. **6**, (2005).

29. Martelli, A. & Puccio, H. Dysregulation of cellular iron metabolism in Friedreich ataxia : from primary iron-sulfur cluster deficit to mitochondrial iron accumulation. **5**, 1–11 (2014).

**SUPPLEMENTARY*****Characterization of Cs-Fe/ATP nanoparticles***

	Critical N/P	Mean hydrodynamic diameter (nm)	pDI	Zeta potential (mV)	Drug loading (% w/w)	Encapsulation efficiency (%)
CS-Fe <sub>20%</sub> /ATP	1.17	125 ± 5	0.09 ± 0.01	25 ± 1	39 ± 4	72 ± 2

**Figure S1.** Physicochemical properties of CS-Fe<sub>20%</sub>/ATP nanoparticles.

**Propidium Iodide Assay on cells treated with different nitrate salts, to exclude the influence of  $\text{NO}_3^-$  on  $\text{Fe}(\text{NO}_3)_3$  observed toxicity**

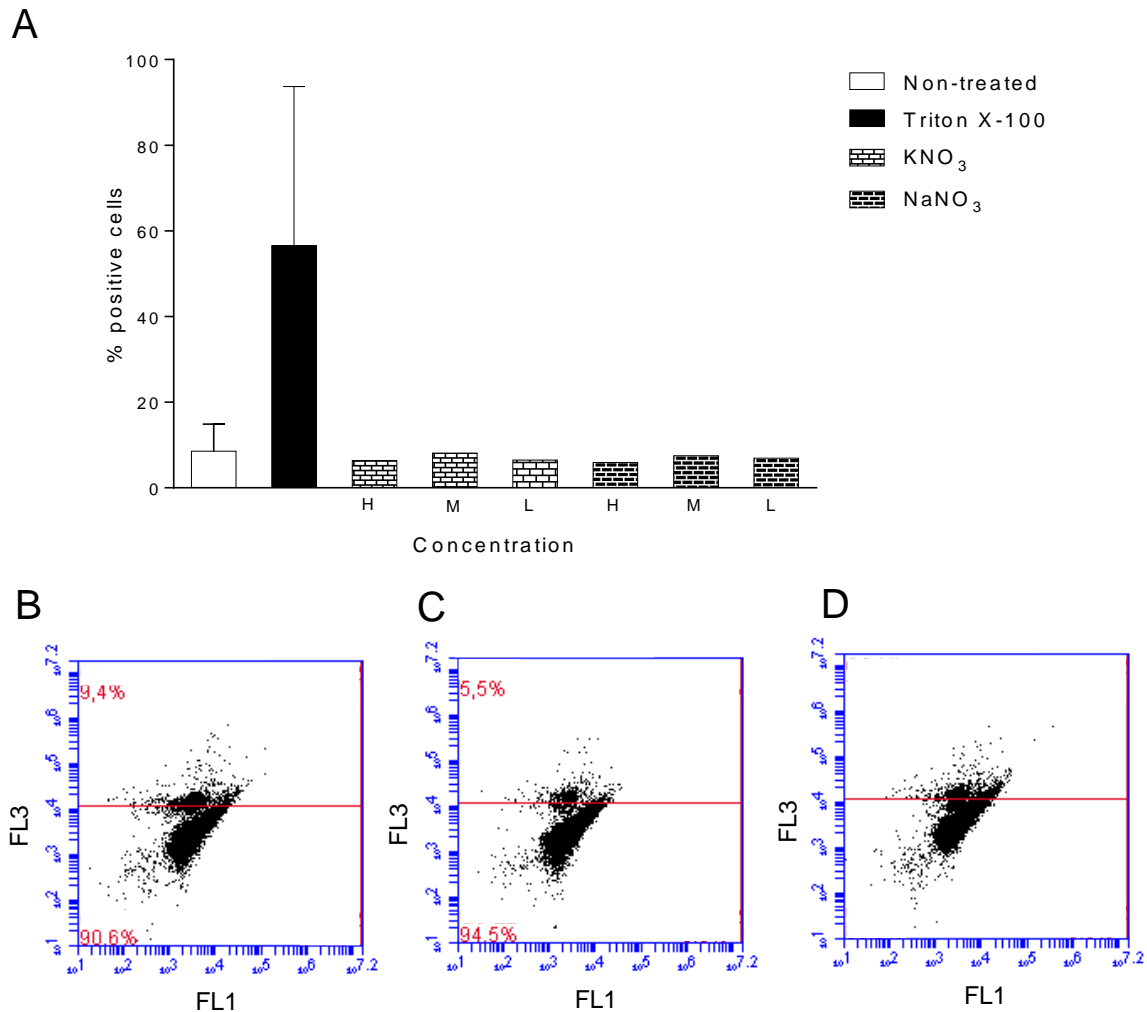


**Figure. S2** Percentages of necrotic RAW cells detected by PI assay after 24 h of exposure to Triton X-100 and different concentration of  $\text{Na}(\text{NO}_3)_3$  and  $\text{K}(\text{NO}_3)_3$  (A). The concentrations tested (Hight, Medium, Low) correspond to the  $\text{NO}_3^-$  concentrations tested with  $\text{Fe}(\text{NO}_3)_3$ . Data presented as mean  $\pm$  S.D., n = 3. Representative flow cytometry analysis of non-treated cells (B), cells treated with  $\text{Na}(\text{NO}_3)_3$  at the highest concentration (C) and cells treated with  $\text{K}(\text{NO}_3)_3$  at the highest concentration (D).

*Detection of intracellular Reactive Oxygen Species (ROS) on cells treated with different nitrate salts, in order to exclude the influence of  $\text{NO}_3^-$  on  $\text{Fe}(\text{NO}_3)_3$  oxidative stress induction*

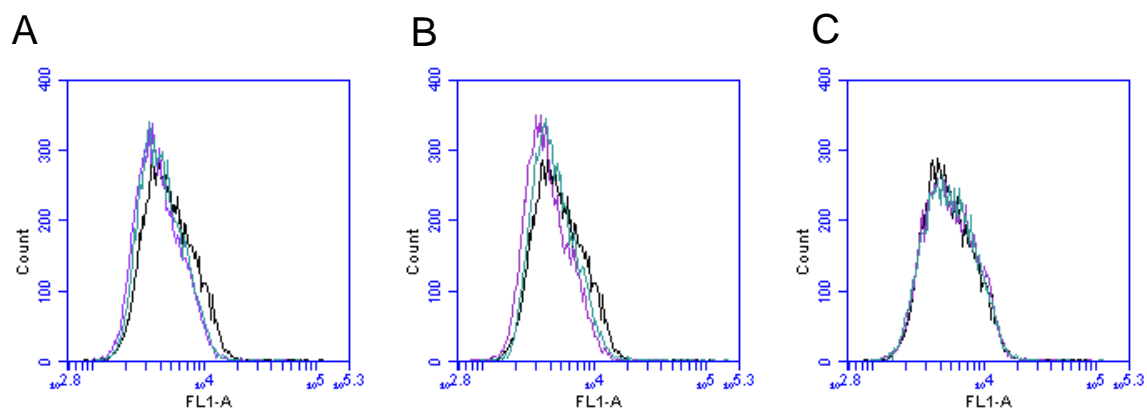


**Figure. S3** Representative FL-1 intensities of cells exposed to  $\text{Na}(\text{NO}_3)_3$  and  $\text{K}(\text{NO}_3)_3$  at the highest concentrations for 1 h (A), 4 h (B) and 24 h (C), compared to non-treated cells.





# Experimental work

---

## Chapter 4

*Nanotoxicology at the particle/micelle frontier:  
influence of core-polymerization on the  
intracellular distribution, cytotoxicity  
and genotoxicity of polydiacetylene micelles*



**Nanotoxicology at the particle/micelle frontier: influence of core-polymerization on the intracellular distribution, cytotoxicity and genotoxicity of polydiacetylene micelles**

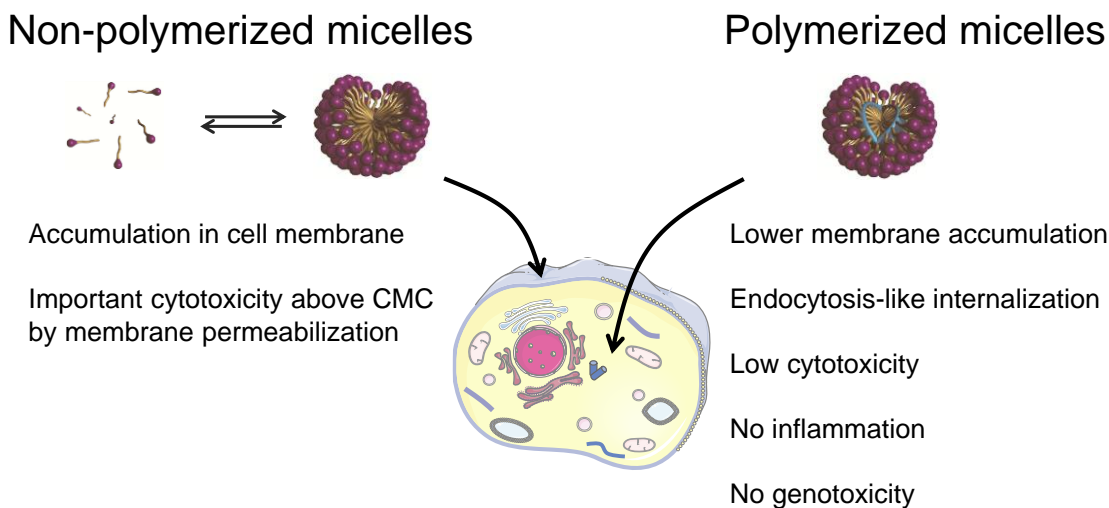
*Federica Costamagna,<sup>1</sup> Hervé Hillaireau,<sup>1</sup> Juliette Vergnaud,<sup>1</sup> Damien Clarisse<sup>2</sup>, Lucie Jamgotchian<sup>2</sup>, Olivier Loreau<sup>2</sup>, Stéphanie Denis,<sup>1</sup> Edmond Gravel,<sup>2</sup> Eric Doris,<sup>2,\*</sup> Elias Fattal<sup>1,\*</sup>*

<sup>1</sup>Institut Galien Paris-Sud, Univ. Paris-Sud, Cnrs, Université Paris-Saclay, Chatenay-Malabry, France; <sup>2</sup>Service de Chimie Bioorganique et de Marquage (SCBM), CEA, Université Paris-Saclay, 91191 Gif-sur-Yvette, France

Chapter published as an article in *Nanoscale*, 2020, 12, 2452-2463 737-742.

**ABSTRACT:** The understanding of the cellular uptake and the intracellular fate of nanoparticles and their subsequent influence on cell viability is challenging as far as micelles are concerned. Such systems are dynamic by nature, existing as unimers under their critical micelle concentration (CMC), and as micelles in equilibrium with unimers above the CMC, making canonical dose-response relationships difficult to establish. The purpose of this study was to investigate the *in vitro* cytotoxicity and uptake of two micellar systems that are relevant for drug delivery. The two micelles incorporate a poly(ethylene glycol) coating and a pentacosadiynoic core which is either polymerized (pDA-PEG micelles) or non-polymerized (DA-PEG micelles), with the aim of evaluating the influence of the micelles status (“particle-like” or “dynamic”, respectively) on their toxicological profile. Intracellular distribution and cytotoxicity of polymerized and non-polymerized micelles were investigated on RAW 264.7 macrophages in order to compare any different interactions with cells. Non-polymerized micelles showed significantly higher cytotoxicity than polymerized micelles, especially in terms of cell permeabilization, correlated to a higher accumulation in cell membranes. Other potential toxicity endpoints of polymerized micelles were then thoroughly studied in order to assess possible responses resulting from their endocytosis. No specific mechanisms of cytotoxicity were observed, neither in terms of apoptosis induction, cell membrane damage, release of inflammatory mediators nor genotoxicity. These data indicate that non-polymerized micelles accumulate in the cell membrane and induce cell membrane permeabilization, resulting in significant toxicity, whereas polymerized, stable micelles are internalized by cells but exert no or very low toxicity.

**KEYWORDS:** engineered nanoparticles; micelles; cytotoxicity; intracellular distribution; genotoxicity



## INTRODUCTION

Engineered nanoparticles, regardless of their route of administration, are able to interact with biological components or systems, leading to biomedical applications, but also potentially inducing adverse effects. Therefore, the different mechanisms behind the *in vitro* and *in vivo* toxicity of such nanomaterials should be investigated in details by nanotoxicology studies. In recent years, nanotoxicology has mostly focused on inorganic nanoparticles, providing extensive data on their cytotoxic properties.<sup>1</sup> Regarding nanoparticles for biomedical applications, most studies have been conducted on liposomes, polymeric and iron oxide nanoparticles. However, less is known about the toxicology of micellar structures used for drug delivery.<sup>2</sup> Such systems are puzzling to evaluate in terms of canonical dose-response relationships, because they are dynamic by nature, existing as unimers below specific critical micelle concentration (CMC),<sup>3</sup> and as micelles in equilibrium with unimers above the CMC. In this respect, they differ from nanoparticles or liposomes, the structure of which is insensitive to dilution. Micelles and unimers might have different behaviors in regard to cellular uptake, membrane accumulation, and intracellular distribution, but results of investigations published to date are quite conflicting and

the mechanisms of interaction not yet clear. In our attempts to shed light on the influence of such a dynamic structure on cell responses, we investigate two nanoobjects of similar composition, in two different states: on the one hand, native micelles as a “dynamic” system; on the other hand, core-polymerized micelles, as a “particle-like” system.

The use of micelles for the delivery of hydrophobic drugs, nucleic acids, proteins, and contrast agents has been widely studied in recent years, especially for cancer diagnosis and therapy,<sup>4,5,6,7</sup> and several clinical trials have been conducted.<sup>8,9,10</sup> Among the different nanoparticulate systems, micelles combine interesting features such as easy assembly, modular surface chemistry and a wide range of available sizes.<sup>11</sup> Conventional polymeric micelles are made of amphiphilic copolymers that, in an aqueous environment, spontaneously assemble into colloidal particles characterized by a core/shell structure.

Since physical and chemical stabilities in plasma still remain the major concerns for polymeric micelles for drug delivery, there has been significant interest in their stabilization especially by using diblock and triblock copolymers with lower CMC values and through covalent cross-linkage, established with disulfides and other redox-sensitive bonds, temperature, and pH-sensitive functional groups.<sup>12,13</sup> Such stabilization of micelles has been shown to increase blood circulation time and improve the antitumor activity when micelles were loaded with anticancer drugs.<sup>14,15</sup> Some of us have recently reported photopolymerized core-stabilized polydiacetylene micelles (pDA-micelles) as promising potential carriers for therapeutics and imaging agents.<sup>16,17,18,19,20</sup> Compared to classical block copolymer micelles, pDA-micelles exhibit smaller size that can allow a deeper diffusion into the target tissues. Such micelles were produced from the assembly of diacetylenic (DA) amphiphilic unimers and subsequently photopolymerized. Higher stability and a greater drug loading were observed for polymerized micelles as compared to non-

photopolymerized analogs. Polymerized pDA-micelles with an outer shell of polyethyleneglycol (PEG) chains were well suited for *in vivo* applications since they showed significant EPR-mediated tumor accumulation and tumor growth inhibition when loaded with paclitaxel, while allowing *in vivo* imaging by near-infrared fluorescence and positron emission tomography.<sup>16</sup> Wagner et al. recently reported that photopolymerized pDA-PEG micelles exhibit decreased cytotoxicity compared to micelles made of monomeric surfactants.<sup>21</sup> However, knowledge is still lacking on the influence of stabilization on the interactions between cells and micelles. The mechanisms of potential toxicity on cells of conventional and stabilized micelles are most probably different and need to be fully understood.

In this study, we have evaluated the influence of the core polymerization on cell responses, by comparing native DA-PEG micelles as a “dynamic system” and core-polymerized pDA-PEG micelles, as a “particle-like” system. In particular, we have investigated *in vitro* uptake and overall cytotoxicity (mitochondrial activity, membrane integrity) on RAW 264.7 macrophages. For pDA-PEG micelles, which exhibited an endocytosis-like behavior, further intracellular toxicity endpoints were assessed, such as apoptosis/necrosis induction, cytokine production, as well as genotoxicity, which has been little studied for such drug delivery systems.

## RESULTS

### 1. Influence of polymerization on cellular uptake and toxicity

#### *1.1 Impact on mitochondrial activity*

The impact of exposure to polymerized pDA-PEG micelles and non-polymerized DA-PEG micelles on overall cell viability was monitored through the quantification of mitochondrial activity (MTT Test). Cell viability percentage is plotted as a function of unimers concentration (semi-log plot) in Figure 1. The test was performed in the concentration range of 0.0003–1 mg/mL after 24, 48 and 72 h of incubation and the results were compared to those obtained with branched 25 kDa polyethyleneimine (PEI) at equivalent concentrations. PEI is a cationic polymer known to display many mechanisms of cytotoxicity.<sup>22</sup> Overall, we observed cytotoxicity in a dose-dependent manner, with a time-dependent trend at high concentrations ( $> 0.1$  mg/mL for polymerized micelles and  $> 0.03$  mg/mL for non-polymerized micelles). Non-polymerized micelles were substantially more toxic than polymerized micelles at all incubation times: at 24 and 48 h, the  $IC_{50}$  values were ten times lower for non-polymerized micelles, while at 72 h the difference between the two types of micelles was less pronounced.

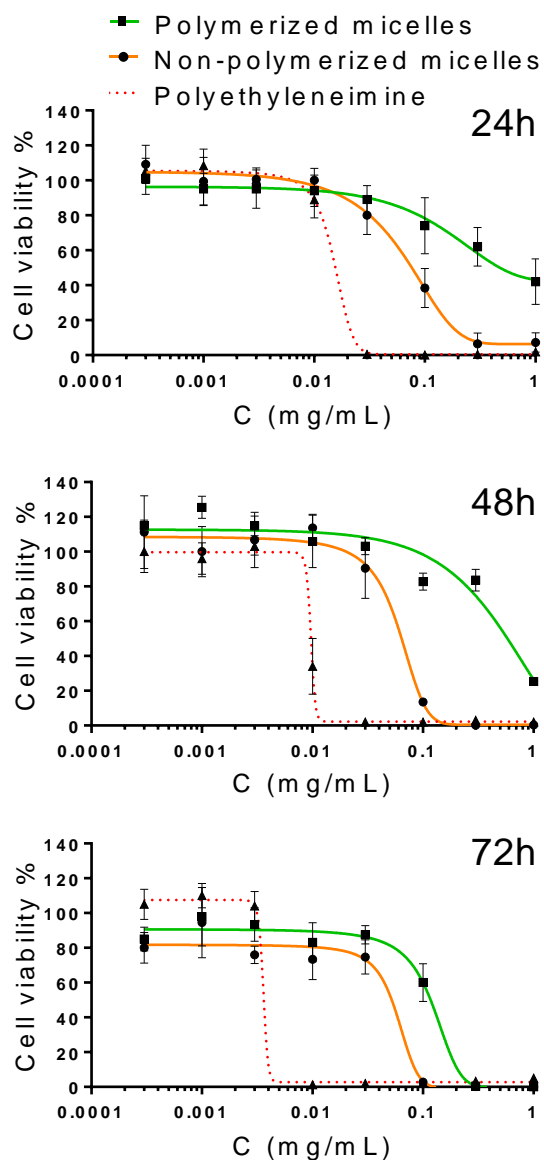


**Figure 1.** Mitochondrial activity of RAW cells treated with polymerized micelles, non-polymerized micelles and Polyethyleneimine (PEI) for 24, 48, and 72 h. Results are fitted by a sigmoidal curve. All data presented as mean  $\pm$  S.D., n = 3.

### 1.2 Membrane damage

Toxicity towards cellular membrane was assessed by LDH release assay. Lactate dehydrogenase (LDH) is a cytosolic enzyme; the increased release of LDH in the extracellular medium is relevant to assess the alteration of the cell membrane. LDH assay was performed after 24 h of incubation with polymerized and non-polymerized micelles in the concentration range of 0.0003–1 mg/mL. LDH release was compared to spontaneous release of non-treated cells and to LDH release in cells exposed to 0.1 mg/mL of Triton X-100. As illustrated in Figure 2, for cells treated with non-polymerized micelles, LDH release is not significant at concentrations < 0.1 mg/mL, but it increases dramatically above 0.1 mg/mL. On the contrary, almost no release can be observed in cells treated with polymerized micelles regardless of the concentration.

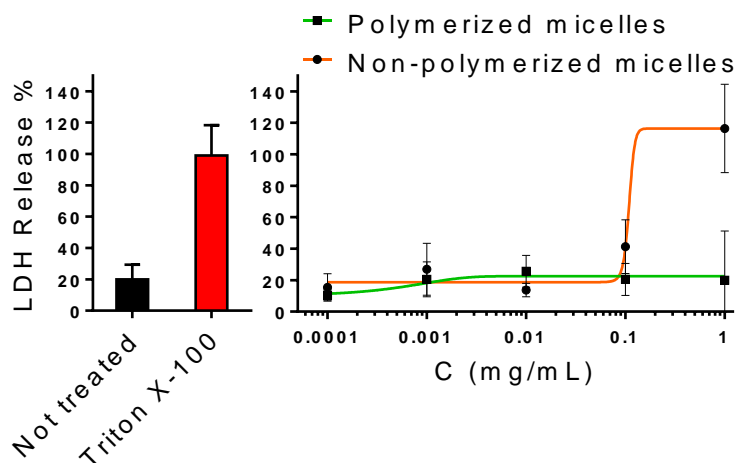


**Figure 2.** LDH release (%) in untreated RAW cells, RAW cells treated by Triton X-100 0.1 mg/mL, RAW cells exposed to polymerized and non-polymerized micelles for 24 h. Results obtained with micelles are fitted by a sigmoidal curve. All data presented as mean  $\pm$  S.D.,  $n = 3$ .

### 1.3 Uptake and intracellular distribution

To study the intracellular uptake of polymerized pDA-PEG and non-polymerized DA-PEG micelles, RAW 264.7 cells were treated with  $^{14}\text{C}$ -labelled micelles for 4 h, 24 h and 48 h at 37 °C and for 4 h at 4 °C. All the experiments were performed at a concentration of 0.01 mg/mL that was non-toxic, as determined by the MTT assay. As shown in Figure 3, RAW 264.7 cells readily internalize micelles, with a time-dependent trend that reaches a plateau at 24 h. At all incubation times, non-polymerized micelles are taken up approximately twice as much as polymerized micelles. The decreased uptake at 4 °C is consistent with an energy-dependent uptake mechanism at 37 °C. However, a more significant uptake observed at 4 °C for non-polymerized micelles which is indicative of some passive uptake.

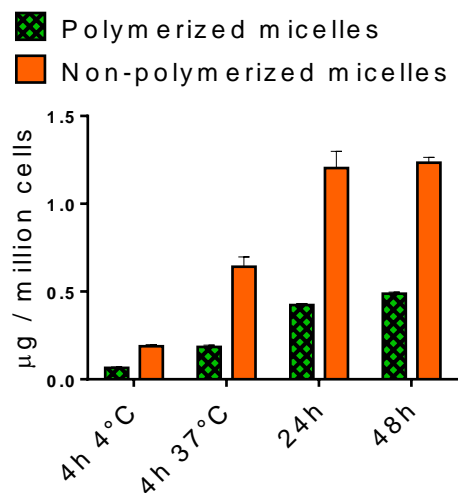


**Figure 3.** Analysis of polymerized and non-polymerized  $^{14}\text{C}$ -labeled micelles uptake by RAW cells after exposure to 0.01 mg/mL micelles at 37 °C (after 4, 24, and 48 h of exposure) and at 4 °C (after 4 h of exposure). All data presented as mean  $\pm$  S.D., n = 2.

To investigate the intracellular distribution of micelles, we optimized a differential detergent fractionation of cells (Figure S1) allowing separation of the following subcellular compartments:

cytosol, membranes and nucleus/cytoskeleton (Figures S2-S4; Table S1). The sub-cellular localization of the radiolabeled micelles was evaluated by radioactivity in each fraction after 4 h and 48 h of incubation at 37 °C, at a non-cytotoxic concentration (0.01 mg/mL). The results from Figure 4 indicate that pDA-PEG micelles accumulate mainly in cellular membranes, with a moderate yet significant concentration in cytosol and nucleus compartments. Membrane accumulation was four times higher for the non-polymerized micelles compared to polymerized micelles after 4 h of incubation and three times higher after 48 h. Interestingly, unlike cells exposed to non-polymerized micelles, cells treated with polymerized micelles had a cytosolic fraction that showed a time-dependent increase, which is consistent with an endocytosis-mediated internalization.

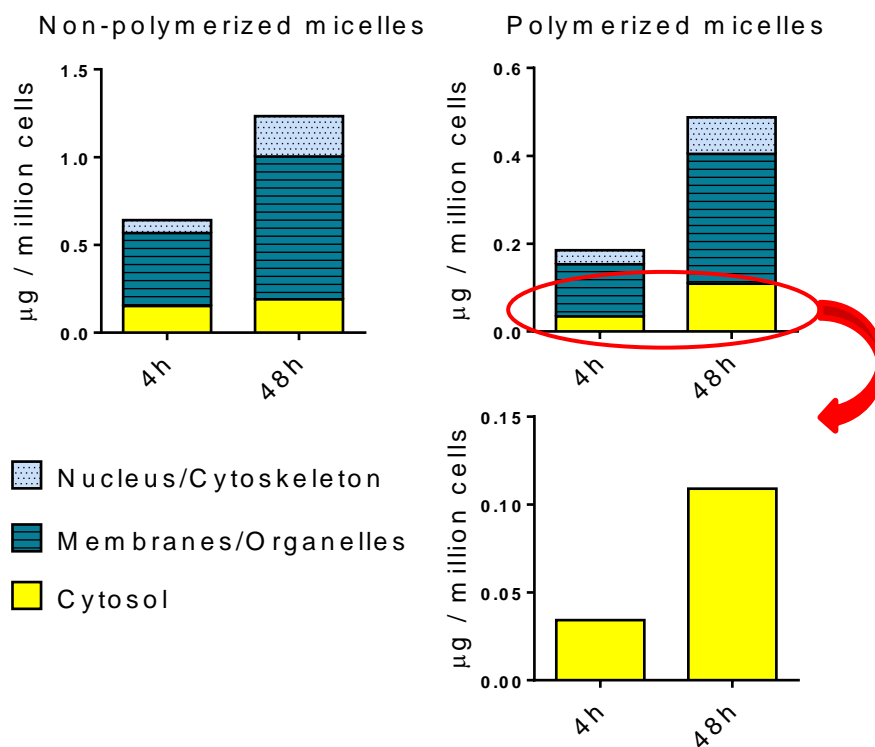


**Figure 4.** Subcellular localization of  $^{14}\text{C}$ -pDA-PEG polymerized micelles and  $^{14}\text{C}$ -DA-PEG non-polymerized micelles in RAW cells after 4 h and 48 h of exposure to 0.01 mg/mL micelles (n = 2).

## 2. Polymerized micelles cytotoxicity studies

### 2.1 Impact on cell morphology

The impact of polymerized pDa-PEG micelles on cell morphology was investigated through flow cytometry analysis. In particular, two parameters were taken into account: the side scattering (SSC) pattern and the height forward scattering (FSC-H). Results showed in Figure 5 evidenced that micelles significantly affected the SSC pattern after 24 h of exposure only at very high concentration (1 mg/mL). In the same way, higher values of FSC-Height (FSC-H) were detected for cells treated for 24 h at 1 mg/mL. On the other hand, 4 h of treatment-induced no detectable effect, regardless of the concentration.

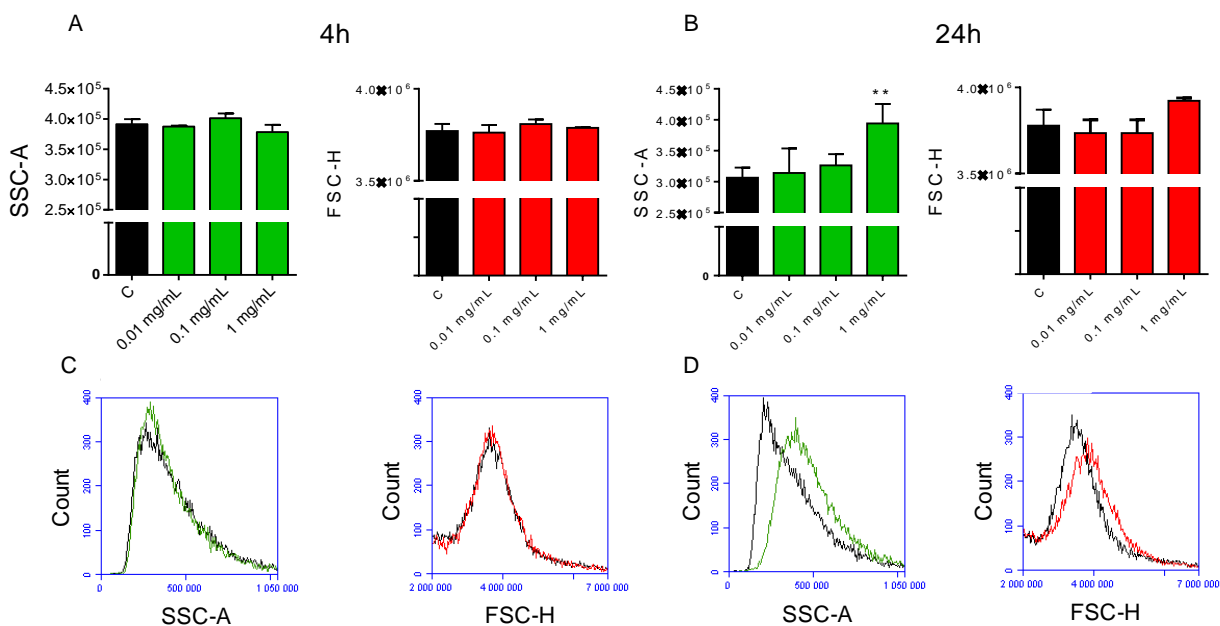


**Figure 5.** Side scatter (SSC) and Forward scatter (FSC) values of RAW cells treated with different concentrations of polymerized micelles for 4 h (A) and 24 h (B), compared with untreated RAW cells. Data presented as mean  $\pm$  S.D., n = 3. Representative side scatter (SSC) and Forward scatter (FSC) curves of RAW cells after 4 h exposure (C) and 24 h exposure (D) to polymerized micelles 1 mg/mL.

## ***2.2 Apoptosis/necrosis induction***

Quantification of apoptotic cells was performed by flow cytometry after staining of phosphatidylserines translocated to the outer leaflet of the membrane with Annexin V, an anticoagulant. To discriminate apoptotic cells from necrotic and intact cells, Annexin V coupled with FITC (green fluorescence) was combined with propidium iodide (PI) (red fluorescence), that can stain permeabilized cells. Unlabeled cells are considered as viable, Annexin V-positive cells as early apoptotic, both Annexin V-positive/PI-positive cells as necrotic and late apoptotic. The Triton X-100 detergent was used as a positive control for necrosis induction, while staurosporine was chosen as a positive control for apoptosis induction.<sup>23,24</sup> Results show that compared to non-treated cells, there was no increase of apoptosis or necrosis in cells exposed to micelles, whatever the time of incubation and micelle concentration (Figure 6).

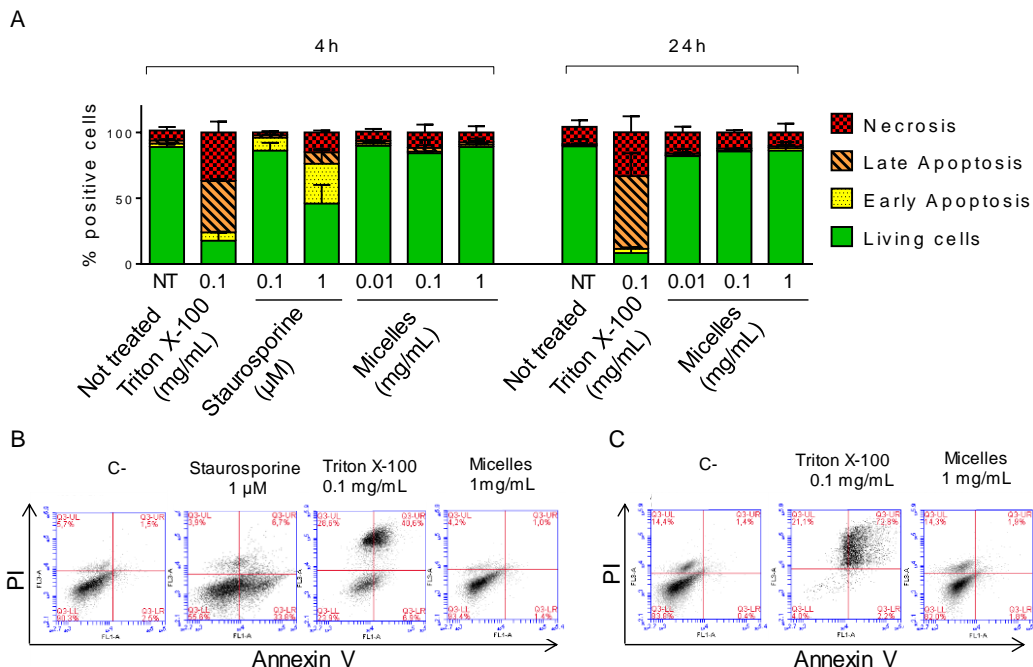


**Figure 6.** Percentages of living cells, necrotic cells, early apoptotic cells and late apoptotic cells detected by Annexin V/PI assay after 4 h and 24 h of exposure (A) (n=3). Representative flow cytometry analysis of Annexin V-FITC / PI stained cells after 4 h (B) and 24 h of exposure (C).

### 2.3 Inflammatory response

To evaluate the inflammatory response, four cytokines (MCP-1, IL-10, IL-6, and TNF- $\alpha$ ) were quantified in cell supernatant after 24 h of pDA-PEG micelles incubation at subtoxic concentrations. The toll-like receptor agonist lipopolysaccharides (LPS) at two different concentrations was used as a positive control since it is known to induce production of pro-inflammatory cytokines.<sup>25</sup> For non-treated cells and cells treated with micelles, IL-6 signal was under detectable levels. As shown in Figure 7, no significant increase in any inflammatory factor has been observed after treatment with micelles at both tested subtoxic concentrations. In the same

way, micelles addition to LPS treatment did not affect the inflammatory effect of LPS, indicating the absence of any potentiation effect.

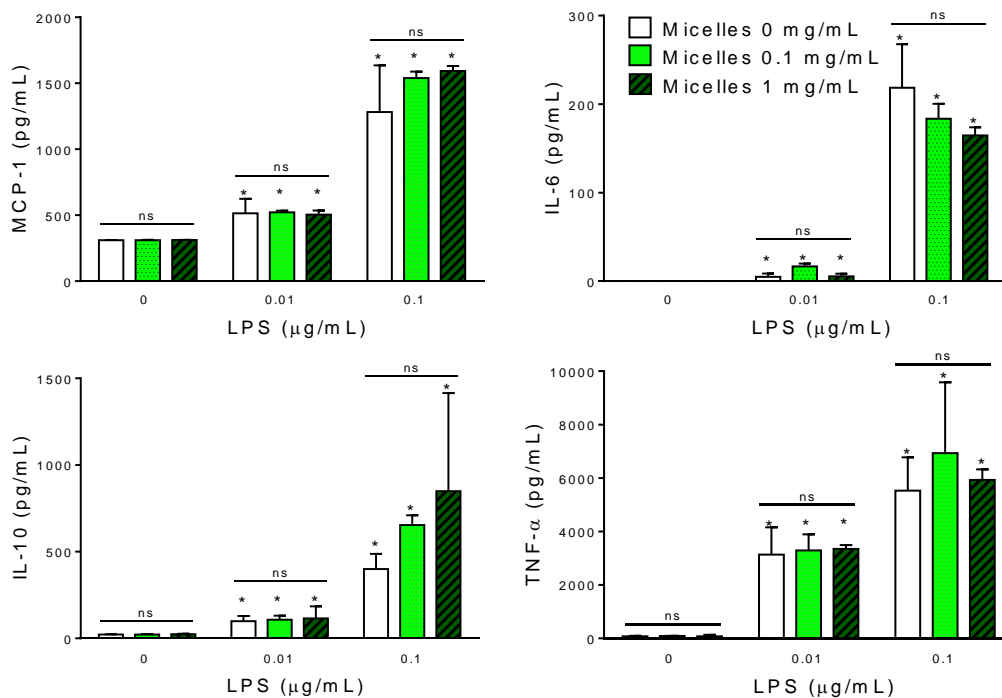


**Figure 7.** Secretions of MCP-1, IL-6, IL-10, TNF- $\alpha$  cytokines by untreated RAW cells and RAW cells treated for 24 h with pDA-PEG micelles, LPS, LPS combined with micelles, quantified with CBA method. All data presented as mean  $\pm$  S.D.,  $n = 3$ .

## 2.4 Genotoxicity

The potential genotoxicity of polymerized pDA-PEG micelles was investigated by the comet assay. The comet assay is a gel electrophoresis-based method that can be used to measure DNA damage caused by double-strand breaks, single-strand breaks, alkali labile sites, oxidative base damage, and DNA cross-linking with DNA or protein. Images of comet assay (Figure 8) were observed to show no significant change for cells treated with pDA-PEG micelles for 24 h at any

concentration compared to untreated cells. The images were further quantified using OpenComet plugin of ImageJ software. Tail parameters used in this study were % tail DNA, tail length, % Tail intensity, Olive Tail Moment and Extent Tail Moment. The Olive Tail Moment was defined by the percentage of DNA in the tail multiplied by the length between the center of the head and tail.<sup>26</sup> The Extent Tail Moment was the product of the tail length and the percentage of DNA in the tail.<sup>27</sup> None of these parameters were altered in images of treated cells compared to images of untreated cells.

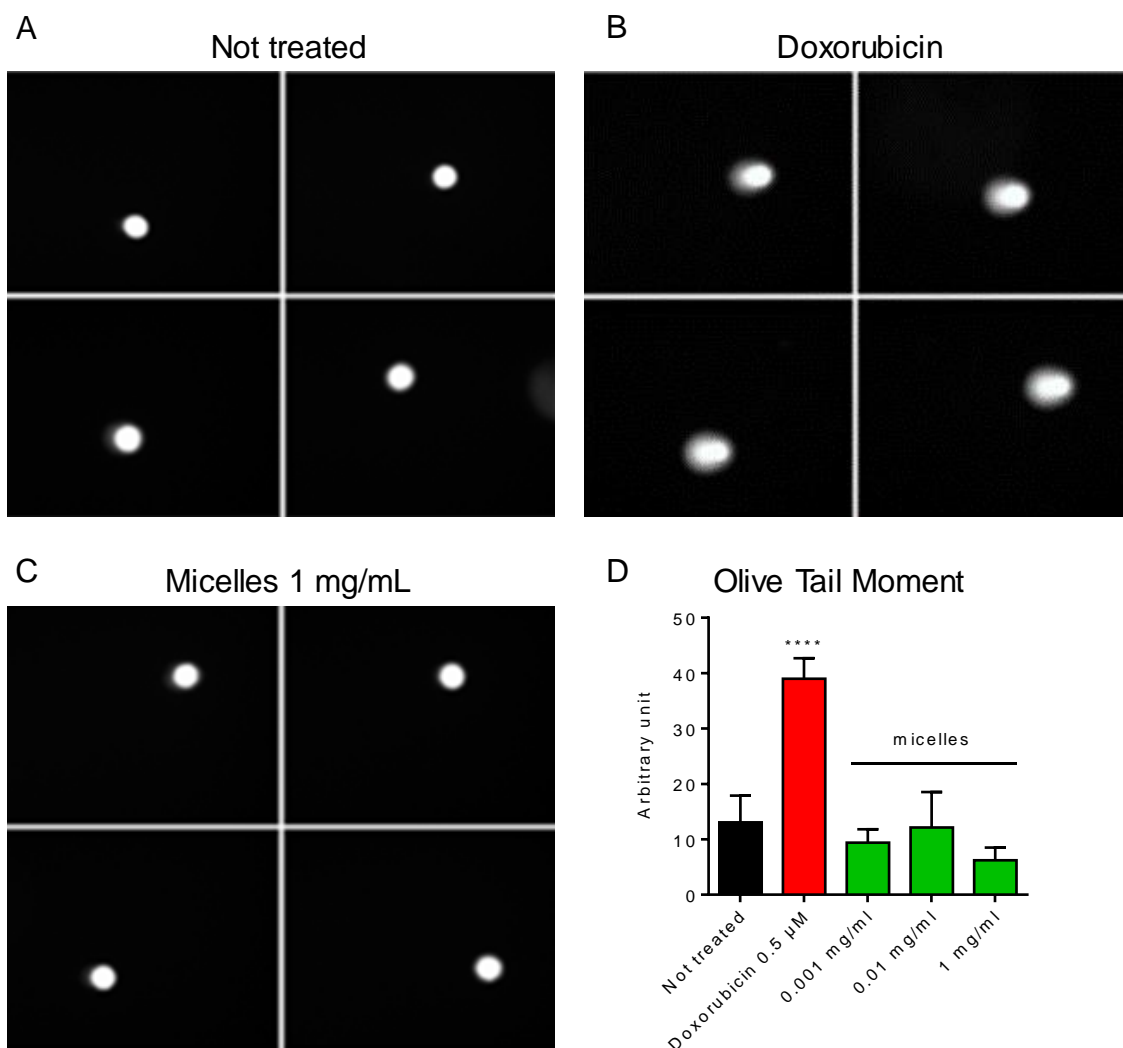


**Figure 8.** Representative comet assays on untreated RAW cells C- (A), RAW cells after 24 h treatment with 0.5  $\mu$ M Doxorubicin (B) and RAW cells treated with 1 mg/mL pDA-PEG micelles (C). Quantification of DNA damage by using the Olive tail moment parameter (D) (product of tail DNA % and distance between intensity weighted-centroids of head and tail). Data are mean values  $\pm$  SD of three independent experiments.

## DISCUSSION

To this day, knowledge is lacking on how chemical and physical characteristics of nanoparticles influence their interactions with cells in terms of mechanisms of toxicity and intracellular distribution. The use of *in vitro* models with endpoints investigating general mechanisms of damage is relevant to assess the potential toxicity of drug delivery systems in a fast and efficient way. Because nanomaterial toxicity is often associated with their uptake by cells, and because many early uptake responses to foreign materials involve sentinel leukocytes and immunomodulatory cells, phagocytic cells are classically used as experimental models for their ability to actively take up foreign particles, as reviewed by Drasler et al.<sup>28</sup> Phagocytic cells of primary interest include peripheral blood monocytes, peritoneal and lung macrophages, and bone-marrow transformed monocytes.<sup>29</sup> Immortalized RAW 264.7 murine macrophages represent this phenotype and have been well characterized and used for nanotoxicology purposes for various nanoparticle types.<sup>30,31,32</sup> They were therefore chosen as a model in this work for investigating micelles toxicity.

Micelles are dynamic structures that can change size or disassemble into single amphiphilic units upon interaction with the surroundings. Stabilization of micelles by core-polymerization can

prevent disassembly, which directly translates into a prolonged circulation time *in vivo*. In the last decade, some of us have been involved in the development of micelles obtained from the self-assembly of specific unimers composed of a diacetylene (DA)-bearing hydrophobic tail and a poly(ethylene glycol) (PEG) headgroup. These DA-PEG unimers spontaneously form small ( $d = 12$  nm) micelles in an aqueous medium. The key feature of these objects is that they can be stabilized through photo-polymerization upon irradiation at 254 nm. Under such conditions, the diacetylene units of neighboring unimers react with one another *via* a topochemical 1,4-addition mechanism and give rise to linear oligomers. The resulting polymerized micelles were previously shown to be more stable than their non-polymerized counterparts.

It is well known that several particle features, such as type, size, shape, zeta potentials, dispersion/agglomeration status, and surface modification should be taken into account in evaluating nanoparticles safety.<sup>33</sup> Nevertheless, few studies are available on the different toxicological profile of nanoparticles with the same composition but a different structure. Some publications compared the cellular internalization of un-cross-linked polymeric micelles and shell-cross-linked polymeric micelles.<sup>34,35,36</sup> Another group investigated the effect of shell-crosslinking on cytotoxicity and immunotoxicity of different nanoparticles for drug delivery.<sup>37,38</sup> The objective of the present study was to investigate the toxicological profile towards RAW 264.7 cells of DA-PEG micelles in their non-polymerized form (DA-PEG), *i.e.* as a “dynamic system”, and in polymerized form (pDA-PEG), *i.e.* as a “particle-like” system, in order to understand the role played by the structure on cellular uptake and toxicity.

In the first part of this work, we compared the uptake and intracellular distribution as well as the overall cytotoxicity of non-polymerized and polymerized micelles. MTT tests showed that non-polymerized micelles were substantially more toxic than polymerized micelles at

concentrations above 0.1 mg/mL at all incubation times. These results indicate that photopolymerization reduces the impact of micelles on cells in terms of cell viability. LDH release assay showed a dramatic increase of the cell membrane permeability for cells treated with non-polymerized micelles from 0.1 mg/mL, *i.e.* just above their CMC (0.065-0.07 mg/mL), while no increase was observed in cells treated with polymerized micelles at any concentration. Data obtained by Trypan Blue Test (Fig. S5) showed similar results. These outcomes tend to indicate that the cytotoxicity of non-polymerized micelles is related to their ability to destabilize and disrupt cell membranes when exposed at concentrations above their CMC, while polymerization of micelles prevents this propensity. To investigate the intracellular distribution of micelle components, we exposed cells to  $^{14}\text{C}$ -labelled micelles at a sub-toxic concentration of 0.01 mg/mL (according to MTT and LDH release data). In the case of non-polymerized micelles, existing as unimers at this concentration, an important accumulation is found in cellular membranes, and a significant uptake observed at 4 °C is indicative of some passive uptake. On the contrary, cells treated with polymerized micelles had a cytosolic fraction that showed a time-dependent increase, which, considering also the decreased uptake at 4 °C, is consistent with an endocytosis-mediated internalization. Taken together, we hypothesise that non-polymerized micelles, because of their dynamic nature, may lose their particle status as they interact with cell membranes and act as surfactants. On the contrary, polymerized micelles would distribute as particles inside of cells following a mechanism of endocytosis. The lower total uptake observed for polymerized micelles could be due to their exocytosis, according to previous studies.<sup>34,35</sup> For these reasons, we reasoned that polymerized micelles could have more specific and complex potential toxicity mechanisms that we sought to investigate.

In the light of the intracellular distribution outcomes, in the second part of our work, we investigated the cell morphology, apoptosis induction, release of inflammatory mediators and genotoxicity following exposure to polymerized micelles. Their impact on cell morphology was first investigated by flow cytometry. The increase in cell volume and granularity upon prolonged exposure to high concentrations of pDA-PEG micelles can be related to the macrophage activation triggering phagocytosis of foreign particles, to the presence of micelles on the cell membrane or to changes in the organelles within cells.

Nanoparticles are described as triggers of extrinsic and intrinsic apoptotic pathways; however, it is difficult to set up a comprehensive mechanism of nanomaterial-induced cell death based on conflicting observations in the literature. To evaluate the potential induction of apoptosis, we performed Annexin V/PI Test on cells treated with polymerized micelles also at high concentrations. The data obtained show that, compared to untreated cells, there is no increase of apoptosis and necrosis in cells exposed to polymerized micelles. Since no evidence of cell death occurred in cells treated with polymerized micelles, the reduction of the cell viability observed in the MTT tests could be attributed to an inhibition of the proliferation or to a reduced mitochondrial activity caused by the accumulation of micelles inside of cells at high doses.

The uptake of polymerized micelles by macrophages could also lead to persistent activation of these cells, associated with the release of various cytokines and reactive oxygen and nitrogen species (ROS/RNS). Cytokines are useful biomarkers for predicting the effect of nanoparticles on the modulation of the immune system and for screening the immunotoxicity. In the case of polymerized micelles, no significant increase of any inflammatory factor was observed even at high concentration; similarly, the combined exposure of polymerized micelles and LPS did not potentiate the intrinsic inflammatory effect of LPS. These results are consistent with previous

outcomes showing that the stabilization of nanoparticles structure can lower their immunotoxicity.<sup>39</sup> In these reports, the authors suggest that immunotoxicity could be due to the reduced accessibility of biomolecules to the core of nanoparticles, to the slower degradation of micelles into the most immunotoxic degradation products or to the limited flexibility of the particle structure.

Various nanoparticle systems have been shown to cause genotoxicity,<sup>40,41,42</sup> but the underlying mechanisms are not yet clearly understood. To this day, it has been reported that nanoparticles can cause DNA damage by direct interaction inside of the nuclear envelope or by inducing oxidative stress. Very few studies have been performed to investigate the potential genotoxicity of polymeric micelles.<sup>43,44</sup> This may, however, be of great importance as one could fear that polymerized micelles, because of their small size, could enter the nucleus and interact with DNA. As polymerized micelles' ability to reach nuclear compartment was not excluded by our intracellular distribution evaluations, genotoxic effects were investigated using a comet assay, a test that has been extensively used to assess genotoxicity of nanoparticles and that shows correlations between effects in cultured cells and exposure in animal models. No differences were observed in cells treated with polymerized micelles compared to untreated cells, suggesting that polymerized pDA-PEG micelles are not genotoxic even at high concentrations.

## **CONCLUSIONS**

To the best of our knowledge, this is the first report in which the effect of core-polymerization on both the uptake and the cytotoxicity of micelles is systematically investigated while keeping the surface characteristics and micelle composition unchanged. According to our results,

macrophages exhibit very different responses to micelles depending on the micelle structure, especially at high concentrations, which is in contradiction with previous reports.<sup>36</sup> Non-polymerized micelle components tend to accumulate into cell membranes leading to an increase of cell membrane permeability, whereas polymerized micelles internalization is consistent with the endocytosis of “particle-like” systems. The toxicity profile of polymerized micelles, thoroughly studied in order to assess possible responses resulting from their internalization, showed no sign of toxicity for concentrations below 0.1 mg/mL, neither in either mitochondrial activity, membrane permeabilization, induction of apoptosis/necrosis, secretions of pro-inflammatory cytokines nor genotoxicity. Such concentrations could be considered in the range (or at the higher end) of therapeutically relevant doses. Taken together, our results suggest that the cytotoxic effects and the intracellular distribution of micelles towards macrophages are related to their “micelle-like” or “particle-like” structure and that core-polymerization of pDa-PEG micelles can improve the safety of these particles when used as drug delivery systems. We believe that this study will provide more scientific understandings on the toxicity of amphiphilic micelles and on the effect of nanoparticles structure on their interactions with cells.

## **EXPERIMENTAL**

### ***Cell culture***

The macrophage-like murine cell line RAW 264.7 was obtained from ATCC (catalog number TIB-71) and cultured in high glucose Dulbecco's Modified Eagle's Medium (Sigma), supplemented with 50 U/mL penicillin, 50 U/mL streptomycin, and 10% fetal bovine serum

(Gibco). Cells were maintained at 37 °C in a 5% CO<sub>2</sub> humidified atmosphere. Twice a week, cells were divided at 1:10 ratio by scraping.

***Synthesis, preparation and characterization of pDA-PEG2000 micelles***

DA-PEG unimers were synthesized by our previously described method (see SI for details).<sup>18</sup> Briefly, commercial pentacosanoic acid was first reduced to its hydroxyl counterpart which was in turn transformed to the corresponding bromide. The latter was treated with the desired PEG chain in the presence of sodium hydride to yield the desired DA-PEG unimer. For this study, two different unimers were synthesized: the first one bearing a methoxy-terminated PEG headgroup (DA-PEG-OMe) and the second bearing a carboxylate-terminated PEG headgroup (DA-PEG-CO<sub>2</sub>H). Critical micelle concentrations were determined for these two surfactants using the du Noüy ring method and found to be 65 and 70 mg/L, respectively. Micelles were obtained by self-assembly of DA-PEG-OMe and DA-PEG-CO<sub>2</sub>H unimers in a 9:1 ratio in water. They were then either studied as such (DA-PEG micelles) or after 5 h of photo-polymerization under UV at 254 nm (pDA-PEG micelles). Micelles were characterized by dynamic light scattering (DLS) and zeta potential measurements. For the synthesis of <sup>14</sup>C-labeled micelles, <sup>14</sup>C-DA-PEG-OMe was synthesized following the procedure described for DA-PEG-OMe but starting from <sup>14</sup>C-labeled pentacosanoic acid (see SI for details). The specific activity was measured by scintillation counting (it is given in μCi per mg of micelles). The physicochemical properties of the different micelles studied in this article are given in Table 1 below.

**Table 1.** Physicochemical properties of micelles

Micelle type	DLS		Zeta potential (mV)	Specific activity ( $\mu\text{Ci}\cdot\text{mg}^{-1}$ )
	Diameter (nm)	PDI		
DA-PEG	13	0.14	-3.5	na
pDA-PEG	12	0.11	-2.5	na
$^{14}\text{C}$ -DA-PEG	12	0.13	na	2
$^{14}\text{C}$ -pDA-PEG	12	0.12	na	2

**MTT Test**

The mitochondrial activity was evaluated using the 3-[4,5-dimethylthiazol-2-yl]-3,5-diphenil tetrazolium bromide (MTT) test. This colorimetric test measures the mitochondrial dehydrogenase cell activity, an indicator of cell viability. The assay is based on the reduction, by living cells, of the tetrazolium salt, MTT, which forms a blue formazan product. RAW 264.7 cells were seeded onto 96-well plates (TTP, Zurich, Switzerland) with 100  $\mu\text{L}$  of growth medium per well at a density of 8,000 cells/well for 24 h incubation, 4,000 cells/well for 48 h incubation and 2,000 cells/well for 72 h incubation. After 24 h (pre-incubation), 100  $\mu\text{L}$  of micelles (polymerized pDA-PEG micelles and non-polymerized DA-PEG micelles) dispersed in growth medium were added onto cells at various final concentrations (0.0003 – 1 mg/mL). After 24 h, 48 h and 72 h of incubation with micelles, 20  $\mu\text{L}$  of a 5 mg/mL MTT solution was added to each well and incubated for 2 h. The medium was then discarded and 200  $\mu\text{L}$  of dimethyl sulfoxide (DMSO) was added to dissolve formazan crystals. The absorbance was measured at 570 nm with a microplate reader (Metertech  $\Sigma$  960, Fisher Bioblock, France). The fraction of viable cells was calculated as the absorbance ratio between micelle-treated and untreated cells. Wells without the addition of MTT were used as blank. Polyethyleneimine (PEI) (25 kDa) was used as a positive control. The  $\text{IC}_{50}$  was calculated as the sample concentration which inhibits the growth of 50% of cells relative to untreated cells,

using the sigmoidal fitting from GraphPad Prism Software. All measurements were performed in quadruplicate.

### ***Micelles uptake and intracellular distribution***

To study the intracellular uptake of micelles (polymerized pDA-PEG micelles and conventional pDA-PEG micelles), RAW 264.7 cells were treated with  $^{14}\text{C}$ -labelled micelles for 4 h, 24 h and 48 h. The subcellular localization of radiolabeled micelles was evaluated by differential detergent fractionation of cells. RAW 264.7 cells were seeded onto 6-wells plates (TTP, Zurich, Switzerland) with 2 mL of growth medium per well at a density of 300.000 cells/well. At each time, the growth medium was replaced by 2 mL of  $^{14}\text{C}$ -labelled micelles dispersed in culture medium at a final concentration of 0.01 mg/mL. After 4 h (at 37 °C and 4 °C), 24 h (at 37 °C), and 48 h (at 37 °C) of incubation, the ProteoExtract Subcellular Proteome Extraction Kit (Merck Millipore) was used to obtain different subcellular fractions (cytosol, membranes, nucleus/cytoskeleton), following kit instructions with some modifications (Suppl. Info). After discarding culture medium, cells were washed with ice-cold Wash Buffer gently agitating at 4 °C for 5 min, twice. Then, cells were incubated with ice-cold Extraction Buffer I for 10 min gently agitating at 4 °C; supernatant corresponding to cytosol fraction was recovered. Subsequently, ice-cold Extraction Buffer II was added and incubated with cells for 30 min gently agitating at 4 °C. Because of the partial detachment of cells, the supernatant was centrifuged at 3000  $\times g$  for 20 min at 4 °C to recover a fraction of membranes content in the supernatant. Afterward, a mixture of Extraction Buffer III and Extraction Buffer IV were added to wells and to pellets of previous centrifugation to solubilize nucleus and cytoskeleton content fraction under gentle agitation at RT until complete solubilization. Hionic Fluor scintillation cocktail (Perkin Elmer) was added to each fraction to

measure its radioactivity on a BECKMAN model LS 6000 TA Liquid Scintillator after thorough homogenization. To estimate the effectiveness of our fractionation methodology to recover these intracellular fractions, lactate dehydrogenase quantification (CytoTox 96 Non-radioactive Cytotoxicity Assay Kit, Promega), Protein concentration determination (Pierce BCA Protein Assay Kit, Thermo Fisher Scientific) and Western blotting were performed on fractions.

### ***LDH Release Assay***

LDH released from the cytoplasm compartment to the extracellular medium was measured through the formation of the red formazan product in medium, measured at 492 nm using a microplate reader. Lactate dehydrogenase (LDH) released in the extracellular medium was quantified using the CytoTox 96 Non-radioactive Cytotoxicity Assay Kit (Promega), according to manufacturer's instructions. RAW 264.7 cells were seeded onto 96-well plates (TTP, Zurich, Switzerland) with 100  $\mu$ L of growth medium per well at a density of 8,000 cells/well and pre-incubated for 24 h. Subsequently, 100  $\mu$ L of micelles (polymerized pDA-PEG micelles and conventional pDA-PEG micelles) dispersed in growth medium were added on cells at various final concentrations (0.0001 – 1 mg/mL) and incubated for 24 h. The LDH release (%) was calculated as the ratio between the LDH released and the total intracellular LDH measured after lysis. 0.1 mg/mL Triton X-100 was used as a positive control. All measurements were performed in triplicate.

### ***Cell morphology analysis***

Cell morphology was studied by analyzing height forward scatter (FSC-H) and side scatter (SSC) using flow cytometry (Accuri C6, BD Biosciences). RAW 264.7 cells were seeded onto 6-

wells plate with 2 mL of growth medium at a density of 300.000 cells/well for 4 h incubation and 150,000 cells for 24 h incubation. After 24 h of pre-incubation, cells were treated with polymerized pDA-PEG micelles at different final concentrations (0.01, 0.1 and 1 mg/mL) for 4 h and for 24 h in the appropriate culture media. Afterward, untreated cells and micelles-exposed cells were rinsed with ice-cold PBS, detached by scraping and suspended in PBS for flow cytometry analysis. All measurements were performed in triplicate.

### ***Trypan blue test***

Micelles effect on cell membrane permeability was also evaluated by Trypan blue test. RAW 264.7 cells were seeded onto 96-well plates (TTP, Zurich, Switzerland) with 100  $\mu$ L of growth medium per well at a density of 7.000 cells/well and pre-incubated for 24 h. Then, 100  $\mu$ L of polymerized pDA-PEG micelles dispersed in growth medium were added on cells at various concentrations (0.0003 – 1 mg/mL). After 24 h exposure, plates were centrifuged for 5 min at 200  $\times$ g and supernatants were discarded paying attention not to remove cells. Cells were subsequently rinsed with PBS and 100  $\mu$ L of Trypan Blue solution 0.4%, in 50:50 (v/v) (Eurobio) were added to wells. Cell counting was performed manually by microscopy and the cell viability was calculated as the ratio between uncolored cells and total cells. PEI and Triton X-100 at various concentrations were used as positive controls. All measurements were performed in triplicate.

### ***Annexin V/Propidium iodide Assay***

Apoptosis/necrosis detection following exposure to polymerized pDA-PEG micelles were performed using the FITC Annexin V Apoptosis Detection Kit I (BD Biosciences). RAW 264.7 cells were seeded with 2 mL of growth medium in 6-wells plates (300,000 cells/well for 4 h

exposure and 150,000 cells/well for 24 h exposure) and pre-incubated for 24 h. Culture medium was replaced with dilutions of polymerized pDA-PEG micelles suspension (0.01-0.1-1 mg/mL). After incubation, plates were centrifuged (200 ×g, 5 min), the culture medium was discarded, and cells were rinsed twice with ice-cold PBS. Annexin V-FITC and PI were added to cells and then removed before rinsing with ice-cold PBS and scraping. Cells were suspended in ice-cold PBS and immediately analyzed by flow cytometry (Accuri C6, BD Biosciences) using the fluorescent channels FL-1 for Annexin V-FITC and FL-3 for PI. Staurosporine (0.1 μM and 1 μM) and Triton X-100 (0.1 mg/mL) were used as positive controls respectively for apoptosis and necrosis induction.

### ***Comet Assay***

The alkaline single cell gel electrophoresis (comet assay) was used for quantifying and analyzing DNA damage, in compliance with previously described protocols.<sup>45,46,47</sup> RAW 264.7 cells were seeded with 1 mL of growth medium per well at a density of 80,000 cells/well and pre-incubated for 24 h. Afterward, the culture medium was replaced with fresh medium, polymerized pDA-PEG micelles dilutions (0.001-0.1-1 mg/mL) and doxorubicin (0.5 μM) as a positive control. After 24 h incubation, cells were scraped in ice-cold PBS and the cell concentration was adjusted at 100,000 cells/mL. 200 μL of cell suspensions were mixed with 800 μL of 1% low-gelling-temperature agarose at 40 °C and rapidly pipet onto 1% Normal Melting Agarose pre-coated slides. All the following steps were sheltered from daylight to prevent the occurrence of additional DNA damage. After agarose has gelled, slides were immersed in a cold lysing solution (2 M NaCl, 100 mM EDTA, 10 mM Trizma base, pH 10, supplemented with 1% vol/vol Triton X-100). After overnight lysis, slides were rinsed three times for 20 min with cold electrophoresis buffer (1 mM EDTA and

300 mM NaOH, pH > 13) to ensure removal of salt and detergent and to allow DNA unwinding and expression of single-strand breaks and alkali labile sites. Electrophoresis was conducted at a voltage of 0.6 V/cm for 20 min. Slides were subsequently neutralized twice with distilled water, placed in Ethidium Bromide solution (2 µg/mL) and incubated for 5 min. After two washes with distilled water, slides were analyzed with a fluorescent microscope (Leitz Diaplan), using a 20× objective, equipped with a Coolsnap ES camera (Roper Scientific). At least 70 selected images per slide were analyzed using OpenComet automated tool.<sup>48</sup> The tail length, olive tail moment (OTM), tail extent moment, percentage of tail DNA and percentage of tail intensity were used as DNA damage indicators. All experiments were performed three times.

### ***CBA Assay***

Cytokine secretions were quantified in the cell supernatants following exposure to polymerized pDA-PEG micelles using the Cytometric Beads Array (CBA) Mouse Inflammation Kit (BD Biosciences) that allows multiplexed dosage of several cytokines known to be involved in the inflammatory response: IL-6, IL-10, TNF- $\alpha$ , and MCP-1. Lipopolysaccharide (LPS) has been chosen as a positive control to induce cytokine secretion. 8,000 cells were seeded with 200 µL in 96-well plates. After 24 h of pre-incubation, supernatants were discarded and replaced by 200 µL of fresh growth medium, alone (non-treated cells) or containing increasing concentrations of LPS (0.1, 1, 10 µg/mL), polymerized pDA-micelles dispersion at 0.01 mg/mL or 0.1 mg/mL, as well as combinations of LPS at 0.1 µg/mL with pDA-micelles or LPS at 1 µg/mL with pDA-micelles. After 24 h exposure, supernatants were sampled and analyzed according to the manufacturer instructions. For TNF- $\alpha$  detection, samples were diluted 1:20. Cytokine results were obtained as pg/mL concentrations. All measurements were performed in triplicate.

## ACKNOWLEDGEMENTS

The “Institut Galien Paris-Sud” and the “Service de Chimie Bioorganique et de Marquage” belong to the Laboratory of Excellence in Research on Medication and Innovative Therapeutics (ANR-10-LABX-0033-LERMIT).

## REFERENCES

1. Soenen, S. J. *et al.* Cellular toxicity of inorganic nanoparticles: Common aspects and guidelines for improved nanotoxicity evaluation. *Nano Today* **6**, 446–465 (2011).
2. Agency, E. M. Joint MHLW / EMA reflection paper on the development of block copolymer micelle medicinal products Joint MHLW / EMA reflection paper on the development of block copolymer micelle medicinal products Table of contents. **44**, 1–15 (2013).
3. Vert, M. *et al.* Terminology for biorelated polymers and applications ( IUPAC Recommendations 2012 )\*. **84**, 377–410 (2012).
4. Lukyanov, A. N. & Torchilin, V. P. Micelles from lipid derivatives of water-soluble polymers as delivery systems for poorly soluble drugs. *Adv. Drug Deliv. Rev.* **56**, 1273–1289 (2004).
5. Lu, Y. & Park, K. Polymeric micelles and alternative nanonized delivery vehicles for poorly soluble drugs. *Int. J. Pharm.* **453**, 198–214 (2013).

6. Movassaghian, S., Merkel, O. M. & Torchilin, V. P. Applications of polymer micelles for imaging and drug delivery. *Wiley Interdiscip. Rev. Nanomedicine Nanobiotechnology* **7**, 691–707 (2015).
7. Navarro, G., Pan, J. & Torchilin, V. P. Micelle-like nanoparticles as carriers for DNA and siRNA. *Mol. Pharm.* **12**, 301–313 (2015).
8. Matsumura, Y. *et al.* Phase I clinical trial and pharmacokinetic evaluation of NK911, a micelle-encapsulated doxorubicin. *Br. J. Cancer* **91**, 1775–1781 (2004).
9. Matsumura, Y. & Kataoka, K. Preclinical and clinical studies of anticancer agent-incorporating polymer micelles. *Cancer Sci.* **100** (4), 572–579 (2009).
10. Deshmukh, A. S. *et al.* Polymeric micelles: Basic research to clinical practice. *Int. J. Pharm.* **532**, 249–268 (2017).
11. Yokoyama, M. Polymeric micelles as drug carriers: Their lights and shadows. *J. Drug Target.* **22**, 576–583 (2014).
12. O'Reilly, R. K., Hawker, C. J. & Wooley, K. L. Cross-linked block copolymer micelles: functional nanostructures of great potential and versatility. *Chem. Soc. Rev.* **35**, 1068 (2006).
13. Radiation, E. Stabilization of Block Copolymer Micelles by UV and Fast Electron Radiation. **408**, 399–408 (1982).
14. Barkey, N. M. *et al.* Development and in vivo quantitative magnetic resonance imaging of polymer micelles targeted to the melanocortin 1 receptor. *J. Med. Chem.* **56**, 6330–6338 (2013).

15. Zhang, F. *et al.* Shell crosslinked knedel-like nanoparticles for delivery of cisplatin: Effects of crosslinking. *Nanoscale* **5**, 3220–3225 (2013).
16. MacKiewicz, N. *et al.* Tumor-targeted polydiacetylene micelles for in vivo imaging and drug delivery. *Small* **7**, 2786–2792 (2011).
17. Gravel, E. *et al.* Drug delivery and imaging with polydiacetylene micelles. *Chem. - A Eur. J.* **18**, 400–408 (2012).
18. Gravel, E. *et al.* Cellular uptake and trafficking of polydiacetylene micelles. *Nanoscale* **5**, 1955 (2013).
19. Theodorou, I. *et al.* Stable and compact zwitterionic polydiacetylene micelles with tumor-targeting properties. *Chem. Commun.* **51**, 14937–14940 (2015).
20. Ogier, J. *et al.* Enhanced drug loading in polymerized micellar cargo. *Org. Biomol. Chem.* **8**, 3902–3907 (2010).
21. Neuberg, P. *et al.* Photopolymerized micelles of diacetylene amphiphile: physical characterization and cell delivery properties. *Chem. Comm.* **58**, 15–17 (2015).
22. Kafil, V. & Omid, Y. Cytotoxic impacts of linear and branched polyethylenimine nanostructures in A431 cells. *BioImpacts* **1**, 23–30 (2011).
23. Yamaki, K. *et al.* Participation of various kinases in staurosporine induced apoptosis of RAW 264.7 cells. *J. Pharm. Pharmacol.* **54**, 1535–44 (2002).
24. Wilhelmi, V. *et al.* Evaluation of apoptosis induced by nanoparticles and fine particles in RAW 264.7 macrophages: Facts and artefacts. *Toxicol. Vitr.* **26**, 323–334 (2012).

25. Beutler, B. & Rietschel, E. T. Rietschel\_Beutler\_Innate Immune Sensing and Its Roots-the Story of Endotoxin. *Nat. Rev. Immunol.* **3**, 169–176 (2003).
26. Olive, P. L., Ban, J. P. & Durand, R. E. DNA Damage and Repair in Tumor Heterogeneity in Radiation-Induced and Normal Cells Measured Using the ‘ Comet ’ Assay. *Radiation Research* **94**, 86–94 (1990).
27. Lee, E., Oh, E., Lee, J., Sul, D. & Lee, J. Use of the tail moment of the lymphocytes to evaluate DNA damage in human biomonitoring studies. *Toxicol. Sci.* **81**, 121–132 (2004).
28. Drasler, B., Sayre, P., Steinhäuser, K. G., Petri, Rothen-rutishauser, B. *Nanoimpact* **8**, 99-116 (2017).
29. Jones, C. F. & Grainger, D. W. In vitro assessments of nanomaterial toxicity. *Adv. Drug Deliv. Rev.* **61**, 438–456 (2009).
30. Chen, L. *et al.* The toxicity of silica nanoparticles to the immune system. *Nanomedicine* **13**, 1939–1962 (2018).
31. Herd, H. L., Bartlett, K. T., Gustafson, J. A., McGill, L. D. & Ghandehari, H. Biomaterials Macrophage silica nanoparticle response is phenotypically dependent. *Biomaterials* **53**, 574–582 (2015).
32. Tripathy, N., Hong, T., Ha, K., Jeong, H. & Hahn, Y. Effect of ZnO nanoparticles aggregation on the toxicity in RAW 264 . 7 murine macrophage. *J. Hazard. Mater.* **270**, 110–117 (2014).
33. Elsaesser, A. & Howard, C. V. Toxicology of nanoparticles. *Adv. Drug Deliv. Rev.* **64**, 129–137 (2012).

34. Kim, Y., Pourgholami, M. H., Morris, D. L., Lu, H. & Stenzel, M. H. Effect of shell-crosslinking of micelles on endocytosis and exocytosis: Acceleration of exocytosis by crosslinking. *Biomater. Sci.* **1**, 265–275 (2013).
35. Lu, H. *et al.* Enhanced transcellular penetration and drug delivery by crosslinked polymeric micelles into pancreatic multicellular tumor spheroids. *Biomater. Sci.* **3**, 1085–1095 (2015).
36. Kim, Y., Pourgholami, M. H., Morris, D. L. & Stenzel, M. H. Effect of cross-linking on the performance of micelles as drug delivery carriers: A cell uptake study. *Biomacromolecules* **13**, 814–825 (2012).
37. Mathias, J. R. *et al.* NIH Public Access. **33**, 1212–1217 (2010).
38. Elsabahy, M. *et al.* Surface charges and shell crosslinks each play significant roles in mediating degradation, biofouling, cytotoxicity and immunotoxicity for polyphosphoester-based nanoparticles. *Sci. Rep.* **3**, (2013).
39. Elsabahy, M. & Wooley, K. L. Data Mining as a Guide for the Construction of Cross-Linked Nanoparticles with Low Immunotoxicity via Control of Polymer Chemistry and Supramolecular Assembly. *Acc. Chem. Res.* **48**, 1620–1630 (2015).
40. Di Bucchianico, S. *et al.* Multiple cytotoxic and genotoxic effects induced in vitro by differently shaped copper oxide nanomaterials. *Mutagenesis* **28**, 287–299 (2013).
41. Ahamed, M. *et al.* Genotoxic potential of copper oxide nanoparticles in human lung epithelial cells. *Biochem. Biophys. Res. Commun.* **396**, 578–583 (2010).
42. Moche, H. *et al.* Tungsten carbide-cobalt as a nanoparticulate reference positive control in in vitro genotoxicity assays. *Toxicol. Sci.* **137**, 125–134 (2014).

43. Bahadori, F., Kocyigit, A., Onyuksel, H., Dag, A. & Topcu, G. Cytotoxic, Apoptotic and Genotoxic Effects of Lipid-Based and Polymeric Nano Micelles, an In Vitro Evaluation. *Toxics* **6**, 7 (2017).
44. Knudsen, K. B. *et al.* In vivo toxicity of cationic micelles and liposomes. *Nanomedicine Nanotechnology, Biol. Med.* **11**, 467–477 (2015).
45. Olive, P. L. & Banáth, J. P. The comet assay: A method to measure DNA damage in individual cells. *Nat. Protoc.* **1**, 23–29 (2006).
46. Dhawan, A. *et al.* PROTOCOL FOR THE SINGLE CELL GEL ELECTROPHORESIS / COMET ASSAY FOR RAPID GENOTOXICITY ASSESSMENT Prepared by : *Electrophoresis* **17**, 1–10 (2007).
47. Kirsch-volders, M. *et al.* Report from the In Vitro Micronucleus Assay Working Group Report from the In Vitro Micronucleus Assay Working Group. *Environ. Mol. Mutagen.* **2280**, 167–72 (2000).
48. Gyori, B. M., Venkatachalam, G., Thiagarajan, P. S., Hsu, D. & Clement, M. V. OpenComet: An automated tool for comet assay image analysis. *Redox Biol.* **2**, 457–465 (2014).

## SUPPLEMENTARY

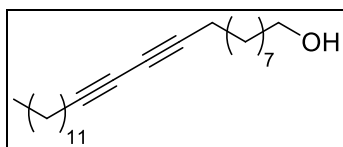
### Chemical Synthesis

#### General

Unless otherwise specified, chemicals were purchased from Sigma-Aldrich and used without further purification. Tetrahydrofuran (THF) was distilled from sodium/benzophenone before use. Flash chromatography was carried out on Kieselgel 60 (230–240 mesh, Merck).  $^1\text{H}$  and  $^{13}\text{C}$  NMR spectra were recorded on a Bruker Avance DPX 400 spectrometer at 400 and 100 MHz respectively. Chemical shifts ( $\delta$ ) are given in ppm relative to the NMR solvent residual peak and coupling constants ( $J$ ) in Hz.

### Synthesis of diacetylene polyethylene glycol (DA-PEG-OMe and DA-PEG-CO<sub>2</sub>H) amphiphiles.

#### *Synthesis of pentacos-10,12-diyne-1-ol (DA-OH).*



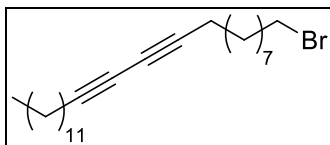
Under nitrogen atmosphere and at 0 °C (ice bath), to a solution of pentacos-10,12-diyne-1-ol (1 g, 2.7 mmol, 1 equiv.) in diethyl ether (50 mL) was added lithium aluminium hydride (205 mg, 2 equiv.). After stirring for 1.5 h at room temperature, the reaction was cooled again to 0 °C and 15% sodium hydroxide (200  $\mu\text{L}$ ) was added, followed by water (600  $\mu\text{L}$ ). The resulting pink precipitate was filtered off on Celite<sup>®</sup>, the organic phase was washed with hydrochloric acid (2  $\times$

20 mL), and dried on magnesium sulfate. After solvent removal under vacuum, product **5** was obtained as a white solid (938 mg, yield = 96%).

**<sup>1</sup>H NMR** (400 MHz, CDCl<sub>3</sub>, δ): 3.63 (t, *J* = 7 Hz, 2H; CH<sub>2</sub>-OH), 2.23 (t, *J* = 7 Hz, 4H; CH<sub>2</sub>-C≡), 1.60-1.45 (m, 6H; CH<sub>2</sub>), 1.44-1.24 (m, 28H; CH<sub>2</sub>), 0.86 ppm (t, *J* = 7 Hz, 3H; CH<sub>3</sub>).

**<sup>13</sup>C NMR** (100 MHz, CDCl<sub>3</sub>, δ): 77.5 (-C≡), 77.4 (-C≡), 65.2 (-C≡), 65.2 (-C≡), 63.1 (CH<sub>2</sub>-OH), 32.7 (CH<sub>2</sub>), 31.9 (CH<sub>2</sub>), 29.6 (3 CH<sub>2</sub>), 29.4 (CH<sub>2</sub>), 29.3 (3 CH<sub>2</sub>), 29.1 (CH<sub>2</sub>), 29.0 (CH<sub>2</sub>), 28.8 (CH<sub>2</sub>), 28.7 (CH<sub>2</sub>), 28.3 (CH<sub>2</sub>), 28.2 (2 CH<sub>2</sub>), 25.7 (CH<sub>2</sub>), 22.6 (CH<sub>2</sub>), 19.2 (CH<sub>2</sub>), 14.1 ppm (CH<sub>3</sub>).

*Synthesis of 1-bromopentacos-10,12-diyne (DA-Br).*

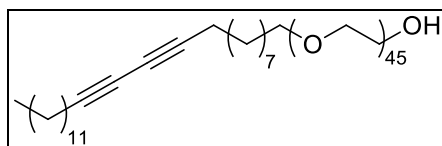


Under nitrogen atmosphere, triphenylphosphine (550 mg, 1.5 equiv.) and **DA-OH** (500 mg, 1.4 mmol, 1 equiv.) were solubilized in dichloromethane (3 mL). Tetrabromomethane (700 mg, 1.5 equiv.) was added in portions and the reaction was stirred at room temperature for 15 min. After addition of cold water (2 mL) the organic phase was separated, dried over magnesium sulfate and purified on a silica plug eluted with pure dichloromethane. Upon concentration under reduced pressure, the desired product **Da-Br** was obtained as a yellowish varnish (585 mg, yield = 100%).

**<sup>1</sup>H NMR** (400 MHz, CDCl<sub>3</sub>, δ): 3.40 (t, *J* = 7 Hz, 2H; CH<sub>2</sub>-Br), 2.24 (t, *J* = 7 Hz, 4H; CH<sub>2</sub>-C≡), 1.85 (td, *J* = 7 Hz, 2H; CH<sub>2</sub>), 1.60-1.45 (m, 6H; CH<sub>2</sub>), 1.45-1.25 (m, 26H; CH<sub>2</sub>), 0.88 ppm (t, *J* = 7 Hz, 3H; CH<sub>3</sub>).

$^{13}\text{C}$  NMR (100 MHz,  $\text{CDCl}_3$ ,  $\delta$ ): 77.6 ( $-\text{C}\equiv$ ), 77.4 ( $-\text{C}\equiv$ ), 65.3 ( $-\text{C}\equiv$ ), 65.1 ( $-\text{C}\equiv$ ), 34.0 ( $\text{CH}_2\text{-Br}$ ), 32.8 ( $\text{CH}_2$ ), 31.9 ( $\text{CH}_2$ ), 29.6 (3  $\text{CH}_2$ ), 29.4 ( $\text{CH}_2$ ), 29.3 ( $\text{CH}_2$ ), 29.2 ( $\text{CH}_2$ ), 29.1 (2  $\text{CH}_2$ ), 28.9 ( $\text{CH}_2$ ), 28.8 ( $\text{CH}_2$ ), 28.7 ( $\text{CH}_2$ ), 28.6 ( $\text{CH}_2$ ), 28.3 ( $\text{CH}_2$ ), 28.2 ( $\text{CH}_2$ ), 28.1 ( $\text{CH}_2$ ), 22.7 ( $\text{CH}_2$ ), 19.2 ( $\text{CH}_2$ ), 14.1 ppm ( $\text{CH}_3$ ).

*Synthesis of pentacos-10,12-diyne-1-oxypentatetraentaethyleneglycol (DA-PEG-OH).*



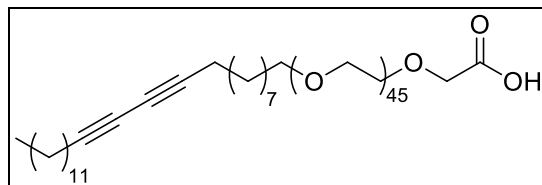
Under nitrogen atmosphere, polyethylene glycol (MW = 2 000, 1.5 g – 0.75 mmol – 1 equiv.) dissolved in anhydrous acetonitrile (15 mL) was added to a suspension of sodium hydride (36 mg, 2 equiv.) in anhydrous acetonitrile (7 mL). The mixture was heated to reflux for 30 min and allowed to cool down to room temperature. Compound **DA-Br** (317 mg – 0.75 mmol – 1 equiv.) dissolved in tetrahydrofuran (3 mL) was slowly added and the reaction was stirred at room temperature for 96 h. After concentration under vacuum, purification by column chromatography (silica gel, dichloromethane/methanol 95:5) yielded the desired **DA-PEG-OH** product as a pale yellow solid (600 mg, yield = 40%).

$^1\text{H}$  NMR (400 MHz,  $\text{CDCl}_3$ ,  $\delta$ ): 3.65 (m, 180H;  $\text{CH}_2\text{-O}$ ), 3.42 (t,  $J = 7$  Hz, 2H;  $\text{CH}_2\text{-O}$ ), 2.22 (t,  $J = 7$  Hz, 4H;  $\text{CH}_2\text{-C}\equiv$ ), 1.60-1.45 (m, 6H;  $\text{CH}_2$ ), 1.35-1.20 (m, 28H;  $\text{CH}_2$ ), 0.88 ppm (t,  $J = 7$  Hz, 3H;  $\text{CH}_3$ ).

$^{13}\text{C}$  NMR (100 MHz,  $\text{CDCl}_3$ ,  $\delta$ ): 77.4 ( $-\text{C}\equiv$ ), 77.3 ( $-\text{C}\equiv$ ), 72.4 ( $\text{CH}_2\text{-O}$ ), 71.4 ( $\text{CH}_2\text{-O}$ ), 70.5 (86  $\text{CH}_2\text{-O}$ ), 70.2 ( $\text{CH}_2\text{-O}$ ), 69.9 ( $\text{CH}_2\text{-O}$ ), 65.3 ( $-\text{C}\equiv$ ), 65.2 ( $-\text{C}\equiv$ ), 61.5 ( $\text{CH}_2\text{-OH}$ ), 31.8 ( $\text{CH}_2$ ), 29.5

(4 CH<sub>2</sub>), 29.4 (CH<sub>2</sub>), 29.3 (3 CH<sub>2</sub>), 29.2 (2 CH<sub>2</sub>), 29.0 (CH<sub>2</sub>), 28.9 (CH<sub>2</sub>), 28.7 (CH<sub>2</sub>), 28.2 (2 CH<sub>2</sub>), 25.9 (CH<sub>2</sub>), 22.6 (CH<sub>2</sub>), 19.1 (CH<sub>2</sub>), 14.0 ppm (CH<sub>3</sub>).

*Synthesis of carboxylic derivative DA-PEG-CO<sub>2</sub>H.*



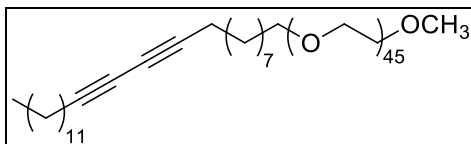
Under nitrogen atmosphere, pentacos-10,12-diyne-1-oxypolyethyleneglycol **DA-PEG-OH** (468 mg – 0.2 mmol – 1 equiv.) dissolved in tetrahydrofuran (5 mL) was added to a suspension of sodium hydride (12 mg, 2.5 equiv.) in tetrahydrofuran (5 mL). The mixture was refluxed for 30 min and allowed to cool down to room temperature. 2-bromoacetic acid (195 mg – 1.4 mmol – 7 equiv.) dissolved in tetrahydrofuran (2 mL) was slowly added and the reaction was stirred at room temperature for 24 h. After concentration under vacuum, purification by column chromatography (silica gel, dichloromethane/methanol 95:5) yielded the desired product as a pale yellow solid (384 mg, yield = 80%).

**<sup>1</sup>H NMR** (400 MHz, CDCl<sub>3</sub>, δ): 4.20 (s, 2H, O-CH<sub>2</sub>-CO<sub>2</sub>H), 3.80-3.60 (m, 180H; CH<sub>2</sub>-O), 3.51 (t, *J* = 7 Hz, 2H; CH<sub>2</sub>-O), 2.24 (t, *J* = 7 Hz, 4H; CH<sub>2</sub>-C≡), 1.65-1.47 (m, 6H; CH<sub>2</sub>), 1.40-1.25 (m, 28H; CH<sub>2</sub>), 0.88 ppm (t, *J* = 7 Hz, 3H; CH<sub>3</sub>).

**<sup>13</sup>C NMR** (100 MHz, CDCl<sub>3</sub>, δ): 169.1 (CO<sub>2</sub>H), 77.5 (-C≡), 77.3 (-C≡), 72.4 (CH<sub>2</sub>-O), 71.6 (CH<sub>2</sub>-O), 70.6 (86 CH<sub>2</sub>-O), 70.1 (CH<sub>2</sub>-O), 70.0 (CH<sub>2</sub>-O), 68.6 (O-CH<sub>2</sub>-CO<sub>2</sub>H), 65.2 (-C≡), 65.1 (-C≡), 61.6 (CH<sub>2</sub>-O), 31.6 (CH<sub>2</sub>), 29.6 (3 CH<sub>2</sub>), 29.5 (CH<sub>2</sub>), 29.4 (CH<sub>2</sub>), 29.3 (2 CH<sub>2</sub>), 29.2

(CH<sub>2</sub>), 29.1 (CH<sub>2</sub>), 29.0 (CH<sub>2</sub>), 28.8 (2 CH<sub>2</sub>), 28.7 (CH<sub>2</sub>), 28.2 (2 CH<sub>2</sub>), 26.2 (CH<sub>2</sub>), 22.6 (CH<sub>2</sub>), 19.2 (CH<sub>2</sub>), 14.0 ppm (CH<sub>3</sub>).

*Synthesis of methyl ether derivative DA-PEG-OMe.*



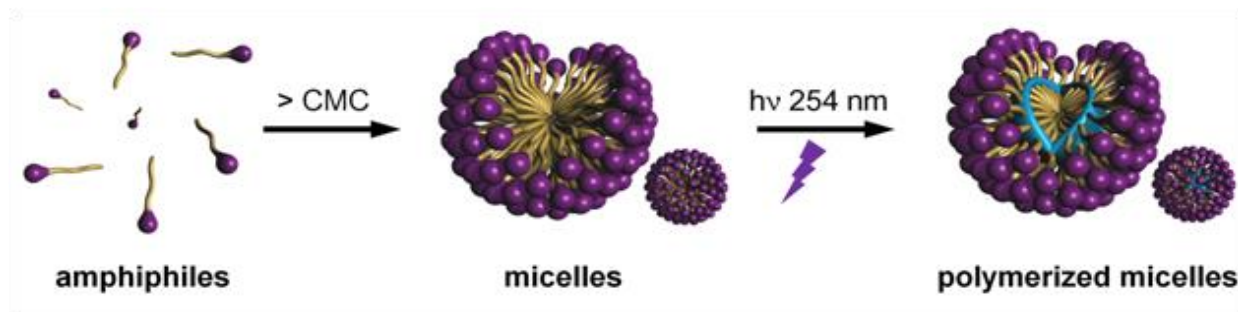
Under nitrogen atmosphere, polyethylene glycol monomethyl ether (MW = 2000, 250 mg – 0.13 mmol – 1 equiv.) dissolved in anhydrous acetonitrile (10 mL) was added to a suspension of sodium hydride (6 mg, 2 equiv.) in anhydrous acetonitrile (2 mL). The mixture was refluxed for 30 min and allowed to cool down to room temperature. Compound **DA-Br** (211 mg, 4 equiv.) dissolved in tetrahydrofuran (2 mL) was slowly added and the reaction was stirred at room temperature for 96 h. After concentration under vacuum, purification by column chromatography (silica gel, dichloromethane/methanol 95:5) yielded the desired product as pale yellow solid (265 mg, yield = 90%).

<sup>1</sup>H NMR (400 MHz, CDCl<sub>3</sub>, δ): 3.80-3.45 (M, 180H; CH<sub>2</sub>-O), 3.33 (s, 3H, O-CH<sub>3</sub>), 2.19 (t, *J* = 7 Hz, 4H; CH<sub>2</sub>-C≡), 1.57-1.45 (M, 6H; CH<sub>2</sub>), 1.37-1.17 (M, 28H; CH<sub>2</sub>), 0.83 ppm (t, *J* = 7 Hz, 3H; CH<sub>3</sub>).

<sup>13</sup>C NMR (100 MHz, CDCl<sub>3</sub>, δ): 77.4 (-C≡), 77.3 (-C≡), 72.5 (CH<sub>2</sub>-O), 71.9 (CH<sub>2</sub>-O), 70.7-70.2 (86 CH<sub>2</sub>-O), 70.3 (CH<sub>2</sub>-O), 70.0 (CH<sub>2</sub>-O), 65.3 (-C≡), 65.2 (-C≡), 61.6 (CH<sub>2</sub>-OH), 58.9 (O-CH<sub>3</sub>), 31.8 (CH<sub>2</sub>), 29.6 (CH<sub>2</sub>), 29.5 (3 CH<sub>2</sub>), 29.4 (CH<sub>2</sub>), 29.3 (3 CH<sub>2</sub>), 29.2 (CH<sub>2</sub>), 29.1 (CH<sub>2</sub>),

29.0 (CH<sub>2</sub>), 28.8 (CH<sub>2</sub>), 28.7 (CH<sub>2</sub>), 28.3 (2 CH<sub>2</sub>), 26.0 (CH<sub>2</sub>), 22.6 (CH<sub>2</sub>), 19.1 (CH<sub>2</sub>), 14.0 ppm (CH<sub>3</sub>).

### Micelles Assembly.



A mixture of **DA-PEG-OMe** and **DA-PEG-CO<sub>2</sub>H** amphiphiles in a 9:1 molar ratio was solubilized in deionized water at a final 10 mg mL<sup>-1</sup> concentration. The solution was sonicated with an ultrasonic probe (300 ms pulses per second, 25 W output power) for 30 min. The solution was then filtered over a 0.2 μm nylon membrane to yield conventional DA-PEG micelles. To obtain core-polymerized micelles, the DA-PEG micelle colloid was further subjected to UV irradiation (254 nm – low pressure mercury UV lamp – Heraeus) for 6 h. The volume of the solution was adjusted to the initial volume by adding deionized water, to compensate the volume lost during the photo-polymerization process. The solution was then filtered over a 0.2 μm nylon membrane to yield pDA-PEG micelle colloid.

The preparation of <sup>14</sup>C-labeled micelles was carried out in the same manner, replacing **DA-PEG-OMe** with <sup>14</sup>C-**DA-PEG-OMe**. The latter was synthesized according to the procedure described above, but starting from <sup>14</sup>C-labeled pentacosanoic acid (prepared according to *Org. Biomol. Chem.* **8**, 3902–3907 (2010)).

Supplementary Figures

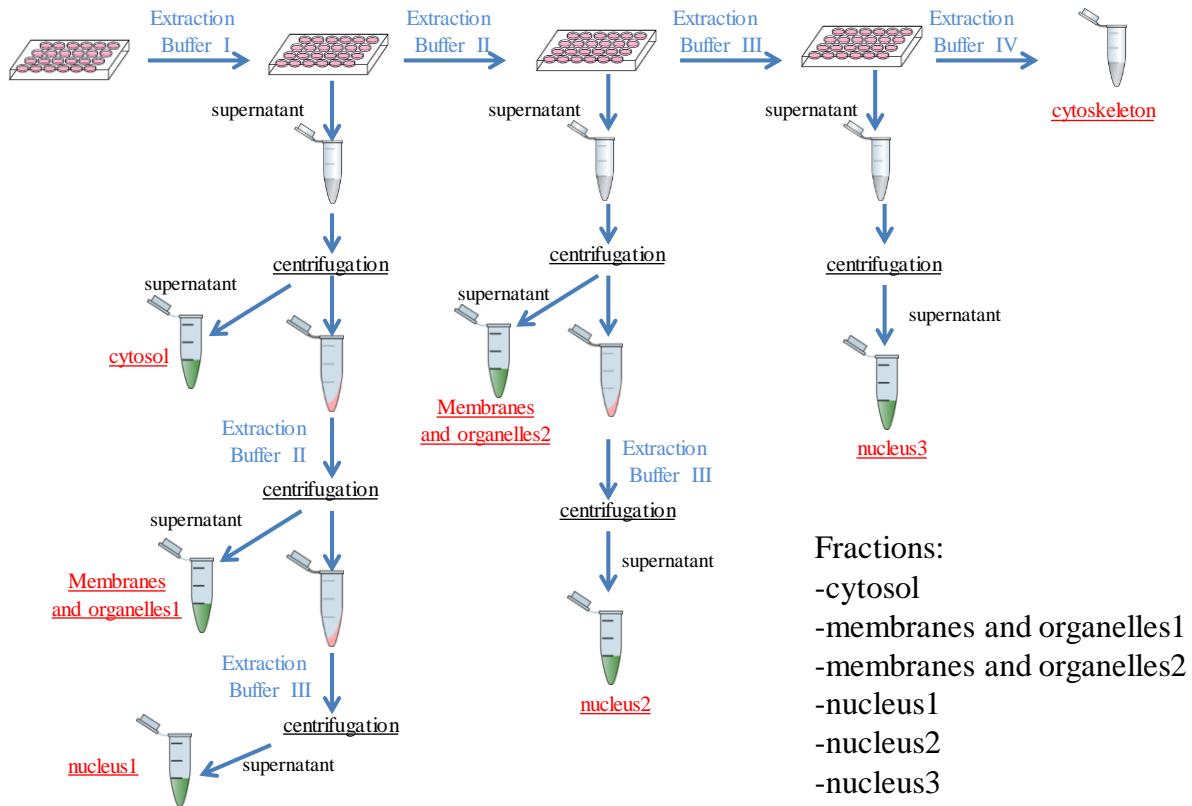


**Figure S1. Initial subcellular fractionation procedure for intracellular distribution studies.**

The standard subcellular fractionation method provided for the ProteoExtract Subcellular Proteome Extraction Kit (Merck Millipore) was optimized to ensure a relevant separation of cytosol, membranes/organelles, nucleus and cytoskeleton in RAW 264.7 cells.

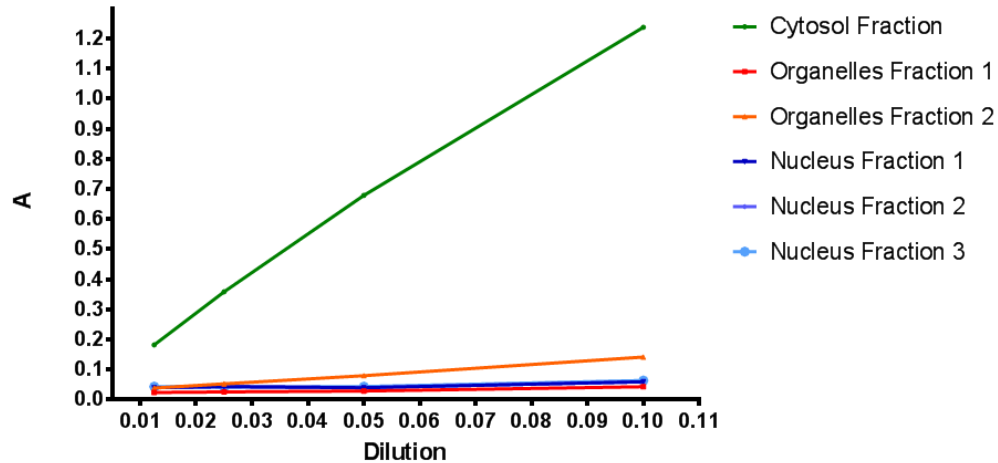


**Figure S2. LDH assay on cell fractions.** All fractions from the initial procedure were diluted in PBS + 1% BSA (1:10, 1:20, 1:40, 1:80) and lactate dehydrogenase (LDH) was quantified in all solutions using the CytoTox 96. Cytosolic LDH was quantified through the formation of the red formazan product in medium, measured at 492 nm. “Cytoskeleton” fraction was collected with “nucleus 3” fraction. The absorbance measured at 492 nm is proportional to the LDH content, showing that almost all the LDH is recovered in the cytosolic fraction, confirming a proper isolation of the cytosol.

**Table S1. Proteins content in cell fractions.** The protein content in all fractions was dosed using a Pierce BCA Protein Assay Kit (Thermoscientific), showing negligible quantities in the “Membranes and organelles 1” and “Nucleus 1” fractions, which were not selected for the optimization of the cellular fractionation procedure.

Fraction	Protein content ( $\mu\text{g}$ )	Proportion to total proteins
Cytosol	637	35%
Membr. and Org. 1	70	3%
Membr. and Org. 2	628	34%
Nucleus 1	9	0.5%
Nucleus 2	379	21%
Nucleus 3	100	5%

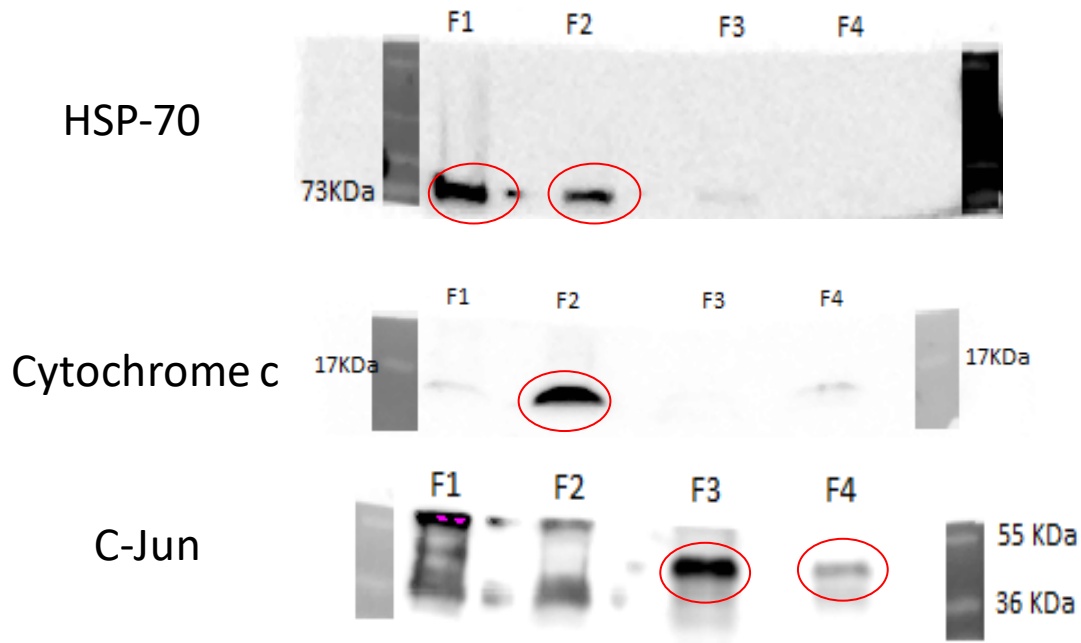


**Figure S3. Identification of compartment-specific proteins in cell fractions.** Three cellular proteins (HSP-70, Cytochrome c and C-Jun) were detected by Western blot on cell fractions after concentration, in the “cytosol” fraction (F1), “membranes and organelles” fraction (F2), combined “nucleus” fractions (F3) and “cytoskeleton” fraction (F4). The ubiquitous Heat shock protein HSP70 (70 kDa) was correctly detected in “cytosol” fraction (F1) and in “membranes and organelles” fraction (F2). The cytochrome complex (12 kDa) was detected only in “membranes and organelles” fraction (F2), confirming that this fraction has been well isolated. The nuclear protein c-Jun (43 kDa) was founded to be present in both the “nuclear” (F3) and the “cytoskeleton” fraction (F4), indicating that nuclear and cytoskeleton fractions were not well separated; the two fractions were therefore combined in the final fractionation protocol.

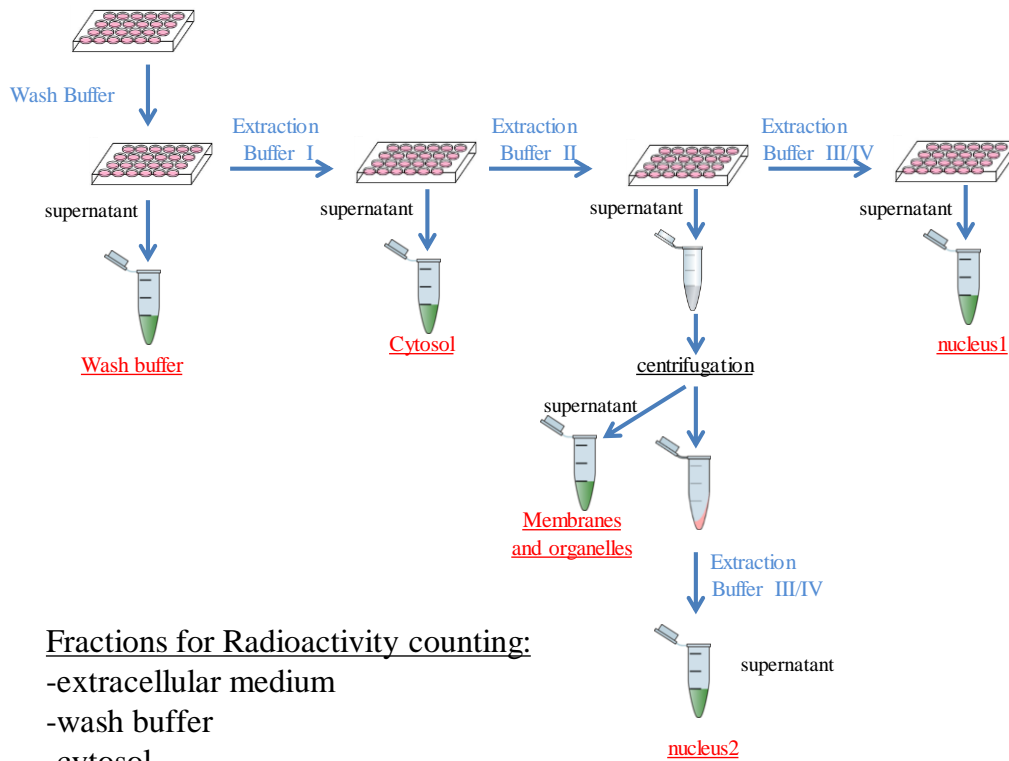


**Figure S4. Final Subcellular fractionation protocol and radioactivity counting.** The final subcellular fractionation protocol set up according to LDH quantification (Figure S2), protein quantification (Table S1) and identification (Figure S3). Radioactivity measurements were performed on all subcellular fractions as well as in the culture medium and in the washing buffer in order to follow the total amount of radioactivity added on cells.

**Table S2. Total uptake of non-polymerized and polymerized  $^{14}\text{C}$ -labeled micelles.** The uptake ( $\mu\text{g}/\text{million cells}$ ) by RAW cells was quantified following exposure to 0.01 mg/mL micelles at 37 °C (4–48 h incubation) or at 4 °C (4 h incubation).

	4h	4h	24h	48h
	4 °C	37 °C	37 °C	37 °C
Non-polymerized micelles ( $\mu\text{g}/\text{million cells}$ )	0.18	0.64	1.20	1.23
Polymerized micelles ( $\mu\text{g}/\text{million cells}$ )	0.06	0.18	0.42	0.48

**Table S3. Subcellular localization of conventional and polymerized  $^{14}\text{C}$ -labeled micelles.** Micelles ( $\mu\text{g}/\text{million cells}$ ) were quantified in subcellular compartments following exposure of RAW cells to 0.01 mg/mL micelles at 37 °C (for 4 h and 48 h incubation).

	4h			48h		
	37 °C			37 °C		
	Cytosol	Membr	Nucleus	Cytosol	Membr	Nucleus
Conventional micelles ( $\mu\text{g}/\text{million cells}$ )	0.15	0.42	0.07	0.19	0.81	0.23
Polymerized micelles ( $\mu\text{g}/\text{million cells}$ )	0.03	0.12	0.03	0.11	0.30	0.08

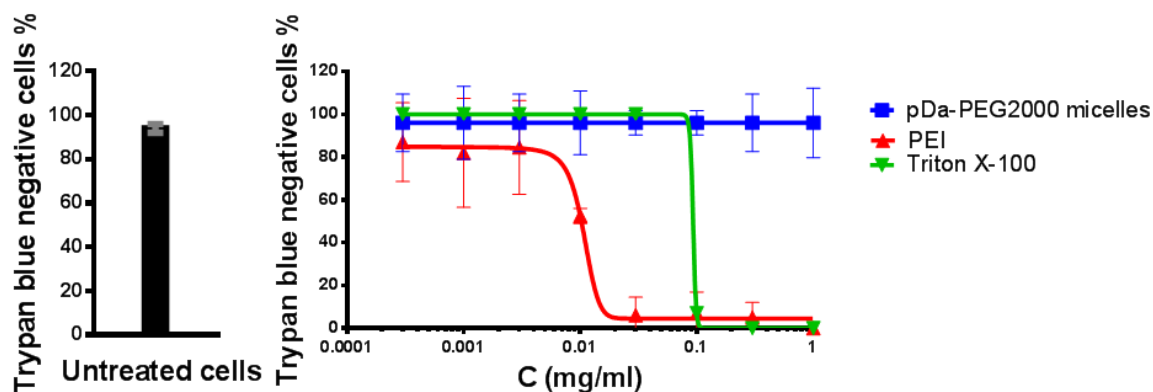


**Figure S5. Evaluation of micelle impact on cell viability by the Trypan Blue test.** RAW cells were treated with polymerized pDA-PEG micelles, polyethylenimine and Triton X-100 at various concentrations (0.0003-1 mg/mL) for 24 h, and further stained with Trypan Blue and observed. Results obtained with micelles were fitted by a sigmoidal curve. Data are mean values  $\pm$  SD of three independent experiments.

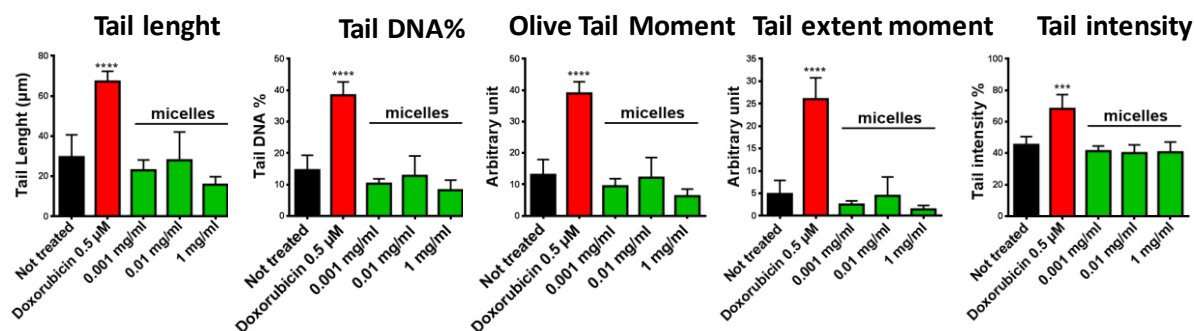


**Figure S6. Comparison of genotoxicity parameters.** The images of the comet assay performed on RAW cells exposed to polymerized micelles and doxorubicin (positive control) were quantified using the OpenComet plugin of the ImageJ software, and expressed by calculating different

parameters: tail length, tail DNA percentage, Olive tail moment, tail extent moment and tail intensity. Data are mean values  $\pm$  SD of three independent experiments.

# General discussion

## **Context and objectives**

In medical applications, **nanotechnology** has led to significant improvements in cancer therapy, diagnostic imaging of diseases, tissue engineering and most importantly in drug delivery systems. Nanotechnology plays nowadays a significant role in the field of medicine and drug delivery because of major limitations and problems that affected conventional pharmaceutical agents and older formulations and delivery systems.<sup>1</sup> Indeed, nanoformulations can deliver drugs more precisely to the targeted tissue and reduce the overall dose and potential toxic side effects. For instance, the enhanced permeability and retention (EPR) effect can allow passive targeting and accumulation of nanosized drugs at malignant tumors and other pathological sites. Beside this, nanocarriers can protect from the degradation fragile drugs that would have very low half-life in physiological conditions.

The design of drug nanocarriers is particularly challenging because the physicochemical properties of nanoparticles can be modified once the formulation is administered in the organism. Controlling and designing the drug/particle association is important but anticipating the in vivo solubilization/release is as much fundamental in order to predict efficacy and toxicity of the nanoformulation. Regarding nanoformulations intended for intravenous injection, anticipating their biodistribution and longterm fate is arduous. The first challenge is related to the colloidal stability of nanoparticles in the blood. Indeed, the complex physiological fluid environment that nanoparticles encounter is populated with a wide range of biomacromolecules, e.g., proteins, vitamins, lipids, and salts/ions that can affect their physicochemical properties and their colloidal stability.

**The objectives of this thesis concerned (1) the improvement of the colloidal stability of two different nanosized delivery systems and (2) the investigation of the influence of the stabilized structure on the biological behavior of nanoparticles and on their interaction**

**with cells.** The present chapter will outline a general discussion and give some perspectives concerning the data we collected during this PhD thesis.

### **Reinforcing the internal structure of nanoparticles**

The Zeta potential of the nanoparticles is the common indicator of their stability based on the electrostatic repulsion between similarly charged particles. Higher surface charge translates into increased electrostatic repulsion and therefore increased stability. However, many other parameters can affect the stability of nanoparticles. Most of studies reported in literature investigated the influence of the surface properties of nanoparticles on their colloidal stability and biological behavior. Together with the surface charge, it is well known that Van der Waals attractive forces regulate the colloidal stability of nanoparticles. This is why researchers usually modify nanoparticles surface properties, with the aim of increasing the electrostatic repulsion and minimizing the Van der Waals attraction. Nonetheless this PhD thesis is centered on different strategies aimed to increase the colloidal stability of nanoparticles, based on the reinforcement of their internal structure. In particular, **two different nanocarriers have been taken into account: (1) chitosan based nanogels and (2) polydiacetylene micelles.** The major concern common to both these systems is related to their instability in physiological media that can lead to their aggregation or more often to their disintegration. The reinforcement of the structure is obtained thanks to the introduction of new bonds. In both cases, the introduction of internal crosslinks does not significantly affect the surface charge of nanoparticles.

In the case of **chitosan nanogels**, crosslinks bonds were obtained by modifying chitosan before nanoparticles formation, namely complexing it with metal ions. The rationale behind this approach is based on the chelation properties of chitosan that can form strong coordination complexes with metals with the lone pairs of electrons on oxygen and azote atoms. Reynaud et

al. notably developed organometallic complexes of chitosan with different metals (Fe<sup>2+</sup>, Fe<sup>3+</sup> and Zn<sup>2+</sup>) formulated as microparticles to remove residual active drugs from the digestive tract.<sup>2</sup> Other groups used chitosan-iron complexes to treat water in order to remove the chromium<sup>3</sup> or chitosan-zinc complexes to improve antimicrobial activity of chitosan.<sup>4</sup>

In this work, chitosan has been modified with two different metal ions (Fe<sup>3+</sup> and Zn<sup>2+</sup>) and different complexation degrees were achieved. Modified polymers were then used to prepare ATP-loaded nanogels. This work is reported in **chapter 1**. The preparation method followed previously reported protocols,<sup>5,6</sup> with some validations. For instance, it has been verified that by inverting the components, that is adding a chitosan solution into a solution of ATP, it was not possible to obtain nanoparticles with such low size and polydispersity.

Chitosan-metal complexes showed to generate more compact and homogenous nanoparticles, which is advantageous for their colloidal stability. According to previous studies, the ionic strength tends to weaken electrostatic interactions inside of nanogels leading to their disintegration. In this work, we observed the disintegration of nanogels in the presence of NaCl 0,9% and, on the contrary, their immediate aggregation in the presence of proteins. Our first and more intuitive hypothesis was based on the fact that positively charged nanogels immediately interact with negatively charged proteins forming aggregates. However, the purification of nanogels allowed us to demonstrate that another mechanism was at the base of the destabilization. In fact, according to the comparison between purified and not purified nanogels, by eliminating free chitosan or chitosan-metal polymer from the formulation, the aggregation in the presence of proteins is strongly limited. This means that positively charged free chitosan chains interact with negatively charged proteins leading to the formation of big aggregates. This leads to a progressive “extraction” of the polymer chains from nanogels caused by the ionic strength of the solution. The presence of iron strongly limits the phenomenon of nanogel disintegration due to the ionic strength, proving that iron effectively forms new “bridges” between the polymer

and the nucleotide leading to the formation of resistant nanoparticles.  $Zn^{+2}$  didn't improved the stability of nanogels in physiological media, suggesting that, contrary to  $Fe^{+}$ , it is not able to form crosslinks between the two components of nanogels. For these reasons, the formulation based on CS- $Fe_{20\%}$  polymer has been selected and used for following studies in chapter 2 and chapter 3 of this thesis.

The colloidal properties and the stability of nanogels have been evaluated by Dynamic Light Scattering analysis (DLS). For the future, DLS results, especially in a complex media, could be compared with results obtained with other techniques. For instance, fluorescence single particle-tracking (fSPT) may be an alternative method to be used under these conditions. Then, to investigate the compactness of nanogels and confirm the impact of the presence of metals, other techniques could be used, such as the Atomic Force Microscopy (AFM) or the calculation of the quantity of water inside of nanogels. Finally, to assess the presence of cross-links inside of nanogels, Infrared Spectroscopy analysis could be attempted on lyophilized nanoparticles.

In the case of **polydiacetylene micelles**, the synthesis and formulation of nanoparticles has been performed at the Service de Chimie Bioorganique et de Marquage (SCBM, département Médicament et Technologie pour la Santé, Institut Joliot). These systems are obtained from the self-assembly of specific unimers composed of a diacetylene (DA)-bearing hydrophobic tail and a poly(ethylene glycol) (PEG) headgroup. DA-PEG unimers spontaneously form small micelles in an aqueous medium that can be subsequently stabilized ("cross-linked") through photo-polymerization upon irradiation at 254 nm.

## Application of chitosan based nanogels to the delivery of nucleotides and nucleotide analogues

Natural nucleotides and nucleotide analogues display important pharmacological activities. The well-known nucleotide adenosine triphosphate (ATP), the most important and ubiquitous source of energy of cells, is used for the treatment of cardiac, hepatic and brain ischemia. 3-OH-modified nucleotide analogues such as azidothymidine triphosphate (AZT-TP) display anticancer and/or antiviral activity by interfering with cancer cells or viral nucleic acid synthesis, respectively. The clinical use of these drugs, however, is limited due to the presence of a triphosphate group, which is prone to hydrolysis and enzymatic degradation and is responsible for the high hydrophilicity of the molecules, thereby strongly limiting their uptake by targeted cells and their access to the intracellular pharmacological targets. To overcome these limitations and enable the administration of nucleotides and nucleotide analogues, several nanocarriers have been investigated,<sup>7</sup> such as liposomes, aqueous-core polymeric nanocapsules, poloxamer-polyethyleneimine copolymer nanoparticles, metal organic frameworks. Various technological locks remain, however, to translate these nucleotides and nucleotide analogues based nanosystems to clinics, such as drug entrapment efficiency, drug loading, material biocompatibility, and, mostly, synthesis complexity.

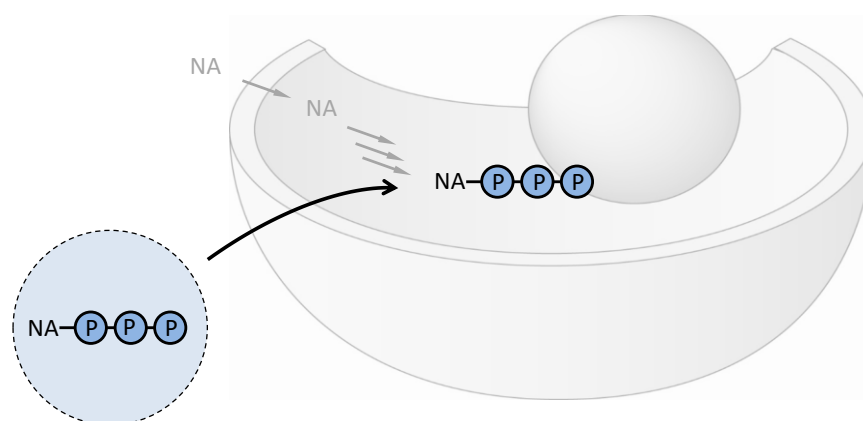


**Fig.1** Improving the intracellular uptake of nucleotides by using nanocarriers.

Recently, Giacalone et Al. have shown that **triphosphate group-containing active drugs** such as ATP and AZT-TP **can induce the** so-called “**ionotropic gelation**” of **chitosan**, leading to CS/ATP and CS/AZT-TP nanoparticles with high drug entrapment efficiency and elevated loading rate.<sup>5</sup> Chitosan is a natural biocompatible and biodegradable polysaccharide obtained from chitin deacetylation that is known to form nanoparticles through complexation with the tripolyphosphate (TPP) polyanion. The simple and easily scalable ionotropic gelation technique gave the name of “nanogels” to the nanoparticles prepared. Since their introduction in 1997 by Calvo et al., Chitosan-TPP based nanogels have been widely used, especially for the delivery of proteins and nucleic acids (DNA, siRNA). In the **chapter 2** of this thesis, the ionotropic gelation has been successfully applied to the encapsulation of other triphosphate derivatives, such as cytidine triphosphate (C-TP) and gemcitabine triphosphate (dFdC-TP), and compared with ATP nanogels. Thanks to its ability to form stable nanoparticles, chitosan-iron complex have been used for the preparation of the aforementioned nanogels. It has been demonstrated that, independently from the nucleotide structure, modified chitosan can form nanoparticles with small size (diameter < 200 nm) and narrow polydispersity, confirming that the electrostatic interactions are the driving force of the nanogels formation. Data obtained on the drug loading reinforce the hypothesis that the structure of nanogels is similar for all nanogels formulations. However, the ITC results and the colloidal stability of nanogels suggest that other parameters related to the nitrogen base can play a role in the interactions between polymer and nucleotides, making them stronger (in the case of purine containing molecules) or weaker (in the case of pyrimidine containing molecules). In the same way, the fluorine atoms on the ribose of dFdC-TP has an impact on these interactions.

For all the formulations, in 0.9% w/v NaCl the nanoparticles mean size was found to remain constant over 24 h, while the scattered light intensity decreased progressively over 24 h, suggesting a particle dissociation without aggregation nor swelling but rather through disentanglement of chitosan chains from the particles and subsequent dissolution. The in vitro drug release in these conditions was evaluated for the CS-Fe<sub>20</sub>%/ATP formulation. The possibility of purchasing the products of hydrolysis of ATP (ADP and AMP) made the HPLC analysis and the interpretation easier to perform. For the future, it will be interesting to compare these data with the release of other nucleotides in the same conditions. The in vitro release of ATP from nanoparticles was found to be extremely low confirming that CS-Fe<sub>20</sub>%/ATP display a very good resistance to the ionic strength. After some hours, the ATP released from nanoparticles is hydrolyzed in ADP that is subsequently hydrolyzed in AMP. This is most probably due to the presence of acetic acid used for nanogels preparation that is not completely removed during the step of purification. In perspective, in order to prove the “protective action” of nanoparticles against the nucleotides degradation, the drug release analysis should be evaluated in absence of an acid buffer in the preparation. Furthermore, with the aim of proving the protective action in a physiological media, the experiment should be performed in presence of phosphatases enzymes. The comparison between the degradation rate of the free ATP and the ATP released from nanoparticles in these conditions would provide important informations on the mechanism of protection of nanogels from nucleotides degradation.

We also have showed that **dFdC-TP (gemcitabine triphosphate) loaded nanogels** could deliver the active triphosphates of therapeutic nucleotides into breast and pancreatic cancer cells inducing an in vitro cytotoxic activity similar to that observed with the parental drug. Moreover, the resistant index of lymphogenic cancer cells has been found to be lower for the nanoformulation compared to the free drug. This result, despite being not easy to interpret, suggests that the mechanisms of cytotoxicity of free dFdC-TP and nanogels-carried dFdC-TP

are different. Furthermore, it demonstrate that nucleotides delivered by chitosan-iron nanogels are immediately released inside of cells after nanoparticles uptake. In perspective, it will be interesting to demonstrate that nanoformulations containing active triphosphate form of nucleoside analogs are able to efficiently reverse the drug-resistant phenotype of cancer cells. In order to do this, cytotoxicity evaluations on nucleoside-kinases deficient cells should be attempted. Additionally, besides overall cell viability assessments, specific toxicity endpoints should be investigated such as the induction or apoptosis or, more importantly in the case of gemcitabine triphosphate, the DNA damage.

### **Cellular uptake of nanoparticles**

The nanoparticles cellular uptake is very important to be considered when evaluating the potential use of colloids for biomedical application, as well as for assessing their possible risks of usage (nanosafety profile). Even if many studies on how physicochemical properties of nanoparticles relate with cellular effects (including uptake) are reported in literature, further investigations on nanoparticle-cell interaction are required.

In order to study the interactions of nanoparticles with cells, macrophages, monocytes and neutrophils are often used. In this thesis, immortalized RAW 264.7 murine macrophages were chosen as a model for investigating nanoparticles uptake. Since these cell types usually have a great propensity for nanoparticles internalization, short incubation times can be considered. To elaborate upon the mechanism of nanoparticles entry and accumulation, a time course approach from 1 h to 24 h or longer can be utilized. Generally, not cytotoxic concentrations are used to study nanoparticles uptake, based on preliminary tests.

A variety of microscopic methods, ranging from simple light microscopy to more complex electron microscopy, can be used to determine the uptake and the intracellular localization of nanoparticles inside cells. Fluorescent confocal microscopy is usually used to identify more

qualitatively the uptake of nanoparticles aggregates into certain organelles in living cells. This technique is based on the use of a fluorescent dye that can be conjugated to the polymer or the lipid constituting the nanocarrier or physically encapsulated into the nanoparticle. The main disadvantages of this technique are (1) that the resolution is insufficient ( $> 100$  nm) to examine individual nanoparticles and (2) that only the dye is detected limiting the informations about the nanoparticles status. In this thesis (**chapter 3**), we used fluorescent confocal microscopy with the aim of proving the effective ability of chitosan-iron nanogels to deliver intracellularly the encapsulated nucleotide (ATP conjugated to BODIPY in this case). The uptake was found to be clearly higher when the molecule was delivered by the carrier compared to the free one. Furthermore, the perinuclear fluorescence observed in median optical slices showed that the molecule was delivered in the cell cytoplasm rather than merely bound to the cell membrane. It would have been interesting to compare these results with the analysis by confocal microscopy of cells treated with ATP-BODIPY-loaded nanogels based on unmodified chitosan, in order to confirm the higher capacity of intracellular delivery of chitosan-iron based nanogels compared to chitosan based ones. With the aim of investigating the kinetic of interaction of chitosan-iron based nanogels with macrophages, confocal microscopy by reflection mode has been used at different incubation times. Thanks to the higher electronic density of iron, it has been possible to determine the kinetic of internalization of nanogels. To the best of our knowledge, this is the first time that this technique is applied to the investigation of the nanoparticles intracellular uptake.

To gain the resolution, transmission electron microscopy (TEM) is typically carried out to determine the uptake and the localization of individual nanoparticles inside cells, as well as to provide clues to the uptake mechanism whether it is endocytic or not.<sup>8</sup> In fact, nanomaterials and cell components, such as organelles, can be clearly imaged by TEM. Metallic and metal oxide nanoparticles (e.g., Au, Ag, TiO<sub>2</sub> and SiO<sub>2</sub>) generate much greater contrast in the TEM

compared with the cellular background. Therefore, this technique can be applied to a diverse range of cell types and particles compositions to determine nanoparticles localization. In the chapter 3 of this thesis, TEM has been used to evaluate the presence of chitosan-iron nanoparticles inside of macrophages after 12 h of exposure. The presence of nanoparticles have not been assessed, probably because of their previous degradation. In the future, we could extend the TEM analysis to cells treated for different times, especially for short incubation times, in order to clarify the mechanism of entrance and degradation of chitosan-iron nanoparticles inside of cells. Furthermore, in perspective, uptake experiments on chitosan-iron nanoparticles could be performed also at 4°C and at 37°C in presence of endocytosis-inhibitors. These additional experiments could provide more informations about the mechanism of cell internalization of nanogels and on their intracellular fate.

Flow cytometry is another technique used to quantify the internalization of nanoparticles, based on the use of fluorescent dye chemically linked to the carrier components or physically entrapped in the carrier. In addition, flow cytometry can be used to investigate the morphology of cells. In some studies, the morphology of cells treated with nanoparticles is correlated to their internalization and/or absorption to the cell membrane. Generally, an increased cell volume and/or a higher granularity are considered to be indicators of nanoparticles accumulation. In this thesis, we reported that RAW cells treated with polymerized DA-PEG micelles at high concentrations (1 mg/mL) display an increased cell volume and granularity. Any difference has been observed on cells exposed to chitosan-iron nanogels, probably because of the lowest concentration used (up to 0.2 mg/mL).

Another strategy for following the intracellular fate of nanoparticles consists on labelling them with radioactive isotopes. In this thesis (**chapter 4**), in order to compare the intracellular distribution of DA-PEG micelles in their conventional form and in their core-polymerized form, macrophages were exposed to <sup>14</sup>C-labelled micelles. DA unimers exhibited an important

accumulation in cellular membranes and a significant uptake at 4 °C that is indicative of some passive uptake. On the contrary, core-polymerized micelles accumulate in cell cytoplasm in a time-dependent way, suggesting an endocytosis-mediated internalization typical of nano-sized particles. These outcomes allowed us to clarify and confirm the mechanism of toxicity of conventional micelles and, together, to elucidate the effect of the core-polymerization on the intracellular fate of micelles.

### **In vitro toxicity of nanoparticles**

**Nanotoxicology** is emerging as an important subdiscipline of nanoscience and nanotechnology because of the finding of increasing toxic effects of nanodrugs and nanomaterials on living organisms. However, the toxicology of nanoparticles is poorly understood as there are no sufficient methods to assess their safety.<sup>9</sup> Nanoparticles can interact with biological systems by either chemical or physical mechanisms.<sup>10</sup> Chemical mechanisms include the production of reactive oxygen species (ROS), dissolution and release of toxic ions, disturbance of the electron/ion cell membrane transport activity, oxidative damage through catalysis, lipid peroxidation or surfactant properties. ROS are considered as being the main underlying chemical process in nanotoxicology, leading to secondary processes that can ultimately cause cell damage and even cell death. Moreover, ROS production is one of the main factors involved in inflammatory processes. Physical mechanisms are mainly a result of particle size and surface properties. This includes disruption of membranes and membrane activity, transport processes, protein conformation/folding and protein aggregation/ fibrillation.

Because of their ability to actively take up foreign particles, **immune cells** are classically used as experimental models for in vitro nanotoxicity studies.<sup>11</sup> As reported before,<sup>12</sup> the general trends of cytotoxicity for nanoparticulate materials are similar for both the murine and human macrophage cell lines. For cytotoxicity studies, the 24 h time point usually provide more

sensitive data, to complete one cell cycle. Issues that we can expect to address in studies > 24 h include cell proliferation, microbial growth and possible removal and reapplication of dosing solutions. Based on these considerations, in this thesis, **RAW 264.7 murine macrophages were used to evaluate the cytotoxicity of CS-Fe<sub>20%</sub>/ATP nanogels and pDA-PEG micelles**, in order to predict the toxicity of these drugs nanocarriers after acute administration in humans. **Chitosan** is a polysaccharide known to be biocompatible and biodegradable. However, the presence of high percentage of iron in the formulation demanded a deep investigation of the eventual mechanisms of toxicity. **Iron** is a transition metal that, due to its inherent ability to exchange electrons with a variety of molecules, is essential to support life. In mammals, iron exists mostly in the form of heme, enclosed within an organic protoporphyrin ring and functioning primarily as a prosthetic group in proteins. Paradoxically, free iron has also the potential to become cytotoxic when electron exchange with oxygen is unrestricted and catalyzes the production of reactive oxygen species. These biological properties demand that iron metabolism is tightly regulated such that iron is available for core biological functions while preventing its cytotoxic effects. Macrophages play a central role in establishing this delicate balance.<sup>13</sup> Moreover, non-transferrin-bound iron assumes greatest clinical importance in various iron-loading disorders, such as haemochromatosis and thalassaemia. Humans have a very limited capacity to excrete iron, so iron that enters the body in excess of metabolic requirements accumulates in the tissues and body fluids and can exceed the body's capacity to sequester it in a relatively harmless protein-bound form. The resulting excessive iron deposits can potentiate tissue damage.<sup>14</sup> Recently, a new form of cell death, named ferroptosis, was discovered. Ferroptosis results from iron-dependent lipid peroxide and ROS accumulation and is characterized mainly by cell volume shrinkage and increased mitochondrial membrane density without typical apoptotic and necrotic manifestations.<sup>15</sup> The oxidation of organic

substrates by iron (II or III) and hydrogen peroxide ( $H_2O_2$ ) is called Fenton chemistry or the Fenton reaction, and was first described by H. J. H. Fenton in 1894.

In **chapter 3**, the possible cytotoxic effects of CS-Fe<sub>20%</sub>/ATP nanogels were evaluated and compared to that of the CS-Fe<sub>20%</sub> free polymer and Fe(NO)<sub>3</sub> (free Fe<sup>3+</sup>), by treating cells with the same amounts of iron (III).

The cell morphology analysis by flow cytometry revealed a strong impact of free iron (Fe(NO)<sub>3</sub>) on the side scatter, contrary to iron complexed to chitosan (CS-Fe<sub>20%</sub>/ATP nanogels and CS-Fe<sub>20%</sub> free polymer). This could be related to the phagocytosis of aggregates formed in the culture medium as a result of the interactions between iron and proteins, to cell damage and/or even to the induction of cell death mechanisms. The higher impact of free iron on cells homeostasis was confirmed by results obtained from Propidium Iodide Assay and ROS production analysis. However, by observing by TEM cells treated with higher concentrations of CS-Fe<sub>20%</sub>/ATP nanogels, some differences have been noticed compared to not treated cells, in particular at the level of mitochondria. By the way, the effect on mitochondria has been also shown through the assessment of the mitochondrial membrane potential by TMRE staining. These outcomes suggest that the eventual toxicity consequent to the accumulation of high quantities of CS-Fe<sub>20%</sub>/ATP nanogels could be related to the toxic effects of iron released by nanogels. In order to better understand this point, it could be interesting to compare the intracellular distribution of iron after cells exposure to free iron Fe(NO)<sub>3</sub> and CS-Fe<sub>20%</sub>/ATP nanogels or CS-Fe<sub>20%</sub> free polymer. Iron could be detected inside of cells by using mass spectrometry, electron spectroscopy imaging X-ray, fluorescence microscopy.<sup>16</sup> Anyway, taken all together, our results suggest that CS-Fe<sub>20%</sub>/ATP nanogels present a low cytotoxicity at therapeutically relevant doses that makes them good candidates for following in vivo studies.

In **chapter 4**, the possible toxic effects of polydiacetylene micelles on macrophages were investigated and compared to those of non-polymerized micelles. The two nanoobjects (native

micelles and core-polymerized micelles) were taken as models of a “dynamic” system and a “particle-like” system respectively. First tests of the impact of micelles on the overall viability evidenced the higher toxicity of non-polymerized micelles compared to polymerized ones. LDH release assay results indicated that the cytotoxicity of non-polymerized micelles is related to their ability to destabilize and disrupt cell membranes when exposed at concentrations above their CMC, while polymerization of micelles prevents this propensity. Uptake studies confirmed the accumulation in membranes of non-polymerized micelles, indicating that, because of their dynamic nature, micelles may lose their particle status and act as surfactants. On the contrary, since polymerized micelles showed to be internalized by endocytosis, eventual intracellular toxic effects were investigated. Any increase of apoptosis and necrosis were observed as well as any significant increase of inflammatory factors. As polymerized micelles’ ability to reach nuclear compartment was not excluded by intracellular distribution evaluations, genotoxic effects were investigated and, according to collected data, were excluded. In this part of the thesis, because of the absence of genotoxic effects of polymerized micelles, the ROS evaluation has been considered to be not necessary. In vivo studies performed until today with pDA-PEG micelles for cancer therapy and imaging purposes, while showing efficient delivery abilities, didn’t evidence any toxic effect confirming the nanocarrier safety profile showed in this thesis.

## **General conclusion**

In conclusion, during this thesis we were able to improve the colloidal stability in physiological conditions of drug nanocarriers intended for parenteral administration and we demonstrated the impact of the colloidal stability of nanoparticles on their interactions with cells. More interestingly, we put in evidence the effects of changing the internal structure of nanoparticles while keeping the same surface properties.

In particular, we obtained chitosan-based nanogels for the delivery of nucleotide analogues resistant to both the disassembly and the aggregation thanks to the introduction of iron in the nanogels structure. Iron, which has been complexed to chitosan before the nanogels formation, is able to act as a “cross-linker” between the polymer and the triphosphate derivative, resulting in a reinforced particles internal structure. Chitosan-iron nanogels showed to have a remarkably higher stability compared to chitosan nanogels and chitosan-zinc nanogels. The formulation containing Adenosine Triphosphate, which has been choose as model, exhibited a very slow drug release in physiological conditions. For these reasons, chitosan-iron nanogels were selected as a scaffold for the preparation of new formulations containing different nucleotide analogues. Chitosan-iron showed to form stable nanogels with any kind of nucleotide, indicating the great potential of this platform for the delivery of different molecules. Preliminary in vitro results on different resistant cancer cell lines allowed us to propose chitosan-iron nanogels as interesting new system for the delivery of chemotherapeutic molecules. The toxicological profile of chitosan-iron nanogels was assessed on macrophages, revealing the absence of acute toxic effects that could be due to the cell exposure to iron. According to our results, we can conclude that chitosan-iron nanogels are able to intracellularly deliver the drug while not releasing toxic iron.

We worked then on another type of drug nanocarrier in the context of a collaboration with the group of Eric Doris. Doris group recently reported the development of photopolymerized core-

stabilized polydiacetylene micelles as promising potential carriers for therapeutics and imaging agents. In this thesis we successfully demonstrated the impact of the core-polymerization on micelles in vitro toxicity and uptake. In fact, core-polymerized micelles were shown to be internalized by endocytosis inside of cells without leading to any intracellular toxic effect, contrary to the non-polymerized ones that accumulate in the membranes causing membrane permeabilization and cytotoxicity.

Taken all together, these results demonstrate that chitosan-iron nanogels and polydiacetylene micelles both represent safe platforms for the delivery of nucleotide analogues and hydrophobic drugs respectively. Furthermore, this thesis demonstrate that the colloidal stability of nanoparticles is a key factor in nanoformulations efficacy and toxicity that has to be severely investigated and anticipated in nanoparticles design.

## REFERENCES

1. Farjadian, F. *et al.* *Nanopharmaceuticals and nanomedicines currently on the market: Challenges and opportunities.* *Nanomedicine* **14**, (2019).
2. Reynaud, F., Tsapis, N., Deyme, M., Vasconcelos, G. & Gueutin, C. Spray-dried chitosan-metal microparticles for ciprofloxacin adsorption : 7304–7312 (2011). doi:10.1039/c1sm05509g
3. Zimmermann, A. C., Mecabô, A., Fagundes, T. & Rodrigues, C. A. Adsorption of Cr(VI) using Fe-crosslinked chitosan complex (Ch-Fe). *J. Hazard. Mater.* **179**, 192–196 (2010).
4. Wang, X., Du, Y. & Liu, H. Preparation , characterization and antimicrobial activity of chitosan – Zn complex. **56**, 21–26 (2004).
5. Giacalone, G., Fattal, E. & Hillaireau, H. Drug-Induced Nanocarrier Assembly as a Strategy for the Cellular Delivery of Nucleotides and Nucleotide Analogues. 0–5 (2013). doi:10.1021/bm301832v
6. Giacalone, G. *et al.* Stabilization and cellular delivery of chitosan – polyphosphate nanoparticles by incorporation of iron. *J. Control. Release* **194**, 211–219 (2014).
7. Hillaireau, H. & Couvreur, P. Nanoencapsulation of antiviral nucleotide analogs. *J. Drug Deliv. Sci. Technol.* **19**, 385–390 (2009).
8. Schrand, A. M., Schlager, J. J., Dai, L. & Hussain, S. M. Preparation of cells for assessing ultrastructural localization of nanoparticles with transmission electron microscopy. *Nat. Protoc.* **5**, 744–757 (2010).
9. Onoue, S., Yamada, S. & Chan, H. K. Nanodrugs: Pharmacokinetics and safety. *Int. J.*

- Nanomedicine* **9**, 1025–1037 (2014).
10. Elsaesser, A. & Howard, C. V. Toxicology of nanoparticles. *Adv. Drug Deliv. Rev.* **64**, 129–137 (2012).
  11. Jones, C. F. & Grainger, D. W. In vitro assessments of nanomaterial toxicity. *Adv. Drug Deliv. Rev.* **61**, 438–456 (2009).
  12. Soto, K., Garza, K. M. & Murr, L. E. Cytotoxic effects of aggregated nanomaterials. **3**, 351–358 (2007).
  13. Soares, M. P. & Hamza, I. Review Macrophages and Iron Metabolism. *Immunity* **44**, 492–504 (2016).
  14. Anderson, G. J. Non-transferrin-bound iron and cellular toxicity. 105–108 (1999).
  15. Yu, H., Guo, P., Xie, X., Wang, Y. & Chen, G. Ferroptosis , a new form of cell death , and its relationships with tumourous diseases Definition and discovery of ferroptosis Differences between ferroptosis and apoptosis / necrosis. **21**, 648–657 (2017).
  16. Manuscript, A. NIH Public Access. **64**, 1363–1384 (2013).

**Titre :** Stabilité colloïdale, devenir intracellulaire et toxicologie des nanovecteurs - Application aux micelles polymérisées et aux nanogels organométalliques

**Mots clés :** nanovecteurs, toxicologie, devenir intracellulaire, stabilité colloïdale, micelles, nanogels

**Résumé :** Une compréhension approfondie de la stabilité colloïdale est nécessaire pour concevoir des nanoparticules pour la vectorisation de molécules actives. En particulier, prévoir le comportement in vivo des particules (désagrégation ou agrégation) est fondamental pour prédire l'efficacité et la toxicité des nanoformulations. Les objectifs de cette thèse concernaient (1) l'amélioration de la stabilité colloïdale en conditions physiologiques et (2) l'étude in vitro du comportement biologique de deux types de nanovecteurs : nanogels à base de chitosane-fer et micelles de polydiacétylène.

**Title :** Colloidal stability, intracellular fate and toxicology of drug nanocarriers - Application to polymerized micelles and organometallic nanogels

**Keywords :** nanocarriers, toxicology, intracellular fate, colloidal stability, micelles, nanogels

**Abstract :** A thorough understanding of the colloidal stability is important to design nanoparticles for drug delivery purposes. In particular, anticipating the in vivo particles disassembly or aggregation is fundamental in order to predict efficacy and toxicity of the nanoformulations. The objectives of this thesis concerned (1) the improvement of the colloidal stability in physiological conditions and (2) the in vitro investigation of the biological behavior of two types of drug nanocarriers: chitosan-iron based nanogels and polydiacetylene micelles.